The University Of Sheffield.

Bidirectional crosstalk between Hypoxia-Inducible Factor and glucocorticoid signalling in zebrafish larvae

By:

Davide Marchi

A thesis submitted in partial fulfilment of the requirements for the degree of Doctor of Philosophy

The University of Sheffield
Faculty of Science
Department of Biomedical Science

August 2020

ACKNOWLEDGEMENTS

Firstly, I would like to thank my supervisor Dr. Freek van Eeden, to whom I am immensely grateful for his outstanding support and guidance throughout my PhD. In particular, I'd like to thank him for his constant effort to let improve my skills and understanding of scientific method. He and the rest of the lab members provided a stimulating and friendly environment which I will always be thankful for.

My most genuine thanks also go to my advisors Dr. Vincent T. Cunliffe and Dr. Mark D. Bass for providing me support, feedback and for our inspiring chats. I am also really grateful both to Eleanor Markham and to Dr. Rosemary Kim for their extremely helpful support and discussions contributing to this study. In addition, this work would not have been possible without the help of the University of Sheffield aquarium staff, who took excellent care of the fish used during my PhD.

A heartfelt thanks to all my great friends and colleagues of the C6 room, C10 lab, Cunliffe and Krone's lab, who played a key role of support and amusement during this PhD journey. I will always happily remember you and all the moments spent together. You made me feel at home. Each of you gave me something special every day that helped me becoming a better person and a better scientist.

Last but not least, a gigantic thank you to the love of my life Claudia, who followed and supported me every day. There are no words to describe my gratitude to her. Finally, a huge thank to both my family and parents in law for their fundamental help and support during this fantastic journey.

ABSTRACT

Hypoxia inducible factor (HIF) and Glucocorticoids (GCs) transcriptional responses play a pivotal role in tissue homeostasis, glucose metabolism and in the regulation of cellular responses to various forms of stress and inflammation. In the last decades few *in vitro* studies highlighted the potential for crosstalk between these two major signalling pathways. However, how this interplay precisely takes place *in vivo* is still unclear.

To this end, the aim of this project is to elucidate how and to what degree hypoxic signalling affects the endogenous glucocorticoid pathway and vice versa, using zebrafish larvae (*Danio rerio*) as an *in vivo* model organism. Indeed, the use of whole animals allows us to show how these pathways interact at a more systemic and complex level than in cell culture, where interactions between different tissues and cell types cannot be easily modelled.

Previous work from my lab identified glucocorticoids as activators of the HIF pathway (Vettori et al., 2017). Counterintuitively, despite their anti-inflammatory action, it was shown that GR loss of function prevents the transcriptional activity linked to immune response (Facchinello *et al.*, 2017). Finally, the glucocorticoid receptor has been also observed to synergistically activate proinflammatory genes by interacting with other signalling pathways (Langlais *et al.*, 2008, 2012; Dittrich *et al.*, 2012; Xie *et al.*, 2019). Nevertheless, how the crosstalk between hypoxic and glucocorticoid signalling occurs *in vivo* is still debated.

By taking advantage of both a genetic and a pharmacological approach I altered these two pathways during the first 120 hours post fertilisation of zebrafish embryos. In particular, I used two different mutant lines I have generated (*hif1β*^{sh544} (*arnt1*) and

gr^{sh543} (*nr3c1*)), coupled to an already existing *vhl*$^{hu2117/+}$*;phd3:eGFP*$^{i144/i144}$ hypoxia reporter line (Santhakumar *et al.*, 2012), to study the effect of HIF signalling on glucocorticoid response and vice-versa, through a "gain-of-function/loss-of-function" approach. Phenotypic and molecular analyses of these mutant lines were accompanied by optical and fluorescence microscope imaging.

Firstly, I have demonstrated that in the presence of upregulated HIF signalling, both glucocorticoid response and endogenous cortisol levels are repressed in 5 days post fertilisation larvae. In addition, despite HIF activity being low at normoxia, my data show that it already impedes glucocorticoid activity and levels.

Secondly, I further analysed the *in vivo* contribution of glucocorticoids to HIF signalling. Interestingly, my results show that both glucocorticoid receptor (GR) and mineralocorticoid receptor (MR) play a key role in enhancing the HIF response.

Finally, I found indications that glucocorticoids promote HIF signalling via multiple routes. Cumulatively, this study suggests a model for how this crosstalk occurs *in vivo* and, more broadly, paves the way for further *in vivo* analysis on the extensive interaction behind these two major signalling pathways.

TABLE OF CONTENTS

INDEX OF FIGURES AND TABLES

FIGURES

TABLES

LIST OF ABBREVIATIONS

3β-HSD – 3β-Hydroxysteroid dehydrogenase/Δ5-4 isomerase

ACTH – adrenocorticotropic hormone

ANOVA – analysis of variance

AP – Alkaline Phosphatase

Asn – Asparagine

arnt – Aryl Hydrocarbon Receptor Nuclear Translocator 1

AVP = Arginine Vasopressin

BAC – Bacterial Artificial Chromosome

BCIP – 5-bromo-4-chloro-3-indolyl-phosphate

bHLH – basis helix-loop-helix

BME – Betamethasone 17,21-dipropionate

BTM – basal transcription machinery

cAMP – cyclic adenosine monophosphate

CBG – corticosteroid-binding globulins

ccRCC – clear cell renal cell carcinoma

CNS – central nervous system

CRF – corticotropin-releasing factor

CRH – corticotropin-releasing hormone

CRISPR – clustered regularly interspaced short palindromic repeats

CRISPant –mutants derived from CRISPR/Cas9-based mutagenesis method

Ct – cycle threshold

cyp11a1 – cytochrome P450 Family 11 Subfamily A Member 1

cyp17a1/2- cytochrome P450 Family 17 Subfamily A Member 1/2

DBD – DNA binding domain

dCAPS – derived Cleaved Amplified Polymorphic Sequence

DEX – Dexamethasone

DMOG – dimethyloxalylglycine

DMSO – dimethyl sulfoxide

dpf – days post-fertilisation

EDTA – ethylenediaminetetraacetic Acid

eef1a1 – Eukaryotic Translation Elongation Factor 1 Alpha 1

eGFP – enhanced Green Fluorescent Protein

egln3 – Egl-9 Family Hypoxia Inducible Factor 3

epo – erythropoietin

EtOH – ethanol

fbp1 – fructose-1,6-bisphosphatase 1

FC – fold change

FIH – asparagine hydroxylase factor inhibiting HIF

fkbp5 – FK506-binding protein 5

FRET – Fluorescent Resonance Energy Transfer

g6pc – Glucose-6-Phosphatase Catalytic Subunit

GC – glucocorticoid

glut1 – glucose transporter 1

GR – glucocorticoid receptor

GRE – glucocorticoid-response elements

H – hinge region

HAF – Hypoxia-associated factor

HIF – Hypoxia-inducible factor

hmgcr – 3-Hydroxy-3-Methylglutaryl-CoA Reductase

HPA – hypothalamic-pituitary-adrenal axis

hpf – hours post-fertilisation

HPI – hypothalamic-pituitary-interrenal axis

HR – homologous recombination

HRE – hypoxia-response elements

HSD17B2 – Hydroxysteroid 17-Beta Dehydrogenase 2

HSP90 – Heat Shock Protein-90 kD

IKKβ – IκB kinase beta

IL – interleukin

IL-1RA – interleukin-1 receptor antagonist

il6st – interleukin 6 Signal Transducer

lamb1b – laminin subunit beta-1

LBD – Ligand binding domain

lipca - lipase, hepatic a

MC2R – melanocortin 2 receptor

MeOH – methanol

MGB - minor groove binder

MR – mineralocorticoid receptor

NBT – nitro blue tetrazolium

NF-κβ – nuclear factor-κB

NFQ – nonfluorescent quencher

NHEJ – non-homologous end joining

NH4Ac – ammonium acetate

NLS – N-terminal nuclear localization signal

nr3c1 – nuclear Receptor Subfamily 3 Group C Member 1

NTD – N-terminal domain

ODDD – oxygen-dependent degradation domain

p300/CBP – p300/CREB-binding protein

P450scc – cytochrome P450 cholesterol side-chain cleavage

PAM – protospacer adjacent motif

PAS – Per-Arnt-Sim

PBS – Phosphate Buffer Saline

PBST – Phosphate Buffer Saline + Tween20

pc – pyruvate carboxylase

pck1 – phosphoenolpyruvate carboxykinase 1

PFA – paraformaldehyde

pfkb1 – phosphofructokinase B-type carbohydrate kinase family protein

pfkfb3 – 6-phosphofructo-2-kinase/fructose-2,6-biphosphatase 3

PHD – prolyl hydroxylases

pi3k – phosphoinositide 3-kinase

PKA – protein kinase A

pomca – proopiomelanocortin-a

Pro – proline

ProtK – proteinase K

PTU – 1-Phenyl-2-thiourea

pVHL – Von Hippel Lindau protein

PVN – paraventricular nucleus

rbx1 – RING box protein-1

ROS – Reactive Oxygen Species

rpm – revolutions per minute

rps29 – Ribosomal Protein S29

RT – Room Temperature

RTqPCR – Quantitative Reverse Transcription Polymerase Chain Reaction

s.e.m – standard error of the mean

siah1a/2 – siah E3 ubiquitin protein ligase 1A

SL – standard length

slc37a4 – Solute Carrier Family 37 Member 4

slc2a1a – solute carrier family 2-member 1a

SSC – Saline-Sodium Citrate

StAR – steroidogenic acute regulatory protein

stat – signal transducer and activator of transcription

TAD-N/C – N- and C-terminal transactivation domains

TAE – Tris-Acetate-EDTA

TBE – Tris-Boric Acid-EDTA

Tg – transgene

tracrRNA – trans-activating CRISPR RNA

UPLC – Ultra-Performance Liquid Chromatography

VBA – Visual Background Adaptation

vegf – vascular endothelial growth factor

vhl – von Hippel Lindau

vll – von Hippel Lindau-like

WISH – whole mount in situ hybridisation

wt – wild type

xg – times gravity

1. INTRODUCTION

1.1. Oxygen homeostasis and hypoxia

Cellular oxygen (O_2) is an essential nutrient that is required to maintain metabolism, bioenergetics and to assure the correct functioning and survival of aerobic animals. It is important to note that while ambient air is 21% O_2 (150 mm Hg), most mammalian tissues are at 2% - 9% O_2 (~40 mm Hg). In vertebrates, oxygen concentration gradients act as signals that guide towards proper development. Indeed, the balance between cell growth and vascularization is able to elicit differential gene expression acting as driving force that directs cell behavior. Moreover, in tissue morphogenesis, the timing of hypoxic exposure can modulate both development and differentiation (Simon and Keith, 2008)

Hypoxia, or decreased oxygen levels, is also a common pathophysiological condition which has profound effects on the cellular transcriptome. Generally, it is characterized by a reduced oxygen availability (below 2%), whereas severe hypoxia or "anoxia" by O_2 levels below 0.02%, to either cells, tissues or organs in the body (Cummins and Taylor, 2005; Bertout, Patel and Simon, 2008; Semenza, 2013). In particular, hypoxia may occur either as a consequence of improper blood supply (i.e. during embryonic development, or in solid tumors) or as a result of the environment (i.e. poorly oxygenated waters or at high altitude) (Webb, Coleman and Pugh, 2009). Cumulatively, hypoxia acts both as a crucial developmental stimulus and physiological stressor to which cells must rapidly respond in order to assure homeostasis.

In all organisms, including vertebrates, homeostasis is the state of optimal internal, physical and chemical conditions, which is maintained by several regulatory apparatus aimed to assure both survival and correct functioning of the body (Biddlestone, Bandarra and Rocha, 2015). One of the main cellular mechanisms that aerobic organisms developed during the course of evolution to cope with decreased oxygen availability is controlled by the hypoxia-inducible factor transcription factors (HIF) family. Being a widely action family of transcription factors, it is made up of primary regulators of the cellular response to low oxygen levels, which mediate several biological functions (i.e haematopoiesis, angiogenesis, maintenance of vascular tone, etc.) in order to provide tissues with blood and oxygen. In addition to that, HIF can also rapidly coordinate a series of metabolic changes (i.e. from aerobic to anaerobic metabolism) that enable the body to prevent both metabolic shutdown and death (Bertout, Patel and Simon, 2008; Semenza, 2013; Ebersole *et al.*, 2018). If these mechanisms fail or are inadequate, they can lead to the development of a wide range of pathological conditions which includes tissue ischemia, inflammation, stroke and the growth of solid tumors (Elks *et al.*, 2015).

As previously mentioned, since cells require oxygen to survive, hypoxia acts as a potent cellular stressor. Indeed, oxygen deprivation leads to reduced mitochondrial oxidative phosphorylation, augmented lactate production and elicits an excessive accumulation of free radicals which further fuel the hypoxic stress (Chandel *et al.*, 2000; Klimova and Chandel, 2008; Solaini *et al.*, 2010). To avoid that, cells must rapidly adapt to match metabolic, redox and bioenergetic requirements to a reduced O_2 supply. In particular, at a protein level these hypoxic responses can be sorted into two different groups: acute and chronic phase. Acute phase responses are prompt and transient and

are mainly based on post-translationally modifications of existing proteins, whereas chronic phase reactions are more persistent and intense.

These changes consist of altering gene transcription and protein biosynthesis to enable cells to temporarily block the cell cycle at G1/S of the interphase. This is usually accompanied by the secretion of survival and proangiogenic factors (mainly in cancer) and by the reduction of energy consumption (Majmundar, Wong and Simon, 2010). Consequently, understanding the molecular mechanisms by which cells sense and respond to hypoxia may provide the basis for novel therapeutic approaches to many disorders.

1.2. The Hypoxia-Inducible Factor pathway

The progression of the cell cycle is an energy requiring process that demands a refined metabolic regulation to occur. Indeed, it is well known that cells must overtake an energy restriction checkpoint during G1 phase, in order to progress through the cell cycle. In this regard, as aerobic organisms require oxygen for metabolically converting nutrients into energy, O_2 represents a vital signalling molecule directing the cell fate. Consequently, assuring oxygen homeostasis is a critical task that must be precisely managed by cells in order to perform correctly and survive in a hostile environment (Semenza, 2011b).

In mammalian cells, this is primarily carried out by the Hypoxia-Inducible Factors (HIFs) which are a family of transcription factors that react both to environmental oxygen and cellular energy alterations (i.e. hypoxia) (Semenza, 2001). HIFs are obligate heterodimers consisting of an O_2-labile α-subunit and a stable β-subunit (also known as aryl hydrocarbon receptor nuclear translocator or ARNT). Both HIF alpha and beta subunits are expressed in the cytoplasm. However, whilst HIF-β/ARNT isoforms are constitutively expressed, HIF-α subunits (HIF1α, HIF2α and HIF3α) are characterized by a very fast turnover that is post-translationally regulated by the PHD3-VHL-E3-ubiquitin ligase protein degradation complex. This mechanism is believed to maintain low basal HIF levels that can rapidly increase in order to promptly respond to decreased oxygen concentrations (Berra *et al.*, 2001; Moroz *et al.*, 2009; Elks *et al.*, 2015; Köblitz *et al.*, 2015).

Under normoxic conditions (normal oxygen levels), a set of prolyl hydroxylases (PHD1, 2 and 3) directly exploit the available molecular oxygen to hydroxylate two prolyl residues (Pro402, Pro564) within the oxygen-dependent degradation domain

(ODDD) of the HIF-α subunits. Then, the hydroxylated HIF-α isoforms are recognized and targeted by the Von Hippel Lindau protein (pVHL), which acts as the substrate recognition component of the E3-ubiquitin ligase complex. Of note, the latter is characterized by a multiprotein complex which consists of Elongin B, Elongin C, Ring-box 1 and Cullin 2 (Iwai *et al.*, 1999). Once this complex ubiquitinates the HIF-α subunits, it directs them towards proteasomal degradation in order to avoid the aberrant stabilization and activation of the HIF pathway under normoxic conditions. In addition, HIF-α may be hydroxylated by factor-inhibiting HIF (FIH) on asparagine 803, which prevents the recruitment of the transcriptional coactivator p300/CREB-binding protein (p300/CBP) and reduces the effectiveness of HIF transcriptional activation (Shay and Simon, 2012). By contrast, the presence of reduced O_2 levels impairs both PHD and FIH enzymatic activity and leads to HIF-α stabilization. As a consequence, pVHL is no more able to recognize and target HIF-α to proteasomal degradation, when the latter is not hydroxylated. This allows the HIF-α and β subunit heterodimer formation, followed by the ARNT-mediated translocation in the nucleus.

Here, p300/CBP may interact with the HIF-αβ transcription complex to further activate the hypoxic response. This implies the upregulation of target genes which are involved in decreasing oxygen consumption and increasing oxygen and nutrient delivery (Nikolaus, Fölscn and Schreiber, 2000). In particular, this occur via HIF-αβ direct recognition and binding to hypoxia-response elements (HREs). The latter are characterized by the presence of a consensus sequence G/ACGTG located within the promoter regions of target genes such as phosphofructokinase, adrenomedullin, erythropoietin and vascular endothelial growth factor (Lando *et al.*, 2002; Leonard *et al.*, 2005; van Rooijen *et al.*, 2009) (**figure 1.1**).

Importantly, the zebrafish (*Danio rerio*) has proved to be a very informative and genetically tractable organism for studying hypoxia and HIF pathway both in physiological and pathophysiological conditions. (C. E. Robertson *et al.*, 2014; Vettori *et al.*, 2017) In the next subchapter, I will describe the main oxygen sensing, signal transduction and transcriptional activation components that characterize the HIF signalling pathway.

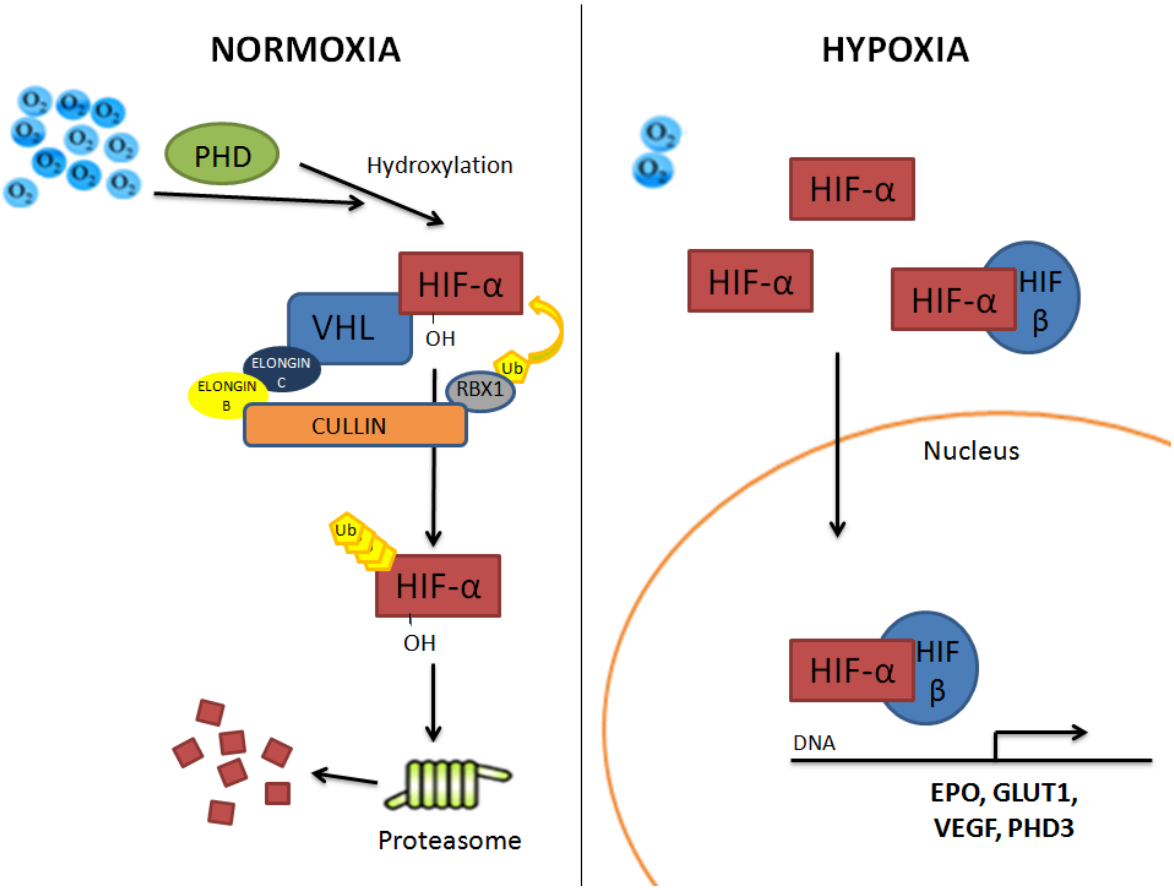

Figure 1.1 Oxygen-dependent post-translational regulation of HIF-α subunit. Under normoxic conditions, the prolyl hydroxylase 3 (PHD3) hydroxylates HIF-α subunit on two specific prolyl residues within the oxygen dependent degradation domain (ODD). In turn, VHL recognizes and binds to hydroxylated HIF-α and then recruits the other components of the E3-ubiquitin ligase complex. The latter promotes the ubiquitin-mediated proteasomal degradation of HIF-α subunit. Conversely, hypoxic conditions inhibit PHDs activity and the subsequent degradation of HIF-α, which can in turn be stabilized and migrate into the nucleus after dimerization with HIF-1β-subunit. Here, the HIF-αβ active complex elicits the expression of genes such as VEGF, GLUT1 and EPO involved in restoring oxygen homeostasis. (modified from Stroka and Candinas, 2010).

1.2.1. Oxygen-dependent regulation of HIF-α

The preservation of oxygen homeostasis is essential to assure the correct functioning of the cell cycle. In this regard, the ability to perceive and quickly respond to changes related to the environmental oxygen availability is initially carried out by a plethora of oxygen sensor proteins. Among them, prolyl hydroxylases (PHD) represents the first line of defence against decrease oxygen levels, by hydroxylating crucial residues in HIF-α subunits.

Within the HIF pathway, the prolyl-hydroxylase domain containing enzymes (PHDs) together with the asparagine hydroxylase factor inhibiting HIF (FIH), are the main molecular oxygen sensors (Schofield and Ratcliffe, 2004; Walmsley *et al.*, 2011; Place *et al.*, 2013; Ivan and Kaelin Jr, 2017). There are three different prolyl-hydroxylases (PHD1-3) which hydroxylate HIF-α subunits on two specific proline residues (Epstein *et al.*, 2001; Kaelin and Ratcliffe, 2008). Among them, PHD2 has proven to be the main mediator of HIF-1α hydroxylation, whereas both PHD's 1 and 3 was shown to participate more significantly to HIF-2α regulation (see also chapter 1.2.2) (Appelhoff *et al.*, 2004). However, PHD3 proved to be more potently upregulated than PHD2 under hypoxic conditions, whilst the expression of PHD1 is insensitive to hypoxia. In addition, PHD3 itself is one the main HIF target genes, as it is required to hydroxylate and degrade the HIF-α subunit. This is because, to control its own levels and to avoid an excessive and prolonged hypoxic response, the HIF pathway is able to trigger an intracellular super short feedback loop. This is based on the upregulation of its regulators aimed to tune HIF activity itself (Aprelikova *et al.*, 2004; Pescador *et al.*, 2005; Henze and Acker, 2010; van Rooijen *et al.*, 2011; Santhakumar *et al.*, 2012).

As a consequence of hypoxia, besides the direct transcriptional regulation of the PHDs, both PHD1 and PHD3 stabilisation are tuned by the Siah1a/2 RING-finger ubiquitin

ligases, which target prolyl hydroxylases to proteasomal degradation. (Nakayama *et al.*, 2004; Khurana *et al.*, 2006).

As previously mentioned, an additional controller of the HIF activation is represented by FIH, which is a Fe^{2+} and oxygen dependent asparagyl hydroxylase with the ability of hydroxylating HIF1-α subunit on a specific asparagine residue (Asn803). Of note, even though this hydroxylation is essentially an oxygen dependent event, due to its high affinity with molecular oxygen, the hydroxylation performed by FIH tends to be more inhibited under severe hypoxic conditions than the PHDs' one (Lisy and Peet, 2008). By doing so, FIH activity avoids HIF to interact with its transcriptional co-activator p300/CBP (Lando *et al.*, 2002). At the same time, it creates a gradual hypoxic response by permitting the HIF-p300/CBP co-activation to occur only under severe hypoxic conditions. This allows the cell to further activate the HIF transcriptional response only when needed.

Another level of complexity in the regulation of the hypoxic response is represented by the fact that both FIH and PHDs are dioxygenases requiring O_2, ferrous iron (Fe^{2+}), 2-oxoglutarate and ascorbate, as co-substrates, in order to hydroxylate HIF-α (Siddiq, Aminova and Ratan, 2007). In this regard, ferrous iron is essential for the enzyme to be assembled into its active conformation, since prolyl hydroxylases contain Fe^{2+} in their hydrophobic active centre. In addition, O_2 binding event requires the ascorbate-dependent maintenance of this iron molecule in its ferrous state. Moreover, HIF-α hydroxylation occurs by transferring one oxygen either to Pro402 or Pro564, while a second oxygen atom reacts with 2-oxoglutarate. This reaction yields both succinate and carbon dioxide as reaction products, making this catalytic process irreversible. Finally, during a complete reaction, Fe^{2+} is transiently oxidized to Fe^{4+} and reduced to the Fe^{2+} state. Interestingly, when α-ketoglutarate is converted into

succinate without hydroxylation of a peptide substrate, this Fe^{2+} is oxidized to Fe^{3+}. In this process, ascorbate is also required to reduce Fe^{3+} back to Fe^{2+} in order to allow the enzyme to be recycled (Pan *et al.*, 2007). So, HIF may also be a response to iron depletion and may explain the HIF-activation properties of iron chelators in cell culture (Bianchi, Tacchini and Cairo, 1999; Buss *et al.*, 2004; Hatcher *et al.*, 2009).

Cumulatively, the vertebrate O_2-sensing pathway primarily involves both prolyl and asparagyl hydroxylation of the HIF-α subunits, which in normoxic conditions contribute to HIF inactivation. By contrast, in hypoxia the lack of molecular O_2 avoids these oxygen sensors to act on HIF-α, allowing the cytoplasmic stabilization of the latter. Finally, not only O_2 concentration, but also multiple mitochondrial products can coordinate PHD activity, HIF stabilization and hence the cellular responses to O_2 depletion (Solaini *et al.*, 2010).

1.2.2. The Hypoxia-Inducible Factor isoforms

As described in the previous subchapter, the adaptive cellular response to an adverse environment consists in the orchestration a transcriptional program based on the upregulation of HIF-dependent target genes, which code for proteins that are involved in restoring and promoting energy homeostasis (i.e. VEGF, GLUT1, EPO, PHD3 etc.) (Schofield and Ratcliffe, 2004; Semenza, 2011a; Moniz, Biddlestone and Rocha, 2014).

In this regard, HIFs are evolutionarily conserved heterodimeric proteins, related to the basic-helix loop-helix–Per-Arnt-Sim homology (class II bHLH– PAS) transcriptional regulators family, which promote metabolic changes that drive cellular adaptation to low oxygen availability (Majmundar, Wong and Simon, 2010; Nath and Szabo, 2012). In mammals, HIF proteins are obligate heterodimers composed by an

oxygen-sensitive α-subunit (HIF-1α, HIF-2α, and HIF-3α) and a constitutively stable aryl hydrocarbon receptor nuclear translocator or β-subunit (ARNT1 and ARNT2).

As also illustrated in figure 1.2, both subunits are bHLH/PAS transcription factors containing transactivation domains (TADs) (Webb, Coleman and Pugh, 2009). In particular, the initial bHLH domain is followed by a Per-Arnt-Sim (PAS) domain which acts as a molecular sensor, an oxygen-dependent degradation domain (ODD), and by an N- and C-terminal transactivation domains (TAD-N and TAD-C) (**figure 1.2**).

Of note, the latter is present in all the HIF-α subunits with the exception of HIF-3α, which only has the TAD-N activation domain, along with the inhibitory PAS domain protein (IPAS) (Li *et al.*, 2006; Makino *et al.*, 2007). On the other hand, HIF-β/ARNT being not targeted and degraded by the pVHL-E3 ligase complex lacks both the ODD and the TAD-N domains, and has a constitutively active N-terminal nuclear localization signal (NLS) (Pollenz, Sattler and Poland, 1994; Eguchi *et al.*, 1997).

Another important difference among HIF isoforms regards their expression pattern. Indeed, if HIF-1α subunit is ubiquitously expressed, HIF-2α is selectively expressed in a tissue-specific manner and it has been observed to be present at high levels only in vascular endothelial cells, lung type-2 pneumocytes and kidney epithelial cells (Bertout, Patel and Simon, 2008). Conversely, Hif-3α highest levels in vertebrates have been observed in heart, placenta, lung, and skeletal muscle, whilst were barely detectable in the liver, brain, and kidney (Zhang *et al.*, 2014; Duan, 2016). In addition, although HIF-1α and HIF-2 α, share multiple structural similarities, their roles differ under a variety of conditions. In this respect, HIF-1α is broadly considered the major regulator of the hypoxic response in hypoxia, whereas HIF-2α is usually more associated with tumorigenesis (Loboda, Jozkowicz and Dulak, 2010).

Furthermore, *in vitro* studies highlighted that under hypoxic conditions HIF-1α tends to occupy more binding sites than HIF-2α, which instead engages a smaller subset of them (Schödel *et al.*, 2011). By contrast, HIF-3α was shown to have multiple variants in human, which can either inhibit or activate the transcription of target genes, according to variant length, the gene targeted and the abundance of HIF-β. These effects can occur via competitive binding to HIF-1α/2α at cytoplasmic level to HIF-β and also to HREs (Heikkilä *et al.*, 2011).

In addition, HIF-1α and HIF-2α usually upregulate overlapping as well as unique transcriptional targets and cooperate in reprogramming metabolic pathways to generate cellular energy especially under different hypoxic conditions (Raval *et al.*, 2005; Koh and Powis, 2012; Shay and Simon, 2012; Suzuki *et al.*, 2014). Interestingly, although both HIF-1 and HIF-2 bind to the same HRE consensus sequence in the regulatory regions of target genes, the DNA binding does not necessarily correspond to the increased transcriptional activity. This suggests that post-DNA binding mechanisms might be required for transactivation (Mole *et al.*, 2009). Moreover, the differential activation of downstream target genes has also been linked to differences among the N-terminal transactivation domains (TADs) of HIF-1α compared to HIF-2α. These findings suggested that differences in HIF-α isoforms' coding sequences might also contribute to isoform-specific function (Hu *et al.*, 2003, 2007).

It is also important to note that previous studies highlighted the presence of HIF switches, which can directly change HIF-α isoform dependency. Indeed, it has been observed that HIF-1α is activated during short periods of severe hypoxia and upregulates genes primarily involved in glycolysis and pyruvate metabolism, whereas HIF-2α is activated under prolonged periods of mild hypoxia and mainly controls genes regulating fatty acid metabolism (Gordan *et al.*, 2007; Majmundar, Wong and Simon,

2010; Koh and Powis, 2012). The temporal regulation of HIF-1/2α is primarily mediated by the oxygen dependent hydroxylases which differently regulate HIF-α isoforms stability and activity. In this regard, PHD2 preferentially interact with HIF-1α than HIF-2α, whereas PHD3 has relatively more influence on HIF-2α than HIF-1α (Appelhoff *et al.*, 2004). HIF-2α is also less efficiently hydroxylated than HIF-1α by both PHDs and FIH-1, resulting in the stabilization and activation of HIF-2α in the presence of higher oxygen tension (Koivunen *et al.*, 2004). Moreover, it has been observed that in addition to post-translational mechanisms, in lung epithelial cells, HIF-1α (but not HIF-2α) mRNA is destabilized under prolonged hypoxia, due to HIF-dependent expression of HIF-1α antisense RNA (Uchida *et al.*, 2004).

Interestingly, the zebrafish HIF signalling pathway shows a remarkable functional conservation with humans (van Rooijen *et al.*, 2011). Moreover, both human and zebrafish liver expresses all HIF-α family members under both physiologic and pathophysiologic conditions, suggesting that HIFs are important mediators of normal liver function and disease (Koh *et al.*, 2012). Unfortunately, due to a genome duplication event occurred in zebrafish during evolution, there are two paralogs for each of the three Hif-α isoforms (Hif-1αa, Hif-1αb, Hif-2αa, Hif-2αb, Hif-3αa and Hif-3αb) and redundancy between the isoforms may occur. However, among these, Hif-1αb has proven to be the main zebrafish homologue in the hypoxic response (Elks *et al.*, 2011, 2015; Köblitz *et al.*, 2015). By contrast, as concerns HIF-1β (ARNT) paralogues, the expression of two genes encoding Arnt1 and Arnt2 proteins has been outlined in zebrafish (Wang *et al.*, 2000; Prasch *et al.*, 2006; Hill *et al.*, 2009; Pelster and Egg, 2018).

In addition to the above considerations, even though microarray analysis have identified over 400 genes regulated by HIF (Mole *et al.*, 2009; Schödel *et al.*, 2011),

subsequent CHIPseq studies have also mapped an extremely larger number of HREs (5177) in the zebrafish genome (Greenald *et al.*, 2015; Kim *et al.*, 2017). Thus, HIF is likely to impact on the transcription of a much larger set of genes. These data also highlighted that the regulation of hypoxia-inducible genes may occur even via interactions with other transcription factors through still unknown mechanisms. Moreover, several studies have reported a differential regulation of specific HIF target genes performed by HIF-1α and HIF-2α (Elvert *et al.*, 2003; Covello and Simon, 2004; Warnecke *et al.*, 2004; Raval *et al.*, 2005; Scortegagna *et al.*, 2005; Holmquist-Mengelbier *et al.*, 2006). However, the mechanism by which HIF-1α and HIF-2α distinguish their respective target genes is still unclear. Of note, it does not seem to be dependent on the core HRE sequence, but possibly on the different expression patterns of the HIFα-subunits and/or on the interaction with other transcription factors (Ruas and Poellinger, 2005; Wenger, Stiehl and Camenisch, 2005).

Finally, the universal importance of HIFs proteins has been demonstrated by the ubiquitous expression of HIF-1α and HIF-1β in almost all adult and embryonic mouse and human tissues. Furthermore, the fact that several functional knock-down studies in mice have often led to premature mortality and/or abnormal physiology with particular relevance to increased tumorigenesis confirmed this assumption (Kapitsinou and Haase, 2008).

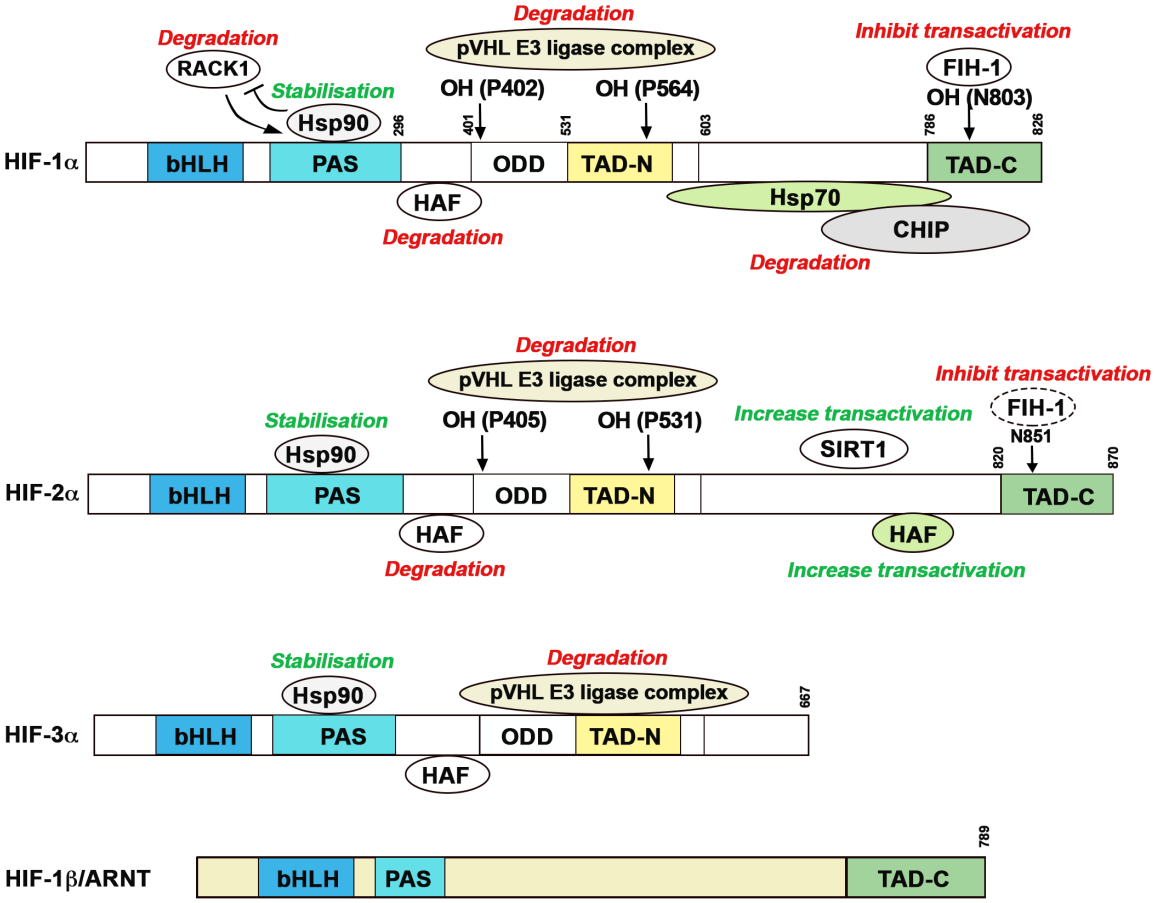

Figure 1.2. Structural domains of HIF-1α, HIF-2α, HIF-3α and their transcriptional binding partner HIF-1β/ARNT. In humans and other vertebrate species, both HIF-1α and HIF-2α contain a basic helix-loop- helix (bHLH) domain; a Per-Arnt-Sim domain (PAS) made up of PAS-A and PAS-B; an oxygen dependent degradation (ODD) domain; an N-terminal transactivation domain (N-TAD) located in the ODD and a C-TAD localized in the C-terminal region (modified from Koh and Powis, 2012).

1.2.3. The role of von Hippel Lindau protein

As previously stated, pVHL controls HIF-α stability and consequently negatively regulates the activation of the HIF response under normoxic conditions. Since HIF activity elicits a potent transcriptional response, HIF-α stability is a process that must be finely regulated. In the cells, this is achieved by a specific multiprotein complex driven by VHL.

pVHL is the main enzyme in the pathway which regulates HIF-stability by recognizing and binding to the hydroxylated HIF-α subunit. Then, being the substrate recognition component of the E3-ubiquitin ligase complex, it is able to engage elongin B, elongin C, cullin 2, and ring-box1 to induce the poly-ubiquitination of HIF-α subunit (**figure 1.1**). As a result, poly-ubiquitination signals the HIF-α degradation to the 26s proteasome (Kallio *et al.*, 1999). By doing so, cells ensure that HIF-α is constantly degraded in the cytoplasm under normoxic conditions.

pVHL is also involved in the termination of the HIF response after reoxygenation upon hypoxia. In addition, it can be present in the nucleus where it has been observed binding to HIF-α subunits in order to trigger their ubiquitination (Groulx and Lee, 2002). Of note, the VHL-ubiquitin ligase complex trafficking has been seen being more dependent on the transcription rate rather than the cellular oxygen levels (Khacho *et al.*, 2008). It is also interesting to observe that since HIF signalling plays a pivotal role in the regulation of cellular oxygen availability by stimulating erythropoiesis, angiogenesis and metabolism through anaerobic glycolysis, it can tune and interact with several other signalling pathways in ways that are still unknown.

Moreover, even if pVHL is well-known to be the key regulator of the HIF signalling, it has been shown to have numerous additional HIF-independent roles. Although some of these may result from VHL's role in the ubiquitination complex,

others appear to be independent of this. For instance, inhibition or loss of VHL has been demonstrated to affect microtubules stability, cilia and mitotic spindle formation and may also contribute to tumorigenesis (Kim and Kaelin, 2004; van Rooijen *et al.*, 2011; Kim *et al.*, 2020).

In particular, the presence of a mutation in the VHL gene is typically associated to the development of familial VHL disease and of sporadic clear cell renal cell carcinoma (ccRCC) forms (Nyhan, O'Sullivan and McKenna, 2008). In this regard, people affected by VHL disease are heterozygous for wide range of mutations at the level of this gene, which makes them more susceptible to develop cysts and highly vascularized tumors following the loss of heterozygosity. Moreover, the form and severity of the disease may vary according to both the location and the type of mutation. Finally, although VHL patients are closely monitored for kidney cancer, biallelic loss of VHL is also a major cause of sporadic kidney cancer. Frustratingly, in these cases ccRCC is usually discovered when it is in an advanced state and has become metastatic. For these patients treatment options are extremely limited (Lonser *et al.*, 2003; Cohen and McGovern, 2005).

The role of VHL in assuring homeostasis has been demonstrated is several studies. Among those, Vhl knock-out studies performed in mice resulted in haemorrhages and defects in placental vascularisation which bring to embryonic death at around 10 embryonic days (Gnarra *et al.*, 1997). By contrast, despite the early lethality in *Vhlh* knockout mice, studies performed on zebrafish *vhl* mutants showed that they are able to complete embryogenesis and survive up to larval stages (8-11 days post fertilization). Thus, zebrafish *vhl* mutants represent an exclusive vertebrate model in which VHL role can be studied during both embryonic and postembryonic stages (van Rooijen *et al.*, 2009).

Another disease associated with VHL mutation is the Chuvash polycythaemia. Interestingly, despite other VHL disease forms characterized by a heterozygous mutation, Chuvash polycythaemia is mostly caused by a homozygous R200W mutation located at the C-terminus of the gene. Interestingly, this results in an exacerbated HIF response followed by the development of polycythaemia, peripheral thrombosis, haemangiomas and in an increased vascular tone, but not hemangioblastomas, pheochromocytoma or ccRCC (Gordeuk *et al.*, 2004; Smith *et al.*, 2006). This highlighted the fact that there may be additional roles played by VHL, besides negatively regulating HIF, that are essential for its role as a tumour suppressor gene (Ang *et al.*, 2002)

In general, the VHL/HIF signalling is also highly relevant in cancer, even when there are no mutations in the HIF pathway itself. This is particularly due to the hypoxic nature of the majority of solid tumours. Since uncontrolled growth is a fundamental characteristic of tumours, oxygen is a central nutrient that quickly runs out especially in the inner part of the tumoral mass. This usually triggers the activation of the HIF pathway which makes the tumour more resistant and able to cope with a hypoxic scenario. Consequently, these series of event are often followed by the expression of growth factors that leads to hypoxic angiogenesis (Semenza, 2012).

As a consequence of the above considerations, unravelling the precise mechanism in which HIF signalling works, how it is regulated and how it affects and interacts and with other pathways may provide entry points for clinical intervention. To this end, the following subchapters will be focused on the description of the main biological pathways affected by HIF in order to mediate the hypoxic response.

1.2.4. The HIF pathway and its role in glucose metabolism

In order to reduce oxygen consumption, HIF pathway orchestrates a rapid metabolic shift from aerobic metabolism to anaerobic glycolysis, leading to upregulation of glycolytic genes (i.e. enolase 1, aldolase A, lactate dehydrogenase A, phosphoglycerate kinase 1, and phosphofructokinase L) (Semenza *et al.*, 1996; Minchenko *et al.*, 2002). In addition, it is able to alter the composition of the electron transport chain (Fukuda *et al.*, 2007), to regulate mitochondrial turnover (Zhang *et al.*, 2007, 2008) and triggers the induction of pyruvate dehydrogenase kinase in order to switch metabolism away from oxidative phosphorylation (Kim *et al.*, 2006; Papandreou *et al.*, 2006). Of note, this switch allows cells to strongly reduce ROS production derived from oxygen starved mitochondria, hence avoiding oxidative stress related damages. Since glycolysis is less efficient in the conversion of glucose into ATP, HIF pathway can also increase glucose trafficking into the cell by up-regulating glucose transporters gene transcription (i.e. GLUT1) (Behrooz and Ismail-Beigi, 1997).

At the same time, HIF pathway may act to increase oxygen delivery by stimulating erythrocyte production via up-regulation of *epo* and a series of iron-absorption related genes (Haase, 2010; Zhang *et al.*, 2012) and by increasing angiogenesis through the transcription enhancement of angiogenic factors, (i.e. VEGF), (Krieg *et al.*, 2000; Pajusola *et al.*, 2005; Hickey and Simon, 2006).

In the last years it has come to light that HIF is also involved in the regulation of lipid metabolism. Indeed it has been observed that mice carrying a hepatic knockout of Vhl develop severe hepatic steatosis with impaired fatty acid oxidation, increased lipid storage capacity and decreased lipogenic gene expression (Rankin *et al.*, 2009; Greenald *et al.*, 2015). Furthermore, the precise effect of the HIF pathway mainly depends on its activation level. For instance, low- activation level of HIF-2α in mouse

liver was shown to have a positive effect on their metabolic profile, as seen in hypomorphic *phd2* mutants (Rahtu-Korpela *et al.*, 2014), whilst high activation level led to hepatic steatosis (Rankin *et al.*, 2009).

In particular, the activation of the hypoxic response in zebrafish can be achieved by homozygous null mutation of the *vhl* gene. Previous work from my laboratory focused on the phenotypic characterization of this mutant, established a linkage among *vhl* mutation, hypoxic response and cancer (Rooijen *et al.*, 2009; van Rooijen *et al.*, 2011). Moreover, by exploiting the highly responding target gene promoter of Prolyl Hydroxylase 3, a unique GFP readout of the VHL/HIF signalling pathway was generated to track HIF signalling *in vivo*. Previous work based on the use of this reporter line also identified glucocorticoid (GC) agonists and a number of hydroxylases inhibitors as potent activators of HIF signalling, especially at the hepatic level (Santhakumar *et al.*, 2012; Vettori *et al.*, 2017).

1.2.5. The HIF pathway and its role in inflammation

The HIF signalling mediated activation of the inflammatory response is a complex mechanism, which is characterized by the simultaneous activation of both pathways in several pathological circumstances such as chronic inflammation, wounds healing and solid tumours (Safronova and Morita, 2010). Here, hypoxia triggers NF-κβ stabilisation, which acts as a master regulator of the inflammatory and anti-apoptotic response. This is achieved, as for HIF-α, via the oxygen dependent inhibition of prolyl hydroxylase activity. Then, this triggers the decrease in IκB kinase beta (IKKβ) hydroxylation, which leads to the activation of NF-κβ (Yamamoto, Yin and Gaynor, 2000; Cummins *et al.*, 2006, 2007; Ziv *et al.*, 2012). The interaction between hypoxia and inflammation has been well studied in a zebrafish model of wound healing, where

HIF-1α pathway activation was observed to delay neutrophil resolution (Elks *et al.*, 2011). This is believed to occur as a consequence of HIF activation inside the neutrophils themselves and seems to be related to an augmented neutrophil apoptosis rate coupled to a decreased trafficking away from the comorbid site (Schild *et al.*, 2020).

Importantly, even if hypoxia is a pro-inflammatory event, previous studies showed links between the anti-inflammatory and GC responses. In this regard, GCs have been observed, primarily *in vitro*, to both potentiate and inhibit HIF pathway activation (Basu *et al.*, 2002; Kodama *et al.*, 2003; Leonard *et al.*, 2005; Wagner *et al.*, 2008; Sun *et al.*, 2010). In a similar way, hypoxia has been shown to attenuate the glucocorticoid anti-inflammatory response and to elicit corticosteroid insensitive inflammation (Charron *et al.*, 2009; Huang *et al.*, 2009). It is also important to note that despite hypoxia is pro-inflammatory, it can positively interact with pathways with apparently opposite effects.

From these data it has become clear that the HIF-GC crosstalk is complex and still unclear and most likely reflects a context-specific activity of the transcriptional regulators in the tissue microenvironment. In particular, it is still unknown how the crosstalk occurs *in vivo,* how HIF affects GC response, and vice versa. In addition, it would be interesting to know if glucocorticoid receptor (GR) is an obligatory factor for HIF response or if it is a synergistic one. Therefore, the aim of my PhD was to further the research on how precisely this crosstalk occurs *in vivo*, as this may have a wide physiological significance in health and disease.

1.3. Glucocorticoids

The name “glucocorticoid” is a portmanteau word (glucose + cortex + steroid), which derives from their key role in the regulation of glucose metabolism, their biosynthesis at the level of the adrenal cortex and their steroidal structure. In particular, GCs represent a well-known class of lipophilic steroid hormones synthetized, with a circadian rhythm, by the adrenal glands in humans and by the interrenal tissue in teleosts. The GC circadian production in teleosts is tuned by the hypothalamic-pituitary-interrenal (HPI) axis, which is the equivalent of the mammalian hypothalamus-pituitary-adrenal (HPA) axis. Both are essential for stress adaptation (Alsop and Vijayan, 2009; Griffiths *et al.*, 2012; Tokarz *et al.*, 2013; Faught and Vijayan, 2018a).

Cortisol is the main GC both in humans and teleosts and controls a series of physiological processes which includes glucose, lipid and protein metabolism, stress response and inflammation (Munck, Guyre and Holbrook, 1984; Macfarlane, Forbes and Walker, 2008; Kuo *et al.*, 2015; Facchinello *et al.*, 2017). Due to their potent anti-inflammatory action, synthetic GCs has been broadly used for the treatment of pathological disorders that are linked to hypoxia, including rheumatoid arthritis, inflammatory, allergic, infectious, autoimmune diseases as well as to prevent graft rejections and against immune system malignancies (Nikolaus, Fölscn and Schreiber, 2000; Neeck, Renkawitz and Eggert, 2002; Chrousos and Kino, 2005; Revollo and Cidlowski, 2009; Busillo and Cidlowski, 2013). However, due to the presence of adverse effects (Moghadam-Kia and Werth, 2010) and GC resistance (Barnes and Adcock, 2009; Barnes, 2011) their therapeutic benefits are limited in patients chronically treated with these steroids. Examples of the most common GC related side

effects include osteoporosis, glaucoma, diabetes, skin atrophy, abdominal obesity, hypertension in adults and growth retardation in children.

Cortisol exerts its functions through direct binding both to the glucocorticoid receptor (Gr) and to the mineralocorticoid receptor (Mr), which in turn bind cortisol with different affinities (Bamberger, Schulte and Chrousos, 1996; Faught and Vijayan, 2018b). Once bound together, they form an active transcription factor complex, which can function either in a genomic or in non-genomic way. For these reasons, GC and their kindred intracellular receptors, represent critical checkpoints in the endocrine control of vertebrate energy homeostasis. Indeed, even if the biological effects induced by GCs are usually adaptive, their abnormal activity may contribute to a series of acute metabolic diseases which includes insulin resistance, obesity and type 2 diabetes (Smith and Vale, 2006; de Guia *et al.*, 2014). Thus, furthering the research on how they precisely work and interact with other pathways, such as the HIF signalling, may provide new routes to treat these diseases (i.e HIF-related ones) and to simultaneously facilitate the development of innovative GCs with a better benefits-risk ratio.

1.3.1. The Hypothalamus-Pituitary-adrenal/interrenal axis

GCs are essential hormones biosynthesized and secreted by the adrenal cortex/interrenal gland both in a circadian manner and in response to stress. The latter is generally defined as a status of real or perceived threat to homeostasis. In particular, assuring homeostasis in the presence of stressors requires the activation of an intricate series of coordinated biological responses performed by the nervous, endocrine and immune systems (Smith and Vale, 2006; Nesan and Vijayan, 2016). In this regard, the key anatomical structures that regulate the stress response are located both in the central nervous system and in peripheral tissues. The primary effectors of the stress

response are localized in the paraventricular nucleus (PVN) of the hypothalamus, in the anterior lobe of the pituitary gland and at the level of the adrenal gland. These three main structures are generally referred to as the hypothalamic-pituitary-adrenal (HPA) axis in humans and to as hypothalamic-pituitary-interrenal axis (HPI) in zebrafish (Tsigos and Chrousos, 2002; Smith and Vale, 2006; Nesan and Vijayan, 2016) (**figure 1.3**).

Among these, the hypothalamus is the initial stressor recognition site for both internal and external signals. In particular, in mammals, neurons localized in the paraventricular nucleus synthesize both corticotropin-releasing factor (CRF) and arginine vasopressin (AVP) which are released into hypophyseal portal vessels that access the anterior pituitary gland. On the other hand, in teleosts there is a direct neuronal connection to endocrine cells through the hypophyseal stalk, since they lack a portal system between the hypothalamus and the pituitary gland (Schmidt and Braunbeck, 2011). Here, CRF binding to its receptor localized on pituitary corticotropes triggers the release of adrenocorticotropic hormone (ACTH) into the systemic circulation. In humans, ACTH derives by posttranslational modification of the protein encoded by the proopiomelanocortin (POMC) gene. Of note, due to genome duplication, two *pomc* genes named *pomca* and *pomcb* have been identified in zebrafish (Gonzalez Nunez, Gonzalez-Sarmiento and Rodrıguez, 2003; Hansen *et al.*, 2003; To *et al.*, 2007). However, only *pomca* seems to be expressed in the pituitary gland and is required for the interrenal organ development. (Wagle, Mathur and Guo, 2011; Shi *et al.*, 2020). Consequently, the main target of ACTH is the adrenal cortex in humans and the interrenal tissue in teleost, where it binds to the melanocortin 2 receptor (MC2R) on the steroidogenic cells. Here, it stimulates cortisol biosynthesis and secretion (Mommsen, Vijayan and Moon, 1999; Smith and Vale, 2006; Nesan and Vijayan, 2013,

2016). Finally, once released into the systemic circulation, GCs can access target tissues (i.e. liver, heart and vascular tissues) to exert metabolic and cardiovascular effects and the brain itself, in order to support cognitive processes required to tackle a threatening situation (Spiga *et al.*, 2014).

Interestingly, GCs may also tune the activity of the HPA/I axis itself and hence their own biosynthesis, in order to cease the stress response and avoid an exacerbated reaction. This is achieved via a GC-GR mediated negative feedback loop, which acts bot at the hypothalamic and anterior pituitary levels, where they inhibit both CRH and ACTH biosynthesis and release (Jones, Hillhouse and Burden, 1977; Dallman *et al.*, 1987; Alsop and Vijayan, 2008; Griffiths *et al.*, 2012). In addition, GCs may indirectly control HPA axis activity through modulation of different brain structures, including the amygdala, the hippocampus and the prefrontal cortex, that can in turn influence the activity of the paraventricular nucleus (Ulrich-Lai and Herman, 2009; Nicolaides *et al.*, 2010, 2015; Spiga *et al.*, 2014).

In zebrafish, even if a functioning HPI axis-dependent stress response starts only after hatching, they already have all the steroid biosynthesis and cortisol action components before hatching. Indeed, in the zebrafish developing hypothalamus, all the CRF-synthetising neurons are fully developed by 36 hpf, and *crf* is quantifiable starting from egg fertilization. The anterior pituitary ACTH-synthetising corticotropes are also differentiated by 26 hpf. Moreover, despite the interrenal tissue is not completely developed until hatching, the steroidogenic cells are already developmentally mature. In addition, the essential steroidogenic enzymes, including hydroxylases and StAR, are present by 28 hpf, but cortisol biosynthesis starts only at 48 hpf (Nesan and Vijayan, 2016). For these reasons, both cortisol and GR transcripts are maternally deposited into oocytes before the spawning phase. However, a complete turnover of these

transcripts occurs just after the mid-blastula transition and the zygotically synthetised *gr* mRNA and protein are measurable in the embryos by 12–24 hpf. By contrast, the endogenous cortisol release in response to stressors followed by the downstream GC-GR mediated gene regulation starts only between 96 and 120 hpf (Alsop and Vijayan, 2008; Nesan *et al.*, 2012; De Marco *et al.*, 2013; Weger *et al.*, 2018; van den Bos *et al.*, 2020).

1.3.2. Cortisol biosynthesis and secretion

In higher vertebrates, GCs are synthesized in the zona fasciculata of the adrenal cortex starting from cholesterol, whereas in zebrafish at the level of the interrenal gland. Here, steroidogenesis is stimulated when ACTH binds to the melanocortin type-2 receptor (MC2R) which is its specific cell surface G-protein coupled receptor (Mountjoy *et al.*, 1994). Following ACTH binding, MC2R undergoes a series of conformational changes that activate adenylyl cyclase. This leads to a raise of the intracellular cyclic adenosine monophosphate (cAMP) levels which, in turn, triggers the downstream protein kinase A (PKA) signaling pathways. The latter is able to stimulate an acute GCs biosynthesis both via genomic and non-genomic ways (de Guia *et al.*, 2014).

The rate-limiting step in the steroid biosynthesis is the transfer of cholesterol from the outer to the inner membrane of mitochondria, which is performed by the steroidogenic acute regulatory protein (StAR) (Lin *et al.*, 1995; Stocco and Clark, 1996). Upon delivery, cholesterol is converted to pregnenolone by cytochrome P450 cholesterol side-chain cleavage (P450scc) enzymatic activity, encoded by *CYP11a1*. Then, pregnenolone can be transformed either into progesterone by the 3β-hydroxysteroid dehydrogenase/Δ5-Δ4 isomerase, encoded by *3β-HSD*, or hydroxylated into 17α-hydroxyprogesterone by cytochrome P450 17α-hydroxylase,

encoded by *CYP17a1*. Progesterone and 17α-hydroxyprogesterone are then metabolized via a number of steps to androgen/estrogen and aldosterone/cortisol, by enzymes such as 17β-HSD and CYP19 (Bremer and Miller, 2014).

Cortisol, which is the primary GC in teleosts and the most abundant in humans, is ultimately bound to corticosteroid-binding globulins (CBG) in order to be transported in the bloodstream from the adrenal/interrenal gland to the target tissues. Of note, CBG not only promotes cortisol distribution but also plays a key role in its release to tissues (R. Oakley, 2013). Finally, since molecular oxygen is fundamental for steroid hormones biosynthesis, recent studies have highlighted the fact that the expression of specific steroidogenic genes such as StAR, CYP17A1, and CYP19 can be controlled by hypoxia (Tan *et al.*, 2017).

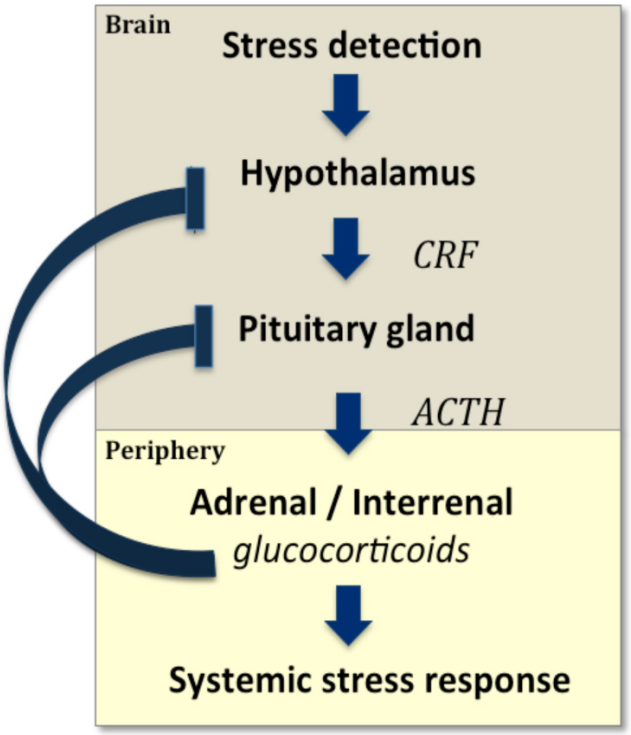

Figure 1.3. The HPA/I axis. In response to stressors, hypothalamic neurons release Corticotropin-releasing factor (CRF) and Arginine vasopressin (AVP), which in turn acts on the anterior pituitary gland to enhance the biosynthesis and release of the adrenocorticotrophic hormone (ACTH) into the blood circulation. The latter, synthetized by post-translational modification of protein encoded by proopiomelanocortin gene (POMC), upon binding to the melanocortin 2 receptor (MC2R) on the steroidogenic cells of the adrenal glands, orchestrates a signal transduction pathway that finally leads to GCs biosynthesis and secretion into the bloodstream. Then, following acute stress, the system turns itself off by way of a negative feedback loop, wherein the receipt of cortisol in the hypothalamus and pituitary gland, suppress the production of ACTH and CRF (modified from Griffiths et al. 2012).

1.3.3. Glucocorticoid receptors and the systemic stress response

GCs can passively diffuse across the plasma membrane into the cytoplasm, thanks to their lipophilic nature. However, their biological availability within the cells is regulated by two enzymes which work in an opposite fashion: 11β-Hydroxysteroid dehydrogenase type 2 (11β-HSD2) oxidizes cortisol into its inactive form, named cortisone, whereas 11β-hydroxysteroid dehydrogenase type 1 (11β-HSD1) transforms cortisone to cortisol. Once inside the cell, GCs can bind to their specific receptors GR and MR (Mangelsdorf *et al.*, 1995; de Kloet, Joëls and Holsboer, 2005; Chrousos and Kino, 2009; Spiga *et al.*, 2014).

Both receptors, in the absence of their ligands (unbound state) are associated in an inactive oligomeric complex with specific regulatory proteins. Among these, heat shock protein-90 kD (HSP90) which binds GR to the C-terminal domain, heat shock protein-70 kD (HSP70), p59 immunophilin, Fkbp51 and Fkbp52 and the small p23 phosphoprotein allow to maintain the correct GR's protein folding (Schoneveld, Gaemers and Lamers, 2004; R. Oakley, 2013; Spiga *et al.*, 2014).

The GR, which belongs to the nuclear receptor transcription factor family, is composed of different conserved structural elements. These include a N-terminal variable region, required for ligand-independent gene transactivation, followed by a central zinc-finger-containing DNA-binding domain, an adjacent hinge region containing nuclear localization signals and a C-terminal ligand-binding domain. The latter also includes residues essential for dimerization and hormone-dependent gene transactivation. Of note, the interaction between GR and HSP90 is fundamental to maintain its C-terminal domain in a favourable conformational state required for ligand binding (**figure 1.4**).

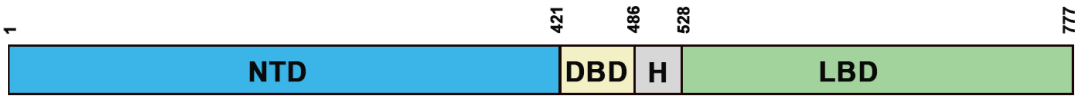

Figure 1.4. **Representative figure of the GR's domains structure.** The N-terminal domain (NTD) which is required for ligand-independent gene transactivation, includes a transcriptional activation function region (AF1). The latter, which interacts with co-regulators and with the basal transcriptional machinery, is the main posttranslational modifications site. The LBD, which is made up of 12 α-helices and 4 β-sheets, forms a hydrophobic pocket needed for GC binding and includes an AF2 domain. The latter allow to interact with coregulators in a ligand dependent way. Finally, two nuclear localization signals, named NL1 and NL2, are localized in the DBD-hinge region junction and within the LBD, respectively.

Upon GC binding, GR undergoes a conformational change within the heterocomplex that involves a FKBP51-FKBP52 exchange, which triggers the translocation of the GC-GR active complex into the nucleus. This structural modification exposes the two GR nuclear localisation signals, which allow the hormone-activated GR to dimerize with another GC-GR molecule and to migrate into the nucleus via nuclear pores (Vandevyver *et al.*, 2013; Presman and Hager, 2017). Importantly, this transcription factor complex can also act non-genomically in the cytoplasm, where it may interact via direct protein-protein interactions with other transcriptional regulators and/or kinases (i.e. basal transcription machinery (BTM); phosphoinositide 3-kinase (PI3K); signal transducer and activator of transcription (STAT)) (Reichardt *et al.*, 1998; Prager and Johnson, 2009; Groeneweg *et al.*, 2011; de Guia *et al.*, 2014) (**figure 1.5**).

Inside the cell nucleus, GC-GR complexes directly binds to specific GREs, as tetramers, in order to regulate the transcription of target genes. Generally, the GRE GGAACAnnnTGTTCT is an imperfect palindromic consensus sequence that consists of two 6 bp half sites. Moreover, the three nucleotides spacing in-between the two half sites is essential for the GR to tetramerize on this sequence. Previous genome-wide

studies showed that the same GRE can mediate both the GC-dependent induction of many genes (positive GRE) and the repression of others (negative GRE) (R. Oakley, 2013; Uhlenhaut *et al.*, 2013). Interestingly, the presence of specific inverted repeats negative GREs (IR nGRE), unrelated to simple GREs has been also reported both in mice and in humans. These DNA binding sequences are palindromic sequences consisting of two inverted repeated (IR) motifs separated by 1 bp. In particular, they act on GC-GR complexes in order to promote the assembly of cis-acting GR-SMRT/NCoR repressing complexes (Guenther, Barak and Lazar, 2001; Surjit *et al.*, 2011)

Consequently, these findings indicate that the broadly different GC effects on various tissues can be partially ascribed to cell type-specific differences in the chromatin landscape that affects the accessibility of specific GREs for GR binding (Ramamoorthy and Cidlowski, 2013; Escoter-Torres *et al.*, 2019). Furthermore, the GCs concentration at which the GR binds to GREs change throughout the genome. Another important feature of the GC-GR complex that makes their effects even more varying is that can tune gene expression in different ways: by binding directly to DNA, by tethering itself to other transcription factors bound to DNA, or via direct binding to DNA and with neighbouring DNA-bound transcriptional regulators (composite manner) (R. Oakley, 2013) (**figure 1.5**).

As previously mentioned, cortisol can bind not only to GR, but also to MR. The latter is a member of the transcription factors steroid hormone receptor family, which is evolutionarily related to the GR. In particular, it has been observed that GCs, even at smaller concentrations than those required to activate the GR, bind to MRs and enhance the activity of several kinases involved in different signal transduction cascades (Nicolaides *et al.*, 2015; Faught and Vijayan, 2018b). Like GR, MR is also

characterized by the four canonical functional domains present in all nuclear hormone receptors (**figure 1.4**).

In mammals, the mineralocorticoid system is essential to regulate potassium and fluid homeostasis upon aldosterone activation of MR. Even though cortisol is a high-affinity ligand for MR, this steroid is deactivated in MR-specific tissues by the 11β-hydroxysteroid dehydrogenase type 2 enzymatic activity. This allows aldosterone, a second corticosteroid present in mammals, to bind to this receptor. Importantly, teleosts do not synthesize aldosterone and cortisol have been shown to mediate the majority of the changes in iono- and osmo-regulatory functions via GR signalling (Faught and Vijayan, 2018b). Moreover, if in teleosts the Gr-mediated cortisol effects regard the stress response and the modulation of intermediary metabolism, behaviour, growth and immune function, the roles of MR is less evident.

Cumulatively, despite its conserved and ancient origin, a clear role for MR has not been defined yet in ray-finned fish. Interestingly a recent *in vivo* study on MR signalling shed light on a key role for this receptor in the regulation of stress axis activation and function in teleosts (Faught and Vijayan, 2018b). As a consequence of the above considerations, due to the MR involvement in controlling HPI axis and since nothing is known about its role in the HIF signalling, deepening the knowledge on MR putative contribution to the HIF pathway is warranted.

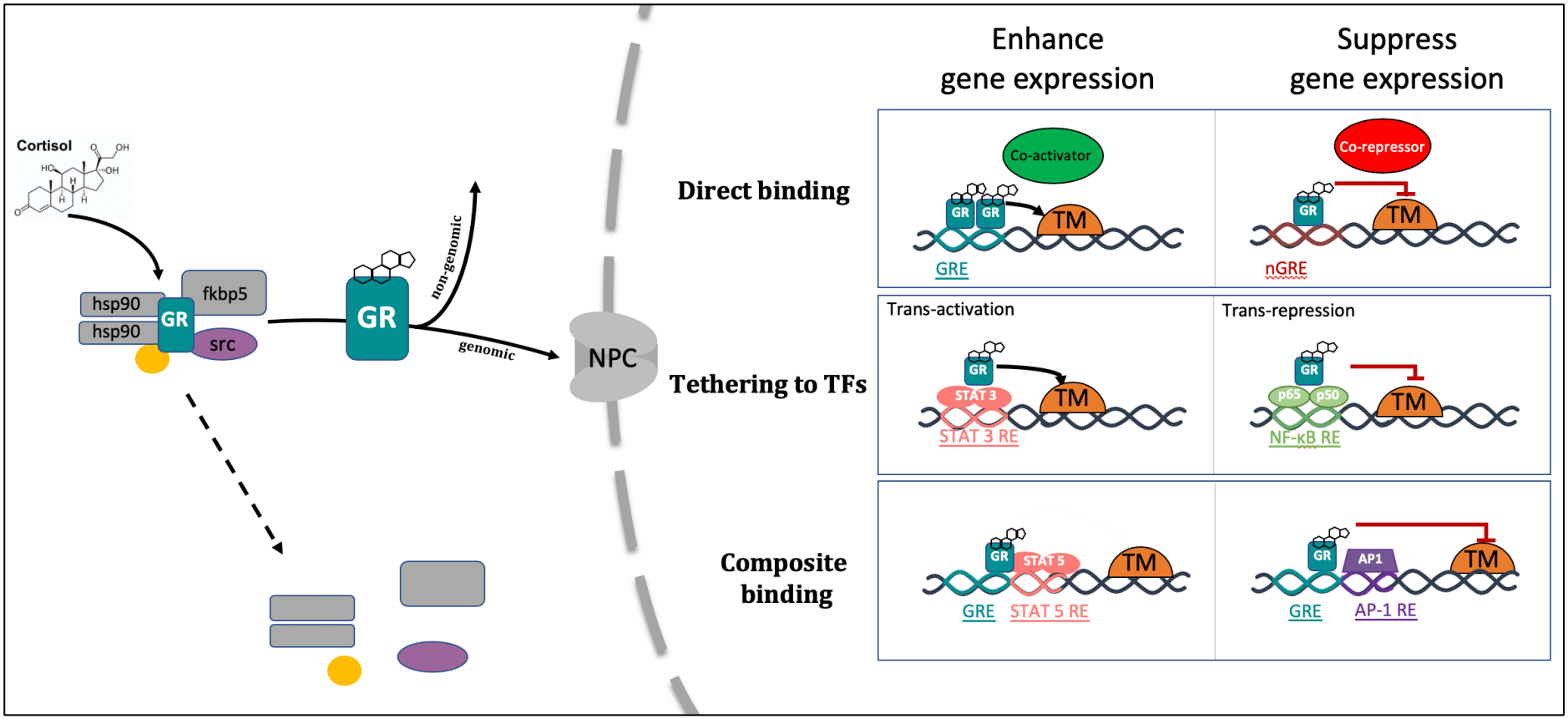

Figure 1.5. Representative picture of the canonical GR signalling pathway. After binding to GC, cytoplasmic GR undergoes a conformational change, becomes hyper-phosphorylated, dissociates from accessory proteins (chaperone complex) and translocates into the nucleus. Here, after dimerization with another GR, regulate gene expression. Interestingly, GR may enhance or repress transcription of target genes by directly binding to palindromic GC response elements (GRE), or by tethering itself to other transcription factors apart from DNA binding, or in a composite manner by both directly binding GRE and interacting with transcription factors bound to neighbouring sites.

1.3.4. GCs and their role on glucose metabolism

The regulation of systemic glucose metabolism requires the presence of a fine-tuned crosstalk between different peripheral organs and the central nervous system (Coll and Yeo, 2013; de Guia *et al.*, 2014). Among these, the liver represents the main organ in the body involved in controlling the mammalian glucose and lipid homeostasis (van den Berghe, 1991; Vegiopoulos and Herzig, 2007). Its primary activities are gluconeogenesis and glycogenolysis during fasting, in order to provide glucose for extrahepatic tissues such as erythrocytes, renal medulla, and brain (Consoli, 1992).

Recently, genome-wide analysis of GC target gene networks highlighted that GR fine-tunes numerous aspects of hepatic energy metabolism, especially the ones related to protein and sugar homeostasis (Yu *et al.*, 2010; Murani *et al.*, 2019; Wang *et al.*, 2019). In particular, GR functionally interacts with other transcription factors to control specific genetic networks (Le *et al.*, 2005), among which only a small amount has been characterized in detail so far. In addition, GCs exert their functions by antagonizing insulin action, promoting hepatic gluconeogenesis and decreasing glucose uptake and its utilization in skeletal muscle and white adipose tissue. These result in a temporary rise in blood glucose, which is thought to be favourable under stressful conditions (Aronoff *et al.*, 2004; Charmandari, Tsigos and Chrousos, 2005).

GCs are also able to promote gluconeogenesis mainly by transcribing specific genes encoding for enzymes involved in the gluconeogenic pathway, such as glucose-6-phosphatase (*G6PC*), pyruvate carboxylase (*PC*), phosphoenolpyruvate carboxykinase 1 (*PCK1*), 6-phosphofructo-2-kinase/fructose-2,6-biphosphatase (*PFKB*), fructose-1,6-bisphosphatase 1 (*FBP1*) and Solute Carrier Family 37 Member 4 (*SLC37A4*). The *G6pc*, *Pck1*, and *Pfkb1* GREs have been defined and the mechanism of GR-regulated *Pck1* transcription has been studied in great details. By contrast, the

mechanisms regulating GC-activated *Pc* and *Fbp1* are still unknown (Kuo *et al.*, 2015). Moreover GCs are able to exert tissue specific effects by increasing glycogen storage in the liver, whilst they promote catecholamine-induced glycogenolysis and/or suppress insulin-dependent glycogen synthesis in skeletal muscle (Kuo, Harris and Wang, 2013; Rafacho *et al.*, 2014). Overall, the physiological GCs response that tunes glucose homeostasis has been well documented. However, the precise way by which GCs regulate glucose homeostasis is still unclear.

1.3.5. GCs and their role in inflammation

As described in the subchapter 1.3.3, GR can regulate gene expression in different ways (Schoneveld, Gaemers and Lamers, 2004) (**figure 1.5**). Among these, the negative regulation of gene transcription may occur via both genomic and non-genomic mechanisms. In particular, this inhibitory effect played by the GC-GR active complex on other transcription factors' function constitutes the GC anti-inflammatory way of action (Stellato, 2004).

In this regard, trans-repression mainly occurs via direct binding between monomeric GC-GR complex and transcription factors (i.e. NF-κB, c-Jun, and c-Fos) activated by cytokines and other pro-inflammatory stimuli, which synergistically coordinate the expression of several proinflammatory genes (Davies, Ning and Sánchez, 2005; Nicolaides *et al.*, 2015). As a result, the mutual antagonism between transcription factors impairs their transcriptional properties and prevents them from binding to their corresponding DNA response elements. An additional GC-mediated anti-inflammatory mechanism consists of increasing the transcription of I-κB which, in turn, may repress NF-KappaB by favouring its retention in the cytoplasm (Li, Wang and Gelehrter, 2003). Moreover, GCs have been observed to inhibit the transcriptional

activity of various pro-inflammatory genes such as cytokines, chemokines, mediator-synthesizing enzymes and adhesion molecules. Contrary to expectations, GR loss of function was speculated by Facchinello and co-workers to prevent the transcriptional activity linked to the immune response (i.e. of cytokines Il6, Il1β, Il8 and Mmp-13) (Facchinello *et al.*, 2017), corroborating the hypothesis of a GC-GR mediated dual-action on the immune system (Busillo and Cidlowski, 2013; Duque and Munhoz, 2016). In addition, GR was shown to synergistically induce proinflammatory genes by acting on other signalling pathways (Langlais *et al.*, 2008, 2012; Dittrich *et al.*, 2012; Xie *et al.*, 2019). Finally, studies also demonstrated that GCs increase the transcription of numerous anti-inflammatory molecules such as interleukin-10 (IL-10), interleukin-1 receptor antagonist (IL-1RA), secretory leukocyte inhibitory protein and neutral endopeptidase (Schaaf and Cidlowski, 2002; van den Bos *et al.*, 2020).

1.4. HIF-GC interaction insights

The modulation of the HIF pathway has the potential to be clinically exploited as therapeutic treatment for a variety of pathological conditions which includes stroke, ischemia, spinal cord injury, inflammation, cancer, wounding, chronic anaemia and bone regeneration (Bernhardt et al., 2006; Shen et al., 2009; Shi et al., 2010; Wan et al., 2008; Ratan et al., 2008 Semenza 2003,2009,2015).

To this end, in the last years, an unbiased chemical screen performed in my laboratory on zebrafish larvae allowed to discover that HIF associated transcriptional responses are potently activated by GC, particularly in the zebrafish liver (Vettori *et al.*, 2017). Moreover, by translating these observations to human tissues, it has been possible to show that GCs are able to promote HIF stabilization, without the need of the GR DNA binding domain (non-genomic action), in primary human hepatocytes and intact liver slices. In this regard, since c-src inhibitor PP2 treatment was able to rescue this effect, this suggested a role for GCs in promoting c-src–mediated proteasomal degradation of pVHL, followed by stabilization of HIF-α subunit (Vettori *et al.*, 2017).

According to these data, since the liver is an important regulator of blood glucose levels, and both GCs and HIF promote gluconeogenesis and glycogen storage in the liver, furthering the knowledge on the crosstalk between these transcriptional regulators may provide an explanation for the GC effects on glucose metabolism and may have a wider physiological significance in health and disease than previously expected.

Indeed, both GCs and hypoxic transcriptional responses are mutually involved in assuring tissue homeostasis by controlling cellular responses to various forms of stress and inflammation, especially affecting glucose metabolism. For this reason, the

interaction between these two stress-responsive pathways has become increasingly appreciated over recent years.

Synthetic GCs have been widely used for years as anti-inflammatory drugs for treating pathological conditions where hypoxia plays a role in disease progression such as rheumatoid arthritis and chronic obstructive pulmonary disease (Nikolaus, Fölscn and Schreiber, 2000; Neeck, Renkawitz and Eggert, 2002; Busillo and Cidlowski, 2013). It has also been shown that GCs release in response to atmospheric hypoxia is linked with high altitude in humans and that the prophylactic treatment with GCs has been broadly exploited to mitigate the related mountain sickness (Wright, Brearey and Imray, 2008). Additionally, it has been observed that GCs protect different organs from ischemic injury, as it has been observed in particular against experimental cerebral and hepatic ischemic/reperfusion injury (Dardzinski *et al.*, 2000; Limbourg *et al.*, 2002; Glanemann *et al.*, 2004; Tokudome *et al.*, 2009).

The presence of an interplay between hypoxia and GC dependent signalling pathways has been previously reported by different *in vitro* studies (Kodama *et al.*, 2003; Leonard *et al.*, 2005; Wagner *et al.*, 2008; Zhang *et al.*, 2015). However, these studies reported conflicting results on the cross-talk between GC action and hypoxia, where the latter limits GR mediated transactivation both in pulmonary endothelial and hepatic epithelial cells (Leonard *et al.*, 2005; Wagner *et al.*, 2008).

The first data about the interaction between HIF and GR was presented by Kodama et al. 2003 (Kodama *et al.*, 2003). By exploiting an artificial approach using Gal4-fusion reporter assays, they found that the ligand-dependent activation of GR increases hypoxia-dependent gene expression and hypoxia response element (HRE) activity in HeLa cells. Moreover, using dexamethasone treated COS7 cells co-transfected with expression plasmids for either GR or GAL4-LBD and GFP-HIF-1α and

exposed to hypoxic conditions, they showed colocalization of the GR and HIF-1α in the nucleus. For this reason, Kodama et al. postulated the presence of a direct protein-protein interaction between the GR LBD and HIF-1α as the main mechanism for GC-dependent enhancement of HIF pathway, but failed to demonstrate it via GST pull-down assays.

Leonard et al. 2005 (Leonard *et al.*, 2005), subsequently confirmed via microarray analysis that GR is upregulated by hypoxia in human renal proximal tubular epithelial cells. Moreover, using a cell-based GRE luciferase reporter system, they showed that hypoxic exposure can potentiate dexamethasone-stimulated GRE promoter-reporter activity.

By using AtT-20 cells, Zhang et al 2015 (Zhang *et al.*, 2015) demonstrated that GR expression levels were enhanced by HIF-1α under hypoxic conditions. However, dexamethasone treatment was able to cause the downregulation of GR expression in a HIF-1α dependent way. Finally, even if this was confirmed by transfecting AtT-20 cells with HIF-1α siRNA and culturing them under normoxia or hypoxic conditions, the involved underlying mechanism remains unclear.

By contrast, a dexamethasone-related inhibition of HIF-1α target genes expression in hypoxic HEPG2 cells was revealed by Wagner et al. 2008 (Wagner *et al.*, 2008). In particular, via western blot analysis they showed that dexamethasone reduces nuclear HIF-1a protein as the HIF-1a amount was higher in cytosolic cell extracts than in the nuclear extracts upon DEX treatment. This cytoplasmic retention of HIF-1a suggested a blockage of nuclear import, via a still unknown mechanism, which resulted in a reduced HIF target gene expression. Moreover, by exploiting a luciferase assay the author revealed that dexamethasone attenuates HIF-1 activity not only in a GR- dependent way, but also that this effect depends on the presence of

functional HREs. Importantly, Wagner et al., attributed these contradicting results (compared to Kodama's ones) to the presence of Fetal Calf Serum (FCS) in all their cell-culture experiments, as many cellular processes depends on the cell cycle phase.

In the following years, Gaber et al., 2011 (Gaber *et al.*, 2011) investigated the interaction between macrophage migration inhibitory factor (MIF), HIF and the GCs effect in human primary nontumor CD4+ Th cells and Jurkat T cells. In contrast to the previous observations, this study showed the presence of a clear dexamethasone-dose dependent inhibition of HIF-1α protein expression, which resulted in a decreased HIF-1 target gene expression. expression. Therefore, conversely to Wagner et al. 2008 hypothesis, they proposed a model based on a rapid DEX-mediated induction HIF-1a suppressors' activity or a quick DEX-mediated inhibition of HIF signalling.

As a result of the above considerations, the interplay between GR and hypoxia mediated responses is complex and still requires additional experimental evidence to be untangled. Importantly, these data most likely reflects a context-specific activity of the transcriptional regulators in the tissue microenvironment. Above all, it remains unsolved how GCs fine-tune the cellular pathways mediating adaptation to hypoxic environment, how HIF affects GC signalling and, in turn, whether they are acting on each other. Further studies are also warranted to uncover the underlying mechanism behind it in an *in vivo* animal model.

1.5. The use of zebrafish as model organism

The zebrafish (*Danio rerio*) has been shown to be an exemplary informative and genetically modifiable organism for studying both HIF and GC pathway not only in physiological, but also in pathophysiological conditions (M.J.M. Schaaf, Chatzopoulou and Spaink, 2009; van Rooijen *et al.*, 2011; Santhakumar *et al.*, 2012; Vettori *et al.*, 2017). In particular the short generation time, transparency, anatomical simplicity, quantity of the progeny obtainable by natural mating and the ex-utero embryos development, allow biological processes to be followed in detail and in a non-invasive way. Moreover, zebrafish allow the use of medium to high throughput drug screening (A. L. Robertson *et al.*, 2014; C. E. Robertson *et al.*, 2014; Vettori *et al.*, 2017) and genetic tractability, especially via the recently improved genome editing CRISPR/Cas9 based mutagenesis technology (Hruscha *et al.*, 2013; Varshney *et al.*, 2015; Burger *et al.*, 2016; Wu *et al.*, 2018).

Taking into account these undeniable advantages, this model organism has become more frequently used especially in the hypoxic and stress science field (M.J.M. Schaaf, Chatzopoulou and Spaink, 2009; Löhr and Hammerschmidt, 2011; van Rooijen *et al.*, 2011; Griffiths *et al.*, 2012a; Santhakumar *et al.*, 2012; Krug Ii *et al.*, 2014). Therefore, during my PhD I have exploited it as an *in vivo* model organism to study how and to what degree hypoxic signalling affects the endogenous GC' response and vice versa. In this regard, the use of whole animals allows also to demonstrate how these signalling pathways interact with each other in a more complete way than *in vitro*, where interactions among different tissues and cell types cannot be easily modelled.

Importantly, zebrafish share all the components of the human HIF signalling pathway and by taking advantage of the *vhl* mutant line coupled to the *phd3:eGFP*

transgenic HIF activity reporter line, it is also possible to reliably activate and quantify the HIF response (van Rooijen *et al.*, 2011; Santhakumar *et al.*, 2012; Elks *et al.*, 2015). Furthermore, analogously to humans, zebrafish are diurnal and use cortisol as the main GC hormone (Weger *et al.*, 2016). In addition, unlike other teleosts which have additional GR paralogs, zebrafish have only a single glucocorticoid (zGr) and mineralocorticoid receptor (zMr) isoform (M.J.M. Schaaf, Chatzopoulou and Spaink, 2009; Faught and Vijayan, 2018b). Finally, zGr shares high structural and functional similarities to its human analogous, making zebrafish a reliable model for studying GC activity *in vivo* (Alsop and Vijayan, 2008; Chatzopoulou *et al.*, 2015; Xie *et al.*, 2019).

1.6. Aims

The aim of this project is to unravel the cellular mechanisms underlying the interaction between hypoxic and GC signalling *in vivo* using the zebrafish as a model. In particular, the primary goal is to understand how and to what degree hypoxic signalling affects the endogenous GCs' response and vice versa.

This is because the presence of a crosstalk between GC and hypoxia dependent signalling pathways has been previously indicated in different *in vitro* studies. In addition, synthetic GCs (i.e. betamethasone and dexamethasone), which are the equivalent of naturally present steroid hormones, have been broadly used for decades as anti-inflammatory medications for treating pathological conditions associated to hypoxia (i.e. ischemic injury, asthma, rheumatoid arthritis etc.). Nowadays, thanks to the available *in vitro* results, it has become evident that the HIF-GC crosstalk is an intricate mechanism and might be cell-specific. For these reasons, furthering the knowledge on how this interplay occurs *in vivo* can have a vast physiological relevance in health and disease.

To this end, previous chemical screens performed in my laboratory, using unique zebrafish HIF reporter, surprisingly identified synthetic GR agonists as activators of the HIF pathway. In view of this, the main hypothesis of my project is that GC and HIF are somehow acting on each other. If so, it is likely that GR activity could be required for HIF signalling to occur.

To test these hypotheses, I planned to exploit both a genetic and pharmacological approach to modulate these two pathways during the first 120 hours post fertilisation of zebrafish embryos. I also took advantage of two different mutant lines I have generated during my PhD, named *hif1β*^{sh544} (*arnt1*) and *gr*^{sh543} (*nr3c1*)

respectively, together with an already existing *vhl*$^{hu2117/+}$*;phd3:eGFP*$^{i144/i144}$ hypoxia reporter line. These lines were required to investigate the effect of HIF activity on GC signalling and vice versa, via a "gain-of-function/loss-of-function" approach. Molecular and phenotypic analyses of these mutants have been coupled to optical and fluorescence microscope imaging.

This is because, by knocking out *vhl* and *arnt1* genes, it is possible to up-and downregulate the HIF signalling, whereas the administration of synthetic GR agonists and the generation of *gr*$^{-/-}$ zebrafish line allows to respectively enhance and inhibit the GC pathway. In this regard to understand whether GCs contribute to HIF phenotype, I planned to knock-out both *gr* and *mr* in a HIF upregulated scenario (*vhl*$^{-/-}$ larvae) to quantify the phenotypic and molecular outcomes, in terms of both *phd3;eGFP* and target genes expression. In a similar way, to investigate the role of HIF on GC pathway, I set up to quantify both the expression of GC transcriptional activity and cortisol biosynthesis in the presence of high and suppressed HIF activity, respectively. Finally, chemical treatment with GR agonist (i.e betamethasone) will be used to check the ability of GCs to trigger the HIF response under different HIF levels.

Of note, these approaches coupled to the use of an animal model allowed me to obtain a much clearer overview about the GC/HIF crosstalk in a more global way than in cell culture and to propose a novel model of interaction between these two major signalling pathways.

2. MATERIALS AND METHODS

2.1. Zebrafish husbandry and maintenance

All zebrafish (*Danio rerio*) lines that were used during my research were raised and maintained under standard conditions (14 hours of light and 10 hours of dark cycle, at 28°C) in the Aquaria facility of the University of Sheffield. All zebrafish embryos used for experiments were reared in E3 medium (5 mM NaCl, 0,17 mM KCl, 0,33 mM $MgCl_2$, 0,33 mM $CaCl_2$, pH 7,2) containing methylene blue (Sigma-Aldrich) at 0.0001% and staged according to standard method (Kimmel *et al.*, 1995) for up to 5,2 days post fertilisation (dpf) in accordance with UK Home Office legislation (licence number PB2866ED0 and PC39B259E). PTU (1-Phenyl-2-thiourea) treatment has been performed at 24 hpf in order to prevent embryos pigmentation, when necessary, as described by Karlsson *et al.,* 2001 (Karlsson, von Hofsten and Olsson, 2001).

2.1.1. Wild-type line

Wild-type (WT) embryos were obtained from the AB line ZDB-GENO-960809-7 and reared up to 5,2 dpf under the same aforementioned conditions (chapter 2.1).

2.1.2. *vhl*$^{hu2117/+}$;*phd3*:eGFP$^{i144/i144}$ mutant line

The transgenic line *Tg*(*phd3*:eGFP)$^{i144/i144}$ is a hypoxia reporter line generated via BAC transgenesis by Santhakumar *et al*., 2012. In particular, BAC clone CHORI73-277E22 was originally engineered in order to contain an EGFP reporter construct, with an SV40

polyadenylation site inserted at the level of prolyl hydroxylase 3 (*phd3*) ATG start site. This fish line was incrossed to create homozygotes. In order to create the *vhl*$^{hu2117/+}$;*phd3*:eGFP$^{i144/i144}$ line used in this project, the *Tg*(*phd3*:eGFP)$^{i144/i144}$ line was originally crossed with the *vhl*$^{hu2117/+}$ line. When incrossed, these fish generate *vhl*$^{hu2117/hu2117}$;*phd3:eGFP*$^{i144/i144}$ embryos (here referred to as *vhl* mutants) in accordance with mendelian ratio and begin to fluoresce starting from 28 hpf (Santhakumar *et al.,* 2012). As previously described by van Rooijen et al., 2009, *vhl* mutants are able to complete embryogenesis and are viable up to larval stages (8-10 dpf). Therefore, unlike *vhl* mutant mice which die during early embryonic stages, *vhl*$^{-/-}$ zebrafish larvae represent an ideal vertebrate animal model to study HIF pathway.

2.1.3. *vhl*$^{hu2117/+}$;*vll*$^{i216/i216}$; *phd3:EGFP*$^{i144/+}$ mutant line

The *vhl;vll*(*phd3:eGFP*) fish line used for this project was obtained by crossing *vhl*$^{hu2117/+}$; *phd3:eGFP*$^{i144/+}$ into the *vll*$^{i216/i216}$ homozygous mutant line (van Eeden, unpublished). This fish strain can be incrossed to generate *vhl*$^{hu2117/hu2117}$;*vll*$^{i216/i216}$;*phd3:eGFP*$^{i144/+}$ embryos at a mendelian ratio, hereafter referred to as *vhl;vll* mutants. Interestingly, despite *vhl* larvae are not viable after 8-10 dpf, *vll*$^{-/-}$ larvae develop normally and adult fish are fertile.

2.1.4. *hif1β*$^{sh544/+}$;*vhl*$^{hu2117/+}$ mutant line

The hif1β$^{sh544/+}$;*vhl*$^{hu2117/+}$ mutant line was created via CRISPR/Cas9-based mutagenesis method, targeting exon 5 in *arnt1* gene. The induced mutation is a D125fsX1 that causes a premature stop codon (TAA) after 1 aa at amino acid 125 in the translated amino acid sequence. Homozygous mutants were obtained by incrossing heterozygous

fish and sorted according both to their phenotype at 3 dpf and their GFP fluorescence starting at 28 hpf.

2.1.5. *gr*$^{sh551/+}$*; vhl*$^{hu2117/+}$*;phd3:eGFP*$^{i144/+}$ and *gr*$^{sh543/+}$ mutant lines

Two different *gr* mutant lines were created via CRISPR/Cas9-based mutagenesis method for this project: *gr*$^{sh551/+}$ *vhl*$^{hu2117/+}$*;phd3:eGFP*$^{i144/+}$ and *gr*$^{sh543/+}$ line. The first one, originally generated by Eleanor Markham (van Eeden laboratory) using *vhl*$^{hu2117/+}$*;phd3:eGFP*$^{i144/+}$ embryos at the background, carried 1bp deletion in exon 2 of *nr3c1* gene (also known as *gr*), which codes for the N-terminal domain (NTD). The second one, created by me, using WT(AB) embryos at the background, carried a 11 bp deletion at the level of *nr3c1*'s exon 3 that codes for the DNA-binding domain. Of note, the mutation is a A377fsX12 that causes a premature stop codon (TGA) after 12 aa at aa 390 in the translated amino acid sequence. Since the GR DBD starts at 384 and ends at 463, the first zinc finger motif occurs at aa 377-480 and the second zinc finger motif occurs at aa 386-453, the mutation occurs at the very beginning of the DNA binding domain. Homozygous mutants for each allele were obtained by incrossing heterozygous fish and sorted according to their visual background adaptation (VBA) response at 5 dpf, as reported in a previous study (Griffiths *et al.*, 2012).

2.1.6. *gr*$^{sh543/+}$*;hif1β*$^{sh544/+}$ *phd3:eGFP*$^{i144/+}$, *gr*$^{sh543/+}$*;vhl*$^{hu2117/+}$ *phd3:eGFP*$^{i144/+}$ and *gr*$^{sh543/+}$*;hif1β*$^{sh544/+}$*;vhl*$^{hu2117/+}$ *;phd3:eGFP*$^{i144/+}$ mutant lines

These fish lines were generated by crossing *gr*$^{sh543/+}$ with *hif1β*$^{sh544/+}$*;vhl*$^{hu2117/+}$*;phd3:eGFP*$^{i144/+}$ fish, in order to obtain all the possible genotype combinations. Subsequently, founders were identified by adult tail-clipping and

consequently by screening the offspring for GFP fluorescence. Homozygous mutants were obtained by incrossing heterozygous fish and sorted according both to their phenotype at 3 dpf and their GFP fluorescence starting at 28 hpf.

2.1.7. *gr*$^{sh543/+}$*; mr*$^{sh562/+}$ mutant line

This fish line was generated by crossing the aforementioned *gr*$^{sh543/+}$ with the *mr*$^{sh562/+}$ fish line. The *mr*$^{sh562/+}$, created by Jack Paveley (Vincent Cunliffe/Nils Krone laboratory, Bateson Centre, TUoS), shares a 46 bp deletion at the level of *mr* exon 3 which codes for the DNA-binding domain. The mutation is a T597fsX16 that causes a premature stop codon after 16 aa at aa 613 in the translated amino acid sequence of the DNA binding domain. The F1 generation was identified by adult tail-clipping and *gr*$^{+/-}$*;mr*$^{+/-}$ fish were consequently selected and incrossed to get all the possible genotype combinations. Finally, F2 generation larvae were VBA sorted at day 5 post fertilisation and raised till adulthood. Homozygous mutants were then obtained by incrossing *gr*$^{+/-}$*;mr*$^{-/-}$ fish and sorted according to their visual background adaptation response at 4 dpf.

2.2. Genotyping protocols

2.2.1. DNA extraction from whole embryos

Genomic DNA was extracted using the HotSHOT method (Wellcome Trust Sanger Institute's protocol modified by Eleanor Markham) from whole embryos, as described below. Single embryos were individually placed in sterile wells of a 96-well plate and 25 μl of 1X base solution (1.25 M KOH crystals and 10 mM EDTA in milliQ water) were added in each sample. The embryos were then incubated for 30 minutes at 95°C and cooled down for 10 minutes at 10°C. Finally, 25 μl of 1X neutralisation solution (2 M TrisHCl in milliQ water) were added to each sample and the plate was vortexed for few seconds to further dissolve the embryos. Lastly, the extract was centrifuged for 2 minutes at maximum speed (4200 rpm) and 1,5 μL of supernatant was used per PCR reaction.

2.2.2. DNA extraction from tail biopsies

Fin clipping procedure was conducted according to Home Office recommendations and tail biopsies from adult fish were transfected directly into 50 μl of 1X base solution into a 96-well plate. Clipped tissues were then incubated for 30 minutes at 95°C, followed by cooling to 10°C. for 10 minutes. To neutralise the acidic pH of the medium, 50 μl of 1X neutralisation solution were added to each sample and vortexed for 5 seconds. Finally, the dissolved tissues were centrifuged for 2 minutes at maximum speed and 1,5 μL of extracted DNA was used per PCR reaction.

2.2.3. *vhl*$^{hu2117/+}$;*phd3*:*eGFP*$^{i144/i144}$ genotyping

Although *vhl* mutants are clearly distinguishable from siblings by morphology and thanks to presence of a strong eGFP-related brightness overall, *vhl* heterozygous are identical to WT embryos. For this reason, an already existing genotyping protocol was used as a proof of concept to confirm the genotype of *vhl* embryos and to sort them for mating purposes. The selected mutation is a C/T transition (Q23X) at the level of *vhl* exon1 (van Rooijen *et al.*, 2009), which introduces a premature stop codon and a BciVI restriction site. A DNA region of 414 bp encompassing the mutation site was amplified via PCR and digested using BciVI restriction enzyme at 37°C, overnight. Digested PCR products were cleaved into different DNA fragments according to the corresponding genotype:

- *vhl*$^{+/+}$: 2 fragments (222 and 192 bp)
- *vhl*$^{hu2117/+}$: 3 fragments (414 bp, 222 and 192 bp)
- *vhl*$^{hu2117/\,hu2117}$: 1 fragment (414 bp)

However, due to the inaccuracy of the restriction enzyme activity, digestion results were often difficult to interpret in the right way. For this reason, I decided to improve this genotyping protocol by exploiting the dCAPS (derived Cleaved Amplified Polymorphic Sequence) method (Neff *et al.*, 1998). dCAPS Finder 2.0 (http://helix.wustl.edu/dcaps/) and Primer3 websites were used to design 3 different primers sets, each containing a mismatch mutation, which allow to create a restriction nuclease sensitive polymorphism based on target mutation. BamHI, AccI and EcoRV -related primers set were selected among the suggested dCAPS primers due to their efficiency, survival and activity in PCR mix. In particular, BamHI-related dCAPS primers showed to work better than AccI and EcoRV's ones and was used for genotyping *vhl* embryos. Primers were designed to amplify a 170 bp region enclosing the original

BciVI mutation site (primers listed on Table 2.1). PCR products were subsequently digested at 37°C for at least 4 hours and 30 minutes as recommended by New England Biolabs. The success of the reaction was assessed via gel electrophoresis on a 3% agarose gel. By design, two bands for wild-types (151 bp and an undetectable 19 bp), three bands for heterozygous (170, 151 and 19 bp) and one band for homozygous mutants (170 bp) were expected. Primers and PCR settings used for these two protocols are listed below.

Primer name	Primer sequence	Stock conc.	Working conc.
vhl forward	TAAGGGCTTAGCGCATGTTC	100 μM	10 μM
vhl reverse	CTATCTACGCGTTTAACTCG	100 μM	10 μM
AccI forward	GGTCTCTGATCAGCCG**T**ATA	100 μM	10 μM
AccI reverse	GCATAATTTCACGAACCCACA	100 μM	10 μM
BamHI forward	GGTCTCTGATCAGCCGGAT**C**	100 μM	10 μM
BamHI reverse	GCATAATTTCACGAACCCACA	100 μM	10 μM
EcoRV forward	AGTCTAACTCGGTGGAAGCA	100 μM	10 μM
EcoRV reverse	GTTACAGAACAGAACGTTGACC**G**	100 μM	10 μM

Table 2.1 List of primers sequences used for vhl^{hu2117} genotyping and relative concentrations.

PCR machine setting (*vhl*):

1. 94°C, 4 minutes
2. 92°C, 1 minute
3. 56°C, 30 seconds
4. 72°C, 40 seconds
5. GOTO step 2, 39x
6. 72°C, 10 minutes
7. 12°C, ∞

PCR machine setting (BamHI-dCAPS):

1. 94°C, 4 minutes
2. 92°C, 1 minute
3. 52°C, 30 seconds
4. 72°C, 15 seconds
5. GOTO step 2, 34x
6. 72°C, 10 minutes
7. 12°C, ∞

2.2.4. *gr$^{sh551/+}$ vhl$^{hu2117/+}$;phd3:eGFP$^{i144/+}$* genotyping

To distinguish *gr$^{sh551/+}$;vhl$^{hu2117/+}$* heterozygous from WT embryos, a genotyping protocol was designed in order to identify and raise only heterozygous adult fish. The mutation is an 1bp deletion at the level of exon 2 of *nr3c1* gene, which causes the destruction of a *BslI restriction* site. Primers have been designed with Primer3 to amplify a 177 bp DNA sequence surrounding the mutation site (primers listed on Table 2.2). PCR product has been subsequently digested using *BslI* restriction enzyme by incubating the digestion mix at 55°C overnight, as recommended by New England Biolabs. The success of the reaction was assessed via electrophoresis by running the digested samples on a 3% agarose gel. By design, one band for the homozygous mutants (177 bp), two bands for the wild-types (150 and 27 bp) and three bands for the heterozygous (177, 150 and 27bp) were expected. However, since the 27 bp DNA fragment is too small to be detected on a 3% Agarose gel, it is possible to visualize only one band for the wild-types (150 bp) and two for the heterozygous (177 and 150 bp). The following table lists the primers sequence and PCR settings used for this protocol.

Primer name	Primer sequence	Stock concentration	Working solution
grex2 forward	GCAAAATGGATCAAGGAGGA	100 μM	10 μM
grex2 reverse	CAGAAACTGGCTGCATCATT	100 μM	10 μM

Table 2.2 List of primers sequences used for gr^{sh551} genotyping and relative concentrations.

PCR machine setting:

1. 94°C, 3 minutes
2. 94°C, 30 seconds
3. 47°C, 30 seconds
4. 72°C, 15 seconds
5. GOTO step 2, 34x
6. 72°C, 5 minutes
7. 12°C, ∞

2.2.5. *gr*^{sh543} genotyping

As *gr*$^{sh551/+}$;*vhl*$^{hu2117/+}$ larvae, *gr*^{sh543} heterozygous were also indistinguishable from WT embryos. For this reason, I used a genotyping protocol designed to identify and raise only heterozygous fish. This method takes advantage of an 11 bp deletion occurring at the level of exon 3 of *nr3c1* gene, which introduces a premature stop codon and causes the loss of a *PvuII restriction* site. A genomic sequence of 216 bp surrounding the mutation site was amplified via PCR (primers listed on Table 2.3) and digested with *PvuII* restriction enzyme by incubating the digestion mix at 37°C for at least 4 hours as recommended by New England Biolabs.

Fish genotype was evaluated via electrophoresis by running the digested samples on a 3% agarose gel. By design, one band for the homozygous mutants (216 bp), two bands for the wild-types (127 and 89bp) and three bands for the heterozygous (216, 127 and 89 bp) were expected. The following table lists the primers sequence and PCR settings used for this protocol.

Primer name	Primer sequence	Stock concentration	Working solution
grex3 forward	CCAAACTTTCAGGCAGCAGT	100 μM	10 μM
grex3 reverse	TCCGCAAGTGAGAACTCCAT	100 μM	10 μM

Table 2.3 List of primers sequences used for gr^{sh543} *genotyping and relative concentrations.*

PCR machine setting:

1. 94°C, 3 minutes
2. 94°C, 30 seconds
3. 51°C, 30 seconds
4. 72°C, 15 seconds
5. GOTO step 2, 34x
6. 72°C, 5 minutes
7. 12°C, ∞

2.2.6. *hif1β*$^{sh544/+}$ *vhl*$^{hu2117/+}$*;phd3:eGFP*$^{i144/+}$ genotyping

As *hif1β* heterozygous were undistinguishable from *hif1β* siblings a genotyping protocol was developed to identify and raise heterozygous fish. This mutant line is characterized by a 7 bp insertion at the level of exon 5 of *arnt1* gene (also known as *hif1β*), which introduce a premature stop codon and causes the destruction of MwoI restriction site.

Primers were designed in order to amplify a 156 bp DNA sequence surrounding the mutation site (primers listed on Table 2.4). PCR products were then digested using MwoI restriction enzyme at 60°C, overnight as recommended by manufacturer's instructions. As expected, one band for homozygous mutants (156 bp), three bands for heterozygous (156, 134 bp and 22 bp) and two bands for wild types (134 bp and 22 bp) were detected on a 3% agarose gel. Primers and PCR setting used for this protocol are the following:

Primer name	Primer sequence	Stock conc.	Working conc.
hif1βex5 forward	AGAGCTGTCGGATATGGTGC	100 μM	10 μM
hif1βex5 reverse	TGGTCTGTGAGAAAGGATGGT	100 μM	10 μM

Table 2.4 List of primers sequences used for hif1β^{sh544} *genotyping and relative concentrations.*

PCR machine setting:

1. 94°C, 3 minutes
2. 94°C, 30 seconds
3. 51°C, 30 seconds
4. 72°C, 15 seconds
5. GOTO step 2, 34x
6. 72°C, 5 minutes
7. 12°C, ∞

2.2.7. *mr*$^{sh562/+}$ genotyping

Since *mr* heterozygous larvae are identical to *mr* siblings a genotyping protocol was created to identify and raise heterozygous fish. This mutant line is characterized by a 46 bp insertion at the level of exon 3 of *mr* gene (*nr3c2*), which introduces a premature stop codon and causes the destruction of the DNA binding site.

Primers were designed in order to amplify a 210 bp DNA sequence surrounding the mutation site (primers listed on Table 2.5). Thanks to the mutation size, PCR was enough to appreciate a substantial difference between mutants and wildtypes in terms of DNA bands size on a 3% agarose gel. For this reason, no restriction enzyme DNA digestion was required. As expected, one band for homozygous mutants (164 bp), two bands for heterozygous (164 bp and 210 bp) and one band for wild types (210 bp) were detected on a 3% agarose gel. Primers and PCR setting used for this protocol are the following:

Primer name	Primer sequence	Stock conc.	Working conc.
mrex3 forward	GACCATGAGAACACCTGCAC	100 μM	10 μM
mrex3 reverse	TGAGTCTTACCTTCTACCGCTC	100 μM	10 μM

Table 2.5 List of primers sequences used for mr^{sh652} line genotyping and relative concentrations.

PCR machine setting:

1. 95°C, 5 minutes
2. 95°C, 30 seconds
3. 58°C, 30 seconds
4. 72°C, 15 seconds
5. GOTO step 2, 34x
6. 72°C, 5 minutes
7. 12°C, ∞

2.3. CRISPR/Cas9-based mutagenesis method

CRISPR/Cas9-based mutagenesis method is a ground-breaking technology which allows the introduction of a mutation at the level of a specific genomic region of interest in a target gene. The system is made up of two components: an RNA-guided DNA endonuclease (Cas9) and a single guide RNA (gRNA), specifically designed against a target sequence within the genome.

It takes inspiration from the adaptive immunity mechanism discovered in *Streptococcus pyogenes* used to recognize, target and destroy exogenous DNA. In a similar manner, thanks to the use of specifically designed gRNAs, it is possible to form a ribonucleoprotein active complex with the effector Cas9 nuclease, in order to recognize, bind and cleave its complementary DNA target sequence, upstream to an NGG (PAM) site.

In this regard, to create the aforementioned stable *gr*^{sh543}, *gr*^{sh551} and *hif1β*^{sh544} mutant lines, I co-injected in one-cell-stage zebrafish embryos a specific gRNA, designed to anneal to a target sequence and the Cas9 protein, as described by Hruscha et al. 2013. As a consequence of that, the activated homologous recombination (HR) and the non-homologous end joining (NHEJ) systems introduce mutations in the attempt of repairing the cleaved site. Among a plethora of mosaic mutations, I selected only the ones that were able to cause a frameshift (non-multiple of three mutations) and that were able to be transferred to the progeny. To achieve that, five different gRNA antisense oligonucleotide sequences (guide-oligos listed on Table 2.8) were obtained using CHOPCHOP website (https://chopchop.cbu.uib.no/) to target each a specific restriction site in the corresponding gene of interest (Montague *et al.*, 2014; Labun *et*

al., 2016). These gRNAs were chosen according to their genomic location, GC content, efficiency and the presence of a PAM site downstream of a restriction enzyme's cut site.

In general, it is preferable to induce a mutation as close as possible to the beginning of the open reading frame, in order to induce a frameshift that could affect the downstream domains. However, especially for GR, a drawback of this approach is related to the presence of conserved alternative start codons (AUG) that could generate progressively shorter but still functional isoforms, which could "rescue" the induced mutation (Oakley and Cidlowski, 2013). For these reasons, I decided to generate a mutation at the level of the DNA-binding domain, which is more likely to produce a non-functional protein.

To design the gRNAs used in this project, an 18 nucleotides sequence upstream to a selected PAM site (guide-oligos listed on Table 2.8) was inserted every time into a scaffold sequence (a.k.a CRISPR backbone, listed on Table 2.6) containing a promoter for the T7 Polymerase. Prior to transcription, the gRNAs were amplified via PCR and then purified from an agarose gel to increase their purity (primers listed on Table 2.7).

Scaffold sequence	5'–AAAGCACCGACTCGGTGCCACTTTTTCAAG TTGATAACGGACTAGCCTTATTTTAACTTGCT ATTTCTAGCTCTAAAACNNNNNNNNNNNNN NNNNNNNCTATAGTGAGTCGTATTACGC–3'

Table 2.6 Scaffold sequence used to insert CRISPR guide-oligos to produce a mutation in specific restriction sites.

Amplification protocol is listed below:

- Resuspend crispr guide oligo in TES buffer (Tris-HCl 10 mM pH8, EDTA 1 mM, 0,1 M NaCl) to make a 100 µM stock.
- Dilute it to 1 µM in milliQ water.
- Prepare PCR mix as follows:
    - 5x Firepol Master Mix 20 µl
    - 10µM guide-oligo primer for 2,5 µl
    - 10µM guide-oligo primer rev 2,5 µl
    - 1µM guide-oligo 2 µl
    - milliQ water up to 100 µl of final volume

- PCR machine program:
    1. 95°C, 1 minute
    2. 95°C, 15 seconds
    3. 60°C, 30 seconds
    4. 72°C, 20 seconds
    5. GOTO step 2, 39x
    6. 72°C, 5 minutes
    7. 10°C, ∞

Primer name	Primer sequence	Stock conc.	Working conc.
guide-oligo primer for	AAAGCACCGACTCGGTGCCAC	100 µM	10 µM
guide-oligo primer rev	GCGTAATACGACTCACTATAG	100 µM	10 µM

Table 2.7 List of primers with relative concentrations used to amplify and increase purity of gRNAs.

The resulting PCR product was run on a 3% agarose gel, purified using a Qiagen MinElute gel extraction kit and transcribed using a T7 megashortscript Ambion kit, using 1µ as a template.

Transcription protocol was set up as follows:

- 10x T7 buffer 2 µl
- ATP 2 µl
- GTP 2 µl
- CTP 2 µl
- UTP 2 µl
- template DNA 2 µl
- T7 Enzyme mix 2 µl
- milliQ water up to 20 µl of final volume

The transcription mix was subsequently incubated for 2 hours at 37°C in the water bath and the following protocol was used:

- Add 1 µl of DNase and incubate it for 30 minutes at 37°C
- Make up to 100 µl volume using milliQ water
- Add 33 µl of 10 M NH4Ac and 350 µl of EtOH 100%
- Precipitate the mix at -80°C for at least 2 hours
- Centrifuge at 4°C, max speed, for 30 minutes
- Wash pellet with 70% EtOH and air-dry it
- Dissolve pellet in 15 µl of milliQ water.

The success of the transcription was determined through gel electrophoresis and the corresponding concentration was quantified using a NanoDrop ND-1000 spectrophotometer.

Finally, the gRNA was injected at 2.4 μg/μl together with Cas9 protein. As an example, I have used the following CRISPR-injection mix:

- gRNA (4.18 μg/μl) 2.87 μl
- CAS9 protein (NEB, M0386, 20μM) 0.5 μl
- Phenol red 0.5 μl
- milliQ water up to 5 μl of final volume

Each embryo was injected with 1 nl of CRISPR-injection mix and raised for 24 hours at 28°C in E3 medium. The success of the injection method was determined via whole-embryo PCR-based genotyping performed on a fraction of injected embryos at 1 dpf, which have been randomly selected.

Gene	Target sequence	Restriction site	Restriction enzyme
gr^{sh551}	GCTTGAGGAACCATAGATCC	CCNN_NNN^NNGG	BslI
gr^{sh543}	CCAGCTGACGATGTGGCAG	CAG^CTG	PvuII
hif1βex2	TTTGTTGGCTTTTTGCACCC	CCNN_NNN^NNGG	BslI
hif1β^{sh544}	TCGGTGCTGGTGTTTCCAG	GCNNNNN^NNGC	MwoI
hif1β^{sh544}	TGCGCAGGATAGTGAGTTT	CCNN_NNN^NNGG	BslI

Table 2.8 List of target sequences inserted into the CRISPR scaffold to produce a mutation in specific restriction sites.

2.3.1. CRISPANT technology

Zebrafish-based genetic screenings coupled to recent advances in reverse genetic approaches (i.e. CRISPR/Cas9 method) represent powerful and efficient tools for probing molecular mechanisms governing vertebrate physiology, development and disease. However, with standard application of CRISPR/Cas9 system injection, null mutants can be obtained and analysed only at the F2 generation stage.

To increase throughput, I exploited a novel and rapid technology for directed gene knock-out created by Burger et al 2016 and implemented by Wu et al., 2018. This method, based on CRISPR/Cas9 technology, allows to generate null phenotypes in G_0 zebrafish through the simultaneous injection of four CRISPR/Cas9 ribonucleoprotein complexes, which redundantly target a single gene (Wu *et al.*, 2018). Notably, the resulting GO nulls have a penetrance (>90% of embryos) which approaches the one of standard germline-transmitted knockouts.

To achieve that, four guide-RNAs selected from a lookup table of guide sets for most zebrafish genes, provided by the authors of the aforementioned paper to facilitate screens, were co-injected with Cas9 protein (diluted 1:10) and tracrRNA (100 μM) in one-cell stage embryos. This method was used to create G_0 CRISPANTS (CRISPR/Cas9-mediated mutants) for the following genes of interest: mineralocorticoid receptor (*mr*, a.k.a *nr3c2*), aryl hydrocarbon receptor nuclear translocator 2 (*arnt2,* a.k.a *hif1β2*) and laminin, beta 1b (*lamb1b*). The latter was used as CRISPR-injection control. gRNAs sequences and stock concentrations used are listed in Table 2.9.

Transcript ID	gRNA name	Target exon	Target sequence	Stock conc.	Working conc.
ENSDART00000158162	arnt2_Target_1	exon 5	ACGGCGCCTACAAACCCTCC	100µM	25 µM
ENSDART00000158162	arnt2_Target_2	exon 6	GGCCGATGGCTTCTTGTTCG	100µM	25 µM
ENSDART00000158162	arnt2_Target_3	exon 11	TTCACGCCACAATTCGGATG	100µM	25 µM
ENSDART00000158162	arnt2_Target_4	exon 14	GTCGCAGGTGCGTAAAAACA	100µM	25 µM
ENSDART00000172111	nr3c2_Target_1	exon 2	GCATTGTGGGGTCACCTCCA	100µM	25 µM
ENSDART00000172111	nr3c2_Target_2	exon 2	AAGGGGATTAAACAGGAAAC	100µM	25 µM
ENSDART00000160637	nr3c2_Target_3	exon 5	CAACCAGCTCGCCGGAAAAC	100µM	25 µM
ENSDART00000172111	nr3c2_Target_4	exon 5	ATATCTGACGCCGTCCGTCT	100µM	25 µM
ENSDART00000066945	lamb1b_Target_1_CD95	5'-UTR	TTGTTAATAGCATAGTACATTGG	100µM	25 µM
ENSDART00000066945	lamb1b_Target_2_CD96	exon 1	GGAGAACAAGCAAAACGATGAGG	100µM	25 µM
ENSDART00000066945	lamb1b_Target_3_CD107	5'-UTR	GCGTGGTGCAGGGTTTGTAG	100µM	25 µM
ENSDART00000066945	lamb1b_Target_4_CD108	exon 2	TCACAATGACATGTGTGCG	100µM	25 µM

Table 2.9 List of gRNAs sequences and relative concentrations used to create rapid and consistent biallelic gene disruption in G_0 embryos.

CRISPANT-injection mix was prepared as follows:

- gRNA (25 μM) 0,5 μl (each)
- Cas9 protein (NEB, M0386, 20 μM) 0.5 μl
- tracrRNA (100 μM) 1 μl
- Phenol red 0.5 μl
- milliQ water up to 5 μl of final volume

Finally, 1 nl of injection mix was injected in each embryo and they were then raised at 28°C till five days post-fertilisation in E3 medium. The criterion for success of the injection was assessed by observing the phenotype and quantifying the *eGFP*-related brightness of 5 dpf larvae and via genotyping.

2.3.2. *lamb1b* CRISPR injected embryos genotyping

To confirm the efficiency and the specificity of CRISPR/Cas9-based mutagenesis method, I chose to target a gene which is not involved in the HIF pathway. In particular, *lamb1b* was selected as CRISPR-injection control gene, whereas *vhl*$^{hu2117/hu2117}$*;phd3:eGFP*$^{i144/i144}$ embryos were used as CRISPR-injection control samples. *lamb1b* is an extracellular matrix glycoprotein involved in a variety of biological processes which include cell adhesion, differentiation and migration. Notably, since it has been reported to exhibit tissue-specific compensation, it is not able to generate any phenotype when mutated (Chris Derrick, Bateson Centre, TUoS, unpublished). For this reason, as *lamb1b*-injected *vhl* mutant embryos were undistinguishable from the uninjected ones, a genotyping protocol was designed as follows:

- Prepare PCR mix as follows:
    - 5x Firepol Master Mix 4 µl
    - [10µM] primer for 1 µl
    - [10µM] primer rev 1 µl
    - DNA 1,5 µl
    - milliQ water up to 20 µl of final volume

- PCR machine program:
    1. 94°C, 3 minutes
    2. 94°C, 30 seconds
    3. 50°C, 30 seconds
    4. 72°C, 15 seconds
    5. GOTO step 2, 34x
    6. 72°C, 5 minutes
    7. 10°C, ∞

Primers have been designed using Primer3 to amplify respectively a 262bp (CD95), 238bp (CD96), 254bp (CD107) and 256bp (CD108) DNA sequence surrounding the mutation sites (primers listed on Table 2.10). Finally, the success of the reaction was assessed via gel electrophoresis by running the PCR amplified samples on a 4% agarose gel diluted into Tris-Boric Acid-EDTA (TBE) buffer for two hours at 100 V. TBE buffer was used instead of TAE (Tris-Acetate-EDTA), because of its buffering capacity and conductivity, which make it less prone to overheating during long runs. Moreover, borate allows to resolve small DNA fragments by preserving DNA integrity better than acetate (Sanderson *et al.*, 2014).

gRNA name	Target exon	Primer name	Target sequence	Stock conc.	Working conc.
lamb1b_Target_1_CD95	5'-UTR	CD97 (forward)	TCACACTAAGACATGGGGCA	100µM	10 µM
		CD98 (reverse)	TCTTGTGCAAATAATCGAGGGA	100µM	10 µM
lamb1b_Target_2_CD96	exon 1	CD99 (forward)	TCTTCTCCCACGATCCACAC	100µM	10 µM
		CD100 (reverse)	ACCAAGCAACCAAAACACTGA	100µM	10 µM
lamb1b_Target_3_CD107	5'-UTR	CD119 (forward)	CGCACCCTGAAAAATCATATCT	100µM	10 µM
		CD120 (reverse)	AGAGCTGTAGTGTGGAAAAGTC	100µM	10 µM
lamb1b_Target_4_CD108	exon 2	CD121 (forward)	AAGTTTCATCGTGCAACCTTTC	100µM	10 µM
		CD122 (reverse)	TTCGTTGGGCCTACCTCTAATA	100µM	10 µM

Table 2.10 List of gRNAs'primer sequences and relative concentrations used to genotype lamb1b injected and uninjected embryos.

2.4. Whole mount *in situ* hybridization

2.4.1. Embryos harvesting, treatment and fixation

Embryos to be analyzed were harvested, treated and fixed to allow the probe to penetrate the tissue, find its mRNA target and form stable, double-stranded mRNA:RNA probe hybrid RNA molecules. To this end, 24 hpf embryos were treated with 16,8 µl of 1-phenyl 2-thiourea (PTU, stock concentration 75mg/ml) diluted in 35 ml E3 medium to inhibit melanogenesis, according to Karlsson et al., 2001 protocol. Afterwards, batches of 15 embryos at 4 dpf were treated into 6-well plates with 30 µM Betamethasone 17,21-dipropionate (BME), with 1% DMSO (Sigma-Aldrich) and left untreated as control for 24 hours (Griffiths *et al.*, 2012). Inside the 6-well plates, embryos were incubated in 3 ml total volume of E3 medium without methylene blue. Afterwards, up to 30 embryos were collected in 1,5 ml Eppendorf tubes and anaesthetized using Tricaine Solution (MS-222, Sigma-Aldrich) prior to fixation in 1 ml 4% PFA solution overnight, at 4°C. The following day, embryos were washed twice for 10 minutes in PBST and post-fixed in 1 ml 100% MeOH. Finally, samples were stored at -20°C.

2.4.2. Whole-mount *in* situ hybridization protocol

Whole mount *in situ* hybridization is a common very informative approach used to detect the location and determine the expression levels of target mRNAs in zebrafish embryos. It is a multi-step technique based on the hybridization of a synthetically produced Digoxigenin-labelled antisense-RNA probe to the complementary mRNA under investigation. Digoxigenin is an organic molecule that is recognised by a specific

monoclonal antibody that is covalently linked to Alkaline Phosphatase. In particular, the location and the expression levels of the hybridized Digoxigenin-labelled probe can be observed by treating samples with a combination of substrate and colour enhancer named BCIP and NBT, respectively. Indeed, Alkaline Phosphatase molecules that are covalently bound to the anti-Digoxigenin monoclonal antibody can convert them into a blue precipitate. The expression level of the targeted mRNA is directly proportional to the intensity of the blue staining in the area where the gene under investigation is expressed. The protocol used, described below, was adapted from Thisse and Thisse, 2008 (Thisse and Thisse, 2008). All solutions are listed on Table 2.11:

- **Day 1 (probe-target mRNA hybridisation)**
  - Rehydrate embryos by successive incubations with 60% MeOH/PBST and 30% MeOH/PBST for 10 minutes each at room temperature (RT);
  - Wash them 4 times for 5 minutes each with 100% PBST, at RT;
  - Permeabilise embryos by incubating them in Proteinase K (15 mg/ml stock, diluted 1:1000 in PBST) at RT for the appropriate amount of time according to the developmental stage used, as follows:

Developmental stage	Mins at RT	ProtK concentration
Early somitogenesis	0	10μg/ml
Late somitogenesis	0	
24 hpf	0	
30 hpf	22	
36/48 hpf	30	
3 dpf	50	
4dpf	70	
5 dpf	90-120	15μg/ml

- Wash embryos one time for 5 minutes with PBST to remove ProtK
- Refix by incubating in 4% PFA for 20 minutes at RT;
- Wash 3 times, 5 minutes each, with PBST at RT;
- Pre-incubate in hybridisation mix with tRNA and heparin (HM+) for at least 3 hours at 70°C;
- Incubate overnight at 70°C in HM+ containing Digoxigenin-labelled probe (750-1000 ng for embryos > 4 dpf)

- **Day 2 (Anti-DIG antibody incubation)**
  - Brief wash with 100% hybridisation mix without tRNA and heparin (HM-);
  - Wash with 75%, 50% and 25% HM- in 2x SSC for 15 minutes each at 70°C;
  - Wash with 2x SSC for 15 minutes at 70°C;
  - Wash twice with 0.2x SSC for 30 minutes each at 70°C;
  - Wash with 75%, 50% and 25% 0.2x SSC in PBST for 10 minutes each at RT;
  - Wash with PBST for 10 minutes at RT;
  - Incubate in blocking solution for at least 3 hours at RT;
  - Incubate in blocking solution with anti-Dig antibody overnight, at 4°C, in dark.

- **Day 3 (NBT/BCIP colorimetric reaction)**
  - Brief wash with PBST, at RT, in the dark, to remove antiserum;
  - Wash 4 times with PBST for 30 minutes each, at RT, in the dark;
  - Wash with Alkaline Phosphatase buffer, without $MgCl_2$ for 15 minutes, at RT, in the dark;
  - Wash twice with Alkaline Phosphatase (AP) buffer, with $MgCl_2$ for 10 minutes each, at RT, in the dark;

- Incubate in staining solution at RT, in the dark, until embryos are stained;
- Stop staining reaction by washing with PBST, for 3 times, at4°C, in dark;
- Post-fix the stained embryos with 4% PFA for 20 minutes at RT;
- Wash embryos four times with PBST, 5 minutes each;
- Wash with 25%, 50% and 80% glycerol in PBST and store them at 4°C.

HM+	**AP+ buffer**	**Blocking buffer**	**PBST**	**Staining solution**
Formamide 25 ml	Tris HCl pH 9.5 5 ml	2% Blocking Powder 1 g in 50mls	PBS 1x 45 ml	NBT[1] 3,4 µl/ml AP+
20x SSC 12.5 ml	$MgCl_2$ 1M 2.5 ml	Malate Buffer 25 ml	milliQ water 5ml	BCIP[2] 3,5 µl/ml AP+
Tween20 25% 200 µl	NaCl 5M 1 ml	milliQ water 25 ml	Tween20 25% 200 µl	
Citric acid 1M 460 µl	Tween20 25% 200 µl			
Heparin 50 mg/ml 50 µl	milliQ water up to 50 ml			
tRNA 50 mg/ml 500 µl				
milliQ water up to 50 ml				

Table 2.11 List of solutions and relative concentrations used for WISH protocol. 1: Nitro Blue Tetrazolium Chloride; 2: 5-Bromo-4-Chloro-3-Indoyl-Phosphate.

2.4.3. Antisense RNA probe design and transcription

Single-stranded antisense-RNA probes, which are perfectly complementary to the mRNA to be detected, were synthesized through *in vitro* transcription using chemically modified ribonucleotide triphosphates that carry a digoxigenin side chain (Table 2.12). Prior to that, each plasmid encoding zebrafish complementary DNA (cDNA) fragments, as templates, were linearized with the appropriate restriction enzyme that cleaves on the 5' side of the insert, such that antisense transcripts can be synthesised from the T7 or SP6 RNA polymerase promoter, located immediately downstream of the 3'end of the cDNA clone. Afterwards, the linearized DNA fragments were purified through phenol/chloroform method and transcribed into antisense RNA probes, as follows:

- Linearized DNA 1 µg
- RNase inhibitor 0,5 µl
- T7/SP6 RNA Polymerase 2 µl
- 5x Transcription buffer 4 µl
- 10x Dig-labelled nucleotides mix 2 µl
- milliQ water up to 20 µl of final volume

The transcription mix was then incubated at 37°C for 2 hours and the following RNA precipitation protocol was used:

- Add 1 µl of DNase and incubate it for 20 minutes at 37°C;
- Add 80 µl of milliQ water and mix;
- Add 33 µl of 10 M NH_4Ac and 350 µl of 100% EtOH;
- Precipitate RNA probe by storing it at -80°C for at least 2 hours;
- Centrifuge at maximum speed for 30 minutes at 4°C;
- Wash pellet with 500 µl 70% EtOH;

- Centrifuge at maximum speed for 10 minutes at 4°C;
- Air-dry pellet for 5 minutes;
- Resuspend in 100 µl of milliQ water;
- Store it at -80°C.

The success of the reaction was evaluated by electrophoresis on a 1% agarose gel and the corresponding probe's concentration was quantified using a NanoDrop ND-1000 spectrophotometer.

Probe name	**Vector**	**Restriction enzyme/Polymerase**	**Reference**
pomca	pCR BluntII-TOPO	SP6/XhoI	Muthu et al., 2016
cyp17a2	pGEM-T Easy Vector	SP6/NcoI	Eachus et al., 2017
ldha	pCMV-SPORT 6.1	T7/EcoRI	van Rooijen H. (van Eeden lab)
phd3	pCMV-SPORT 6.2	SmaI/T7	Santhakumar K. (van Eeden lab)

Table 2.12 List of RNA probes used for in situ hybridization analysis.

2.5. TaqMan Real Time-qPCR assay

For many years TaqMan has been the gold standard chemistry for real time PCR due to its unequalled specificity, sensitivity and ease of use. Similar to other types of real-time PCRs, TaqMan-based reactions require double-stranded template and two fairly standard target specific primers to work. Indeed, unlike the ones used in regular PCR reactions, TaqMan assay requires two PCR primers with a preferred product size of 50-150 bp and a third sequence-specific fluorogenic "probe". The latter is a single stranded oligonucleotide of 20-26 nucleotides designed to bind only the DNA sequence in-between the two PCR primers. Notably, the probe cannot be extended by Taq Polymerase, as it lacks a free hydroxyl group. Moreover, TaqMan probes are covalently joined to two other molecules:

- a fluorescent FAM™ or VIC™ dye label called "reporter", located on the probe's 5'-end, which enables the detection of a specific PCR product, as it accumulates during PCR cycles;
- a minor groove binder (MGB) linked to a nonfluorescent quencher (NFQ) on the 3' end, which quenches the fluorescent signal from the reporter via Fluorescent Resonance Energy Transfer (FRET), when the latter is in close proximity to the reporter.

For this reason, as long as the probe remains intact, there is no permanent increase in fluorescent signal from the reporter. Vice versa, if the reporter and the quencher are permanently separated during the polymerase reaction, the reporter does fluoresce, producing a signal that is detected by the RTqPCR machine.

At the beginning of real-time PCR, the temperature is raised at 95°C to denature the double-stranded cDNA. During this step, the fluorescent signal from the "reporter" on the 5' end is silenced by the "quencher" on the 3' end. In the following step, the temperature is lowered to 60°C in order to allow the primers and the probe to anneal to their specific target sequences. Finally, Taq DNA polymerase synthesizes new strands using the unlabeled primers and the cDNA template. In particular, due to its endogenous 5'-nuclease activity, when it reaches the probe, the polymerase cleaves it, separating the dye from the quencher. After each PCR cycle, more reporter molecules are released, resulting in a raise in fluorescence intensity, which is directly proportional to the amount of target amplicon synthesized. By the way, the cycle threshold (Ct) value, defined as the number of cycles required for the fluorescent signal to cross the threshold (background level) are inversely proportional to the expression level of the target gene analysed.

2.5.1. Drug treatment, RNA extraction and cDNA synthesis

Three biological replicates of 10 larvae, at 5 dpf each, were treated for 24 hours starting from 96 hpf, with 30 μM Betamethasone 17,21-dipropionate and with 1% DMSO used as control.

RNA was extracted from 5 dpf larvae derived from the following incrossed mutant lines: WT (AB), *vhl*$^{hu2117/hu2117}$*;phd3:eGFP*$^{i144/i144}$, *vhl*$^{hu2117/+}$*;vll*$^{i216/i216}$*; phd3:eGFP*$^{i144/+}$, *hif1β*$^{sh544/+}$*;vhl*$^{hu2117/+}$*;phd3:eGFP*$^{i144/i144}$, *hif1β*$^{sh544/+}$*;phd3:eGFP*$^{i144/i144}$, *gr*$^{sh543/+}$*; vhl*$^{hu2117/+}$*;phd3:eGFP*$^{i144/+}$ and *gr*$^{sh543/+}$, using the protocol described below:

- **Phase separation**
  - Homogenize samples in 500 μl Trizol for 5 minutes at RT;
  - Add 100 μl chloroform and shake vigorously for 15 seconds;
  - Leave at RT for 2-3 minutes;
  - Centrifuge at 12000 xg for 15 minutes at 4ºC;
- **RNA precipitation**
  - Remove clear, upper aqueous phase to new tubes;
  - Mix upper phase with 250 μl isopropanol;
  - Leave at RT for 10 minutes;
  - Centrifuge at 12000 xg for 10 minutes at 4ºC;
- **RNA wash**
  - Discard supernatant;
  - Wash the pellet with 500 μl 75% EtOH;
  - Centrifuge at 7,500xg for 5mins at 4ºC;
- **Re-dissolving RNA**
  - Discard supernatant;
  - Air-dry the pellet for 5 minutes;
  - Dissolve pellet in 20 μl RNase-free milliQ water

RNA extracted was then quantified using a Nanodrop ND-1000 spectrophotometer. Afterwards, cDNA was synthesized from RNA through reverse transcription using Protoscript II First Strand cDNA Synthesis Kit – easy protocol (NEB), as recommended by manufacturer's instructions. cDNA mix was set up as describe in Table 2.13:

Components	Concentrations
template RNA	up to 1 μg
oligo d(T)23 VN	2 μl
ProtoScript II Reaction Mix (2X)	10 μl
ProtoScript II Enzyme Mix (10X)	2 μl
Nuclease-free water	up to 20 μl of final volume

Table 2.13 List of reagent and relative concentrations used for cDNA synthesis.

Finally, synthesized cDNA was quantified using a Nanodrop ND-1000 spectrophotometer.

2.5.2. TaqMan RT-qPCR protocol and settings

RTqPCR was performed using CFX96 Touch™ Real-Time PCR Detection System (BioRad) paired with CFX Maestro™ Analysis Software. Each assay contains target primers and an optimized sequence-specific probe with no extra design, optimization or lengthy melt-curve analysis necessary. RTqPCR mix was prepared as follows:

- cDNA (100ng/μl) 1 μl
- TaqMan Universal Master Mix 10 μl
- FAM™ Probe 1 μl
- milliQ water up to 20 μl of final volume

The following RTqPCR machine setting was used:

1. 95°C, 10 minutes
2. 95°C, 15 seconds
3. 60°C, 30 seconds
4. GOTO step 2, 39x

Cycle threshold (Ct) values were automatically calculated by the software with ROX as passive reference dye. Three technical replicates for each biological replicate were used for each RTqPCR reaction. Notably, due to the use of a 96 well plate format coupled to the presence of drug treated samples, only one target gene and one housekeeping gene were tested each time. Finally, 1 µl of MilliQ water, in triplicate, was used as negative control instead of cDNA, both for target and housekeeping genes.

2.5.3. Target and reference TaqMan probes used

Four hypoxia-inducible factor pathway-dependent (*egln3, pfkfb3, vegfab and slc2a1a)* and four GC pathway-dependent (*fkbp5*, *il6st, pck1 and lipca)* target genes expression were respectively tested against *eef1a1* and/or *rps29* housekeeping gene expression. The list of TaqMan probes used for RTqPCR analysis is described in the Table 2.14.

2.5.4. Fold change calculation

ΔΔCT method was used to calculate the fold change value (Livak and Schmittgen, 2001). Firstly, the difference between Ct values of target gene and reference gene was calculated both for control samples (ΔCt control) and for treated samples (ΔCt treatment). Then, the difference between the average ΔCt (treatment) and the average ΔCt (control), used as normalizer, was used to obtain the ΔΔCt value. Finally, due to the exponential nature of qPCR, "fold change" is calculated as 2^-ΔΔCt.

ΔCt (ctrl)= Ct(target gene) - Ct(reference gene)

ΔCt (treatment)= average Ct(target gene)-average Ct(reference gene)

ΔΔCt = ΔCt(treatment) – ΔCt (ctrl)

$FC= 2^{-\Delta\Delta CT}$

See the link below, page 57 for additional details.

https://assets.thermofisher.com/TFS-Assets/LSG/manuals/cms_042380.pdf

Gene name	Gene symbol	Assay ID	Dye label	Concentration
Egl nine homolog 3 (phd3)	*egln3*	Dr03095294_m1	FAM-MGB	20x
6-phosphofructo-2-kinase/fructose-2,6-biphosphatase 3	*pfkfb3*	Dr03133482_m1	FAM-MGB	20x
vascular endothelial growth factor Ab	*vegfab*	Dr03072613_m1	FAM-MGB	20x
Solute carrier family 2, member 1a (glut1)	*slc2a1a*	Dr03103605_m1	FAM-MGB	20x
FK506 binding protein 5	*fkbp5*	Dr03114487_m1	FAM-MGB	20x
interleukin 6 signal transducer	*il6st*	Dr03431389_m1	FAM-MGB	20x
phosphoenolpyruvate carboxykinase 1 (soluble)	*pck1*	Dr03152525_m1	FAM-MGB	20x
lipase, hepatic a	*lipca*	Dr03113728_m1	FAM-MGB	20x
eukaryotic translation elongation factor 1 alpha 1, like 1	*eef1a*	Dr03432748_m1	FAM-MGB	20x
ribosomal protein S29	*rps29*	Dr03152131_m1	FAM-MGB	20x
actin beta 1	*actb1*	Dr03432610_m1	FAM-MGB	20x

Table 2.14 List of TaqMan probes used for RTqPCR analysis on HIF and GC target genes expression.

2.6. Cortisol extraction and quantification

By collaborating both with Nan Li (Nils Krone laboratory, University of Sheffield, UK) and Karl-Heinz Storbeck laboratory (Department of Biochemistry, Stellenbosch University, South Africa) I performed cortisol extraction and quantification in both *hif1β*$^{sh544/+}$;*phd3:eGFP*$^{i144/+}$ and *vhl*$^{hu2117/+}$*; phd3:eGFP*$^{i144/+}$ mutant lines. These lines were chosen among the available ones, due to their opposite effect on GC target genes expression, as demonstrated via RTqPCR analysis.

Three biological replicates of 150 larvae at 5 dpf each, of *hif1β*^{sh544} mutants, *hif1β*^{sh544} siblings, *vhl*^{hu2117} mutants and *vhl*^{hu2117} siblings were used for steroid hormones extraction, according to (Eachus *et al.*, 2017) protocol, as follows:

- Transfer 150 larvae into silanized low-binding Eppendorfs and snap-freeze them on dry ice;
- Add 1 ml of phosphate-buffered saline (PBS) to the sample;
- Perform three rounds of freeze/thawing using dry ice and hot water at 55°C to lyse the cells;
- Homogenize samples with a tissue homogenizer (Power Gen 125, Fisher Scientific) equipped with blades (SN-04727-87, Disposable Plastic Tip Homogenizer Probes - LabGEN® Tip Probes, 0.25 to 50 mL, Soft Tissue, 50/pack);
- Perform a fourth freeze/thawing round;
- Store the tubes at -20°C

Once all the samples were collected, I freeze-dried them to make the material more convenient for shipping to Karl-Heinz Storbeck laboratory, which performed cortisol quantification. In particular, the dried steroids were resuspended in 150 mL 50% MeOH and were separated and quantified with an Acquity UPLC System (Waters, Milford, CT) in combination to a Xevo TQ-Standem mass spectrometer (Waters). Finally, chromatographic separation was carried out via ultra-performance liquid chromatography high-strength silica T3 column (2.1 mm, 350 mm, 1.8 mm) (Waters), as described by O'Reilly *et al.*, 2016.

2.7. Visual background adaptation assay

Visual background adaptation (VBA) is a well-characterized GR-dependent neuroendocrine response that causes zebrafish skin pigment cells to shrink when exposed to bright illumination. This is because it is a natural defence strategy against predators to camouflage themselves according to the colour of the background (Kramer *et al.*, 2001; Kurrasch *et al.*, 2009). For this reason, since $gr^{sh543/sh543}$ mutants were indistinguishable from siblings, a quick way to identify their genotype was to assess their VBA response. To achieve that, clutches of $gr^{sh543/+}$ incrossed derived larvae were subjected to VBA assay at 5 dpf, as follows:

- keep petri dishes containing larvae in a dark environment for at least 60 minutes (covered with aluminium foil inside a Styrofoam box);
- expose them under bright, whole-field illumination, using a Leica CLS 150 Microscope Light Source Fibre Optic Lab from the top (maximum light intensity), mounted 50 cm above the petri dishes, with their lid removed, for 20 minutes.
- the plates are placed on a DVV ViewBoxes Light Box (turned on) used as white bright background. This allow to illuminate larvae with a strong bright light both from the top and the bottom.
- move the dishes on a white surface (A4 paper sheet)

Finally, larvae were sorted according to their VBA response by eye. The success of the experiment was assessed via genotyping, as described in section 2.2.5. These conditions are able to reliably trigger VBA response in zebrafish larvae at 5 dpf (Muto *et al.*, 2005; Hatamoto and Shingyoji, 2008).

2.8. Microscopy

2.8.1. Fluorescent stereo microscope

Live zebrafish embryos and *in situ* experiments related pictures were captured using a Leica M165FC fluorescent stereo microscope, equipped with a digital colour camera (DFC310FX) and a Leica external fluorescent light source (EL6000).

2.8.2. Phenotypic analysis of live embryos

Embryos were anesthetized via incubation in Tricaine methanesulfonate (MS-222), diluted 1:25 in the petri dish, and placed on a 2% methylcellulose (Sigma) drop, located on the inner part of a petri dish lid. All embryos were oriented with their anterior to the left side up, so that the lateral left sagittal plane was visible.

2.8.3. Analysis of whole-mount embryos

In situ hybridization-processed whole-mount embryos were mounted in 80% glycerol in a glass embryo-dish. Embryos were oriented either with their anterior to the left or dorsal side up, so that either the lateral left sagittal plane or the pituitary gland region were visible.

2.9. Image analysis

2.9.1. Quantifying *phd3:eGFP*-related rightness

Pictures were acquired using Leica Application Suite version 4.9, which allowed to capture both bright-field and GFP-fluorescent images. To quantify the *phd3:eGFP*-related brightness of live embryos derived from each incrossed mutant line used in this project, I used Fiji (Image J) software v.2.0.0. This software allows to measure the mean grey value of an image, by converting it in a 8-bit format and subsequently by summing the grey values of all the pixels in the selected area, divided by the number of pixels. By default, since value = 0 is assigned to black and value = 255 to white, the quantified mean grey values are proportional to the intensity of the *eGFP*-related brightness present in the embryos. In particular, head, liver and tail (from the anus to the caudal peduncle) (**figure 2.1**) related brightness were selected and measured in all the mutant lines used in this project.

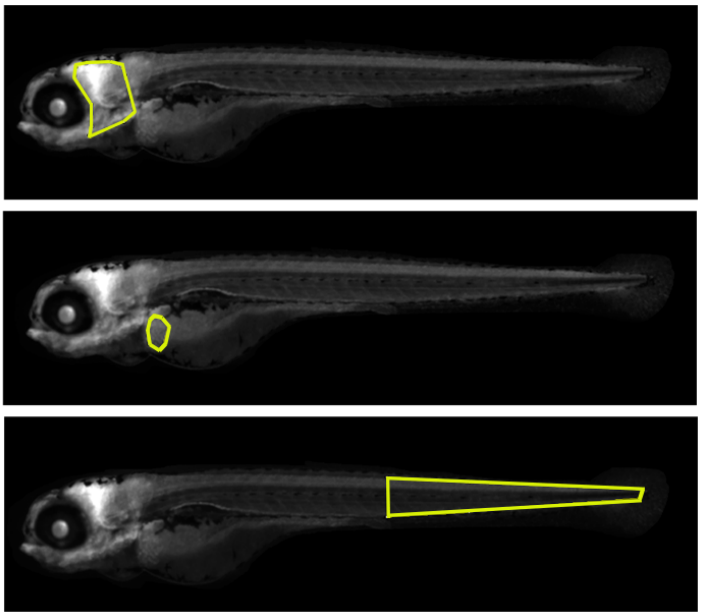

Figure 2.1 Representative picture of the head, liver and tail areas selected in each embryo to quantify the *phd3:eGFP*-related brightness via mean grey value quantification. The embryo shown in the picture above is 5 dpf *vhl* mutant.

2.10. Statistical analysis

GraphPad Prism version 8.4.0 for MacOS (GraphPad Software, La Jolla, California, USA, www.graphpad.com) was used to perform statistical analysis on all the samples analysed. D'Agostino and Pearson's normality test was initially run on all datasets prior to analysis. Unpaired t test was used to check the presence of significant differences between two normally distributed sample groups (i.e. for cortisol quantification). Vice versa, not normally distributed populations were analysed using the non-parametric Kruskal-Wallis test. For the comparison of means of more than two sample groups, One- or Two-way ANOVA method followed by Sidak's post hoc test was used. In particular one-way ANOVA was used for assessing mean grey values data quantification, whereas two-way ANOVA was used to evaluate RTqPCR data. As post-hoc correction tests, Sidak's method for multiple comparisons was used on normally distributed populations, whereas Dunn's correction was used for not normally distributed populations.

3. GENERATION AND CHARACTERIZATION OF ZEBRAFISH MUTANT LINES

3.1. Introduction

In the last decades *in vitro* studies have highlighted the presence of a crosstalk between hypoxia inducible factor- and GC- signalling pathways (Kodama *et al.*, 2003; Leonard *et al.*, 2005; Wagner *et al.*, 2008; Zhang *et al.*, 2015, 2016). However, how this interplay precisely works *in vivo* and which is the molecular mechanism behind it are questions that still remain unanswered.

In this project the comprehension of the molecular mechanisms underlying the interaction between GC and HIF signalling has been initially tackled *in vivo* through the modulation of these two pathways via a "gain-of-function/loss-of-function" approach.

In particular, both a genetic and pharmacological method have been utilised to alter these two pathways during the first 120 hours post fertilisation of zebrafish embryos. On the one hand, CRISPR/Cas9-based mutagenesis has been used as gene editing tool to generate both *hif1β*^{sh544} (*arnt1*) and *gr*^{sh543} (*nr3c1*) mutant lines into an already existing *vhl*$^{hu2117/+}$*;phd3:eGFP*$^{i144/i144}$ hypoxia reporter line (Santhakumar *et al.*, 2012). On the other hand, Betamethasone 17,21-dipropionate (BME, Sigma Aldrich), a synthetic GR agonist, has been used as pharmacological tool to upregulate HIF signalling pathway in zebrafish larvae (Vettori *et al.*, 2017).

The zebrafish is an exceptional genetic vertebrate model system for endocrine studies, because analogously to humans, they are diurnal and use cortisol as the main GC hormone (Weger *et al.*, 2016). Additionally, both the human GC and HIF pathways

components are also present in zebrafish. Consequently, they are informative and genetically modifiable organisms to study both hypoxia and HIF signalling *in vivo* (van Rooijen *et al.*, 2011; Santhakumar *et al.*, 2012; Elks *et al.*, 2015).

In this chapter, the generation and characterisation of the mutant lines used in the present study will be described in detail. Finally, thanks to the presence of the aforementioned *phd3:eGFP*$^{i144/i144}$ hypoxia reporter, it has been possible to outline not only the differences between mutants and wild types, but most importantly to better understand how the interplay between HIF and GC signalling occurs *in vivo*.

3.2. Generation and characterization of *arnt1* and *arnt1;vhl* knockout in zebrafish

The first questions I was keen to answer were the following: how does crosstalk between hypoxia-dependent signals and GC-mediated regulation of gene expression occur? If Hif and GCs are able to act on each other, how do they fine-tune the cellular pathways mediating adaptation to hypoxic environment? Are GCs contributing to Hif functions? Is Hif contributing to GC functions as well? Is GR an obligatory factor for the Hif response or vice versa?

I believed that answers to these questions could be provided through the creation and the analysis of *gr* and *hif1β* mutant lines. To this purpose, to enable an effective downregulation of the HIF pathway I chose to create a *hif1β* mutant to study the effect of HIF on GC signalling. In this regard, knocking out HIF-α was considered impracticable due the presence of 6 isoforms (*hif-1A,B, hif-2A,B* and *hif-3A,B*) (Köblitz *et al.*, 2015).

Hif-1β (hypoxia-inducible factor 1 beta, or Arnt1) is a basic helix-loop-helix-PAS protein which translocates from the cytosol to the nucleus after ligand binding to the Hif-α subunit, following the stabilization of the latter in the cytoplasm. It represents the most downstream protein in the HIF pathway and for this reason it is the most suitable target to efficiently repress it. In particular, zebrafish have two Arnt1 homologues named Arnt1a and Arnt1b, with the shorter one (Arnt1a) apparently non-functional as demonstrated in a previous *in vitro* study (Prasch *et al.*, 2006).

For this reason, I chose to target the *arnt1b* gene at the level of the exon 5, because of its favourable length, its genomic location and the presence of ideal restriction sites for the gRNA make-up. An additional important advantage is that

alternative start codons cannot rescue that mutated allele. Furthermore, since it codes for the DNA binding domain (DBD), a mutation in that region was predicted to block the ability of the protein to act as a transcription factor. In particular, a 7 bp insertion (**figure 3.1**) was obtained using CRISPR/Cas9 based mutagenesis in *vhl;phd3:eGFP* heterozygote embryos. The resulting frameshift mutation (allele name *sh544*) was expected to cause a premature stop codon at the level of the DNA-binding domain, which would result in a severely truncated protein. Consequently, I predicted to observe a strong downregulation of the HIF reporter related brightness in 5 dpf mutant larvae.

The *phd3:eGFP* hypoxia reporter line was previously generated in my laboratory via BAC transgenesis. The *phd3* locus plus >30 kb 3' and a 5' flanking sequence was inserted into a Bacterial Artificial Chromosome (BAC) and recombinereed to replace the translation initiation codon (ATG) of *phd3* itself with a eGFP reporter construct (Santhakumar *et al.*, 2012). The already existing *vhl*$^{hu2117/+}$ line (van Rooijen *et al.*, 2009) was crossed into the Tg(*phd3:eGFP*)$^{i144/i144}$ line in order to create the aforementioned *vhl* $^{hu2117/+}$*;phd3:eGFP* $^{i144/i144}$ fish. In this work, the resulting *hif1β*$^{sh544/+}$*;vhl*$^{hu2117/+}$*;phd3:eGFP*$^{i144/i144}$ line will be called *artn1*$^{+/-}$*;vhl*$^{+/-}$, whereas the *vhl*$^{hu2117/+}$*;phd3:eGFP*$^{i144/i144}$ line will be called *vhl*$^{+/-}$ hereafter.

Figure 3.1. Schematic representation of zebrafish *hif1β* (*arnt1*) gene. Exons are shown as black boxes, whereas introns as lines. The red arrowhead shows the position of a 7 bp insertion in exon 5 (encoding the bHLH DNA binding domain). In the *arnt1* wt and mutant sequence: CRISPR target site: bold. Protospacer-adjacent-motif (PAM) sequence: red. Underlined nucleotide sequence: bp inserted.

Initial analysis performed on *arnt1*$^{+/-}$;*vhl*$^{+/-}$ incross-derived 5 dpf larvae (F1 generation) confirmed the suppressive effect that *arnt1* mutation was expected to have on the HIF signalling in *vhl* mutants. As predicted, *arnt1*$^{-/-}$;*vhl*$^{-/-}$ larvae showed a substantially attenuated *vhl* phenotype, characterized by a reduced *phd3:eGFP* related brightness, especially at the hepatic level, coupled to the absence of pericardial oedema, excessive caudal vasculature and improved yolk usage compared to *vhl*$^{-/-}$ larvae (**figure 3.2A**). In particular, this was quantified as a 39% downregulation ($P<0.0017$) at the level of the head, a 75% downregulation ($P<0.0001$) in liver and a 58% downregulation ($P<0.0001$) in the rest of the body (from the anus to the caudal peduncle), in terms of *phd3:eGFP*-related brightness, compared to *vhl*$^{-/-}$ larvae (**figure 3.2B**). Of note, the HIF-reporter brightness observed in the double mutants was still slightly higher than the wildtype's one (**figure 4.7B compared to D**). Finally, *arnt1*$^{+/-}$;*vhl*$^{+/-}$ larvae (siblings) were identical to wildtypes in terms of both phenotype and hypoxia reporter expression levels.

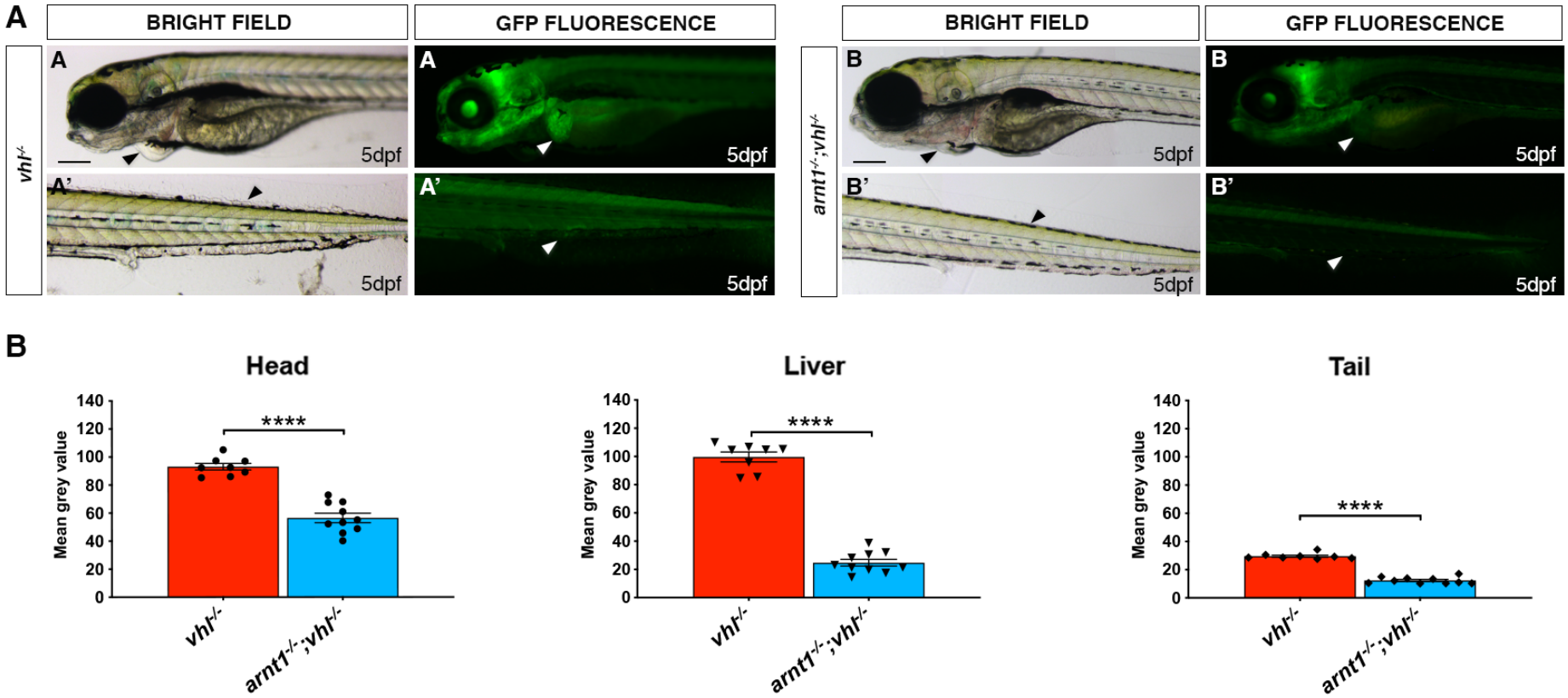

Figure 3.2. A. Magnified pictures of a representative 5 dpf *vhl*$^{-/-}$ larva compared to 5 dpf *arnt1*$^{-/-}$;*vhl*$^{-/-}$. Among the 120 GFP^{+} embryos derived from *arnt1*$^{+/-}$;*vhl*$^{+/-}$(*phd3:eGFP*) x *arnt1*$^{-/-}$;*vhl*$^{+/-}$(*phd3:eGFP*), 15 larvae were characterized by the absence of pericardial oedema, no ectopic extra vasculature at the level of the tail, no bright liver and a reduced brightness in the rest of the body (black and white arrowheads). Genotyping post phenotypic analysis on sorted larvae confirmed genotype-phenotype correlation. Fluorescence, exposure = 2 seconds. Scale bar 200 µm. **B.** Statistical analysis performed on mean gray value quantification (fluorescence, exposure = 991,4 seconds) at the level of the head, liver and tail, after phenotypic analysis on the aforementioned larvae (n=245). *vhl*$^{-/-}$ n=10 larvae: head 93.10 ± 2.33 (mean ± s.e.m); liver 99.64 ± 3.49 (mean ± s.e.m); tail 29.57 ± 0.73 (mean ± s.e.m). arnt1$^{-/-}$;vhl$^{-/-}$ n = 10 larvae: head 56.49 ± 3.36 (mean ± s.e.m); liver 24.69 ± 2.35 (mean ± s.e.m); tail 12.39 ± 0.75 (mean ± s.e.m). Unpaired t-test (*P < 0.05; **P < 0.01; ***P <0.001; ****P < 0.0001).

Homozygous *vhl* mutants are lethal by 8-10 dpf (van Rooijen *et al.*, 2009). To analyse the efficacy of *arnt1* mutation in rescuing the *vhl* phenotype over time, I attempted to raise *arnt1*$^{-/-}$;*vhl*$^{-/-}$ after day 5 post fertilization. Notably, double mutants survived beyond 15 dpf, but failed to grow and thrive when compared to wildtypes, which led us to euthanise them due to health concerns at 26 dpf (**figure 3.3**). *Arnt1* homozygote mutants, both in a *vhl*$^{+/-}$ or wild-type background, are instead morphologically indistinct from wildtypes, and adults are viable and fertile. In contrast, the previously published *arnt2*$^{-/-}$ zebrafish larvae were embryonic lethal around 216 hpf (Hill *et al.*, 2009).

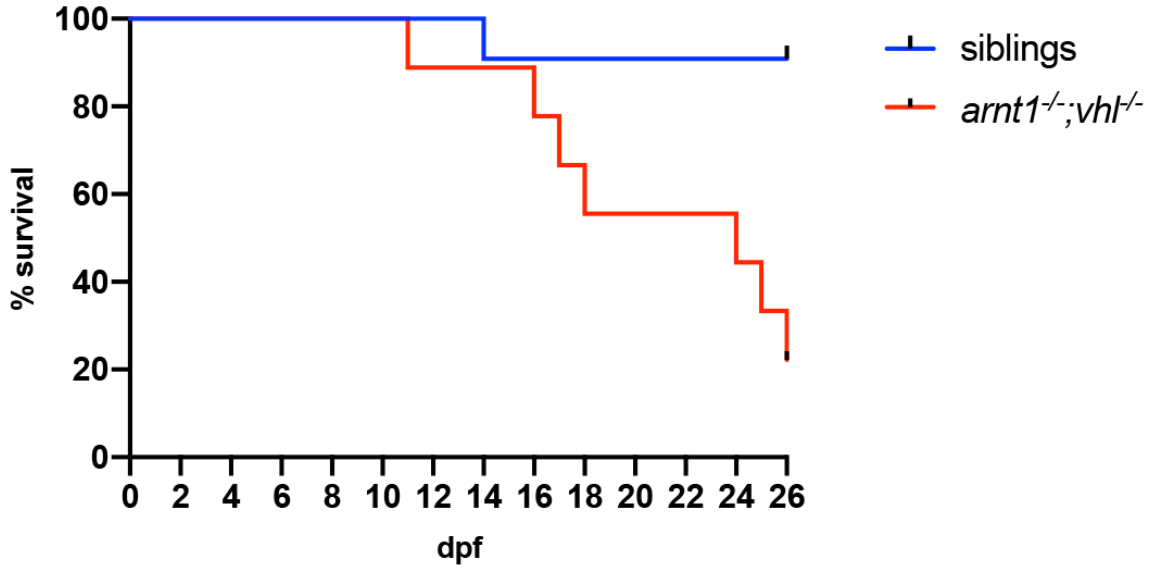

Figure 3.3. Kaplan-Meier survival curves of the zebrafish *arnt1*$^{+/-}$; *vhl*$^{+/-}$*(phd3:eGFP)* line analysed in this study. Time is shown in days. Siblings n = 30; *arnt1*$^{-/-}$; *vhl*$^{-/-}$*(phd3:eGFP)* n = 8. The Log-rank (Mantel-Cox) test was used for statistical analysis. *arnt1*$^{-/-}$; *vhl*$^{-/-}$*(phd3:eGFP)* vs. siblings: **P < 0.0027.

Phenotypic analysis performed both on 26 dpf *arnt1*$^{-/-}$;*vhl*$^{-/-}$ and wildtype siblings showed the presence of substantial morphological differences between these two groups (**figure 3.4**). A common strategy to determine fish maturation is the measurement of the standard body length (SL), assessed from the tip of the snout to the base of the tail (caudal peduncle). Moreover, since fish size may be influenced by genetics and also environmental factors, the combination of standard body length with the evaluation of the maturation of external traits is currently the most reliable measure of fish maturation (Singleman and Holtzman, 2014).

Double mutant body length (SL = 5.05 mm) was comparable to the one of a 13-15 dpf wild-type larva, as reported by Parichy et al. 2009 work (Parichy *et al.*, 2009), but not to its corresponding developmental stage traits. In particular, 26 dpf *arnt1*$^{-/-}$;*vhl*$^{-/-}$ larvae showed a clear body compared to a fully pigmented wild-type one. In addition, it was characterized by a larval-like anteriorly protruding open mouth and a clearly visible gut beneath the swim bladder, which are typical of a 4.9 mm total body length larva (13-15 dpf) (Kimmel *et al.*, 1995). An early larval pigment pattern with melanophores in stripes over the dorsal and ventral myotomes (no longer dispersed over the yolk sac) was also observable. Interestingly, even if the presence of food in the final tract of the intestine is a clear evidence of active feeding, the reduced body length and the absence of properly developed traits, are all distinct signs of a considerable developmental delay.

In addition, the head did not exhibit the dorsal indentation at the level of the pineal gland, which normally appear in 5.7 mm SL larvae. An increasingly pronounced caudal fin condensation, coupled to the presence of the first fin rays, which typically appear by ~4.9 mm SL were visible. On the other hand, the slight bulge in the dorsal fin fold (where the dorsal fin condensation usually arises), as well as the one on the

ventral side were not yet apparent. Finally, the distal end of the larval fin fold was still relatively rounded over the developing caudal fin which resembled, once again, the traits of a 13-15 dpf larva. Vice versa, the body length of the 26 dpf *arnt1*$^{+/-}$;*vhl*$^{+/-}$ sibling (SL = 12.22 mm) matched the standards of the corresponding wild-type larvae and no particular phenotypic traits were observed in them (Parichy *et al.*, 2009) (**figure 3.4**).

Consequently, these results suggest that *arnt1* mutation is able to partially rescue the Vhl phenotype and to triple the lifespan of *vhl* mutant larvae. However, since *arnt1*$^{-/-}$;*vhl*$^{-/-}$ did not show fully rescued traits, I speculate that this could be due to the presence of other Hif1β isoforms (mainly *arnt2*) that could still interact with HIF-α subunits. In support of this, *arnt1*$^{-/-}$;*vhl*$^{-/-}$ showed a slightly higher *phd3:eGFP* expression than the wildtypes.

Since double mutants' head was the brightest region in the body (in terms of *phd3:eGFP*-related brightness), both in 5 dpf and 26 dpf double mutant larvae (**figure 3.2A & 3.4**), this strengthened the hypothesis that mainly Arnt2 compensates for the lack of Arnt1 within the CNS to mediate the hypoxic response (Michaud *et al.*, 2000; Hill *et al.*, 2009). On the other hand, *arnt1*$^{-/-}$;*vhl*$^{-/-}$ liver was the organ with the lowest *phd3:eGFP* related brightness observed. This phenotypic analysis confirmed that zArnt1 is particularly expressed in organs outside the central nervous system and predominantly in the liver of zebrafish larvae (Hill *et al.*, 2009). This is also broadly consistent with mouse data (Jain *et al.*, 1998).

As a consequence of the above considerations, since my data show that HIF pathway could still be partially activated in 5 dpf *arnt1*$^{-/-}$;*vhl*$^{-/-}$ larvae, I set up to test whether this was due to the presence of other *arnt* isoforms. To this end, I took advantage of a novel and rapid CRISPR/Cas9-based technology for directed gene

knock-out, initially developed by Burger *et al.*, 2016 and improved by Wu et al. 2018, as described in the chapter below.

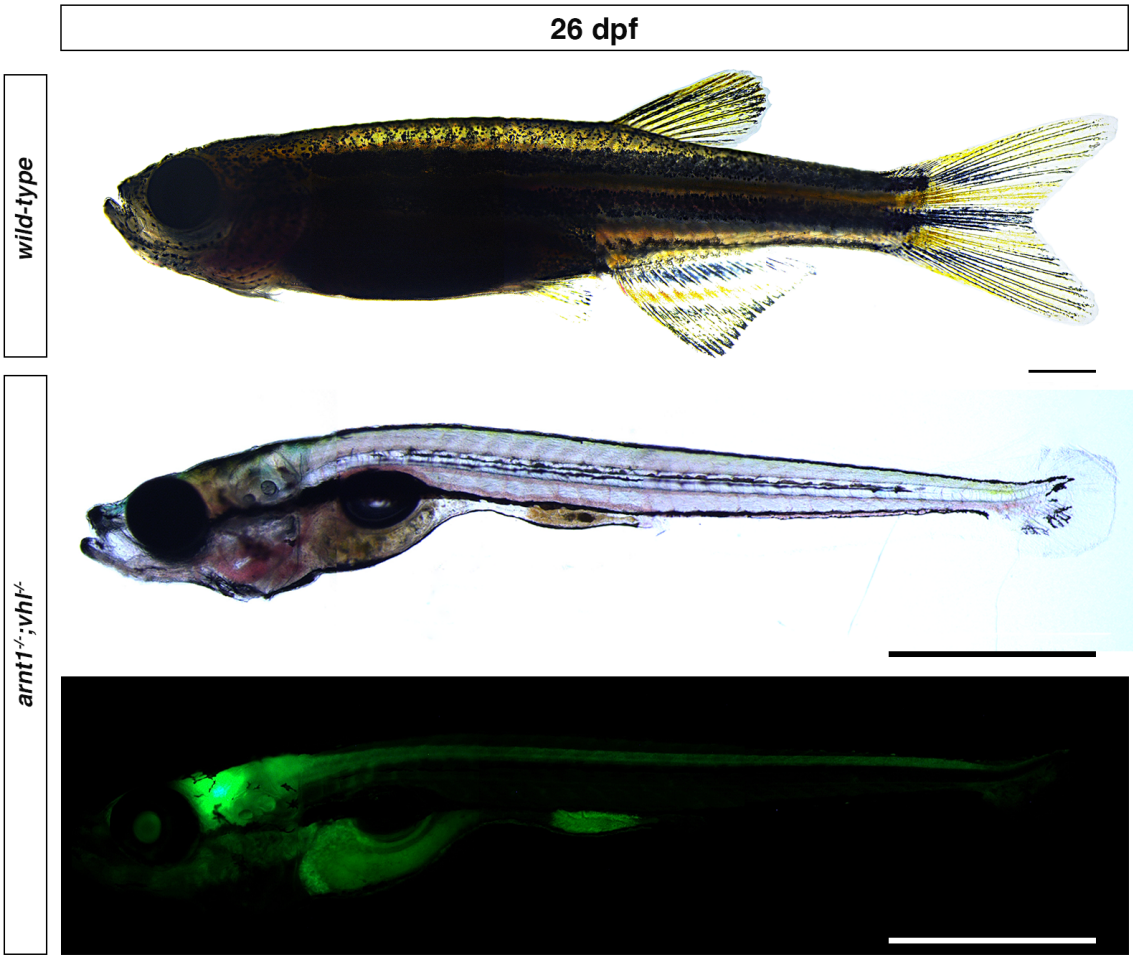

Figure 3.4. Representative picture of a 26 dpf zebrafish *arnt1*$^{+/-}$*; vhl*$^{+/-}$(*phd3:eGFP*) (top image, SL= 12.22 mm) and a *arnt1*$^{-/-}$*; vhl*$^{-/-}$*(phd3:eGFP)* (middle and bottom image, SL= 5.05 mm) larva analysed in this study. Scale bar: 1 mm. Fluorescence, exposure 2 sec.

3.3. Arnt1 and Arnt2 are mutually involved in assuring HIF response in zebrafish

As arnt1;*vhl* double mutants still moderately activate the *phd3:eGFP* HIF reporter, this chapter will be mainly focused on clarifying the differential expression pattern of Arnt1 and Arnt2 isoforms in the zebrafish and their relative importance in the HIF signalling.

The aryl hydrocarbon receptor nuclear translocator (ARNT) is a member of the bHLH/PAS protein super-family. It can dimerize with several PAS superfamily members, which mainly includes members of the hypoxia inducible factors family to assure adaptation to hypoxic conditions.

Both in mammals and in zebrafish ARNT is coded by *arnt1* and *arnt2* (Li, Dong and Whitlock, 1994; Drutel *et al.*, 1996; Hirose *et al.*, 1996; Prasch *et al.*, 2006). However, even if both genes are expressed in almost all the tissues during zebrafish embryonic development, tissue distribution of *arnt2* seems to be more limited than *arnt1* (Hill *et al.*, 2009).

Arnt2 has been the first Arnt isoform to be identified (Tanguay *et al.*, 2000; Wang *et al.*, 2000; Prasch *et al.*, 2006) and its mutation has been shown to be embryonic lethal in zebrafish larvae around 216 hpf (Hill *et al.*, 2009). Previous work also showed that Arnt2 isoform is predominantly expressed at the level of the brain, heart, liver and vascular endothelium in mice (Andreasen *et al.*, 2002). However, the function of Arnt2 still remains poorly understood. On the other hand, Arnt1 is primarily expressed in organ outside the central nervous system and is thought to be required for normal liver development in mice (Jain *et al.*, 1998; Walisser, Bunger, Glover and Bradfield, 2004; Walisser, Bunger, Glover, Harstad, *et al.*, 2004). In addition, there are no indications in

the literature about the spatial and temporal expression patterns of the zebrafish *arnt1* isoform.

To provide further insights about it, I compared the gene expression of both isoforms by knocking out one of them and by observing the corresponding phenotypic outcomes and the relative *phd3:eGFP*-related brightness of the other one. To this aim, I exploited the novel and rapid Wu et al 2018 mutagenesis protocol to generate G_0 CRISPants. Phenotypic analysis of Arnt2 CRISPant larvae created both in a *vhl*$^{+/-}$ and *arnt1*$^{+/-}$;*vhl*$^{+/-}$ background, was carried out on 5 dpf larvae using a Leica M165FC fluorescent stereo microscope.

By comparing the phenotype of *arnt1*$^{-/-}$;*vhl*$^{-/-}$ with the one of 4x *arnt2 gRNAs* CRISPR-injected *vhl*$^{-/-}$ (that will be called *arnt2*$^{-/-}$;*vhl*$^{-/-}$ hereafter), it was possible to show the presence of similarities between these two lines. In particular, the absence of both pericardial oedema and of excessive caudal vasculature, coupled to improved yolk usage and the presence of an inflated swim bladder were all noticeable traits in both double mutants at 5 dpf. Furthermore, *arnt1*$^{-/-}$;*arnt2*$^{-/-}$;*vhl*$^{-/-}$ CRISPants (triple mutants) exhibited an even more rescued *vhl* phenotype, which strongly resembled wild-type larvae (**figure 3.5A**).

Interestingly, by analysing and quantifying the expression of the *phd3:eGFP* transgene, it was possible to appreciate that *arnt2* CRISPR injected *vhl* mutants were characterized by a significant downregulation of the HIF reporter-related brightness at the level of the head (equals to 53%, P<0.0001), in the liver (equals to 54%, P<0.0001) and in the rest of the body (equals to 46%, P<0.0001), compared to uninjected *vhl* mutant larvae (**figure 3.5A & B**). On the other hand, *arnt1*$^{-/-}$;*vhl*$^{-/-}$ showed a weaker *phd3:eGFP* downregulation in the head (equals to 39%, P<0.0017), coupled to a stronger one both at the hepatic level (equal to 75%, P<0.0001) and in the

rest of the body (equals to 58% downregulation, P<0.0001), compared to *vhl*$^{-/-}$ larvae. Furthermore, when both *arnt1* and *arnt2* isoforms were simultaneously knocked-out, the downregulation of the hypoxia reporter was even stronger at the level of the head (equals to 74%, P<0.0001), liver (equals to 86%, P<0.0001) and in the rest of the body (equals to 83%, P<0.0001) compared to *vhl*$^{-/-}$ larvae (**figure 3.5A & B**). Of note, the *phd3:eGFP*-related brightness in the triple mutants (*arnt2* CRISPR injected arnt1$^{-/-}$; *vhl*$^{-/-}$) was similar to the one observed in wildtypes, at the level of the liver, the gut and the tail (**figure 3.5A, white arrowheads)**.

Overall, these data allow me to better understand the partial redundancy of these two isoforms in zebrafish larvae. My data allowed also to confirm that even if Arnt1 is not fundamental for survival, it is the main Arnt isoform expressed at the hepatic level, whereas Arnt2 is more expressed in the developing central nervous system (CNS), as supported by (Hill *et al.*, 2009). Finally, since both isoforms can form a functional complex with HIF-α and both appear to function in the same organs, this demonstrates that they have partially overlapping functions *in vivo* and they synergistically contribute to the HIF signalling pathway.

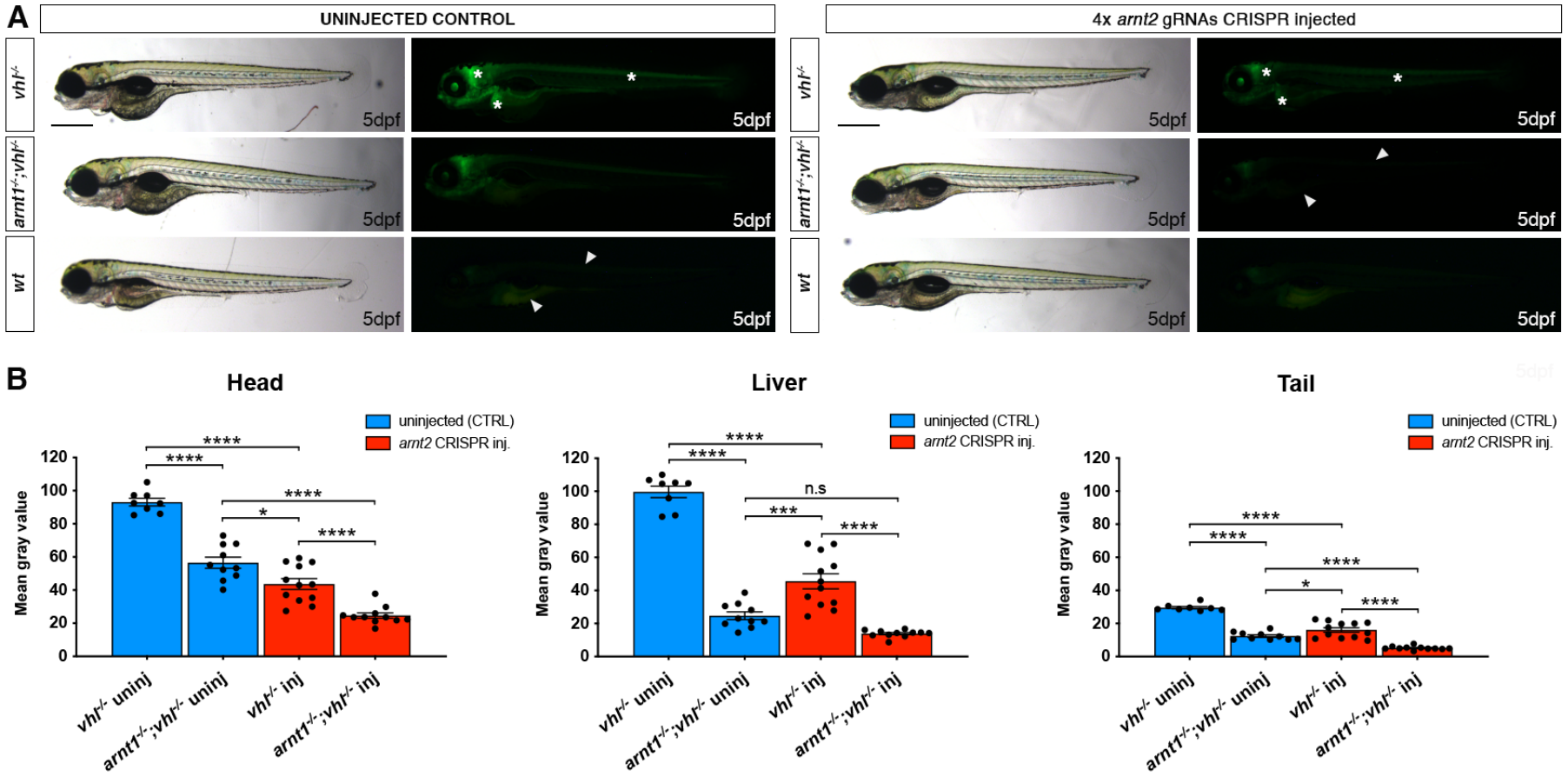

Figure 3.5. A Representative picture of 5 dpf CRISPANT mutants created by redundantly targeting *arnt2* gene via co-injection of 4x gRNAs in *arnt1*$^{+/-}$*;vhl*$^{+/-}$(*phd3:eGFP*) x *arnt1*$^{-/-}$*; vhl*$^{+/-}$(*phd3:eGFP*) derived embryos (n=300). Uninjected embryos were used as control (n=120). Fluorescence, exposure = 991,4 ms. Scale bar 500 µm. **B**. Statistical analysis performed on mean grey values quantification (at the level of the head, liver and tail), after phenotypic analysis on 5 dpf *arnt2* 4x gRNAs injected and uninjected larvae. *vhl*$^{-/-}$ uninjected n = 8 larvae: head 93.1 ± 2.33 (mean ± s.e.m); liver 99.65 ± 3.49 (mean ± s.e.m); tail 29.58 ± 0.73 (mean ± s.e.m). *arnt1*$^{-/-}$*;vhl*$^{-/-}$ uninjected n = 10 larvae: head 56.49 ± 3.36 (mean ± s.e.m); liver 24,7 ± 2.36 (mean ± s.e.m); tail 12.39 ± 0,75 (mean ± s.e.m). *vhl*$^{-/-}$ injected n = 12 larvae: head 43.69 ± 3.25 (mean ± s.e.m); liver 45.54 ± 4.57 (mean ± s.e.m); tail 16.09 ± 1.37 (mean ± s.e.m). *arnt1*$^{-/-}$*;vhl*$^{-/-}$ injected n = 11 larvae: head 24.66 ± 1.63 (mean ± s.e.m); liver 13.88 ± 0.66 (mean ± s.e.m); tail 5.16 ± 0.33 (mean ± s.e.m). Ordinary One-way ANOVA followed by Sidak's multiple comparison test (*P < 0.05; **P < 0.01; ***P <0.001; ****P < 0.0001).

3.4. Generation and characterisation of *gr* and *gr;vhl* knockout in zebrafish

3.4.1. Generation and characterisation of zebrafish *gr*$^{sh551/+}$;*vhl*$^{hu2117/+}$ line

Previous chemical screens carried out in my laboratory allowed the identification of GCs as potent activators of the HIF pathway (Santhakumar *et al.*, 2012; Vettori *et al.*, 2017). However, it still remains uncertain how GCs contribute to the HIF functions, if the GR is an obligatory factor for assuring the HIF response or vice versa, and how the interaction between these two major pathways occurs *in vivo*. For these reasons, a novel zebrafish *gr*^{sh551} mutant line was initially created in my laboratory.

The *gr*$^{sh551/+}$;*vhl*$^{hu2117/+}$ line was generated by Eleanor Markham (van Eeden lab, Bateson Centre, TUoS) in a *phd3:eGFP;vhl*$^{+/-}$ background, using CRISPR/Cas9-based mutagenesis. It was characterized by a 1bp deletion located at the beginning of exon 2 (first coding exon) which codes for the N-terminal domain (NTD). The injected embryos were partly genotyped to test CRISPR efficiency and partly raised till adulthood. Once fertile, this fish line was outcrossed with a wildtype AB fish, to test the presence of carriers for the mutated *gr* gene. To this end, I initially performed PCR-based genotyping on live adult zebrafish tail biopsies. The identified cluster of carriers (10 males and 9 females) was then incrossed and the resulting progeny was genotyped at 120 hpf, in order to raise the F1 generation. Finally, phenotypic analysis was carried out on F1 incrossed-derived embryos by using a fluorescent stereo microscope both on 3 dpf and 5 dpf larvae. Results showed that despite the presence of the *phd3:eGFP;vhl*$^{+/-}$ background, no significant *gr*-related phenotypes were detected in those larvae.

Since previous experiments performed in my lab showed that the strongest GC effect in terms of hypoxia reporter activation occurred at the hepatic level, I tried to sort larvae according to the *phd3:eGFP* related brightness in the whole body and, most of all, in the liver. To this end, I predicted to observe reduced *phd3:eGFP* expression in $gr^{sh551/sh551};vhl^{hu2117/2117}$ compared to $vhl^{hu2117/2117}$ larvae. However, genotyping results showed that there was no clear correlation between reduction in *phd3:eGFP* expression levels and having a mutant phenotype for gr^{sh551}.

To better test this mutant line, I performed a whole-mount Gr antibody staining on $gr^{sh551/+}$ incrossed 100 µM Betamethasone 17,21-dipropionate (BME, Sigma Aldrich) treated and untreated (DMSO, vehicle compound) embryos at 1 dpf. A clutch of both BME treated and untreated samples, with no primary antibody added, were also used as negative controls. BME treatment was used because, being a GR agonist, it might enhance the difference between $gr^{-/-}$ and wild-types. As a consequence of that, I would have expected to observe 25% of antibody stained embryos (putative *gr* mutants) with a loss of staining. However, no differences were detectable in all the clutches.

Whole-embryo genotyping analysis was also repeated on 5 dpf larvae sorted according to their brightness at the level of the liver. These larvae came from the same clutch of embryos that were antibody stained. I chose this developmental stage in order to exclude any possible maternal cortisol and *gr* transcripts contribution. Once again, no genotype-phenotype correlation was present (**figure 3.6**).

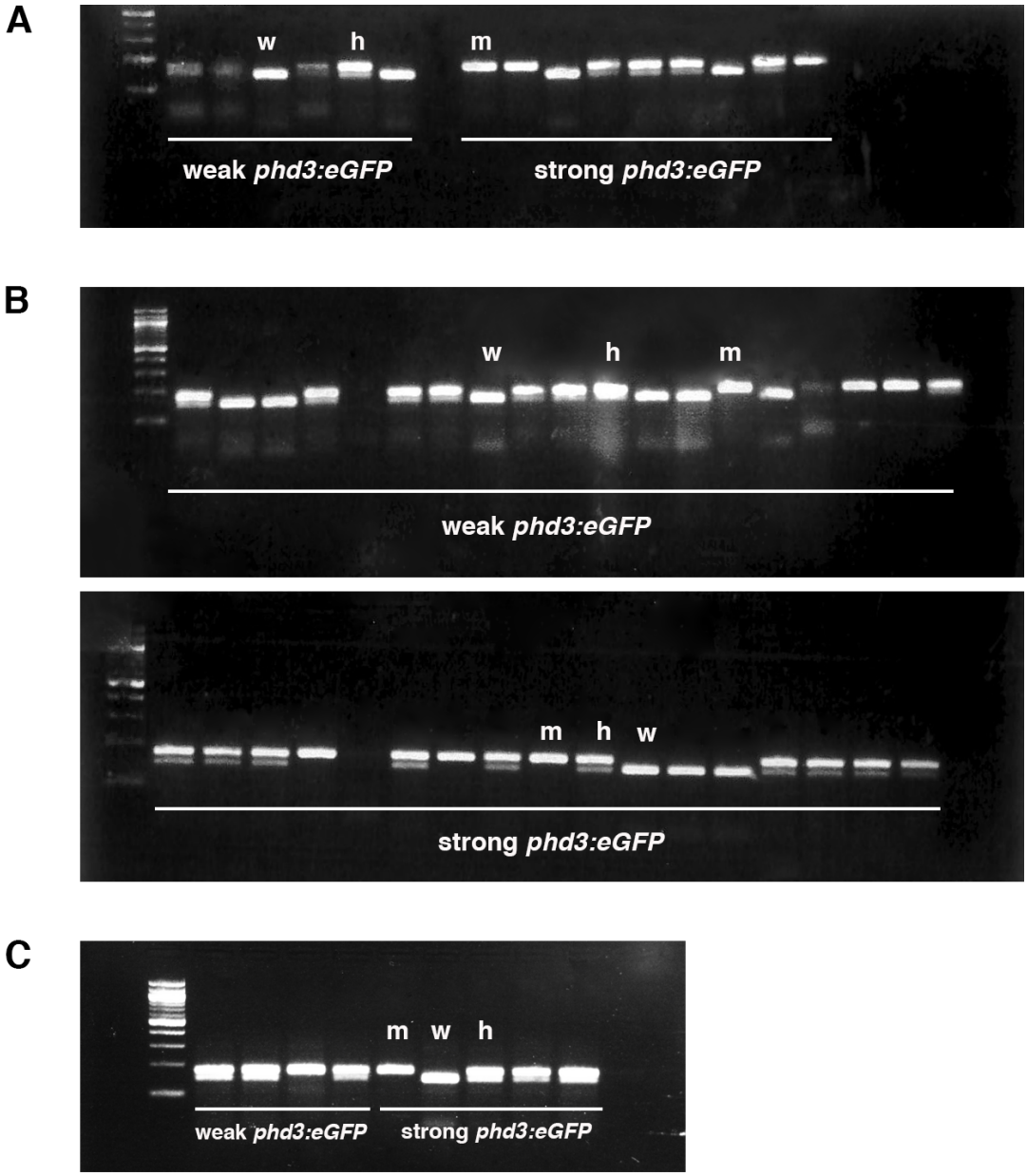

Figure 3.6. **A. Whole-embryo genotyping analysis on *gr*^{sh551} (*phd3:eGFP;vhl*$^{+/-}$) larvae sorted according to their *phd3*:e*GFP* brightness at 5 dpf**, deriving from the same clutch of embryos that were antibody-stained (n = 15). Samples A1-A6 showed weak *phd3:eGFP* brightness; samples A8-B4 showed strong *phd3:eGFP* brightness.

B. Genotyping results on *GFP* sorted *gr*^{sh551} (*phd3:eGFP;vhl*$^{+/-}$) 5 dpf larvae (n = 40). A1-B7: weak *phd3*:e*GFP* brightness; B8-C12 showed strong *phd3*:e*GFP* brightness. I have selected larvae which were not *vhl* mutants, sorting the ones that were brighter and the ones that were less bright among the weak ones. I did that in the expectation that if I had *gr* loss-of-function mutants, they might end up in the least bright group. Indeed, since previous work showed that GCs are able to activate the *phd3*:e*GFP* hypoxia reporter, I could expect that *phd3*:e*GFP* levels will be reduced in *gr* mutants.

C. Whole-embryo genotyping analysis on GR antibody stained 1dpf embryos. Embryos have been sorted according to their *phd3*:e*GFP* related brightness (n = 9). A1-A4: weak *phd3*:e*GFP*. A5-A9: strong *phd3*:e*GFP*.

In all cases shown here (**A, B, C**) the results did not show a clear genotype-phenotype correlation.

To further check whether this fish line carried a true null allele for *gr*, I also performed whole mount *in situ* hybridization (WISH) on DMSO and BME [30 µM] treated 5 dpf *gr*$^{sh551/+}$ incross derived larvae, using pro-opiomelanocortin a (*pomca*) as probe. I chose it because it plays a pivotal role at the level of the pituitary gland in the regulation of the GC-mediated stress response. For this reason, it provides a reliable readout of Gr function in zebrafish larvae (Griffiths *et al.*, 2012; Ziv *et al.*, 2012).

The administration of a synthetic *gr* agonist is supposed to elicit a strong GC response, which in turn triggers the so called "GC-GR mediated negative feedback loop" aimed to shut down their own biosynthesis. Notably, this mainly occurs at the level of the pituitary gland by downregulating the expression of *pomca* gene. This is because the stress-mediated activation of the HPI axis helps the organism to quickly cope with stressful situations and to allow adaptation aimed to restore homeostasis (de Kloet, Joëls and Holsboer, 2005). On the other hand, chronic HPI axis/*pomca* activation would generate constantly elevated GC levels, which would be detrimental to the organism (Laryea *et al.*, 2015).

In this regard, if Gr is not functional, the GC-GR negative feedback loop cannot occur and *pomca* expression cannot be downregulated (Griffiths *et al.*, 2012), resulting in an uncontrolled cortisol biosynthesis. Importantly, *in situ* hybridization analysis on 5 dpf *gr*$^{sh551/+}$ incross derived larvae revealed that both BME-treated *gr* wildtypes and mutants had reduced levels of *pomca* transcripts at the level of the anterior part of the pituitary gland (black arrowheads). This allowed to show that the existing *gr*^{sh551} was not a strong loss of function allele, as true null mutants should not be able to respond to BME treatment and should show upregulated *pomca* expression at the level of the anterior part of the pituitary gland (**figure 3.7**).

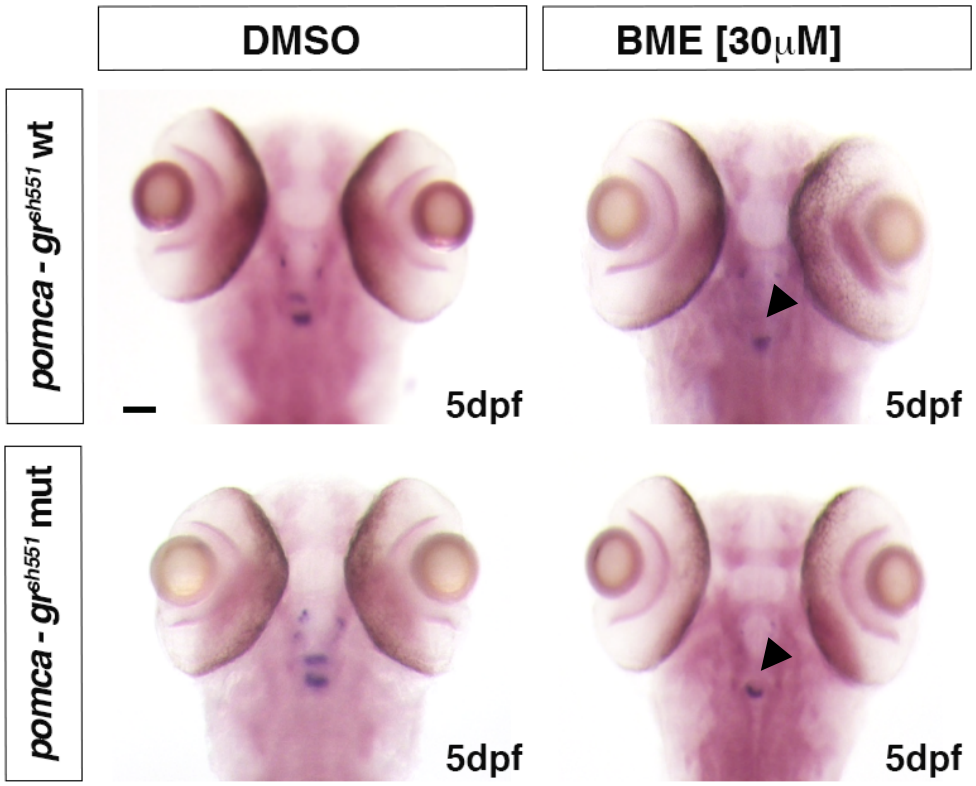

Figure 3.7. R**epresentative pictures of WISH performed on DMSO and BME [30 μM] treated *gr*$^{sh551/-}$*;vhl*$^{+/-}$*(phd3:eGFP)* mutant line, at 5 dpf, using *pomca* as probe.** *gr* siblings DMSO treated (n= 20/20 larvae) showed normal *pomca* expression; *gr* siblings BME treated (n= 20/20 larvae) showed downregulated pomca expression after BME treatment. On the other hand, DMSO treated (n= 18/20) *gr*$^{-/-}$ larvae showed upregulated pomca expression, whereas BME treated (n= 20/20) *gr*$^{-/-}$ larvae showed downregulated expression. As a consequence of that, since *gr*^{sh551} mutants were still able to activate the GC-GR negative feedback loop and to downregulate the pomca expression at the level of the anterior part of the pituitary gland, I showed that this mutant line was not a true null. Anterior part of the pituitary gland (black arrowhead). Scale bar 50 μm.

Finally, although the N-terminal transactivation domain (NTD) is conserved, literature reviews and sequence alignments of human, monkey, rat and mouse GRs revealed that there are other 8 conserved AUG start codons in the exon 2. In human, these were shown to produce various GR isoforms with progressively shorter N-terminal transactivation domain (NTD) (**figure 3.8**). These are formed due to the presence of alternative Kozak translation initiation sequences which can cause either ribosomal shunting or ribosomal leaky scanning mechanisms. This allow the generation of different GR subtypes with truncated N-termini (Yudt and Cidlowski,

2001, 2002; Oakley and Cidlowski, 2011; Merkulov and Merkulova, 2012; Rafacho *et al.*, 2014). As a consequence of the above considerations, even if the alternative Kozak translation initiation sequences have not been identified in zebrafish, it is plausible to speculate that these isoforms are also present in teleosts (*Kino et al.,2017*). For this reason, I speculate that these are still functional in *gr*^{sh551} mutant larvae and are able to compensate for the induced mutation. As a consequence of the above considerations, it was clear that a mutation in a different exon of *gr* gene was warranted.

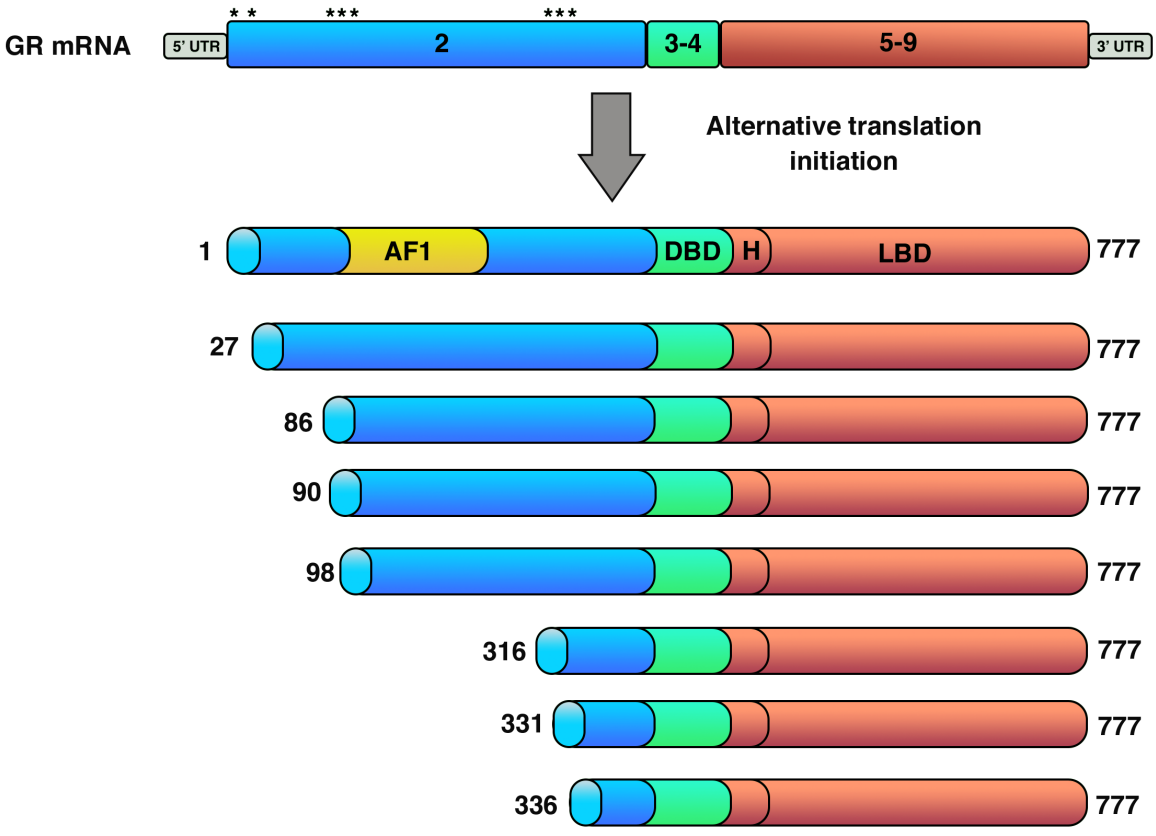

Figure 3.8 Representative picture of the hGR translational isoforms. Eight GR isoforms with progressively shorter N-terminal domains are produced as a consequence of the presence of eight different AUG start codons at the level of exon 2 in the GRα mRNA (location of the 8 AUGs is indicated by asterisks). The initiator methionine in each isoform (indicated by numbers) and the AF1 region (located at 77-262aa) are for the human GRα protein. (modified from R. Oakley, 2013)

3.4.2. Generation and characterisation of zebrafish *gr*$^{sh543/+}$ line

Since the *gr*^{sh551} mutant line proved to be not a null and the already existing *gr*^{s357} allele may still retain some activity via non-genomic pathways or tethering, promoting HIF activation upon GC treatment (Griffiths *et al.*, 2012; Ziv *et al.*, 2012; Vettori *et al.*, 2017), I generated a novel *gr* mutant line, as described below.

Of note, true null *gr* mutants has been proven to be hypercortisolaemic (Facchinello *et al.*, 2017; Faught and Vijayan, 2018b), due to the inability of GC to bind to their functional receptor (Gr). As a result, they fail to provide a negative feedback at the pituitary level and to consequently shut down their own biosynthesis (Facchinello *et al.*, 2017; Faught and Vijayan, 2018b).

In this regard, by exploiting the CRISPR/Cas9 method, I generated a zebrafish line characterized by an 11 bp deletion at the level of *gr* exon 3. The latter was predicted to have a truncated DNA binding domain, to lack the C-terminal ligand binding domain and for these reasons to be a true null (**figure 3.9**).

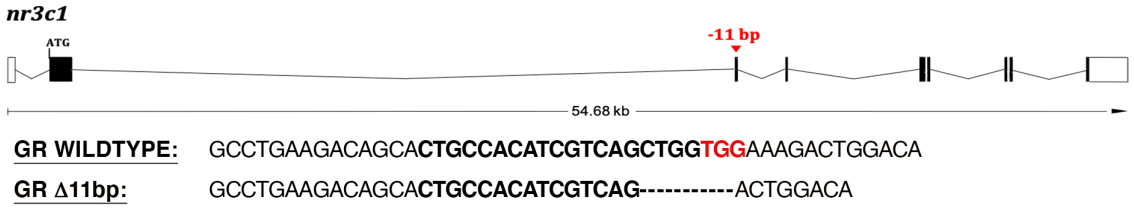

Figure 3.9. **Schematic representation of zebrafish *gr* (*nr3c1*) gene.** Exons are shown as boxes, introns as lines. The red arrowhead shows the position of a -11 bp deletion in exon 3 (encoding the DNA binding domain). In the *gr* wt and mutant sequence the CRISPR target site is bolded and the protospacer-adjacent-motif (PAM) sequence is denoted in red. Dotted line: bp deleted.

To confirm the efficiency of this mutation, I initially incrossed *gr* heterozygous fish and I treated the resulting clutch at 4 dpf for 24 hours with DMSO and BME [30 μM], respectively. Phenotypic analysis carried out on 5 dpf larvae revealed that vehicle treated *gr* mutants were morphologically similar to wild types, except for the presence of a reduced yolk usage and a flattened swim bladder (**figure 3.10A, right column**). As expected, synthetic GC treatment was ineffective on $gr^{-/-}$ larvae which showed only a mild pericardial oedema (**figure 3.10B, right column**). On the other hand, DMSO treated $gr^{+/-}$ and $gr^{+/+}$ larvae looked normal (**figure 3.10A, left column**), whereas betamethasone treatment was able to cause a more severe phenotype to them. In particular, it was possible to observe both an acute pericardial and periorbital oedema, coupled to a reduction of yolk usage and a not completely inflated swim bladder, compared to DMSO treated siblings (**figure 3.10B, left column**).

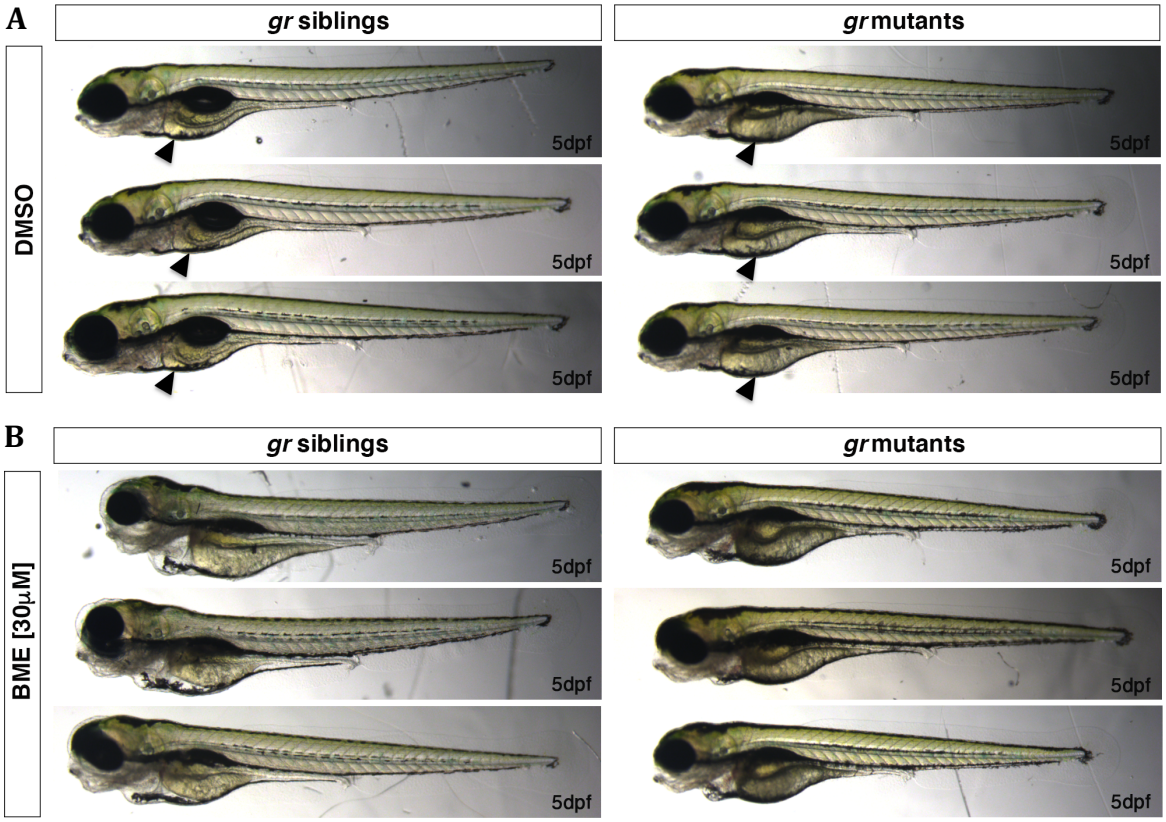

Figure 3.10 A. Representative pictures of DMSO treated 5 dpf *gr*$^{sh543/+}$ incross derived larvae (n = 120). Phenotypic analysis carried out at 5 dpf allowed to show the presence of a reduced yolk usage and a flattened swim bladder in DMSO treated *gr* mutants compared to wild types.

B. Representative pictures of BME [30 μM] treated 5 dpf *gr*$^{sh543/+}$ incross derived larvae (n = 120). Phenotypic analysis carried out at 5 dpf showed the presence of severe pericardial and periorbital oedemas in *gr* siblings as a consequence of BME treatment, which was instead negligible in *gr* mutants (black arrowheads: yolk usage).

To further confirm the *gr* loss-of-function, I repeated the same fish cross and I subjected *gr* larvae to visual background adaptation (VBA) test. Since VBA is a Gr-dependent neuroendocrine response, it can be exploited to check the presence of impairments related to GC biosynthesis and action (Griffiths *et al.*, 2012; Muto *et al.*, 2013).

Larvae derived from $gr^{+/-}$ incrossed fish were pre-sorted via VBA test according to dorsal melanophores size at 4 dpf, and finally sorted again and photographed at 5 dpf. As illustrated in the figure below, statistical analysis performed on melanophores size quantification at the level of the head, highlighted the presence of statistically significant differences between wild types (VBA+, 0.0009 mm^2, P=0.0123), and heterozygous (VBA+, 0.0015 mm^2, P<0.0001) and mutants' melanophores (VBA-, 0.0028 mm^2, P<0.0001) (**figure 3.11A**). In particular, only melanophores on the dorsal side of the head were used for the measurements and this region was always kept constant in order to improve the reliability of measurements. This is because the head is the main region containing the biggest melanophores and where VBA-induced changes are more evident. Moreover, since the head is wider than the tail, it is possible to precisely count all the melanocytes (even the partially overlapped ones) by observing both the cell membrane and the nucleus inside each melanophore, thanks to their darker colour.

To further demonstrate the presence of a true null allele, complementation test was also performed by crossing two *gr* heterozygous fish, which carried a different mutation at the level of the same exon (11 bp deletion and 1 bp insertion, respectively) and by analysing the resulting progeny via VBA test at 5 dpf. Importantly, a similar result was obtained for the trans-heterozygous incross-derived larvae, compared to the previously mentioned one. Indeed, a statistically significant difference was

quantified between wild-types (0.0008 mm^2), heterozygous (0.0013 mm^2) and mutant melanophores size (0.0021 mm^2) (**figure 3.11B**).

In both cases, PCR-based genotyping on negative VBA-response sorted samples revealed that most larvae were homozygous for the *gr* allele, whereas positive VBA-response sorted larvae were always *gr* siblings. Finally, since the same VBA responses were observed and quantified in trans-heterozygotes at 5 dpf, it confirms that the phenotype is due to a defect in GR and not due to mutation of a nearby gene.

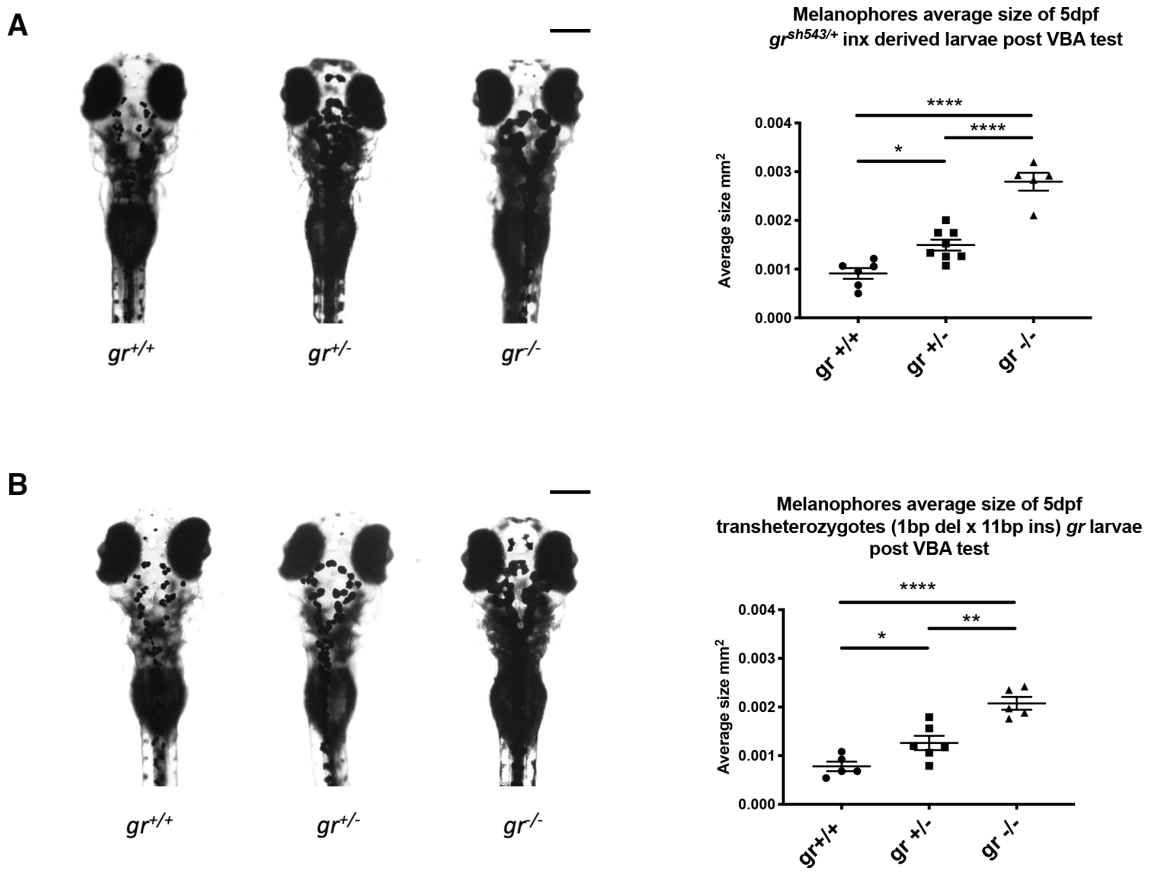

Figure 3.11 A. VBA test performed on *gr*$^{+/-}$ incross-derived 5dpf larvae (n=240), followed by genotyping and statistical analysis. Statistical analysis was performed on melanocytes average size (expressed in mm^2) of 5 dpf larvae post VBA test. Wildtype melanocytes size 0.0009 ± 0.0001 mm^2 (mean ± s.e.m, *P= 0.0123, n = 6 larvae), heterozygous melanocytes size 0.0015 ± 0.0001 mm^2 (mean ± s.e.m, ****P<0.0001, n=8 larvae) and mutant melanocytes size 0.0028 ± 0.0002 mm^2 (mean ± s.e.m, ****P<0.0001, n=5 larvae). One-way ANOVA followed by Sidak's multiple comparisons test has been used for calculating significance (*P<0.05; **P<0.01; ***P<0.001; ****P<0.0001). Scale bar 200 μM.

B. VBA test performed on *gr*$^{+/-}$ (1 bp deletion) x *gr*$^{+/-}$ (11 bp insertion) derived 5 dpf larvae (n = 130), followed by genotyping and statistical analysis. Statistical analysis was performed on melanocytes average size (expressed in mm^2) of 5 dpf larvae post VBA test. Wildtype melanocytes size 0.0008 ± 0.0001 mm^2 (mean ± s.e.m, *P= 0,0494, n=5 larvae), heterozygous melanocytes size 0.0013 ± 0.0001 mm^2 (mean ± s.e.m, ****P<0.0001, n=6 larvae) and mutant melanocytes size 0.0021 ± 0.0001 mm^2 (mean ± s.e.m, **P= 0.0017, n=5 larvae). One-way ANOVA followed by Sidak's multiple comparisons test has been used for calculating significance (*P<0.05; **P<0.01; ***P<0.001; ****P<0.0001). Scale bar 200 μM.

To test the effectiveness of the mutation at a transcriptional level, I performed whole mount *in situ* hybridisation (WISH) on 5 dpf DMSO and BME treated *gr*$^{sh543/+}$ incross derived larvae, using *pomca* as probe.

As expected, results showed the presence of upregulated *pomca* expression in DMSO treated *gr*$^{-/-}$ larvae at the level of the anterior part of the pituitary gland, compared to DMSO treated *gr* wild-types (**figure 3.12**, **top and bottom left, black asterisks**). This is because the absence of a functional GR avoids the GC-GR negative feedback loop to occur. For this reason, it was also possible to observe the presence of unvaried (still upregulated) pituitary *pomca* levels in BME treated *gr*$^{-/-}$ larvae, compared to DMSO treated *gr*$^{-/-}$ ones.

Vice versa, in BME treated *gr* wild types thanks to the presence of functional Gr, the synthetic GC treatment was able to trigger the negative feedback loop. Consequently, it was possible to observe a strong downregulation of *pomca* in BME treated *gr* siblings, compared to BME treated *gr* mutant larvae (**figure 3.12, top and bottom left, black arrowheads**). As a consequence of the above considerations, the fact that *gr*$^{-/-}$ larvae were insensitive to GC and showed an unvaried upregulated *pomca* expression after synthetic GC treatment confirmed the presence of a true null *gr* allele in my *gr*^{sh543} mutant line.

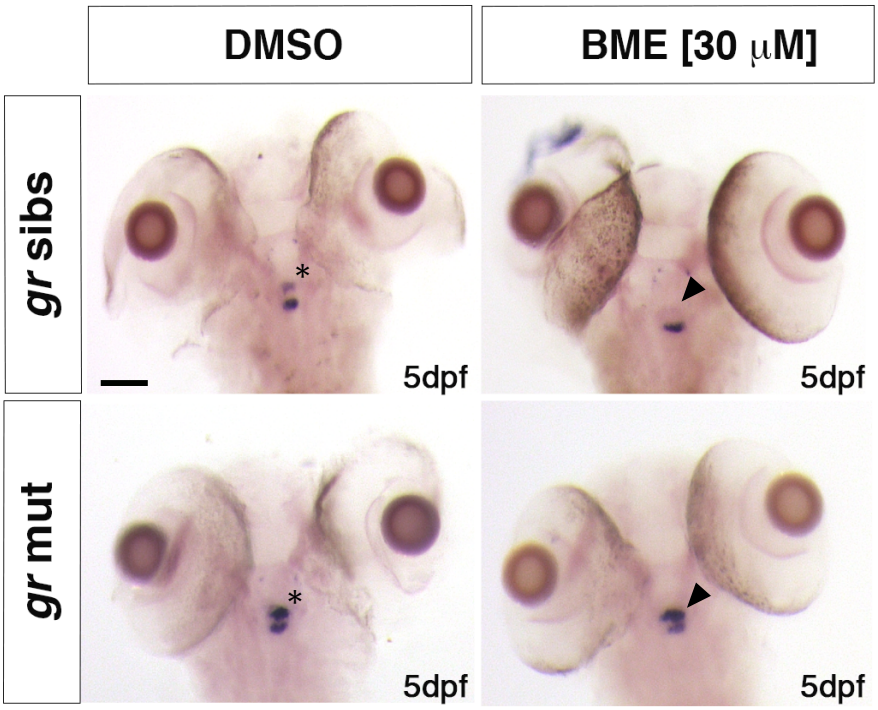

Figure 3.12. Representative pictures of WISH performed on DMSO and BME [30 μM] treated *gr* mutant line, at 5 dpf, using *pomca* as probe. Scale bar 100 μm. *gr* siblings DMSO treated (n = 30/30 larvae) showed normal expression (top left); BME treated *gr* siblings (n= 29/30 larvae) showed downregulated pomca levels (top right). On the other hand, both DMSO treated (n= 30/30) (bottom left) and BME treated (n= 30/30) (bottom right) $gr^{-/-}$ larvae showed upregulated *pomca* expression. Of note, the fact that BME treatment was not able to downregulate pomca expression in $gr^{-/-}$ allowed to confirm that these mutants were true nulls.

Lastly, Gr loss of function was also confirmed via RTqPCR analysis carried out in 5 dpf *gr* mutants. Once again, as expected, a strong downregulation of *fkbp5* mRNA levels quantified in $gr^{-/-}$ larvae both in the presence (BME treated, fold change = 0,01; P<0,0001) and in the absence of synthetic GC treatment (DMSO treated, fold change=0,01; P<0,0001) (**figure 3.13**) corroborated this. On the other hand, both in the presence and in the absence of synthetic GR agonists no significant alterations were quantified in the expression levels of the other three GC target genes selected (*pck1, il6st* and *lipca*). This could be due to the fact that *fkbp5* is a well-established readout of Gr activity (M. J M Schaaf, Chatzopoulou and Spaink, 2009), whereas the other aforementioned genes by not directly taking part of the GC-GR negative feedback loop, might have other inputs and developmental regulation as well.

In this regard, I set up to assess the expression levels of Fkbp5 (FK506 binding protein 51) as it plays a key role in the multiprotein Hsp90/Hsp70-based chaperone machinery which governs GR's sensitivity. It is also critical for assuring GR's correct folding, maturation, trafficking to the nucleus and DNA binding. Finally, both Fkbp5 mRNA and protein expression can be induced by Gr activation via intronic hormone response elements, which provides a super-short feedback loop for Gr-sensitivity (Binder, 2009). Consequently, this makes it the most reliable target gene to assess GR activity.

By contrast, the other aforementioned genes have been selected from previous zebrafish and mice studies (Le *et al.*, 2005; Facchinello *et al.*, 2017; Vettori *et al.*, 2017) as reliable readouts for hepatic lipid metabolism (*lipca*), inflammation (*il6st*) and glucose metabolism (*pck1*). So, they were supposed to provide a general overview of the changes that take place in an organism to adapt to hypoxic conditions. However, unlike *fkbp5* is expressed at early developmental stages, the endogenous cortisol-GR

mediated transcriptional regulation in response to stressors starts only at 96 hpf in zebrafish (Alsop and Vijayan, 2008; Nesan *et al.*, 2012; De Marco *et al.*, 2013; Weger *et al.*, 2018). For this reason, since these developmental changes occur during the synthetic GC treatment step (at 4 dpf), it is plausible to infer that the cortisol-induced expression of these specific target genes was not yet responsive.

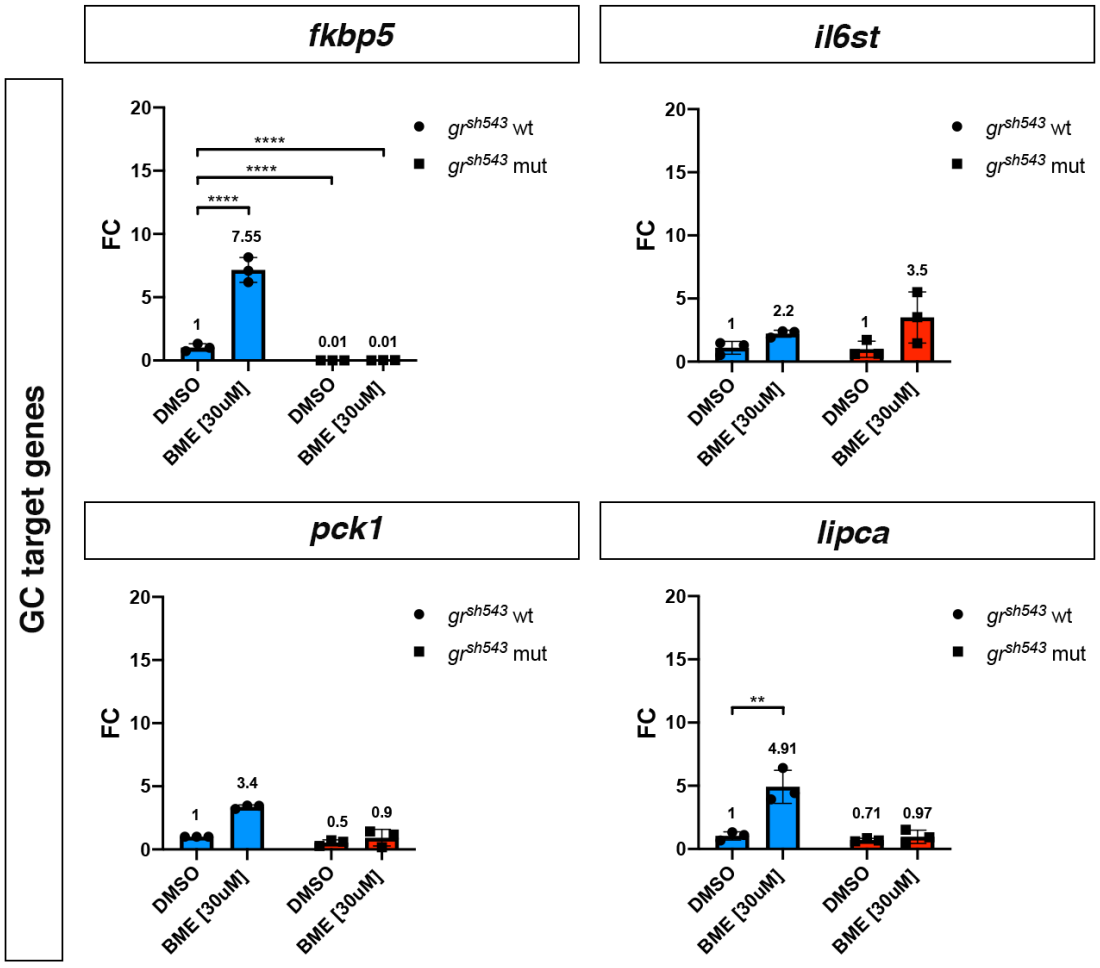

Figure 3.13. **RTqPCR analysis performed on four GC target genes expression (*fkbp5, il6st, pck1 and lipca*) has been carried out on both DMSO and BME [30 μM] treated *gr*$^{-/-}$ and siblings at 5 dpf**, (n = 10 larvae, per group, in triplicate). Statistical analysis, based on ΔΔCt values, was performed using Ordinary Two-way ANOVA followed by Dunnett's multiple comparison test. Data in the graph are instead shown as fold change values to facilitate understanding (*P < 0.05; **P < 0.01; ***P <0.001; ****P < 0.0001). Blue bars: wild-types and/or heterozygotes (siblings); red bars: mutants.

Observational analysis carried out during pair-mating on *gr*$^{-/-}$ adult fish also revealed the absence of distinctive chromatic and sexual traits which make them difficult to identify by gender. However, the typical body shape of a WT male zebrafish characterized by a slender body with its characteristic pinkish cast was not discernible in adult *gr*$^{-/-}$ fish, which looked more feminine and with a darker blue tint compared to wild-types.

Finally, due to the absence both of a functional glucocorticoid receptor and of a *gr* mediated negative feedback loop, *gr*$^{-/-}$ adult fish were not able to properly cope with stress, as previously described in the literature (Griffiths *et al.*, 2012; Ziv *et al.*, 2012; Facchinello *et al.*, 2017).

3.5. Discussion

The main focus of this chapter has been the generation and characterisation of novel zebrafish mutant lines aimed to investigate how the interaction between hypoxic and GC signalling occurs *in vivo*. To date, this scientific question has been primarily tackled through the use of *in vitro* studies, where interactions between different tissues and cell types are not easily modelled (Kodama *et al.*, 2003; Leonard *et al.*, 2005; Wagner *et al.*, 2008; Zhang *et al.*, 2015, 2016). Therefore, many questions regarding how this interplay precisely occurs in a whole organism and which is the molecular mechanism behind it still remain unanswered.

Previous research in my laboratory based on the use of an unbiased chemical screen identified synthetic GCs as activators of hypoxia-inducible factors (HIF) pathway, especially in the liver of zebrafish embryos. Importantly, a model for GCs to stabilize HIF via Von Hippel Lindau degradation has also been proposed (Vettori et al., 2017). In addition, in a counterintuitive way, GR loss of function was described by Facchinello and colleagues to hamper the transcriptional activity linked to immune response (i.e. of cytokines Il1β, Il8 and Il6 and of the metalloproteinase Mmp-13) (Facchinello et al., 2017). Finally, GR has been also found to synergistically activate proinflammatory genes by interacting with other signalling pathways (Langlais et al., 2008, 2012; Dittrich et al., 2012; Xie et al., 2019)

However, there are currently still controversial *in vitro* data and no clear indications about how the crosstalk between these two major signalling pathways precisely occur *in vivo.* In this regard, the elucidation of this intricated interplay may represent an important stepping-stone to reduce GC-related side effects and to treat

pathological conditions that are linked to hypoxia (i.e., asthma, rheumatoid arthritis, COPD, cancer, inflammation, VHL disease, High altitude sickness etc.).

To this end, I used both a genetic and pharmacological approach to alter these two pathways during the first 5 days post fertilisation of zebrafish embryos. In particular, I took advantage of two different mutant lines I have generated: *hif1β*^{sh544} (*arnt1*) and *gr*^{sh543} (*nr3c1*) respectively, coupled to the already existing *vhl*$^{hu2117/+}$*;phd3:eGFP*$^{i144/i144}$ hypoxia reporter line (Santhakumar *et al.*, 2012).

Initial analysis carried out on the *arnt1;vhl* mutant line showed that *arnt1* loss of function substantially attenuated *vhl* phenotype. Of note, double mutants were characterized by a reduced *phd3:eGFP* related brightness, improved yolk usage, properly developed and air-filled swim bladder as well as by the absence of pericardial oedema and excessive caudal vasculature, compared to *vhl*$^{-/-}$ larvae. However, beyond 5 days, the double mutants exhibited only partial recovery from the *vhl* phenotype, they developed well till 15 dpf, but subsequently failed to grow and thrive when compared to their siblings. Of note *arnt1* homozygous mutants were found to be viable and fertile, in contrast to both *vhl* and *arnt2* homozygous mutants, which are embryonic lethal by 8-10 dpf (Hill et al., 2009; van Rooijen et al., 2009).

Given these data, I set out to understand which was the difference in terms of spatial expression pattern of the two ARNT isoforms in zebrafish larvae. So far, the temporal and spatial expression of *arnt1* has been described only in developing mice (Jain *et al.*, 1998; Walisser, Bunger, Glover and Bradfield, 2004; Walisser, Bunger, Glover, Harstad, *et al.*, 2004) and there are just few information about *arnt2* expression pattern in zebrafish (Andreasen *et al.*, 2002; Hill *et al.*, 2009). Furthermore, in both cases, there are no information in the literature about their expression levels under upregulated HIF conditions. To examine this aspect, I exploited the rapid state-of-the-

art CRISPR method to generate G_0 mutants (Burger *et al.*, 2016; Wu *et al.*, 2018) to create *arnt2* mutants both in a *vhl* and in a *vhl;arnt1* background.

My data allowed to show that Arnt1, even if not fundamental for survival, is predominantly expressed in the liver and in organs outside the central nervous system of zebrafish larvae. Conversely, Arnt2 is mainly expressed in the developing central nervous system (CNS), as also reported by Hill et al. in 2009. However, the similarities observed in terms of *phd3:eGFP*-related brightness in both *arnt1*$^{-/-}$*;vhl*$^{-/-}$ and *arnt2* CRISPR injected *vhl* mutants suggest there is no strong functional separation. Finally, when both isoforms were simultaneously knocked out in a *vhl*$^{-/-}$ background, triple mutant larvae exhibited an even more rescued Vhl phenotype, which strongly resembled the wild-type's one. Importantly, an even weaker *phd3:eGFP*-related brightness overall coupled to normal yolk usage, properly developed and air-filled swim bladder and the absence of both pericardial oedema and excessive caudal vasculature were observed in *arnt2*-injected *arnt1;vhl* double mutants, compared to the uninjected ones. As a consequence of the above considerations, since both Arnt1 and Arnt2 can form a functional complex with HIF-α subunits and are expressed in the same organs, I speculate that both Arnt2 and Arnt1 have partially overlapping functions *in vivo* and are synergistically involved in assuring HIF response.

To further investigate the reverse role of GCs on HIF pathway, I initially tested the already existing *gr* mutant line, *gr*^{sh551}, for true null mutation. This line has been created in Van Eeden's laboratory because the existing *gr*^{s357} allele may still act non-genomically or via tethering method, promoting HIF activation upon GC treatment (Griffiths et al., 2012; Ziv et al., 2012; Vettori et al., 2017). Of note, due to the inability of GCs to bind to a functional receptor (GR), it has been proved that *gr* mutants are

hypercortisolaemic (Facchinello et al., 2017; Faught and Vijayan, 2018). This is because GCs, by failing to provide negative feedback cannot shut down their own biosynthesis (Griffiths *et al.*, 2012; Facchinello *et al.*, 2017; Faught and Vijayan, 2018a). Interestingly, this was translated into the presence of reduce yolk usage, coupled to a flattened swim bladder in *gr* mutants compared to wt siblings. In this regard, due to the importance of *gr* both in physiology and development, I speculate that *gr* mutants viability and phenotype could also be due to an overstated MR response induced by the presence of high cortisol levels. Of note, this aspect will be discussed in detail in the following chapter.

To confirm loss-of-function, I initially subjected gr^{sh551} larvae to a series of molecular and pharmacological analysis. Importantly, all the tests carried out on this mutant line showed no differences between wild-types and *gr* mutants, proving that the existing gr^{sh551} line does not carry a strong loss of function allele. In particular, the fact that gr^{sh551} mutants were able to respond to betamethasone treatment and to consequently downregulate *pomca* expression, as wild-type larvae did, confirmed the presence of a still functional Gr. Finally, detailed literature review unveiled the presence of 8 conserved start codons in the first coding exon (exon 2), which were shown to produce various GR isoforms with progressively shorter N-terminal transactivation domain (NTD) (Oakley and Cidlowski, 2011).

Given the need for a true null mutant line, I set out to generate a novel glucocorticoid receptor mutant line, named gr^{sh543}, which was predicted to have a truncated DNA binding domain and, therefore, no C-terminal ligand binding domain too. The absence of shrunk dorsal melanophores observed in gr^{sh543} mutants at 5 dpf, typical of a positive visual background adaptation response, represented the first evidence that the *gr*-dependent negative feedback was missing in mutants.

Furthermore, the failure of *gr*$^{sh543/sh543}$ to respond to betamethasone treatment by inhibiting *pomca* expression, as observed in wt larvae, via WISH analysis was the main evidence of *gr* loss of function. Finally, decreased baseline levels of *fkbp5* both in the presence and in the absence of BME treatment, as quantified via RTqPCR analysis, also supported this assumption.

Having fully tested these two fish lines (*gr*^{sh543} *and arnt1*^{sh544}) for true null mutations, I then attempted to answer to the questions: how does the inactivation of one of the two pathways affects the other one, and *vice versa*?

4. EFFECTS OF GC SIGNALLING ON HIF PATHWAY ACTIVATION

4.1. Introduction

GCs constitute a well-characterized class of lipophilic steroid hormones, which act as peripheral effectors of the hypothalamic-pituitary-adrenal/interrenal axis, playing a pivotal role in the stress response and the regulation of carbohydrate, lipid and protein metabolism (Alsop and Vijayan, 2009; Griffiths et al., 2012; Tokarz et al., 2013; Faught and Vijayan, 2018). GCs exert their function via direct binding to the intracellular GR (Bamberger, Schulte and Chrousos, 1996), and together act as a transcription factor, which can function either in a genomic or in non-genomic way (Stahn and Buttgereit, 2008; Mitre-Aguilar, Cabrera-Quintero and Zentella-Dehesa, 2015; Facchinello *et al.*, 2017; Panettieri *et al.*, 2019).

Synthetic GCs (i.e. betamethasone and dexamethasone), which are analogous to naturally occurring steroid hormones, have been extensively used for decades as anti-inflammatory drugs for treating pathological conditions which are very often related to hypoxia (i.e. acute mountain sickness, rheumatoid arthritis, ischemic injury, asthma, etc.) (Nikolaus, Fölscn and Schreiber, 2000; Neeck, Renkawitz and Eggert, 2002; Busillo and Cidlowski, 2013).

However, conflicting results have been reported in the last decade about the crosstalk between GC action and hypoxia (Kodama *et al.*, 2003; Wagner *et al.*, 2008). Moreover, due to the presence of adverse effects (Moghadam-Kia and Werth, 2010) and GC resistance (Barnes and Adcock, 2009; Barnes, 2011), their use has been

restricted. Therefore, extending the research on how precisely this interplay occurs *in vivo*, may have a wide physiological significance in health and disease.

In this chapter, the effect of GC on HIF signalling will be furthered via both a genetic and a pharmacological approach aimed to alter these two pathways during the first 5 days post fertilisation of zebrafish embryos. To this end, I took advantage of a GR mutant line (*gr*^{sh543}) I have generated, coupled to the aforementioned *vhl*$^{hu2117/+}$*;phd3:eGFP*$^{i144/i144}$ hypoxia reporter line (Santhakumar et al., 2012).

Of note, since cortisol has high affinity not only for GR but also for MR and they have been recently shown to be differentially involved in the regulation of stress axis activation and function in zebrafish (Faught and Vijayan, 2018), I also analysed the role of *mr* in the HIF response. To achieve this, I knocked-out *mr* in *gr*$^{+/-}$*;vhl*$^{+/-}$*;phd3:eGFP* incrossed derived embryos using the aforementioned G_0 mutagenesis CRISPant technology (Wu et al., 2018). Both phenotypic and molecular analysis of these mutant lines were carried out in combination with fluorescence and optical microscope imaging.

4.2. *gr* mutation partially rescues Vhl phenotype

To extend the knowledge on the role of GC on HIF signalling I started to analyse the effect of *gr* loss of function on *vhl* phenotype. To this purpose, I have initially crossed the glucocorticoid receptor mutant line ($gr^{sh543/+}$) I generated with the aforementioned $vhl^{hu2117/+}$;$phd3{:}eGFP^{i144/i144}$ HIF-reporter line. Genotyping analysis following fin-clipping procedure on 3 months old fish allowed to select carriers for both mutations.

Phenotypic analysis carried out on 5 dpf larvae, derived from a $gr^{+/-}$;$vhl^{+/-}$;*phd3:eGFP* incross revealed that *nr3c1* knockout may cause an efficient, but not complete rescue of *vhl* phenotype, in a way that resembled *arnt1* mutation (**figure 3.2A**). In particular, in accordance with the Mendelian ratio, one sixteenth of GFP positive larvae showed a 43% downregulation at the level of the head ($P<0.0005$), a 66% downregulation in the liver ($P<0.0005$) and a 51% downregulation in the tail (from the anus to the caudal peduncle) ($P=0.0020$), in terms of *phd3:eGFP*-related brightness, compared to 5 dpf $vhl^{-/-}$ larvae (**figure 4.1B**). PCR-based genotyping carried out on these larvae revealed that they were $gr^{-/-}$;$vhl^{-/-}$, which allowed me to confirm the presence of a genotype-phenotype correlation.

Of note, rescue was evident by morphology as well. Indeed, even if $gr^{-/-}$;$vhl^{-/-}$ displayed reduced yolk usage, they showed no pericardial oedema, a reduction in the ectopic vessel formation in the dorsal tail fin and a developed air-filled swim bladder (**figure 4.1A**). On the other hand, once again, *gr* homozygote mutant embryos in a $vhl^{+/-}$ or wild-type background, were morphologically similar to wild-types, except for the presence of reduced yolk usage, and adult $gr^{-/-}$ fish were viable and fertile.

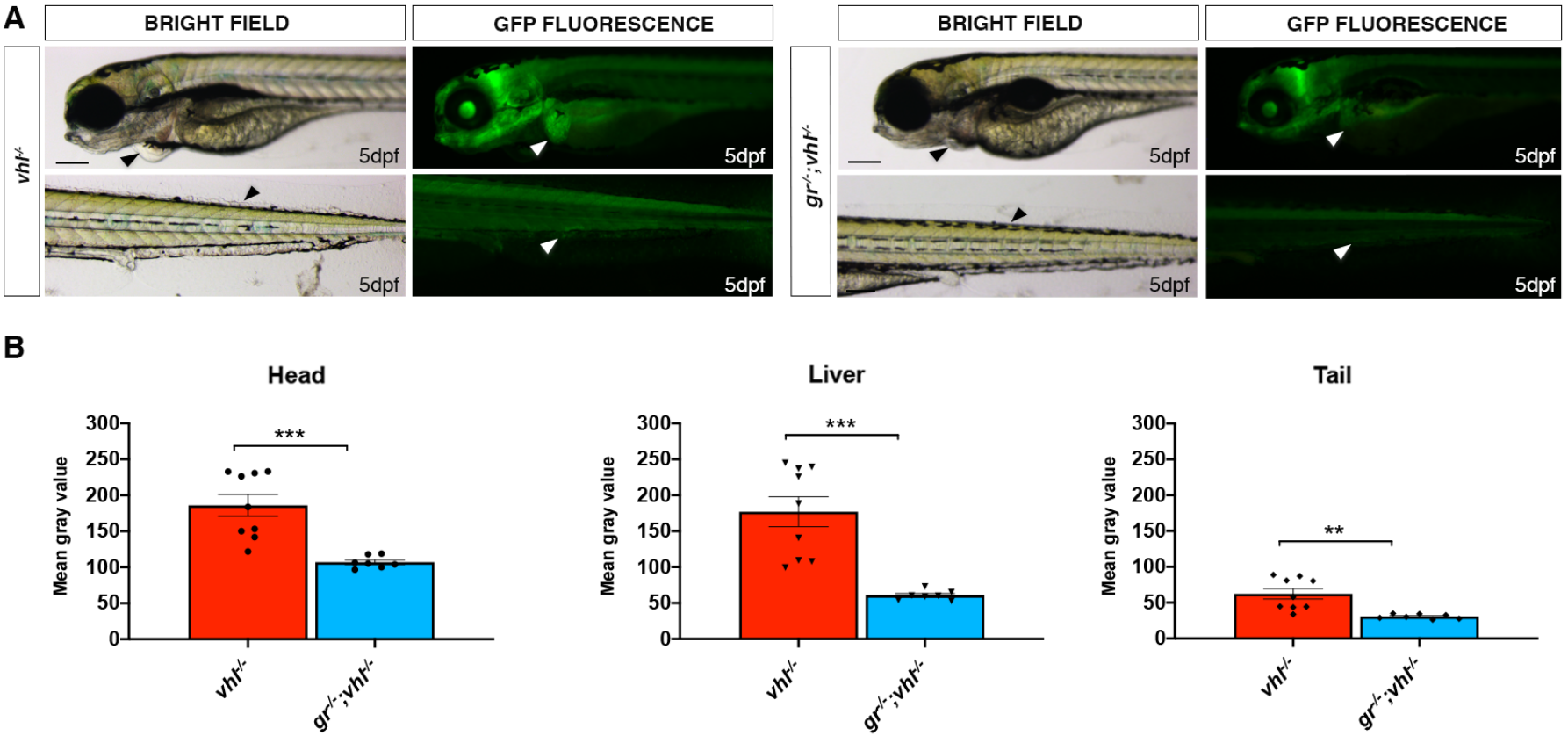

Figure 4.1. A. Magnified pictures of a representative 5 dpf *vhl*$^{-/-}$ larva compared to 5 dpf *gr*$^{-/-}$*;vhl*$^{-/-}$. Among the 450 GFP^{+} embryos derived from *gr*$^{+/-}$*;vhl*$^{+/-}$ (*phd3:eGFP*) x *gr*$^{-/-}$*;vhl*$^{+/-}$(*phd3:eGFP*), 27 larvae were characterized by the absence of pericardial oedema, no ectopic extra vasculature at the level of the tail, no bright liver and a reduced brightness in the rest of the body (black and white arrowheads). Genotyping post phenotypic analysis on sorted larvae confirmed genotype-phenotype correlation. Fluorescence, exposure = 2 seconds. Scale bar 200 μm. **B.** Statistical analysis performed on mean gray value quantification (fluorescence, exposure = 2 seconds) at the level of the head, liver and tail, after phenotypic analysis on 5dpf *gr*$^{+/-}$*;vhl*$^{+/-}$*(phd3:eGFP)* incross derived larvae. *vhl*$^{-/-}$ n= 9 larvae: head 186 ± 15.12 (mean ± s.e.m); liver 177.01 ± 20.85 (mean ± s.e.m); tail 62.34 ± 7.27 (mean ± s.e.m). *gr*$^{-/-}$*;vhl*$^{-/-}$ n = 7 larvae: head 106.96 ± 3.21 (mean ± s.e.m); liver 60.75 ± 2.56 (mean ± s.e.m); tail 30.67 ± 1.27 (mean ± s.e.m). Unpaired t-test (*P < 0.05; **P < 0.01; ***P <0.001; ****P < 0.0001).

In addition, by exploiting the *phd3:eGFP* transgene at the background, it was possible to check the effect of *gr* loss of function on the HIF-signalling pathway also in *gr* mutants larvae, in the presence or absence of synthetic GC treatment.

Interestingly, phenotypic analysis carried out at 5 dpf on the aforementioned clutch of larvae revealed that DMSO treated *gr* mutants were characterized, not only by a reduced yolk usage, but also by a significant downregulation of the *phd3:eGFP*-related brightness at the level of the liver, where HIF is mainly expressed, (equals to 27%, P=0.0406), compared to DMSO treated *gr* siblings (**figure 4.2 and 4.3**). This result strengthened the hypothesis that the presence of functional GR is fundamental to assure the HIF response at the hepatic level and to demonstrate that its function is detectable even in the presence of normoxic HIF levels.

Moreover, as expected, BME treated $gr^{-/-}$ larvae did not show any significant change in terms of *phd3:eGFP* expression levels, compared to DMSO treated *gr* siblings at the level of the head, liver and tail (**figure 4.3, red bars**). Vice versa, as expected, BME treated *gr* siblings were able to respond to synthetic GC administration as indicated by the upregulation of the hypoxia reporter both at the level of the head (equals to +41%, P=0.0077) and the liver (equals to +123%, P<0.0001), compared to DMSO treated *gr* siblings (**figure 4.2 and 4.3, blue bars**). These data confirmed once again that the gr^{sh543} mutation is a true null, and that BME is able to act as an activator of the HIF signalling pathway in zebrafish larvae.

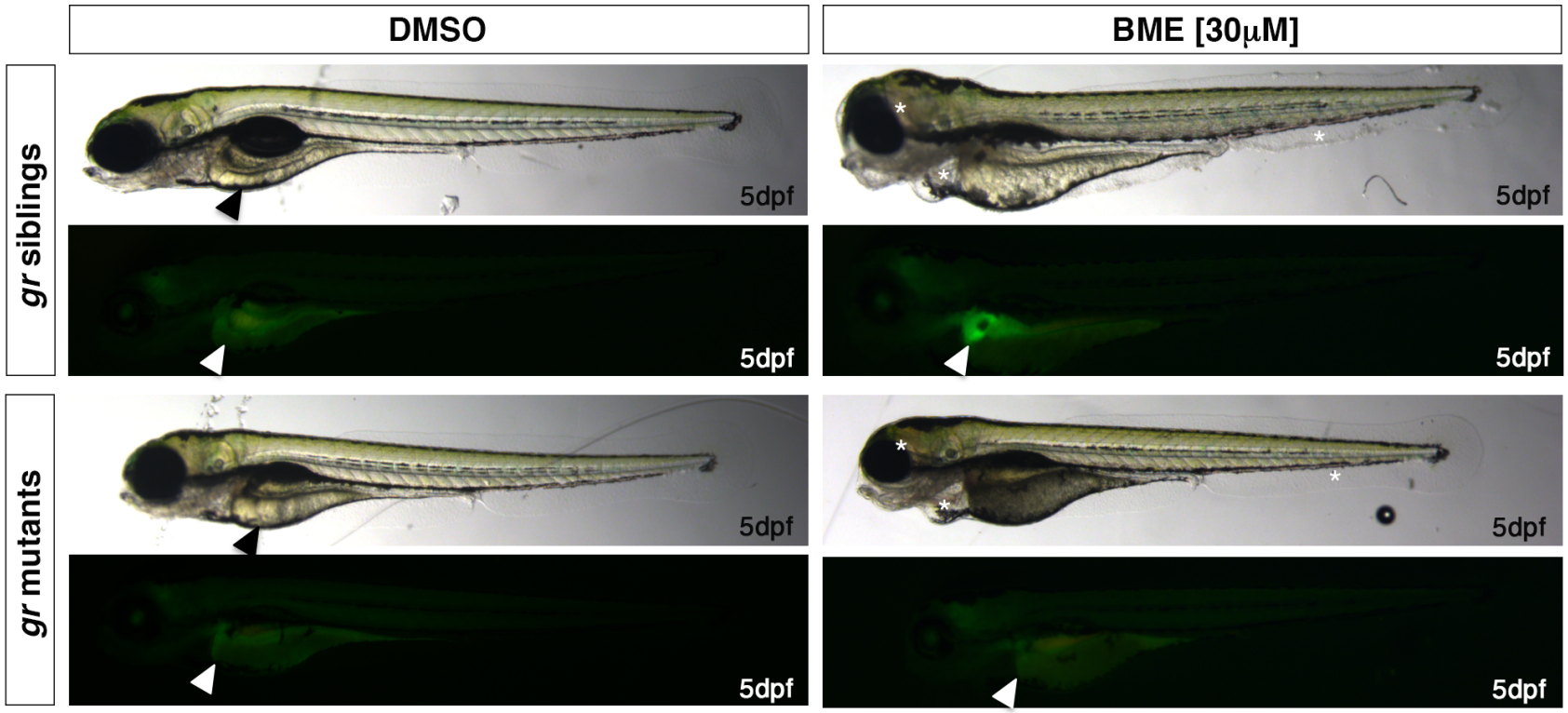

Figure 4.2 Representative pictures of DMSO and BME [30 μM] treated 5 dpf *gr*$^{sh543/+}$(*phd3:eGFP*) and *gr*$^{sh543/\ sh543}$ (*phd3:eGFP*) larvae (n=120). Phenotypic analysis carried out at 5dpf allowed to show the presence of a reduced yolk usage and a flattened swim bladder in DMSO treated *gr* mutants, coupled to a reduced *phd3:eGFP*-related brightness quantified at the hepatic level, compared to wild-types. As expected, BME treated *gr* mutants were not able to respond to the administration of synthetic GCs. In this regard, they only showed a mild pericardial oedema coupled to a still downregulated *phd3:eGFP*-related brightness, especially at the hepatic level. On the other hand, as a consequence of BME treatment, *gr* siblings were characterized by a severe pericardial and periorbital oedema, coupled to an increased hypoxia reporter expression in the liver (black arrowheads: yolk; white arrowhead: liver's GFP brightness; white asterisks: oedema).

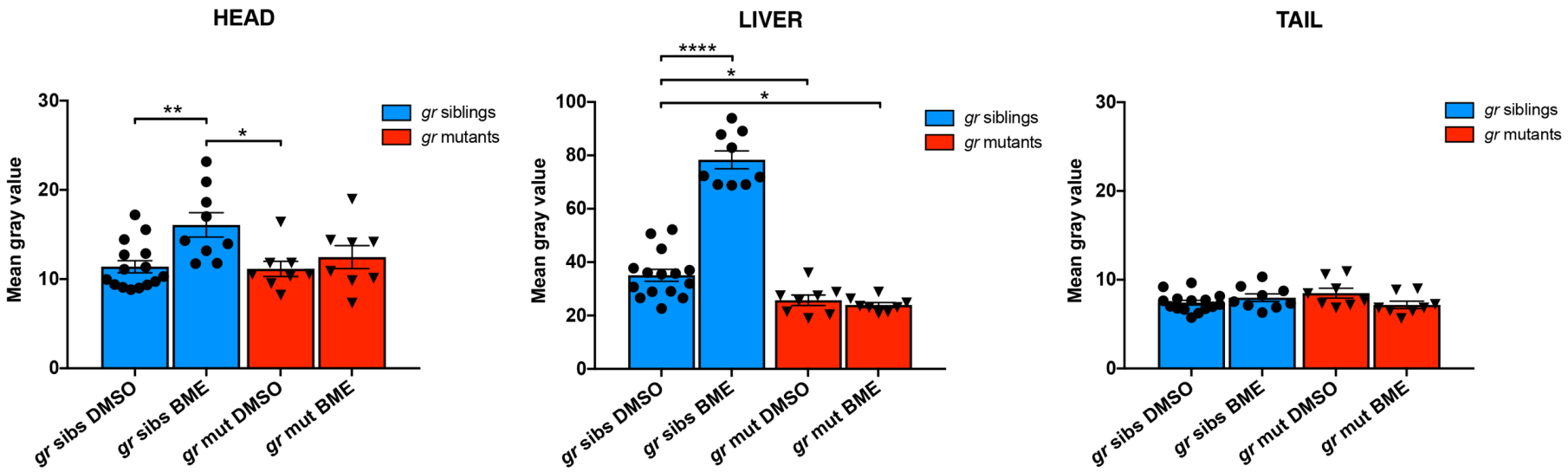

Figure 4.3 Statistical analysis performed on mean grey values quantification (at the level of the head, liver and tail), after phenotypic analysis on 5 dpf DMSO and BME [30 µM] treated *gr*$^{sh543/+}$(*phd3:eGFP*) incross-derived larvae. DMSO treated *gr* siblings n = 15 larvae: head 11.39 ± 0.68 (mean ± s.e.m); liver 35.08 ± 2.24 (mean ± s.e.m); tail 7.41 ± 0.27 (mean ± s.e.m). BME treated *gr* siblings n = 9 larvae: head 16.08 ± 1.37 (mean ± s.e.m); liver 78.33 ± 3.35 (mean ± s.e.m); tail 7.97 ± 0,43 (mean ± s.e.m). DMSO treated *gr* mutants n = 8 larvae: head 11.14 ± 0.86 (mean ± s.e.m); liver 25.73 ± 1.96 (mean ± s.e.m); tail 8.49 ± 0.56 (mean ± s.e.m). BME treated *gr* mutants n = 8 larvae: head 12.46 ± 1.29 (mean ± s.e.m); liver 23.95 ± 0.93 (mean ± s.e.m); tail 7.17 ± 0.42 (mean ± s.e.m). Ordinary One-way ANOVA followed by Sidak's multiple comparison test (*P < 0.05; **P < 0.01; ***P <0.001; ****P < 0.0001).

Finally, as previously done with the *arnt1*$^{+/-}$;*vhl*$^{+/-}$ mutant line, I also tested the efficacy of *nr3c1* mutation in rescuing the *vhl* phenotype. To this end, I attempted to raise *gr*$^{-/-}$;*vhl*$^{-/-}$ larvae after day 5 post fertilization. Three different tanks with the same size and the same amount of larvae (n = 20) have been used in this experiment: one for *gr*$^{-/-}$;*vhl*$^{-/-}$, one for *gr*$^{+/-}$;*vhl*$^{+/-}$ and one for wild-type AB larvae. Interestingly, whereas *vhl* mutants are inevitably deceased by 8-10 dpf (van Rooijen *et al.*, 2009), it has been possible to raise *gr*$^{-/-}$;*vhl*$^{-/-}$ larvae beyond 15 dpf. Then, similarly to the *arnt1*$^{-/-}$;*vhl*$^{-/-}$ larvae scenario, they failed to grow and thrive when compared both to their heterozygous siblings and wild-type (AB). This led me to euthanise them due to welfare concerns at 21 dpf (**figure 4.4**).

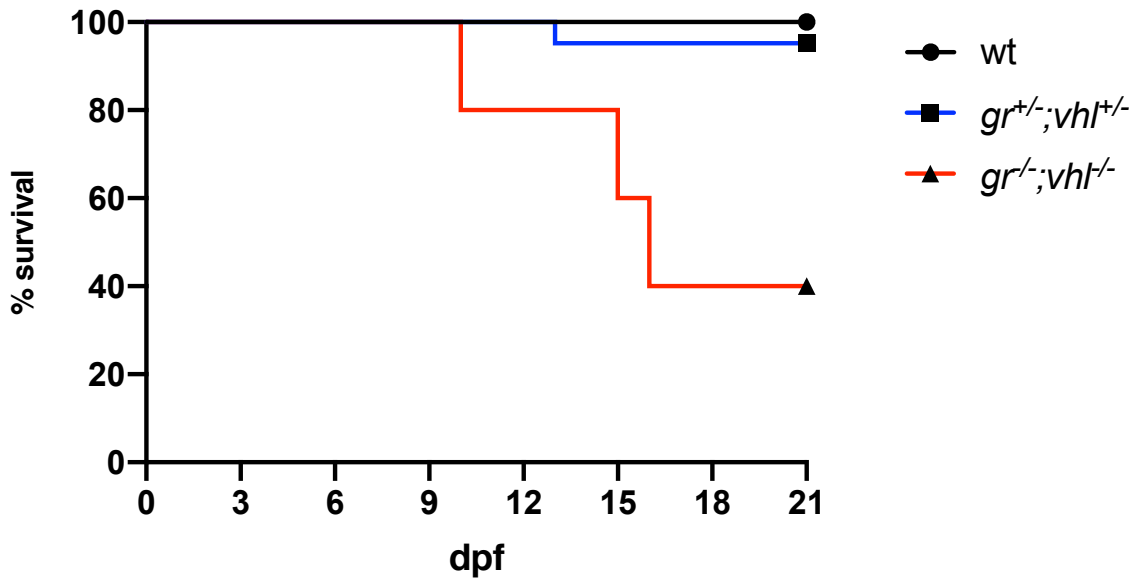

Figure 4.4 Kaplan-Meier survival curves of the zebrafish *gr*$^{+/-}$; *vhl*$^{+/-}$*(phd3:eGFP)* line analysed in this study. Time is shown in days. Wildtypes n = 20; *gr*$^{+/-}$; *vhl*$^{+/-}$ n = 20; *gr*$^{-/-}$; *vhl*$^{-/-}$(*phd3:eGFP*) n = 5. The Log-rank (Mantel-Cox) test was used for statistical analysis. *gr*$^{-/-}$; *vhl*$^{-/-}$(*phd3:eGFP*) vs. *gr*$^{+/-}$; *vhl*$^{+/-}$, ****P < 0.0001; *gr*$^{-/-}$; *vhl*$^{-/-}$(*phd3:eGFP*) vs. wt, ****P < 0.0001.

Phenotypic analysis performed on *gr*$^{-/-}$;*vhl*$^{-/-}$ larvae at 21 dpf showed the presence of substantial morphological differences compared to both with wild-types and *gr;vhl* siblings (**figure 4.5**). Double mutant body length (standard length (SL) = 4,66 mm) was comparable to a 13 dpf wild-type larva, according to Parichy et al. 2009 study (Parichy *et al.*, 2009), but not to its corresponding developmental stage. Vice versa, the body length of 21 dpf *gr*$^{+/-}$;*vhl*$^{+/-}$ siblings (SL = 10,94 mm) matched the standard length of wild-type larvae (SL = 10,74 mm) and no particular phenotypic traits have been observed in them.

Interestingly, 21 dpf *gr*$^{-/-}$;*vhl*$^{-/-}$ larvae showed a still clear body, a larval-like anteriorly protruding open mouth and a visible gut beneath the swim bladder, which are typical traits of a 11-13 dpf wildtype larva (Kimmel *et al.*, 1995). An early larval pigment pattern with small melanophores in stripes was also observable over the dorsal and ventral myotomes (not dispersed over the yolk sac). As previously observed in the *arnt1*$^{-/-}$;*vhl*$^{-/-}$ larvae, the head of 21 dpf *gr*$^{-/-}$;*vhl*$^{-/-}$ did not exhibit the expected dorsal indentation at the level of the pineal gland, which normally appear in 5.7 mm SL larvae. In addition, an increasingly pronounced caudal fin condensation, coupled to the appearance of the first fin rays, typical of a ~4.9 mm SL larva, were not yet visible. Moreover, the slight bulge in the dorsal fin fold as well as the one on the ventral side were not yet apparent. Finally, the distal end of the larval fin fold was still relatively rounded over the caudal fin (**figure 4.5**). Consequently, despite the increased lifespan of these double mutants, the absence of properly developed traits coupled to a reduced body length are all distinct signs of a substantial developmental delay.

As a consequence of the above considerations, these results confirmed that *gr* mutation is able to partially rescue the Vhl phenotype and to double the lifespan of *vhl* mutant larvae. However, since *gr*$^{-/-}$;*vhl*$^{-/-}$ did not show fully rescued traits, I speculate

that this could be due to the presence of the mineralocorticoid receptor (MR) that could still act on the HIF signalling pathway.

Since both double mutant embryos and wild-type siblings have been sorted according to their *phd3:eGFP*-related brightness at 5 dpf, a further confirmation of their genotype was provided by the presence of a still moderately upregulated brightness in 21 dpf $gr^{-/-};vhl^{-/-}$ larvae, compared to the low basal levels observed in $gr^{+/-};vhl^{+/-}$ siblings (**figure 4.5**).

Altogether, these data indicate for the first time in an *in vivo* animal model, that Gr function is essential to assure a proper HIF response in zebrafish larvae. Furthermore, the fact that Gr loss of function was able to partially ameliorate the phenotype of *vhl* mutant and to double the lifespan of $vhl^{-/-}$ larvae, may shed light on important clinical applications. Finally, the fact that only a partial rescue was observed, highlighted the possibility that also MR might have a key role in assuring the HIF signalling.

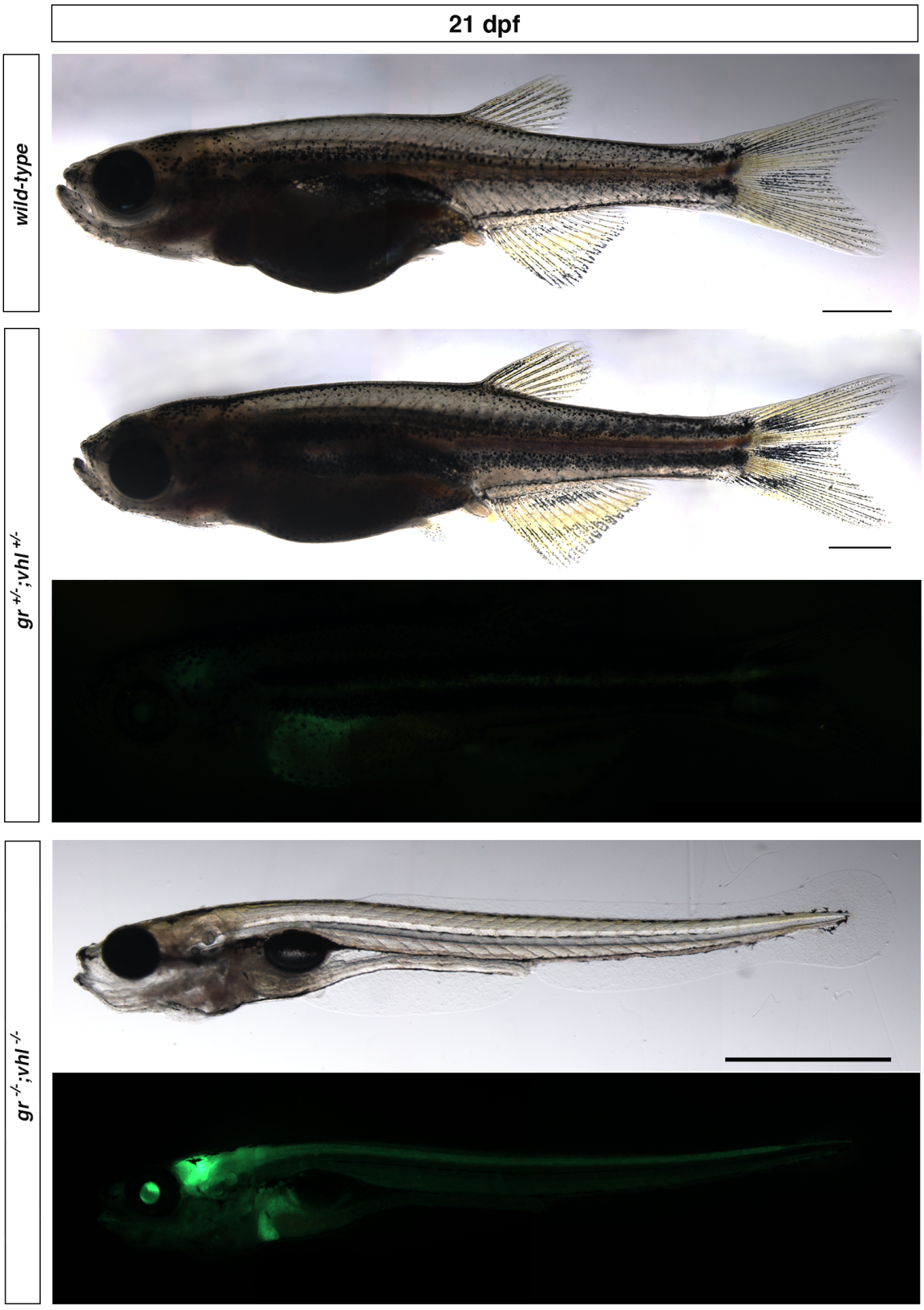

Figure 4.5 Representative picture of a 21 dpf zebrafish WT (top image, SL = 10.74 mm), a 21 dpf *gr*$^{+/-}$*; vhl*$^{+/-}$(*phd3:eGFP*) (middle image, SL= 10.94 mm) and a 21 dpf *gr*$^{-/-}$*; vhl*$^{-/-}$*(phd3:eGFP)* (bottom images, SL= 4,66 mm) larva analysed in this study. Scale bar: 1 mm. Fluorescence, exposure 2 sec.

4.3. *gr* loss of function can further reduce HIF signalling in *arnt1*$^{-/-}$;*vhl*$^{-/-}$ larvae

The similarities between *arnt1* and *gr* mutations could mean that they work in a single linear "pathway". If this assumption was true, mutation of both should not lead to a further attenuation of the reporter expression. To test this, I bred the *gr*^{sh543} mutant line with the *arnt1;vhl* double mutant line and then I crossed *gr*$^{+/-}$;*arnt1*$^{+/-}$;*vhl*$^{+/-}$ triple carrier fish, once adults.

Phenotypic analysis performed on 5 dpf *phd3:eGFP* positive larvae (n = 488) showed a small class of larvae with an even more rescued phenotype and a stronger downregulation of the *phd3:eGFP* related brightness, compared to both *gr*$^{-/-}$;*vhl*$^{-/-}$ and *arnt1*$^{-/-}$;*vhl*$^{-/-}$ double mutants (**figure 4.6**). Moreover, these larvae were characterized by the absence of pericardial oedema (black arrowheads, left) and the lack of ectopic extra vasculature at the level of the tail (black arrowheads, right). Of note, they were also characterized by an even more reduced expression of the hypoxia reported in the head and in the rest of the body (white arrowheads, right) coupled to the absence of a visible *phd3:eGFP* expression in the liver (white arrowheads, left). These 7 putative very weak eGFP^{+} larvae were selected and genotypic analysis confirmed that 5 out of 7 were indeed *gr*$^{-/-}$; *arnt1*$^{-/-}$;*vhl*$^{-/-}$ larvae.

Of note, these triple mutants showed a 54% downregulation at the level of the head, a 71% downregulation in the liver and a 72% downregulation in the tail region, in terms of *phd3:eGFP*-related brightness compared to *vhl*$^{-/-}$ (**figure 4.6**). As a consequence of the above considerations, these data suggest that GCs are likely to act on both Arnt1 and Arnt2 mediated HIF signalling pathway.

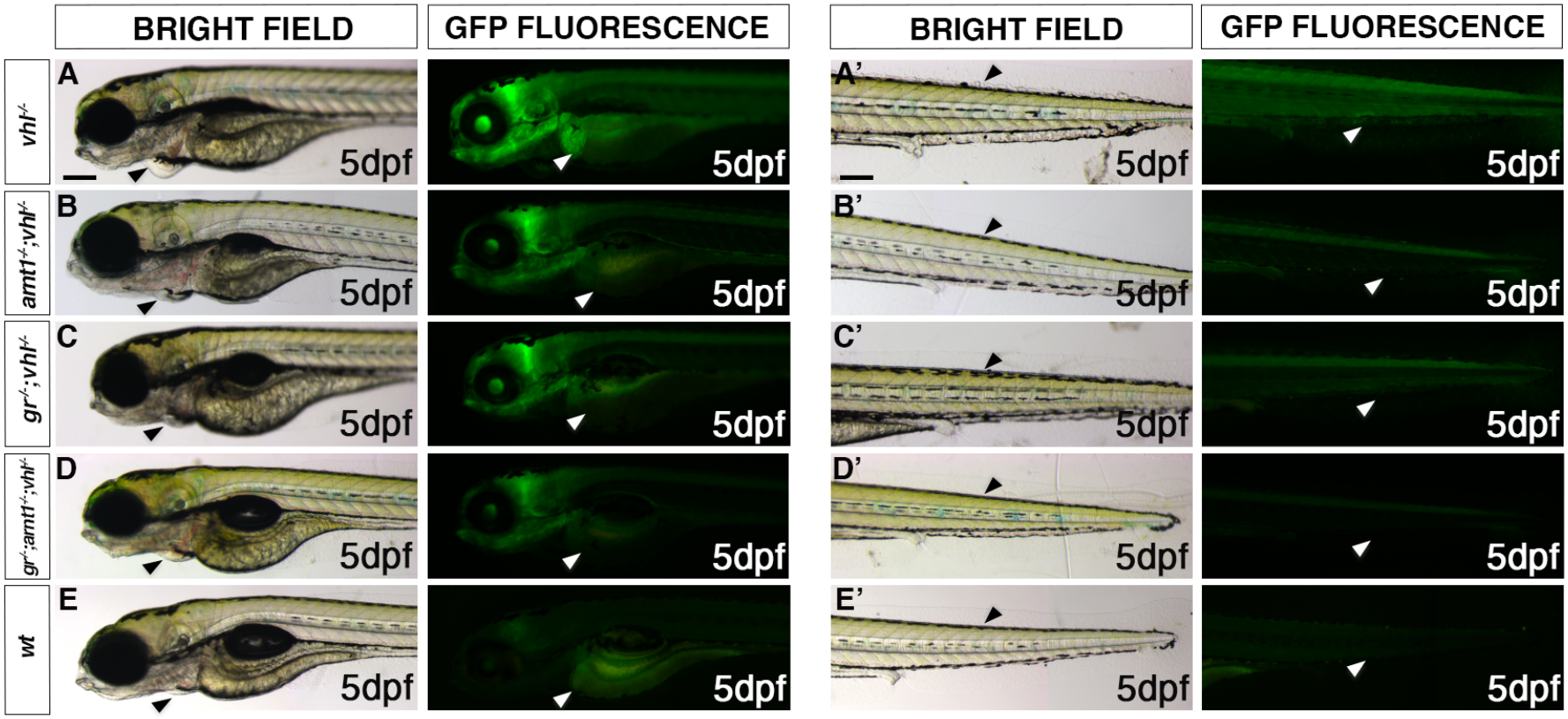

Figure 4.6A. *gr* loss of function effect is stronger when HIF-signalling is moderately upregulated. A-E. Representative picture of the main differences between *vhl*$^{-/-}$, *arnt1*$^{-/-}$;*vhl*$^{-/-}$, gr$^{-/-}$;vhl$^{-/-}$ and triple *gr*$^{-/-}$;*arnt1*$^{-/-}$;*vhl*$^{-/-}$ larvae at 5 dpf. Among the 488 *phd3:eGFP* positive larvae analysed, 7 larvae were characterized by the absence of pericardial oedema (black arrowheads, left), no ectopic extra vasculature at the level of the tail (black arrowheads, right), no visible phd3:eGFP HIF reporter in the liver (white arrowheads, left) and even more reduced levels of this marker in the head and in the rest of the body (white arrowheads, right). Genotypic analysis allowed to confirm the presence of a genotype-phenotype correlation in 5 out 7 samples and to prove that they were triple mutants. Fluorescence, exposure = 2 seconds. Scale bar 200 μm.

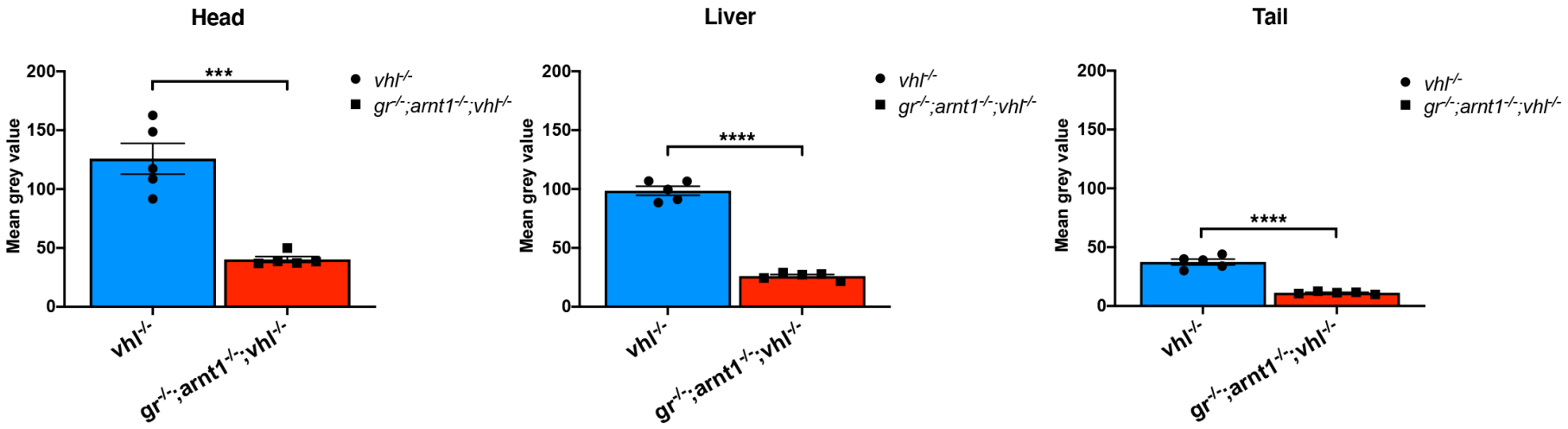

Figure 4.6B. Statistical analysis performed on mean grey values quantification (at the level of the head, liver and tail), after phenotypic analysis on 5 dpf *gr+/-;arnt1+/-;vhl*$^{+/-}$*(phd3:eGFP)* incross-derived GFP+ larvae (n = 488). *vhl*$^{-/-}$ n = 5 larvae: head 125.82 ± 13.05 (mean ± s.e.m); liver 98.52 ± 3.8 (mean ± s.e.m); tail 37.43 ± 2.45 (mean ± s.e.m). *gr*$^{-/-}$*;arnt1*$^{-/-}$*;vhl*$^{-/-}$ n = 5 larvae: head 40.24 ± 2.46 (mean ± s.e.m); liver 26.07 ± 1.31 (mean ± s.e.m); tail 11.22 ± 0.47 (mean ± s.e.m); unpaired t-test (***P = 0.0002; ****P < 0.0001).

4.4. Betamethasone-induced HIF response is Arnt1 dependent

To further study the effect of GCs on the HIF signalling pathway, I performed BME [30 μM] treatment on all the available mutant lines. Of note, unlike cortisol, betamethasone has a really high affinity for GR, but has an insignificant affinity for MR (Montgomery *et al.*, 1990; Fromage, 2012). Moreover, its effect has been mainly appreciated in the zebrafish liver.

In particular, I observed in 5 dpf *gr* wildtypes larvae the presence of a mild upregulation of the HIF reporter-related brightness at the hepatic level, compared to untreated controls (**figure 4.2, *gr* siblings: DMSO vs BME treated**). Interestingly, betamethasone treatment was also able to further increase the *phd3:eGFP*-related brightness at the level of the head and the liver of 5 dpf *vhl*$^{-/-}$ larvae, compared to the DMSO treated counterpart. (**figure 4.7A-A'**). Of note, this was quantified as a 20% upregulation at the level of the head (P=0.017) and as a 61% upregulation in the liver (P<0.0001) of the hypoxia reporter expression, compared to DMSO treated *vhl*$^{-/-}$ larvae (**figure 4.7E**).

This data was also confirmed by whole-mount *in situ* hybridisation carried out on *vhl*$^{+/-}$ incrossed-derived larvae at 5 dpf analysis using both lactate dehydrogenase A (*ldha*) (**figure 4.8B–B', black arrowheads**) and prolyl hydroxylase 3 (*phd3*) as probes (**figure 4.8D–D', black arrowheads**). These two genes were chosen as antisense RNA probes, as they provide a reliable readout of HIF signalling pathway in zebrafish larvae. Indeed, both are upregulated by HIF itself under hypoxic conditions or in a *vhl*-deficient background. In particular, phenotypic analysis performed post *in situ* hybridisation, showed for the first time *in vivo* that both *ldha* and *phd3* expression are upregulated in DMSO treated *vhl*$^{-/-}$*(phd3:eGFP)* mutants compared to *vhl* siblings, (**figure 4.8B-A, and**

4.8D-C), and that their expression can be further enhanced as a consequence of BME treatment (**figure 4.8B'-B, and 4.8D'-D**).

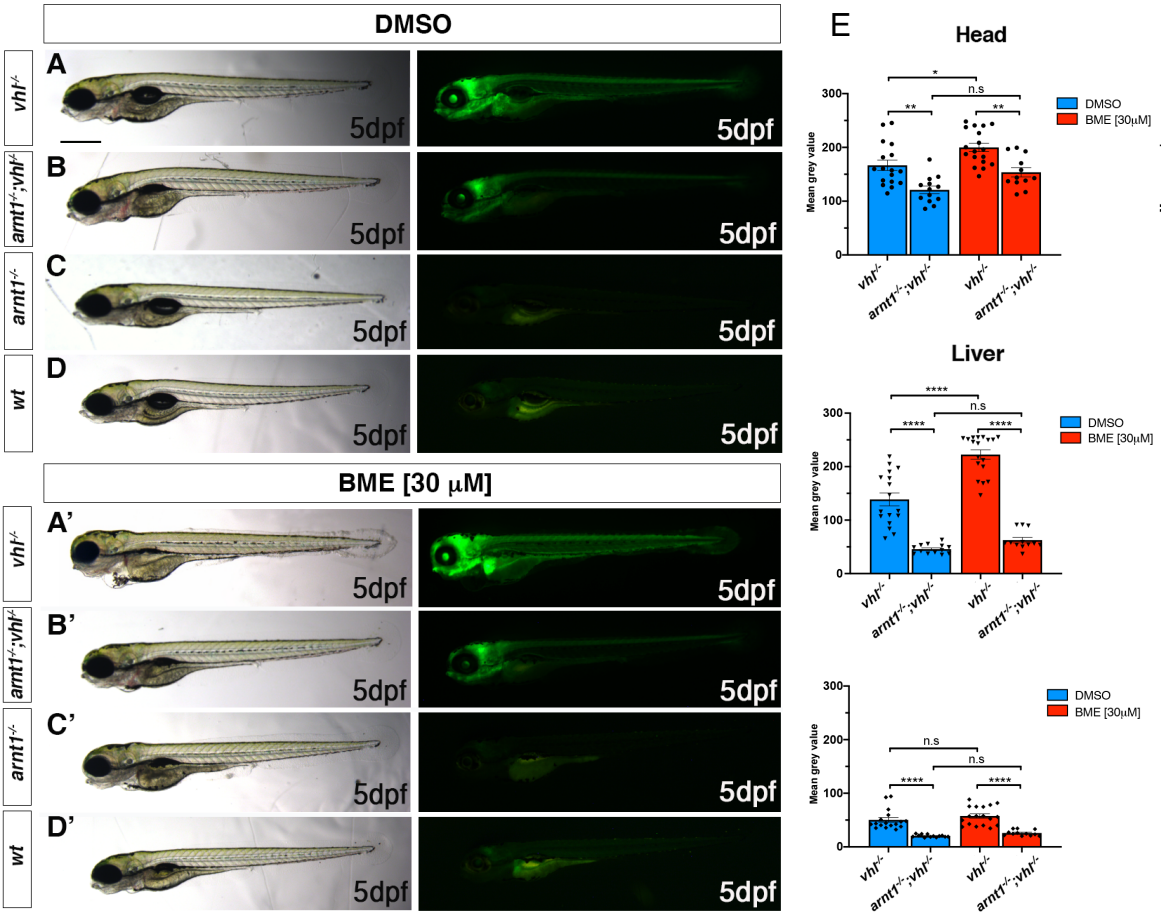

Figure 4.7 A-**D'. Representative picture of phenotypic analysis performed on DMSO and BME [30 μM] treated 5 dpf larvae, derived from *arnt1*$^{+/-}$*;vhl*$^{+/-}$*(phd3:eGFP)* x *arnt1*$^{-/-}$*;vhl*$^{+/-}$*(phd3:eGFP)* (n=540).** All the genotype combinations observed are represented in the figure. Among the 405 GFP^{+} larvae, all the 25 *arnt1*$^{-/-}$*;vhl*$^{-/-}$ showed the aforementioned partially rescued *vhl* phenotype. Moreover, all the *vhl*$^{-/-}$ larvae analysed showed an upregulated expression of the hypoxia reporter both in the head and the liver at 5 dpf. Fluorescence, exposure = 2 seconds. Scale bar 500 μm.

E. Statistical analysis performed on mean gray value quantification (at the level of the head, liver and tail), after phenotypic analysis on 5dpf DMSO and BME [30 μM] treated *arnt1*$^{+/-}$*;vhl*$^{+/-}$*(phd3:eGFP)* x *arnt1*$^{-/-}$*; vhl*$^{+/-}$(*phd3:eGFP*) derived larvae (n=540).** *vhl*$^{-/-}$ DMSO treated n=17 larvae: head 166.67 ± 9.63 (mean ± s.e.m); liver 138.61 ± 12.05 (mean ± s.e.m); tail 50.31 ± 4.51 (mean ± s.e.m). *arnt1*$^{-/-}$*;vhl*$^{-/-}$ DMSO treated n = 13 larvae: head 121.05 ± 6.99 (mean ± s.e.m); liver 49.61 ± 3.88 (mean ± s.e.m); tail 21.75 ± 1.12 (mean ± s.e.m). *vhl*$^{-/-}$ BME treated n = 18 larvae: head 199.88 ± 7.71 (mean ± s.e.m); liver 222.57 ± 8.72 (mean ± s.e.m); tail 57.57 ± 4.11 (mean ± s.e.m). *arnt1*$^{-/-}$;vhl$^{-/-}$ BME treated n = 12 larvae: head 153.71 ± 8.66 (mean ± s.e.m); liver 62.58 ± 5.16 (mean ± s.e.m); tail 25.82 ± 1.54 (mean ± s.e.m). Ordinary One-way ANOVA followed by Sidak's multiple comparison test (*P < 0.05; **P < 0.01; ***P <0.001; ****P < 0.0001).

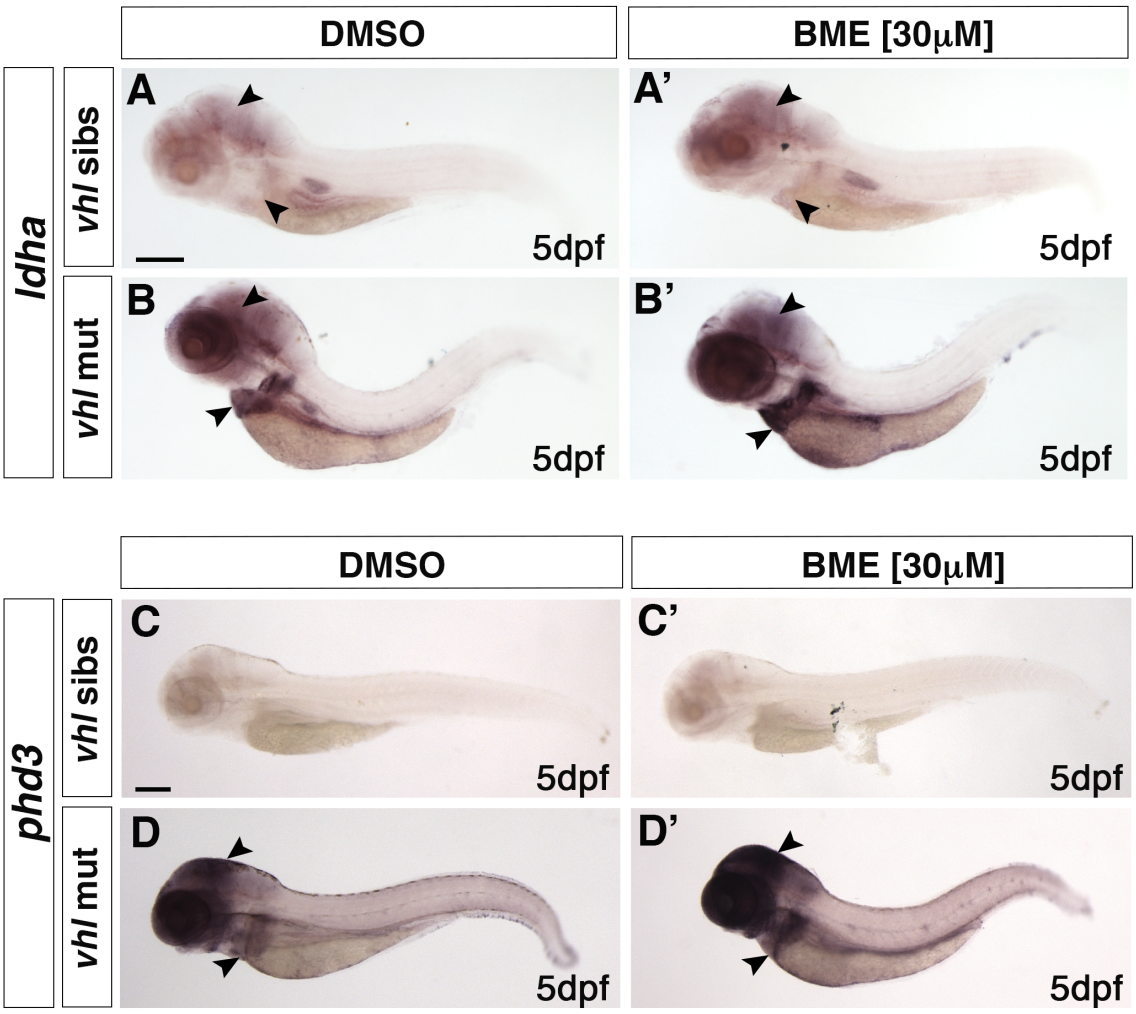

Figure 4.8 A-B'. Representative pictures of WISH performed on DMSO (A-B) and BME [30 μM] (A'-B') treated *vhl*$^{+/-}$ incross derived larvae, at 5 dpf, using *ldha* as probe. DMSO treated *vhl* siblings showed basal *ldha* expression (34/35 larvae), which showed to be upregulated after BME treatment (33/35 larvae). On the other hand, DMSO treated *vhl*$^{-/-}$ showed upregulated *ldha* expression (32/35 larvae), which was further upregulated after BME treatment (34/35 larvae) (black arrowhead: head and liver) Chi-square test (****P < 0.0001). Scale bar 200 μm.

C-D'. Representative pictures of WISH performed on DMSO (C-D) and BME [30 μM] (C'-D') treated *vhl*$^{+/-}$ incross derived larvae, at 5 dpf, using *phd3* (*egln3*) as probe. As expected, *vhl* siblings DMSO treated (n= 30/30 larvae) showed basal *phd3* expression, which was mildly increased after BME treatment (n= 27/30 larvae). *Vhl*$^{-/-}$ DMSO treated (n= 28/30 larvae) showed upregulated *phd3* expression, which was further increased after BME treatment (n= 26/30 larvae) (black arrowhead: head and liver) Chi-square test (****P < 0.0001). Scale bar 200 μm.

To further the analysis, I also treated *arnt1*$^{+/-}$*;vhl*$^{+/-}$*(phd3:eGFP)* incrossed-derived larvae with BME [30 μM] at 4 dpf and I observed the phenotypic outcomes at 5 dpf. Once again, these data confirmed that BME was able to upregulate the hypoxia reporter expression in the liver and the head of *vhl*$^{-/-}$ larvae and to mildly do that only at the hepatic level of wild-type larvae (**figure 4.7A'-A and D'-D**).

Vice versa, as expected, the *phd3:eGFP*-related brightness both of *arnt1*$^{-/-}$ and *arnt1*$^{-/-}$*;vhl*$^{-/-}$ larvae was unaffected after BME treatment (**figure 4.7B-B' and 4.7C-C'**). In the same way, *gr*$^{-/-}$ and *gr*$^{-/-}$*;vhl*$^{-/-}$ mutants were unaffected due to the absence of functional Gr and showed no significant differences overall in terms of hypoxia reporter expression, following Betamethasone treatment (**figure 4.9B'-B and C'-C**). Of note, RTqPCR analysis carried out on both double mutant larvae on HIF (*vegfab* and *egln3*) and GC target genes (*fkbp5*) expression confirmed these data (**figure 4.10**).

Interestingly, since the head was the brightest region observed in these double mutants, I speculate that mineralocorticoid receptor could compensate for the absence of Gr and maintain moderate levels of HIF, particularly within the CNS. Since recent study has shown that both Gr and Mr are differentially involved in the regulation of the stress axis activation and function in zebrafish (Faught and Vijayan, 2018b), I set up to test this hypothesis via WISH and CRISPant method, as it will be thoroughly described in the next subchapters 4.5 and 4.6.

Altogether, these data indicate that in *vhl*$^{-/-}$ larvae BME treatment can upregulate HIF signalling in a Vhl independent way. This is because, as described in a previous study from my lab (Vettori *et al.*, 2017) the activation of GR signalling can negatively regulate VHL protein in human liver cells. However, my analysis shows that in zebrafish larvae there must be an additional point of interaction between these two pathways.

To further test why BME can still activate HIF pathway, even in the absence of functional Vhl, I have repeated the same BME treatment on the already existing *vhl*$^{+/-}$*;vll*$^{-/-}$*(phd3:eGFP)* fish line using incross-derived 4 dpf larvae, followed by phenotypic analysis at 5 dpf. This is because, in zebrafish, the function of human VHL is split over two genes, named *vhl* and *vhl-like* (*vll*). Interestingly, unlike pVhl, Vll seems to play minor, non-essential HIF-negative regulation functions in zebrafish. Here, I speculate that this is due to the fact that Vll functions can be compensated by Vhl activity, but not vice versa. Consequently, *vll*$^{-/-}$ larvae develop normally and adult fish are viable and fertile.

In this scenario, phenotypic analysis performed at 5 dpf on DMSO and BME treated *vhl*$^{+/-}$*;vll*$^{-/-}$ and *vhl*$^{-/-}$*;vll*$^{-/-}$ larvae showed that betamethasone is able to potently activate HIF pathway also in a Vll-independent way (**figure 4.11A**). This was quantified as a 34% upregulation at the level of the head ($P<0.0001$), a 16% upregulation in the liver ($P=0.0007$) and a 72% upregulation in the tail ($P<0.0001$) of the HIF-reporter expression in BME treated *vhl*$^{-/-}$*;vll*$^{-/-}$ larvae, compared to the DMSO treated counterpart (**figure 4.11B**). Moreover, also *vhl*$^{+/-}$*;vll*$^{-/-}$ showed and increased HIF-reporter expression in the head and the liver, as usually occurs in wild types (**figure 4.11A**).

Importantly, these data reveal for the first time that Vll is also involved in counteracting HIF pathway overactivation induced by Betamethasone in zebrafish.

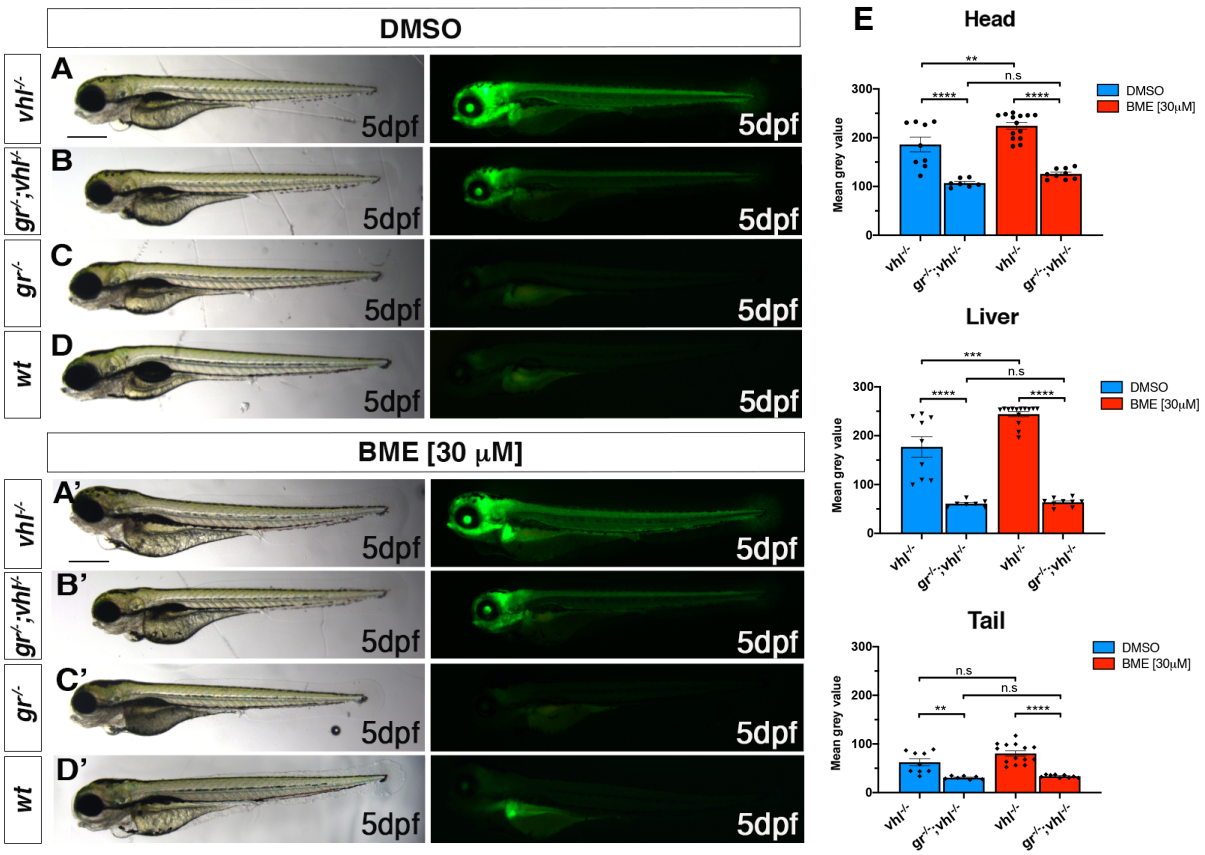

Figure 4.9 A-D'. Representative picture of phenotypic analysis performed on DMSO and BME [30 μM] treated *gr*$^{+/-}$*;vhl*$^{+/-}$*(phd3:eGFP)* incross-derived 5 dpf larvae (n = 600). All the genotype combinations observed are represented in the figure. Among the 450 GFP^{+} larvae analysed, 28 showed a partially rescued *vhl* phenotype which resembled the *arnt1*'s one. Three experimental repeats. In all panels: *P < 0.05; **P < 0.01; ***P <0.001; ****P < 0.0001. Fluorescence, exposure = 2 seconds. Scale bar 500 μm.

E. Statistical analysis performed on mean gray value quantification (at the level of the head, liver and tail), after phenotypic analysis on 5 dpf DMSO and BME [30 μM] treated *gr*$^{+/-}$*;vhl*$^{+/-}$*(phd3:eGFP)* x *gr*$^{-/-}$*; vhl*$^{+/-}$*(phd3:eGFP)* derived larvae. *vhl*$^{-/-}$ DMSO treated n = 9 larvae: head 186 ± 15.12 (mean ± s.e.m); liver 177.01 ± 20.85 (mean ± s.e.m); tail 62.34 ± 7.27 (mean ± s.e.m). *gr*$^{-/-}$*;vhl*$^{-/-}$ DMSO treated n = 7 larvae: head 106.96 ± 3.21 (mean ± s.e.m); liver 60.75 ± 2.56 (mean ± s.e.m); tail 30.67 ± 1.27 (mean ± s.e.m). *vhl*$^{-/-}$ BME treated n = 14 larvae: head 224.32 ± 6.83 (mean ± s.e.m); liver 244.07 ± 5.31 (mean ± s.e.m); tail 80.51 ± 5.49 (mean ± s.e.m). *gr*$^{-/-}$*;vhl*$^{-/-}$ BME treated n = 9 larvae: head 125.85 ± 3.6 (mean ± s.e.m); liver 63.56 ± 2.91 (mean ± s.e.m); tail 33.67 ± 1.02 (mean ± s.e.m). Ordinary One-way ANOVA followed by Sidak's multiple comparison test (*P < 0.05; **P < 0.01; ***P <0.001; ****P < 0.0001).

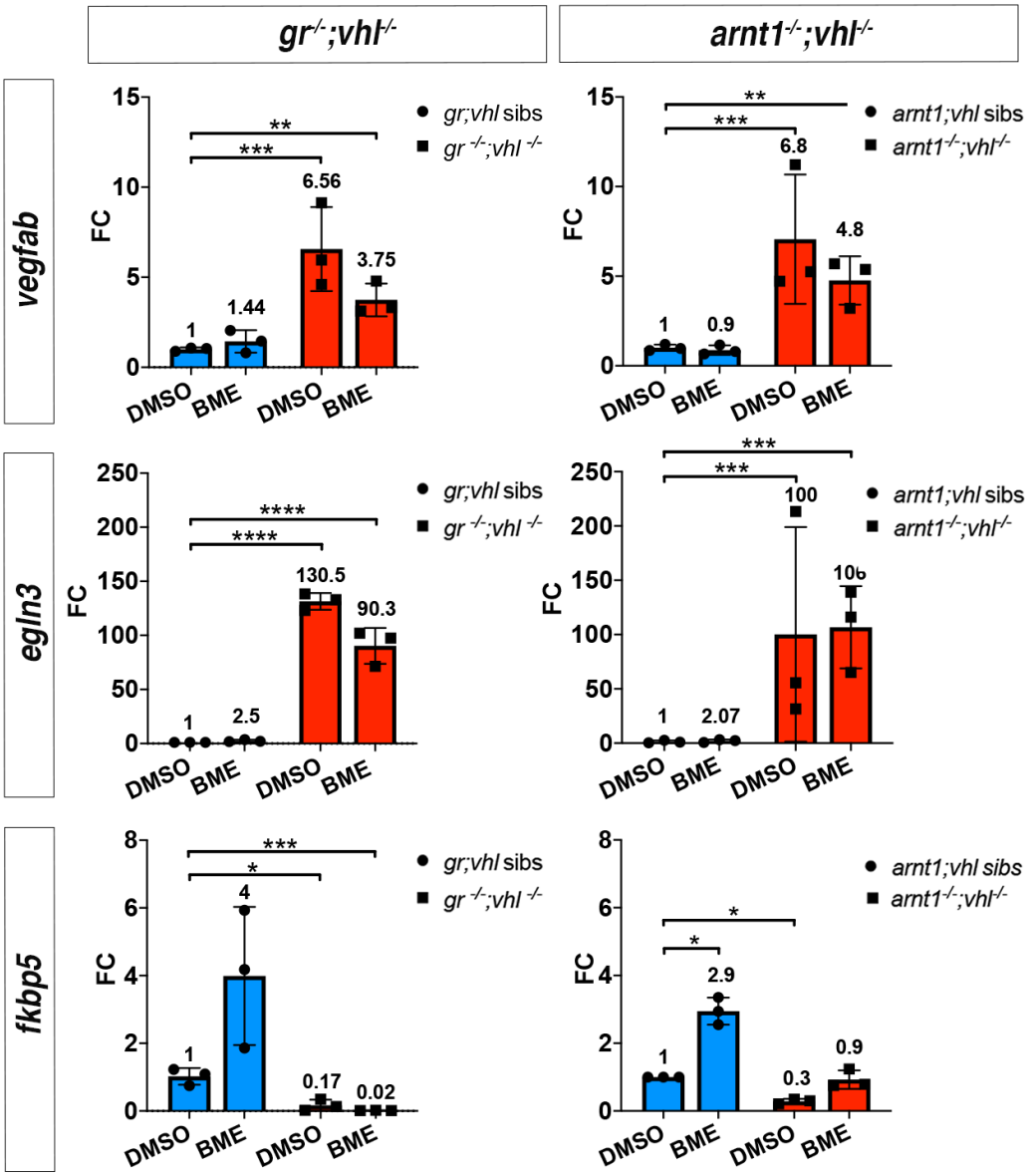

Figure 4.10 RTqPCR analysis carried out both on HIF and GC target genes expression on *gr*$^{-/-}$*; vhl*$^{-/-}$ and sibling at 5 dpf, (n = 10 larvae, per group, in triplicate) compared to *arnt1*$^{-/-}$*;vhl*$^{-/-}$ larvae and siblings, at 5dpd (n = 10 larvae, per group, in triplicate). Both *vegfab* and *egln3* are HIF target genes, whereas *fkbp5* is a GC target gene. Statistical analysis was performed on ΔΔCt values, whereas data are shown as fold change values, Ordinary Two-way ANOVA followed by Dunnett's multiple comparison test.

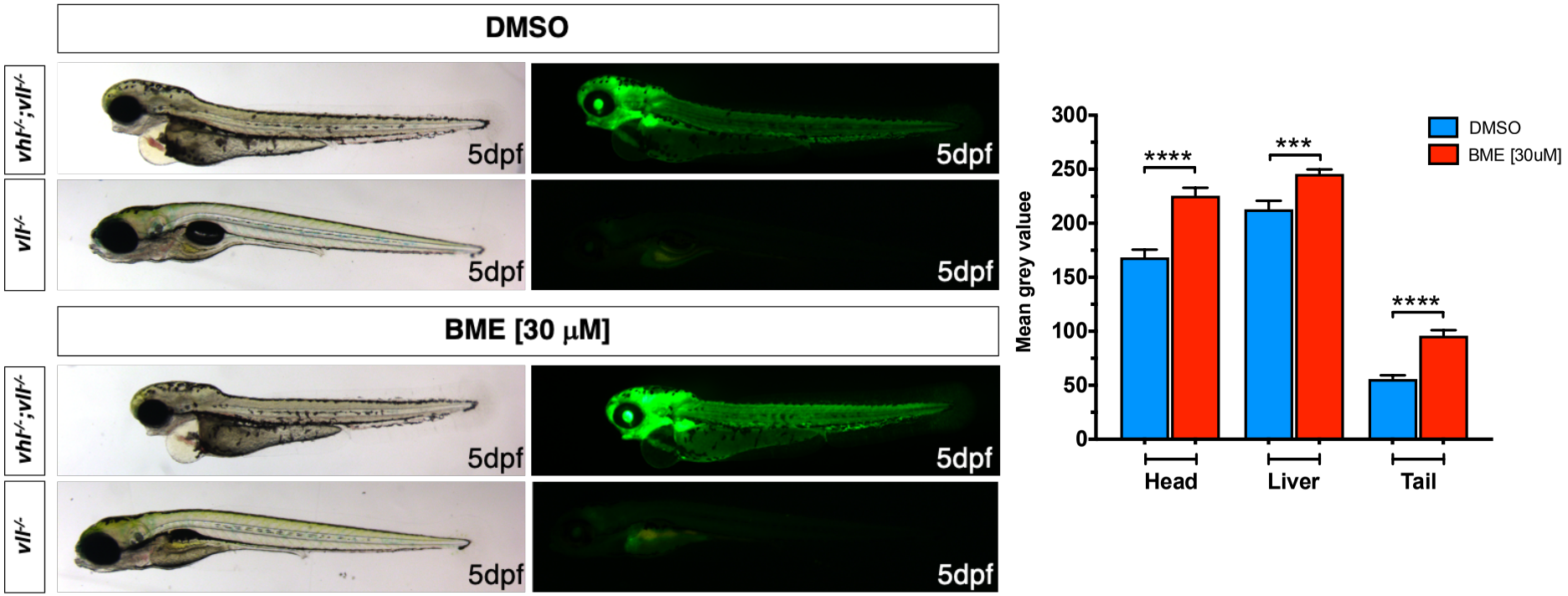

Figure 4.11. A. Representative pictures of phenotypic analysis performed on DMSO and BME [30 μM] treated *vhl*$^{+/-}$;*vll*$^{-/-}$*(phd3:eGFP)* incross-derived 5dpf larvae (*n*=140). Statistical analysis allowed to show that betamethasone is able to significantly activate the *Tg*(*phd3:eGFP*) expression in a Vhl and Vll-independent way. **B.** Statistical analysis performed on mean gray value quantification (at the level of the head, liver and tail), after phenotypic analysis on DMSO and BME [30μM] treated *vhl*$^{-/-}$;*vll*$^{-/-}$*(phd3:eGFP)* larvae. *vhl*$^{-/-}$;*vll*$^{-/-}$ DMSO treated n = 17 larvae: head 168.42 ± 7.18 (mean ± s.e.m); liver 212.91 ± 7.95 (mean ± s.e.m); tail 55.76 ± 3.50 (mean ± s.e.m). *vhl*$^{-/-}$;*vll*$^{-/-}$ BME treated n = 17 larvae: head 225.32 ± 7.32 (mean ± s.e.m); liver 245.73 ± 4.14 (mean ± s.e.m); tail 95.98 ± 5.05 (mean ± s.e.m). Ordinary One-way ANOVA followed by Sidak's multiple comparison test (***P < 0.001; ****P < 0.0001).

4.5. *gr* loss of function overrides HIF-mediated *pomca* downregulation in a *vhl* mutant scenario

To deepen the knowledge about the effect of GCs on the HIF signalling I examined the effect of *gr* loss of function on steroidogenesis in *a vhl* mutant scenario. To this purpose, I performed a whole mount *in situ* hybridisation on 5 dpf $gr^{+/-};vhl^{+/-}$ incross-derived larvae using proopiomelanocortin a (*pomca*) as probe. Interestingly, unlike normal expression of *pomca* observed at the level of the anterior part of the pituitary gland in the *gr;vhl* wild-type siblings (**figure 4.12A**), *vhl* mutants displayed a downregulated expression (**figure 4.12B**). In contrast, in line with previous observations, *gr* mutants showed upregulated *pomca* (**figure 4.12C**). The latter phenotype is known to be induced by the absence of a functional GC-GR mediated negative feedback loop, which triggers the upregulation of *pomca* gene at the level of the pituitary gland. This has been shown to be followed by an overproduction of cortisol at the level of the interrenal gland, which makes zebrafish hypercortisolaemic (Facchinello *et al.*, 2017; Faught and Vijayan, 2018b). Since *vhl* mutants, which are characterized by an upregulated HIF signalling pathway, displayed a downregulated *pomca* expression, I speculated that this might occur via HIF-mediated activity at the pituitary level, aimed to downregulate the cortisol-mediated stress response.

Since GCs control a broad range of physiological processes, act on almost every tissue and organ in the body to maintain homeostasis and are characterized by a robust immunosuppressive and anti-inflammatory actions, their secretion must be finely tuned at the level of the HPA/I axis. In addition, since previous data from my laboratory identified GCs as HIF activators (Santhakumar *et al.*, 2012; Vettori *et al.*, 2017), I inferred that, being HIF particularly expressed at the level of the head, it might in turn

regulates GC levels by acting on *pomca* expression. If this was true, it would enable HIF signalling not only to tune its own levels, but also to ensure homeostasis. Moreover, being HIF signalling a master regulator of pro-inflammatory responses to hypoxia, it would counteract the anti-inflammatory activity played by GCs. To this end, I speculate that the concomitant expression of both upregulated HIF and GC pathway would be detrimental to homeostasis. In particular, the following chapter will be focused on testing and confirming these hypotheses.

Additionally, WISH analysis carried out on the aforementioned mutant line, showed that a strong *pomca* upregulation was present in $gr^{-/-};vhl^{-/-}$ larvae (**figure 4.12D**), compared to both $vhl^{-/-}$ and wild types. Then, PCR analysis carried out post *in situ* hybridisation allowed to confirm the presence of genotype-phenotype correlation. In this regard, if my hypothesis was true, it would suggest that *gr* loss of function mutation overrides the HIF-mediated *proopiomelanocortin a* inhibition.

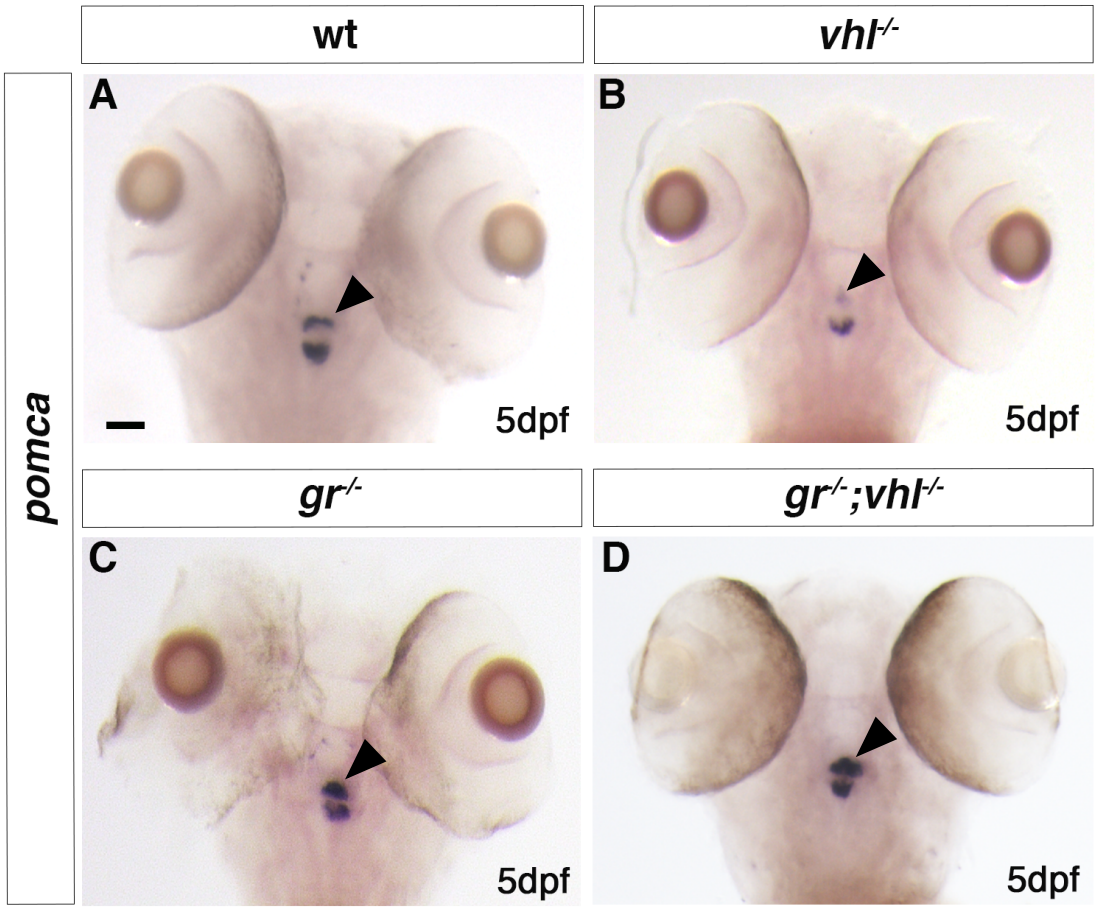

Figure 4.12 A-D'. Representative pictures of whole-mount *in situ* hybridisation carried out on *gr*$^{+/-}$*; vhl*$^{+/-}$ incross derived larvae at 5 dpf, using *pomca* as probe. Of note, *gr*$^{-/-}$*;vhl*$^{-/-}$ larvae showed upregulated *pomca* expression (20/20 larvae), as observed in *gr*$^{-/-}$ (20/20 larvae); vhl mutants showed downregulated *pomca* expression (20/20 larvae), whereas wild types showed normal *pomca* expression (19/20). Chi-square test ($P < 0.0001$). Scale bar 50 μm.

4.6. Both Gr and Mr are directly required for properly assuring HIF response

Endogenous cortisol has high affinity more for Mr than Gr and both have been lately shown to be differentially involved in the control of the stress axis activation and function in zebrafish larvae (Faught and Vijayan, 2018b).

For these reasons, I have speculated that also the GC-MR complex might contribute to trigger the HIF response in zebrafish larvae. To test this, I knocked-out *mr* gene in the *gr*$^{+/-}$*;vhl*$^{+/-}$*;phd3:eGFP* incrossed derived embryos using the aforementioned CRISPant technology (Burger *et al.*, 2016; Wu *et al.*, 2018).

Interestingly, phenotypic analysis performed on 5 dpf injected and uninjected larvae revealed that *mr* CRISPR injected *vhl* mutants were characterized by a decreased *phd3:eGFP*-related brightness at the level of the head (equals to 49%, P<0.0001), in the liver (equals to 56%, P<0.0001) and in the rest of the body (equals to 47%, P<0.0001), compared to *vhl* mutant uninjected larvae (**figure 4.13D compared to 4.13A**). Furthermore, the downregulation was even stronger at the level of the head (equals to 62%, P<0.0001), the liver (equals to 77%, P<0.0001) and the rest of the body (equals to 63%, P<0.0001) when *mr* was knocked-out in *gr*$^{-/-}$*;vhl*$^{-/-}$larvae, compared to uninjected *vhl* mutants (**figure 4.13E compared to 4.13A**). Notably, *mr* injection in *vhl*$^{-/-}$ larvae was also more efficient in downregulating the HIF-reporter expression only at the level of the head (equals to 31%, P = 0.0087) compared to uninjected *gr*$^{-/-}$*;vhl*$^{-/-}$ larvae (**figure 4.13D compared to 4.13B**). This led me to hypothesise that Mr could play a key role at the level of the CNS in terms of HIF pathway regulation, compared to Gr.

At this point, to confirm the specificity of Wu et al., 2018 method, I chose to target a gene which was not involved in the HIF pathway. Laminin, beta 1b (*lamb1b*), which codes for an extracellular matrix glycoprotein, was injected as CRISPR-injection control in *vhl*$^{+/-}$ incross-derived embryos at 1 cell stage. Genotypic analysis carried out on these larvae confirmed that these guides were effective.

As expected, quantification of *phd3:eGFP*-related brightness performed on 5 dpf injected and uninjected larvae, showed no significant differences between these two groups (**figure 4.14A-C and 4.14E**). Overall, these data further supported my hypothesis that not only GR but also MR play an essential role in assuring a proper HIF response in zebrafish.

In light of these facts, understanding the precise role of MR and mineralocorticoid in the HIF signalling is warranted and will require further testing.

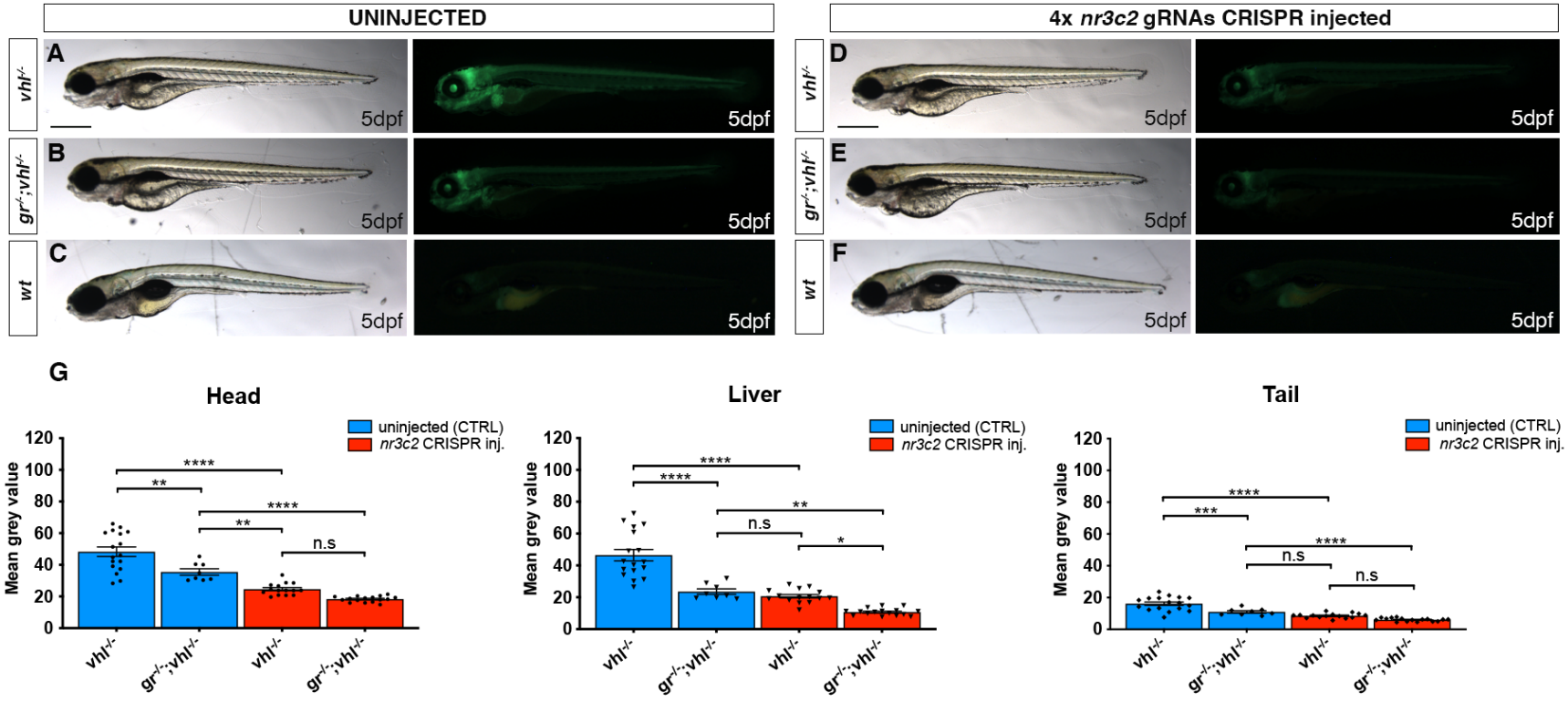

Figure 4.13 A-F. Representative pictures of 5 dpf CRISPANT mutants created by redundantly targeting *nr3c2 (mr)* gene via co-injection of 4x gRNAs in *gr*$^{+/-}$*;vhl*$^{+/-}$*(phd3:eGFP) x gr*$^{-/-}$*; vhl*$^{+/-}$*(phd3:eGFP)* derived embryos (n=344). Uninjected embryos were used as control (n=170). Fluorescence, exposure = 991,4 ms. Scale bar 500 µm. G. Statistical analysis performed on mean grey value quantification (at the level of the head, liver and tail), after phenotypic analysis, on 5 dpf *mr* 4x gRNAs injected and uninjected larvae. *vhl*$^{-/-}$ uninjected n = 17 larvae: head 48.28 ± 2.99 (mean ± s.e.m); liver 46.47 ± 3.55 (mean ± s.e.m); tail 16.15 ± 1.06 (mean ± s.e.m). *gr*$^{-/-}$*;vhl*$^{-/-}$ uninjected n = 8 larvae: head 35.48 ± 2.03 (mean ± s.e.m); liver 23.56 ± 1.72 (mean ± s.e.m); tail 10.98 ± 0.75 (mean ± s.e.m). *vhl*$^{-/-}$ injected n = 15 larvae: head 24.62 ± 0.97 (mean ± s.e.m); liver 20.67 ± 1.1 (mean ± s.e.m); tail 8.57 ± 0.39 (mean ± s.e.m). *gr*$^{-/-}$*;vhl*$^{-/-}$ injected n = 16 larvae: head 18.33 ± 0.46 (mean ± s.e.m); liver 10.71 ± 0.56 (mean ± s.e.m); tail 6.07 ± 0.26 (mean ± s.e.m); ordinary One-way ANOVA followed by Sidak's multiple comparison test.

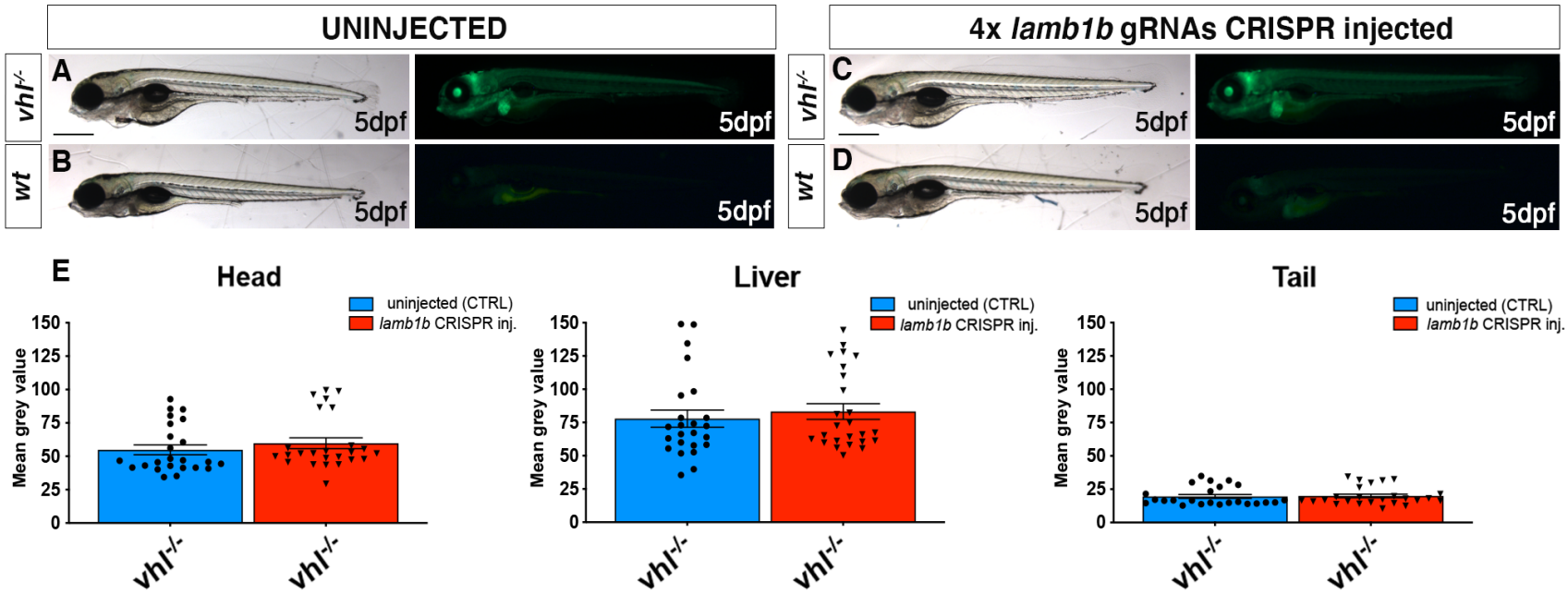

Figure 4.14 A-D. Representative pictures of 5 dpf CRISPANT mutants created by redundantly targeting *lamb1b* gene via co-injection of 4x gRNAs in *vhl*$^{+/-}$*(phd3:eGFP)* incross-derived embryos (n=400). Uninjected embryos were used as control (n=470). Fluorescence, exposure = 991,4 ms. Scale bar 500 µm. E. Statistical analysis performed on mean grey values quantification (at the level of the head, liver and tail), after phenotypic analysis on 5 dpf *lamb1b* 4x gRNAs injected and uninjected *vhl*$^{+/-}$(*phd3:eGFP*) incross-derived larvae. *vhl*$^{-/-}$ uninjected n = 24 larvae: head 54.83 ± 3.68 (mean ± s.e.m); liver 77.86 ± 6.46 (mean ± s.e.m); tail 19.56 ± 1.43 (mean ± s.e.m). *vhl*$^{-/-}$ injected n = 25 larvae: head 59.74 ± 4.05 (mean ± s.e.m); liver 83.23 ± 5.92 (mean ± s.e.m); tail 19.9 ± 1.38 (mean ± s.e.m); unpaired t-test (all panels: *P < 0.05; **P < 0.01; ***P <0.001; ****P < 0.0001).

4.6.1. Generation and characterisation of zebrafish *gr*$^{sh543/+}$;*mr*$^{sh562/+}$ line

To further the knowledge on the MR role on the–HIF signalling when the latter is normally expressed, I initially created the *gr*$^{sh543/+}$;*mr*$^{sh562/+}$ mutant line as mentioned in the subchapter 2.1.7 of the Material and Methods. Then, fin-clipping procedure followed by genotyping analysis on 3 months old fish allowed to select carriers for both mutations. As previously described in chapter 4.2, *gr* mutation is able to partially rescue Vhl phenotype, *gr*$^{-/-}$ larvae can be sorted via visual background adaptation test and have a visible phenotype. On the other hand, *mr* mutation is known not to cause any phenotype, *mr*$^{-/-}$ larvae cannot be VBA sorted and its role in the HIF pathway is still unknown (Cruz *et al.*, 2013; Facchinello *et al.*, 2017; Faught and Vijayan, 2018b). As a consequence of the above considerations, since my data showed that Mr mutation is able to further downregulate the HIF signalling in zebrafish larvae, I decided to check whether the simultaneous knockout of both *mr* and *gr* was able to modulate the phenotype and/or the viability of *gr*$^{-/-}$ mutant larvae.

Phenotypic analysis carried out on VBA sorted *gr*$^{+/-}$;*mr*$^{-/-}$ incross-derived larvae at 5 dpf, revealed that *gr*$^{-/-}$;*mr*$^{-/-}$ mutants are characterized by a slightly improved yolk usage compared to the previously described *gr*$^{-/-}$ larvae (**figure 4.15B compared to 4.15A, white asterisk**). At the same time, double mutants display a still rounded head compared to wild types and a VBA negative response as observed in *gr*$^{-/-}$ larvae (**figure 4.15B compared to 4.15A, black arrowhead**). Vice versa, *mr*$^{-/-}$ didn't show any particular phenotype and they looked like wild-type larvae, as expected (**figure 4.15C**). Genotyping post phenotypic analysis on these VBA sorted larvae confirmed the presence of a genotype-phenotype correlation. Consequently, I inferred that since cortisol cannot bind neither to GR nor to MR anymore, it is unable to elicit any effect, other than the one caused by a cortisol resistance-like state.

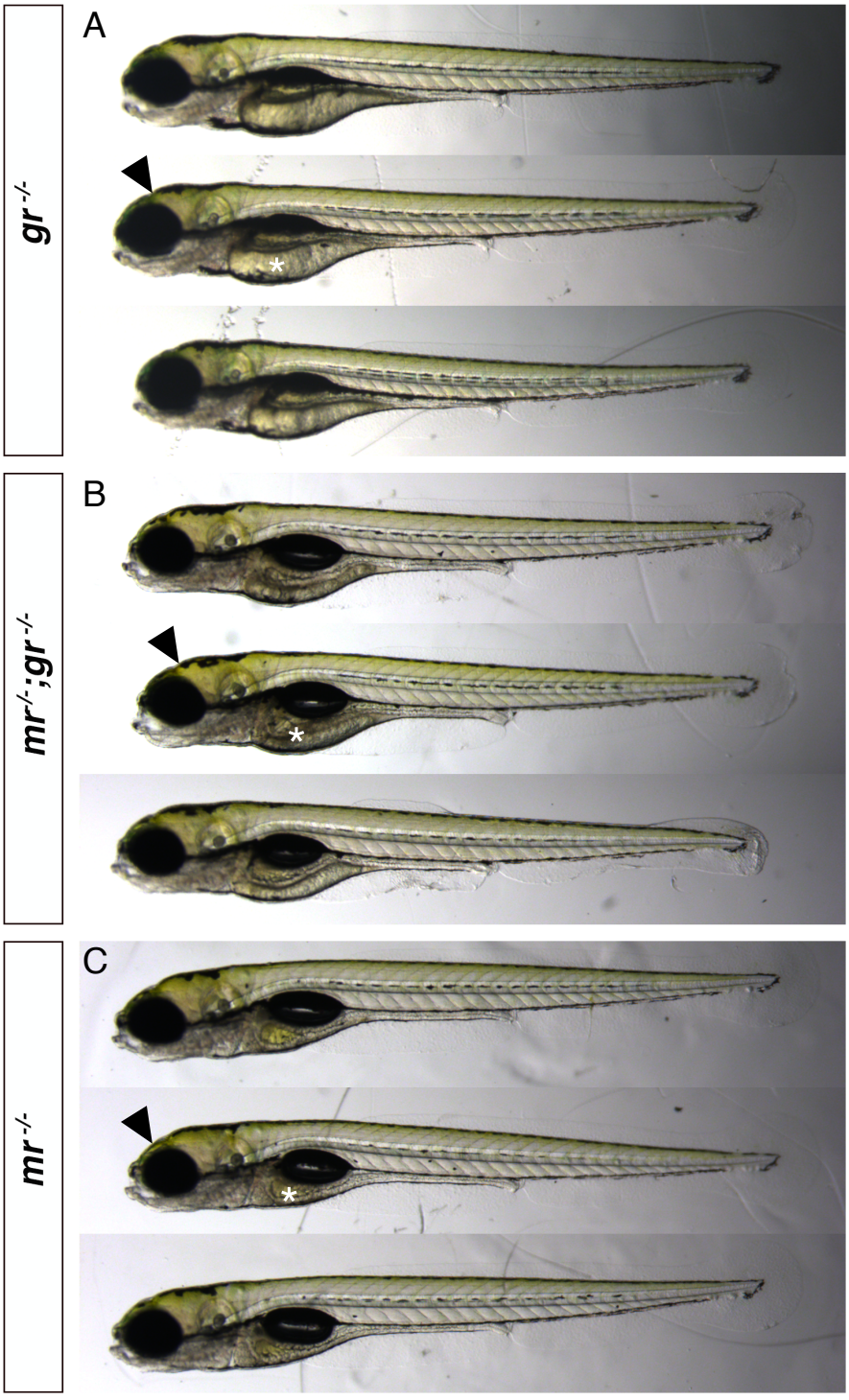

Figure 4.15 A-C. Representative pictures of 5 dpf *gr*$^{+/-}$;*mr*$^{-/-}$ incross-derived larvae (n=600), after being VBA tested and sorted according to their phenotype in three different dishes (n=60 each). In the first dish, there were VBA negative *gr*$^{-/-}$ larvae derived by a *gr*$^{+/-}$ fish incross used as control. The second dish (B) contained VBA negative larvae with a bigger yolk than the wild-types one, but smaller than *gr*$^{-/-}$ larvae (white asterisk), coupled to the presence of a still rounded head (back arrowhead). Finally, the third dish (C) included VBA positive larvae with a normal phenotype. Of note, PCR-based genotyping carried out on 12 larvae per group, allowed to confirm the presence of a genotype-phenotype correlation. White asterisk: yolk/gut; black arrowhead: head.

Since it is well known that in zebrafish GCs regulate a variety of physiological processes and are essential in the stress response, hatching and swim activity at early developmental stages (Oakley and Cidlowski, 2011; Wilson *et al.*, 2013; Timmermans, Souffriau and Libert, 2019), I inferred that these double mutants were unable to cope with stress and were not viable or fertile at adult stages.

To test this, I set up to raise $gr^{+/-};mr^{-/-}$ incrossed derived larvae at 5 dpf till adulthood. Surprisingly, PCR-based genotyping on adult zebrafish tail biopsies, revealed that double mutants were viable and adult males showed feminised secondary sex characteristics, including a slightly bigger belly and bluish stripes. Moreover, both sexes showed an increased average size.

To better examine this aspect, I collaborated with Jack Paveley (PhD student in Vincent Cunliffe lab, The University of Sheffield) to weigh 58 nine-month old fish derived from the same aforementioned cross together with wild type AB fish with the same age, used as control. Each fish was anesthetised with tricaine and gently dried on a tissue to remove the excess of water. Then, it was quickly weighed on an analytical balance and was put back in a new tank. Weighing results allowed to confirm that both wild types and $mr^{-/-}$, which share the same phenotype, have also the same weight (wt = 0.383g compared to $mr^{-/-}$ = 0.396g). On the other hand, as expected, $gr^{-/-}$ showed an increased weight compared to both wild-types AB (equals to 0,505, P<0.0038) and $mr^{-/-}$ (P<0.0001). Finally, $gr^{-/-}; mr^{-/-}$ fish surprisingly weighed more than double the wild types (equals to 0,933, P<0.0001) and almost twice as much as $gr^{-/-}$ (P<0.0001) (**figure 4.16**). Of note, the sex ratio was kept the same among all the groups analysed and a similar amount of fish was raised in each tank according to their genotype.

Consequently, we wanted to check whether the knockout of both *gr* and *mr* was able to affect the ability of these fish to perform the typical male breeding behaviours.

Of note, *gr*$^{-/-}$ adult fish are viable and can be mated without any issue like wild types and *mr*$^{-/-}$ fish. However, unlike the latter, they are unable to properly cope with stress and show freezing behaviour when put in a new environment. For this reason, I wanted to test the ability of *gr*$^{-/-}$*;mr*$^{-/-}$ adult fish to perform breeding. Notably, preliminary behavioural analysis carried out in collaboration with Jack Paveley, showed that these double mutants were less motile, failed to show chasing behaviour (the typical mating ritual) and they did not lay eggs every time we pair-mated them (> 4 times). As a consequence of the above consideration, since reproductive events are also regulated by hypothalamic-pituitary-adrenal axis (Whirledge and Cidlowski, 2013) and double mutants cannot sense cortisol at all, I speculated that this could be the main reason behind this behaviour. Consequently, understanding whether the concomitant presence of both mutations is able to cause defects at the level of the reproductive system in zebrafish is warranted and will require further testing.

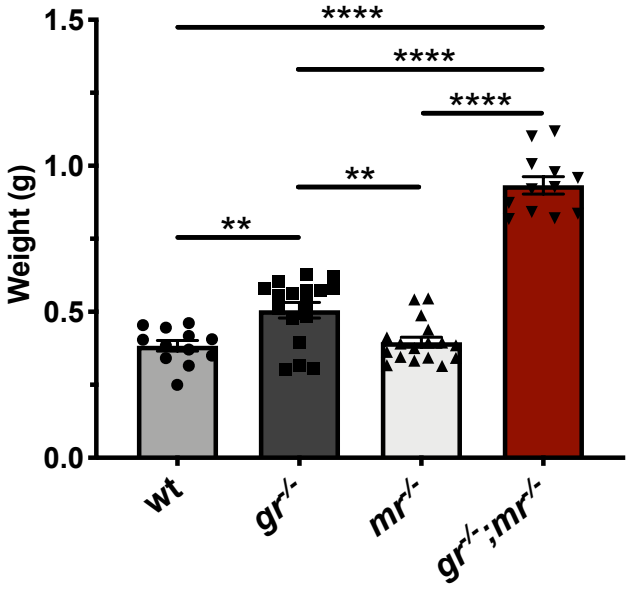

Figure 4.16. Statistical analysis carried out on weighing results of 60 nine-month-old fish derived from the aforementioned *gr*$^{+/-}$*;mr*$^{+/-}$ incross. Wild types fish (n=12): 0.383 ± 0.018 (mean ± s.e.m). *gr*$^{-/-}$ fish (n=17): 0.505 ± 0.027 (mean ± s.e.m); *mr*$^{-/-}$ fish (n=17): 0.396 ± 0.017 (mean ± s.e.m); *gr*$^{-/-}$;*mr*$^{-/-}$ fish (n=12): 0.933 ± 0.030 (mean ± s.e.m). Ordinary One-way ANOVA followed by Sidak's multiple comparison test (all panels: *P < 0.05; **P < 0.01; ***P <0.001; ****P < 0.0001).

4.7. Discussion

This chapter is intended to provide further insights regarding the role of GCs on the HIF signalling. Since previous work from my lab showed that synthetic GC can activate the *phd3:eGFP* hypoxia reporter particularly in the zebrafish liver (Vettori *et al.*, 2017), however the question whether GR activity is essential for proper HIF pathway activation was yet unanswered.

The best way to answer this question was to analyse the effect of *gr* loss of function in a HIF upregulated scenario (*vhl*$^{-/-}$). Here, phenotypic analysis performed on 5 dpf larvae showed that *gr* mutation is able to cause an efficient, but not complete rescue of the *vhl* phenotype. This is interesting because the phenotype induced by *gr* mutation resembled the one generated by knocking down *arnt1* gene in the *vhl*$^{-/-}$ background. Indeed, in both cases it was possible to observe a downregulation of the hypoxia reporter equals to 39% in *arnt1;vhl* double mutants and to 43% in *gr*$^{-/-}$*;vhl*$^{-/-}$ larvae at the level of the head, compared to 5 dpf *vhl* mutants larvae. Moreover, a 75% downregulation in the liver of *arnt1*$^{-/-}$*;vhl*$^{-/-}$ larvae and a 66% downregulation was instead observed in the same organ in *gr;vhl* double mutants. Finally, a 58% and a 51% downregulation of the *phd3:eGFP*-related brightness were quantified from the anus to the caudal peduncle both in *arnt1*$^{-/-}$*;vhl*$^{-/-}$ and *gr*$^{-/-}$*;vhl*$^{-/-}$ larvae, respectively.

In line with these observations, *gr*$^{-/-}$*;vhl*$^{-/-}$ larvae survived much longer than the *vhl*$^{-/-}$ (>=21 dpf compared to max. 10 dpf) but then, similarly to the *arnt1*$^{-/-}$*;vhl*$^{-/-}$, failed to grow and thrive when compared both to their siblings and wild types. Moreover, both double mutants showed lots of morphological similarities with each other, in terms of development stage and anatomical traits, compared to normally developed wild-type siblings.

Cumulatively, the analogies appreciated between *arnt1* and *gr* mutations in a Vhl mutant scenario could suggest that they work in a single linear "pathway". If this assumption was true, the mutation of both genes should not lead to a further attenuation of the hypoxia reporter expression.

Importantly phenotypic analysis carried out on *gr*$^{+/-}$;*arnt1*$^{+/-}$;*vhl*$^{+/-}$ triple carrier fish's progeny showed that the addition of *gr* mutation in a *arnt1;vhl* double mutant scenario generates a stronger downregulation of the *phd3:eGFP* expression and a more rescued Vhl phenotype than the one induced by single mutations. This allowed me to strengthen the hypothesis that these two major signalling pathways are not acting in a linear way.

To then study the effect of *gr* loss of function on the HIF signalling when the latter is not constantly overactivated (i.e. in wild type-like scenario), I analysed the hypoxia reporter gene expression in *gr*$^{+/-}$; *phd3:eGFP* incrossed derived larvae at 5 dpf. Quantification data based on the HIF-reporter expression in the aforementioned progeny showed that *gr* loss of function is able to cause a reduction of the *phd3:eGFP*-related brightness even in the absence of a HIF upregulated pathway. As a consequence, these data indicate for the first time in an *in vivo* animal model that Gr is essential to ensure high HIF signalling levels. In addition, the fact that Gr loss of function was able to partially rescue the Vhl phenotype and to double the lifespan of *vhl*$^{-/-}$ larvae, may have important clinical applications. In this regard, I speculate that the inhibition of glucocorticoid receptors might be a potential avenue to downregulate HIF for clinical purposes.

Furthermore, WISH data derived from *g*$^{+/-}$;*vhl*$^{+/-}$ incross-derived larvae suggested that in *gr*$^{-/-}$;*vhl*$^{-/-}$ larvae the upregulation of *pomca* induced by the lack of a functional Gr, cannot be inhibited with the same efficiency by the HIF signalling activity

at the level of the pituitary gland. For these reasons, I speculate that the resulting upregulated endogenous cortisol can interact only with Mr to stimulate the HIF pathway. This would also explain the presence of a moderately upregulated *phd3:eGFP* reporter expression in *gr*$^{-/-}$*;vhl*$^{-/-}$ larvae (**figure 4.9B**), whose levels are in-between the ones observed in *vhl* mutants and wild-type larvae (**figure 4.9A and D**).

If this was true, I predicted to obtain an even more rescued phenotype by knocking-out *mr* in a *gr*$^{-/-}$*;vhl*$^{-/-}$ background. This is important because nothing is known so far about mineralocorticoid receptor contribution to the HIF signalling. Moreover, a recent work published by Faught and Vijayan, 2018 showed that both Gr and Mr are differentially involved in the regulation of zebrafish stress axis activation and function.

Interestingly, my data showed that both *mr* injected- *vhl*$^{-/-}$ and *gr*$^{-/-}$*;vhl*$^{-/-}$ 5 dpf larvae displayed a significant reduction of *phd3:eGFP*-related brightness. This suggests that, in fish, not only the GR, but also the MR is involved in promoting HIF pathway activation, as a consequence of cortisol stimulation. In addition to that, phenotypic analysis performed on VBA sorted *gr*$^{+/-}$*;mr*$^{-/-}$ incross-derived larvae revealed the presence of an intermediate phenotype in *gr*$^{-/-}$*;mr*$^{-/-}$ that was in-between the on of *gr*$^{-/-}$ and wild types (**figure 4.15**). However, once adults, these double mutants were characterized by an increased size compared to both wild types and *gr*$^{-/-}$ fish. Consequently, I speculate that the additional presence of *mr* mutation in a *gr*$^{-/-}$ scenario makes larvae resistant to cortisol and promote a normal yolk usage, by protecting the body from an overexposure of GC-MR activity. However, although the absence of both functional genes is surprisingly not critical for survival in zebrafish, it causes a significant increase of weigh compared to both wild types and *gr*$^{-/-}$ fish once adults (**figure 4.16**). Since both Gr and Mr are involved in adipose tissue differentiation,

expansion and proinflammatory capacity (Marzolla *et al.*, 2012; Geer, Islam and Buettner, 2014), this could explain the phenotype observed in these double mutants.

Moreover, in contrast to mammals, teleosts lack aldosterone and cortisol is the primary GC hormone which can interact with both Gr and Mr to assure the correct HPI axis functioning (Cruz *et al.*, 2013; Tokarz *et al.*, 2013; Baker and Katsu, 2017; Faught and Vijayan, 2018b). Of note, my hypothesis is also supported by Faught and Vijayan, 2018 elegant work, showing that both Gr and Mr signalling is involved in the negative feedback regulation of cortisol biosynthesis during stress. In conclusion, although Mr contribution to HIF response in other organisms remains unclear, my work suggests research into its function is warranted.

To finally examine the role of GCs on the HIF signalling, I next analysed the effect of betamethasone treatment on *gr*$^{-/-}$;*vhl*$^{-/-}$, *arnt1*$^{-/-}$;*vhl*$^{-/-}$, *arnt1*$^{-/-}$ *and vhl*$^{-/-}$ mutants. Importantly, my data besides confirming that BME acts as a potent HIF activator, indicate a key role for Arnt1 in regulating the BME-induced HIF response. In particular, the fact that BME did not increase *phd3:eGFP*-related brightness both in *arnt1*$^{-/-}$ and in *arnt1*$^{-/-}$;*vhl*$^{-/-}$ larvae, even if other functional Arnt isoforms were present, confirmed that. Indeed, if BME activity was not Arnt1 dependent, it should have been be able to enhance the HIF signalling in both mutants. These data are surprising and would be best explained by assuming that a BME-Gr complex would preferentially interact with a HIFα/ARNT1 complex, instead of with a HIFα/ARNT2 complex. Finally, whether this holds up in mammalian cells would be interesting to address and requires further testing.

Additionally, unlike previous work from my lab showed that activation of GR signalling negatively regulates VHL protein, via c-src upregulation, in human hepatic

cells (Vettori *et al.*, 2017), my current research demonstrates that there must be an additional point of interaction in zebrafish larvae between these two pathways. Indeed, a further activation of the hypoxia reporter was observable after BME treatment even in the absence both of functional Vhl and Vll. For this reason, it is plausible to infer that in BME treated *vhl*$^{-/-}$ larvae, not all the Vhl proteins are broken down, allowing Vll to partially degrade HIF-α subunits and to counteract BME-induced HIF activation. Consequently, I speculate that GC must act downstream, rather than at the level of Vhl and Vll. Indeed, as it will be confirmed in the following chapter, betamethasone can act not only downstream of Vhl and Vll, but also of the HPI axis itself to upregulate the HIF response (**figure 4.7A-A', 4.8B-B' and D-D', 4.97A-A'**).

These data highlighted for the first time *in vivo*, that the absence of functional Gr is able to cause an efficient inhibition of the HIF signalling, both under normoxic and hypoxic-like (*vhl*$^{-/-}$) scenario. Indeed, although GC-GR activity is expected to be basal under non-stressful conditions (i.e. normoxia), its function is detectable with respect to assuring proper HIF activity. By contrast, the BME-mediated HIF activation can occur in a Vhl/Vll independent way in zebrafish and requires Arnt1 function to occur.

Cumulatively, this current study permitted to further the knowledge on the importance of the GCs and their receptors in the hypoxia-inducible factor pathway.

5. ROLE OF HIF SIGNALLING ON GC PATHWAY

5.1. Introduction

Hypoxia is a prevalent pathophysiological condition to which cells have to quickly reply in order to avoid metabolic shutdown and consequent death. Oxygen levels are continuously monitored via the activity of Hypoxia-Inducible Factors (HIFs) family, which is made up of key oxygen sensors that manage the ability of the cell to cope with lowered oxygen levels. In particular, this is tackled by orchestrating a metabolic shift from aerobic (oxidative phosphorylation) to anaerobic metabolism (glycolysis) aimed to reduce oxygen consumption.

Albeit the HIF response aims to reinstate both tissue oxygenation and perfusion, it can in some cases be inappropriate, and might contribute to a variety of pathological conditions such as: inflammation, stroke, tissue ischemia and the growth of solid tumours (Cummins and Taylor, 2005; Murdoch, Muthana and Lewis, 2005; Cummins *et al.*, 2007; Elks *et al.*, 2015). In this respect, synthetic GCs have been exploited for decades, being the equivalent of naturally occurring steroid hormones, due to their potent anti-inflammatory action, in order to treat pathological conditions that are linked to hypoxia (i.e. asthma, rheumatoid arthritis, ischemic injury). Interestingly, previous *in vitro* studies have point out the presence of a crosstalk between HIF and GC signalling (Kodama *et al.*, 2003; Leonard *et al.*, 2005; Wagner *et al.*, 2008; Zhang *et al.*, 2015, 2016). Of note, it has been recently reported that under hypoxic conditions HIF-1 is also able to negatively regulate steroidogenic acute regulatory (StAR) protein expression and steroidogenesis in mouse granulosa cells (Kowalewski, Gram and Boos, 2015). Moreover, both hypoxia and HIF-1α overexpression were shown to

downregulate the expression of StAR also in zebrafish embryos, but to simultaneously upregulate the expression both of CYP11a and 3β-HSD gene. Since the expression of these three genes were reversed in zHIF-1α knockdown embryos under normoxic conditions, this fact suggested that these genes were likely regulated by Hif-1 (Tan *et al.*, 2017).

However, the existence of two paralogs for each of the three zHIF-α isoforms (*hif-1A,B, hif-2A,B* and *hif-3A,B*) (Köblitz *et al.*, 2015), coupled to the lack of a proper reverse genetics approach used in the above-mentioned studies, highlighted the need to further the research on this topic. In particular, it still remains unclear how HIF contributes to GC functions, how the interplay between hypoxia-dependent signals and GC-mediated regulation of gene expression precisely occurs in an organism and what the molecular mechanism is behind it.

In this chapter a thorough molecular analysis on the role of hypoxia-inducible factor signalling on GC pathway will be provided. To tackle this, I took advantage mainly of the *vhl*$^{+/-}$(*phd3:eGFP*) line together with the aforementioned *arnt1*$^{+/-}$ (phd3:eGFP) mutant line I created. Of note, all the data I collected from RTqPCR analysis, whole mount *in situ* hybridisation (WISH) and cortisol quantification converged towards the same direction and allowed me to propose a logical model of interaction between HIF and GC signalling, *in vivo*. Once again, both phenotypic and molecular tests performed on these mutant lines were followed by optical and fluorescence microscope imaging.

5.2. Modulation of the HIF signalling affects GC response

To investigate the role of HIF signalling on GC pathway, I initially set up to test the expression of four potential GC target genes from mammalian studies (*fkbp5, il6st, pck1 and lipca*) in a HIF upregulated (*vhl*$^{-/-}$) and downregulated scenario (*arnt1*$^{-/-}$), compared to wild types, via RTqPCR analysis on 5 dpf larvae. The aim was indeed to check how the GC response varies according to different HIF activation levels.

As previously stated in chapter 3.4, the aforementioned target genes have been selected as potential GC response reporters, however it is important to note that they may have both other inputs and developmental regulation. In this regard, my data confirmed that in 5 dpf zebrafish larvae *fkbp5* is the most well-established and sensitive readout of Gr activity, whereas the other aforementioned genes (*il6st, pck1 and lipca)* were observed to be less reliable (**figure 5.1A-H**). For this reason, I focused this analysis on *fkbp5* expression (**figure 5.1I-L)**.

Importantly, qPCR data obtained from my analysis shows that *fkbp5* expression is downregulated (fold change = 0.1; P = 0.0035) in the presence of an upregulated HIF pathway (*vhl*$^{-/-}$ larvae) compared to DMSO treated *vhl* siblings (**figure 5.1I**). On the other hand, when the HIF pathway is downregulated (*arnt1*$^{-/-}$ larvae), *fkbp5* expression is upregulated (fold change = 24.1; P<0.0001), compared to DMSO treated wild-type levels (**figure 5.1L**). Of note, these data highlighted the presence of a 240 fold difference in the *fkbp5* expression between *vhl*$^{-/-}$ (HIF overexpressed) and *arnt1*$^{-/-}$ larvae (HIF suppressed).

To further investigate the role of HIF signalling on GC response, I also performed betamethasone treatment [30 μM] on the aforementioned mutant lines, followed by RTqPCR analysis. Notably, the administration of synthetic GCs was able to increase

fkbp5 expression in *vhl* siblings but was only able to weakly do that in *vhl* mutants. In particular, its induction levels were not only lower in BME treated *vhl* mutants (fold change = 2.1) than in BME treated wild-type siblings (fold change = 7, P = 0.0286), but also *fkbp5* expression was not substantially different from DMSO treated wild types (**figure 5.1I**). Vice versa, when the HIF pathway was suppressed (*arnt1*$^{-/-}$ larvae), betamethasone treatment was able to further upregulate the expression of *fkbp5* (fold change = 107,5; P = 0.0031), compared to DMSO treated *arnt1* mutant larvae (**figure 5.1L**).

Cumulatively, these results indicate that upregulated HIF levels are somehow able to repress GR activity and can blunt or abolish its sensitivity to an exogenous GR agonist (BME treatment). On the other hand, it is interesting to note that although HIF activity is expected to be low in wild-type larvae in a normoxic environment, its function is also detectable with respect to suppression of GR activity. Indeed, if *arnt1* gene is knocked-out (*arnt1*$^{-/-}$) an increased GR responsiveness is observed (**figure 5.1L**).

Consequently, since these data shed lights on a novel route mediated by HIF to control the GC response, I asked whether this was due to any potential upstream effect of HIF signalling on steroidogenesis. To this end, in order to further analyse whether this had repercussions either on steroidogenesis and/or cortisol levels, I tested them both in a HIF upregulated (*vhl*$^{-/-}$) and downregulated scenario (*arnt1*$^{-/-}$). In this regard, the following section will focus on a series of experiments performed to verify this hypothesis.

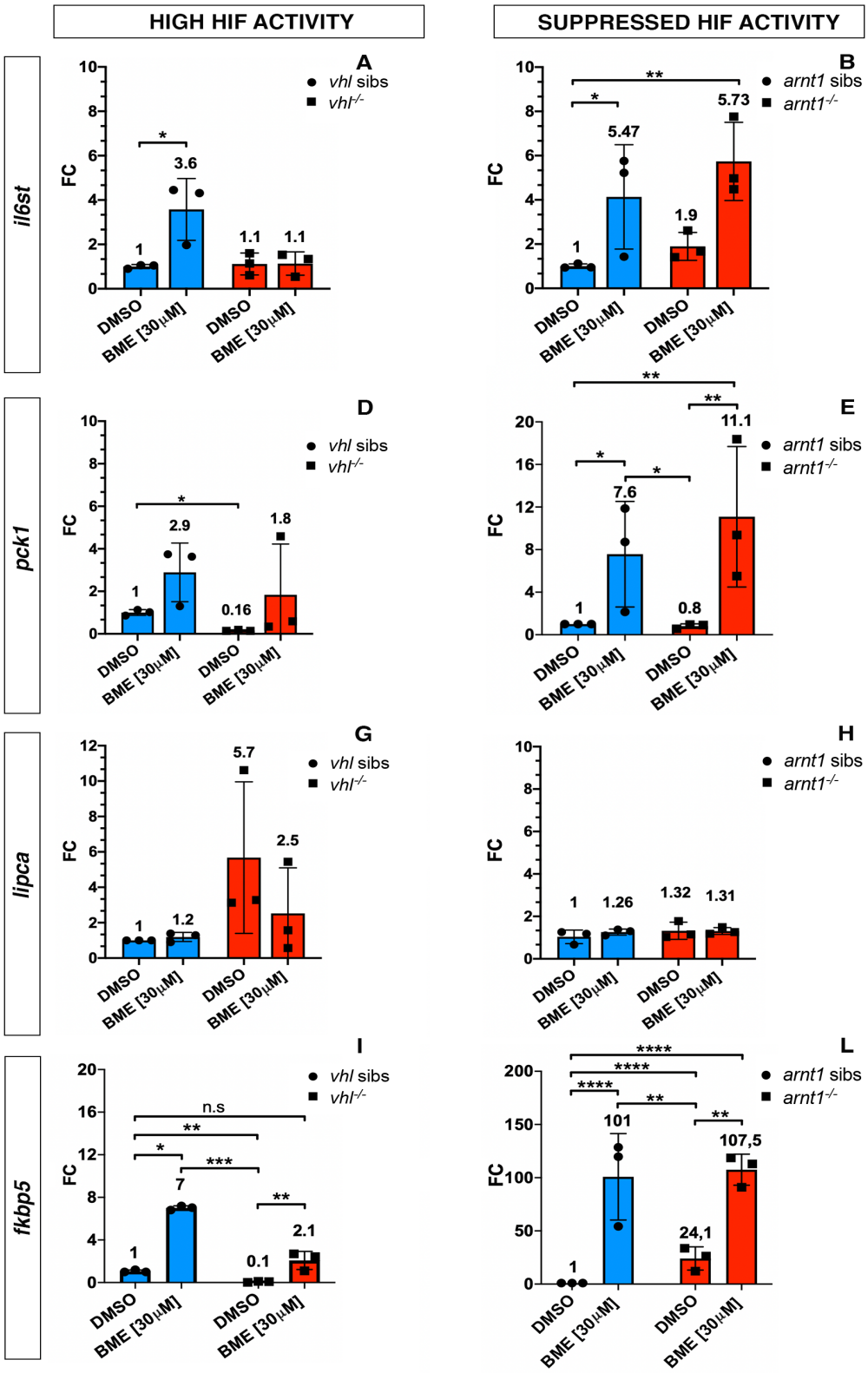

Figure 5.1. Schematic view of RTqPCR analysis on il6st, pck1, lipca and fkbp5 (GC target genes) expression carried out both on *vhl*$^{+/-}$(*phd3:eGFP*) and *arnt1*$^{+/-}$*(phd3:eGFP)*. The aim was to quantify GC target genes expression in the presence of upregulated and downregulated HIF signalling pathway. Statistical analysis performed on ΔΔCt values; data are shown as fold change values for RTqPCR analysed samples; ordinary Two-way ANOVA followed by Dunnett's multiple comparison test (*P < 0.05; **P < 0.01; ***P <0.001; ****P < 0.0001). Blue bars: wid-types and/or heterozygotes (siblings); red bars: mutants.

5.3. HIF signalling acts as negative regulator of steroidogenesis

5.3.1. *arnt1* loss of function derepressed GC responsiveness and upregulates *cyp17a2* expression

To better examine the interplay between HIF signalling and steroidogenesis, I initially tested the expression of *pro-opiomelanocortin* (*pomca*) and *Cytochrome P450 family 17 polypeptide 2* (*cyp17a2*), via whole mount *in situ* hybridisation, on DMSO and BME [30 μM] treated 5 dpf *arnt1* sibling and mutant larvae.

I have chosen these two probes because they are reliable and well-known readouts of HPI axis functioning and steroidogenesis. In particular, Pomca is the precursor molecule of the adrenocorticotropic hormone (ACTH), which is transported via the peripheral circulation to its effector organ, the interrenal tissue, where it stimulates the synthesis and secretion of GCs. Furthermore, it is mainly synthetized by the pituitary anterior lobe corticotropes and the intermediate lobe melanotrophs, in response to stressor recognition and corticotropin-releasing factor (CRF) release. Moreover, *pomca* is also negatively regulated by increased blood cortisol levels via GC-GR mediated negative feedback loop, as part of the HPI axis regulation (Griffiths *et al.*, 2012; Ziv *et al.*, 2012). For these reasons, its expression is a well-established readout of the HPI axis functioning in zebrafish larvae. Finally, previous study carried out in mice suggested that HIF promotes POMC activity in the pituitary gland (Zhang *et al.*, 2011).

By contrast, Cyp17a2 plays a pivotal role in steroidogenesis, as it is one of the steroid-oxidizing cytochromes in the interrenal gland which catalyses the two-step oxidation reaction of progesterone and pregnenolone into 17-OH-progesterone and

17-OH-pregnenolone. For this reason, it is one of the main enzymes required for the conversion of cholesterol into cortisol in zebrafish, upon ACTH stimulation (Ramamoorthy and Cidlowski, 2016; Eachus *et al.*, 2017; Weger *et al.*, 2018).

As expected, data derived from whole mount *in situ* hybridisation analysis on 5 dpf larvae showed that *arnt1* siblings displayed normally expressed *cyp17a2* (**figure 5.2C-C'**) and *pomca* expression (**figure 5.2A**), which were observed to be suppressed only as a result of BME treatment (**figure 5.2D-D' and 5.2A'**). Interestingly, on the other hand, 5 dpf *arnt1*$^{-/-}$ larvae displayed an upregulated *cyp17a2* expression (**figure 5.2E-E'**) coupled to downregulated *pomca* (**figure 5.2B**), compared to *arnt1* siblings.

For this reason, since *arnt1*$^{-/-}$ larvae were characterized by an upregulated GC responsiveness (**figure 5.1L**), I hypothesize that in a HIF suppressed scenario, in the absence of functional *arnt1*, the observed *pomca* downregulation is most likely to occur as a result of the GC-GR induced negative feedback loop, triggered by the presence of putatively high cortisol levels (**figure 5.5**). Of note, if this was true, this would also explain the presence of high *cyp17a2* expression levels observed in DMSO treated mutant larvae (**figure 5.2E-E'**), compared to *arnt1* siblings (**figure 5.2C-C'**)

Finally, in accordance with this hypothesis, I also speculate that the administration of an exogenous source of synthetic GCs, by signalling for the presence of upregulated *pomca* and high cortisol levels, triggers the downregulation of *pomca* at the level of the pituitary gland and consequently of the interrenal *cyp17a2* gene even further (**figure 5.2F-F' and 5.2B'**).

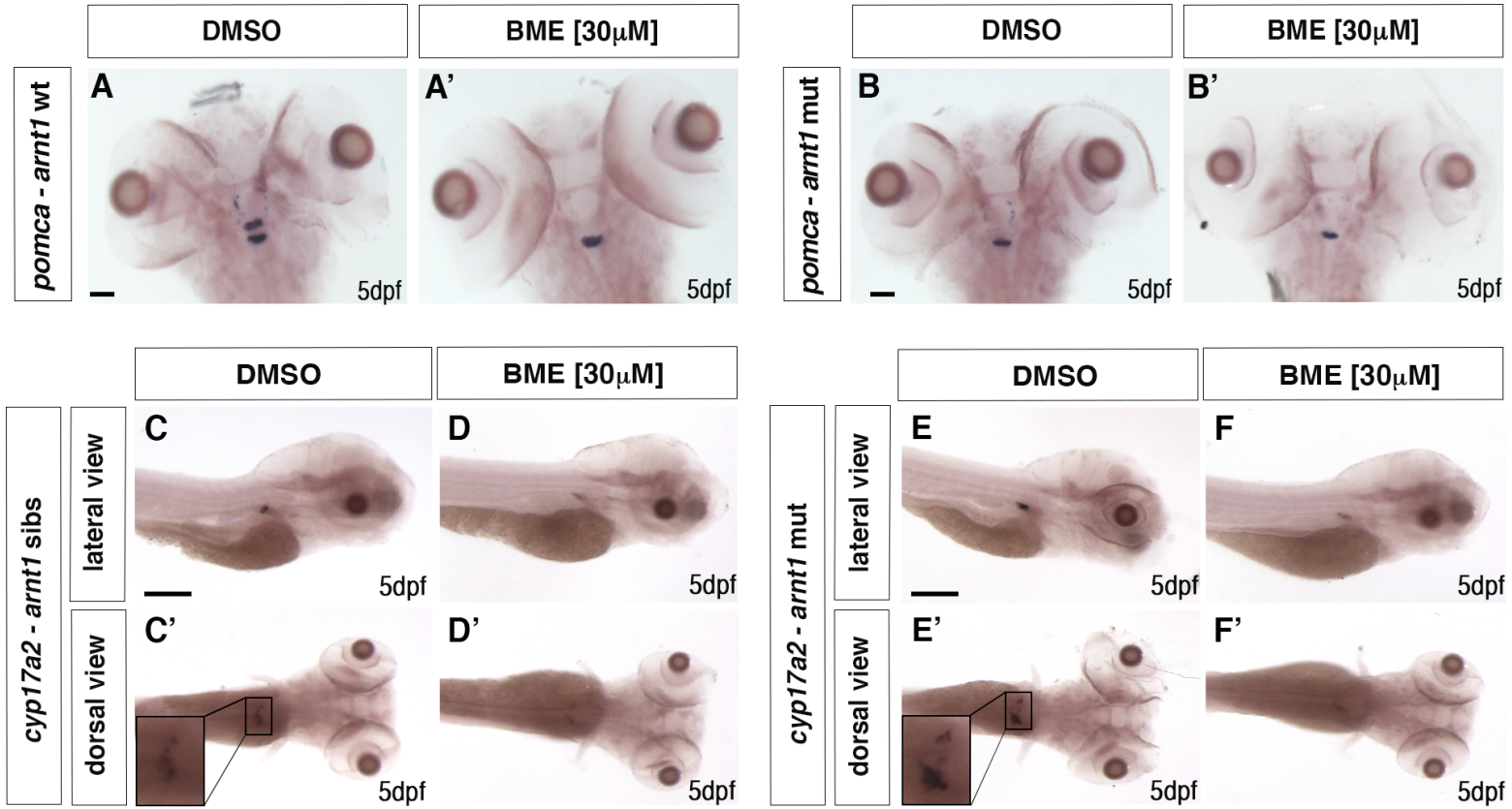

Figure 5.2 Representative pictures of WISH performed on DMSO and BME [30 μM] treated *arnt1* mutant line at 5 dpf, using *pomca* as probe. *arnt1* wt DMSO treated (n= 30/30 larvae) showed normal pomca expression; *arnt1* wt BME treated (n= 29/30 larvae) showed downregulated pomca expression. In contrast, *arnt1*$^{-/-}$ DMSO treated (n= 28/30) and *arnt1*$^{-/-}$ BME treated (n= 30/30) larvae showed downregulated pomca expression. Chi-square test (****P < 0.0001). Scale bar 50 μm. Representative pictures of WISH performed on DMSO and BME [30 μM] treated *arnt1* mutant line at 5 dpf, using *cyp17a2* as probe. *arnt1* wt DMSO treated larvae (n= 26/28) showed normal *cyp17a2* expression, whereas 2/28 larvae showed a weaker one; *arnt1* wt BME treated larvae (n= 28/30) showed downregulated *cyp17a2* expression, whereas 2/30 larvae showed a normal one. In contrast, *arnt1*$^{-/-}$ DMSO treated larvae (n= 24/28) showed upregulated *cyp17a2* expression, whereas 4/28 larvae showed a weaker one. *arnt1*$^{-/-}$ BME treated larvae (n= 25/29) showed downregulated *cyp17a2* expression, whereas 4/29, showed a normal one. Chi-square test (****P < 0.0001). Scale bar 200 μm.

5.3.2. Overexpressed HIF signalling represses GC responsiveness and downregulates *cyp17a2* expression

To further study the effect of HIF pathway on GC signalling, I subsequently investigated both *pomca* and *cyp17a2* expression in the opposite - HIF upregulated - scenario, by carrying out *in situ* hybridization on the *vhl* mutant line. As expected, *vhl* siblings displayed normally expressed *pomca* (**figure 5.3A**) and *cyp17a2* (**figure 5.3C-C'**), which were observed to be downregulated only as a consequence of BME treatment (**figure 5.3A' and 5.3D-D'**).

Interestingly, on the other hand, 5 dpf *vhl*$^{-/-}$ larvae which were characterized by a suppressed GR activity (**figure 5.1I**), showed downregulated *cyp17a2* (f**igure 5.3E-E'**), and downregulated *pomca* expression (**figure 5.3B**) compared to *vhl* siblings (**figure 5.3C-C' and 5.3A**). Here, as previously monitored in the *arnt1* mutant line, betamethasone treatment was observed to decrease *cyp17a2* expression at the level of the interrenal gland even further.

Therefore, I speculate that in the absence of functional *vhl* (HIF upregulated scenario), *proopiomelanocortin-a* downregulation is most likely to occur as a consequence of a HIF-mediated downregulation of *pomca* expression (**figure 5.5**).

As a consequence of the above considerations, if this was true, I predicted to observe reduced levels of endogenous cortisol in *vhl*$^{-/-}$ larvae and normal or even increased cortisol levels in *arnt1*$^{-/-}$ larvae at 5 dpf.

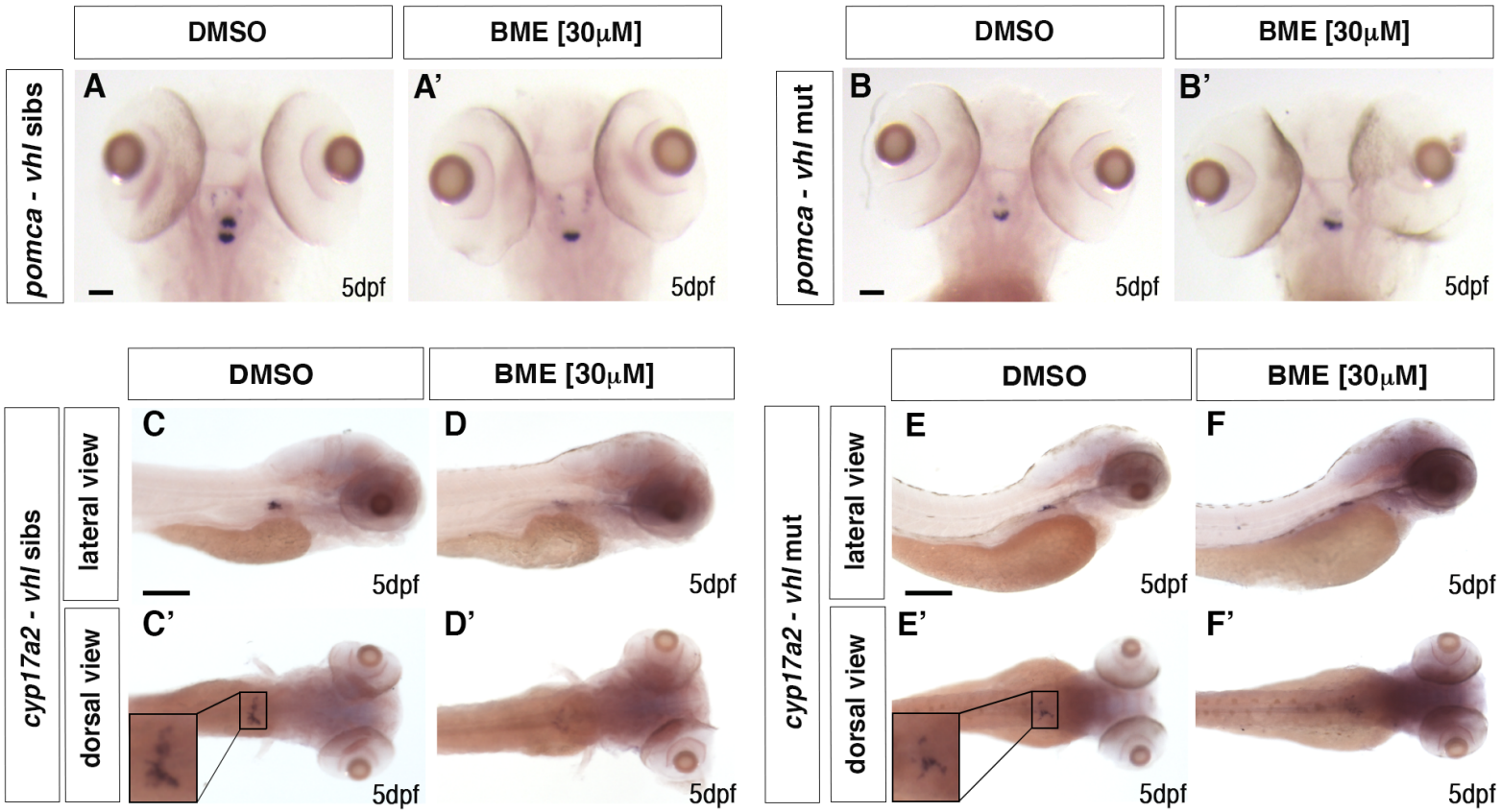

Figure 5.3. Representative pictures of WISH performed on DMSO and BME [30 μM] treated *vhl* mutant line, at 5 dpf, using *pomca* as probe. DMSO treated *vhl* siblings (n= 26/28) showed normal *pomca* expression; BME treated *vhl* siblings (n= 28/30) showed downregulated *pomca* expression. In contrast, *vhl*$^{-/-}$ DMSO (n= 28/29) and BME (n= 28/28) treated larvae showed downregulated *pomca* expression. Chi-square test (****P < 0.0001). Scale bar 50 μm. Representative pictures of WISH performed on DMSO and BME [30 μM] treated *vhl* mutant line, at 5 dpf, using *cyp17a2* as probe. DMSO treated *vhl* siblings (n= 18/21) showed normal *cyp17a2* expression, whereas 3/21 larvae showed a weaker one; BME treated *vhl* siblings (n= 28/30) showed downregulated *cyp17a2* expression, whereas 2/30 larvae showed a normal one. On the other hand, *vhl*$^{-/-}$ DMSO treated larvae (n= 27/28) showed weak *cyp17a2* expression, whereas 1/28 larvae showed a normal *one. vhl*$^{-/-}$ BME treated larvae (n= 30/30) showed downregulated *cyp17a2* expression. Chi-square test (****P < 0.0001). Scale bar 200 μm.

5.3.3. Steroidogenesis is impaired in *vhl* mutant and is enhanced in *arnt1* mutant zebrafish larvae

To confirm the hypothesis that overexpressed HIF levels negatively act not only on GC responsiveness but also on steroidogenesis, whereas *arnt1* loss of function derepresses them, I quantified cortisol levels on the aforementioned *vhl* and *arnt1* mutant lines, respectively. Three biological replicates of 150 larvae each for *hif1β*^{sh544} mutants, *hif1β*^{sh544} siblings, *vhl*^{hu2117} mutants and *vhl*^{hu2117} siblings at 5dpf were respectively used for steroid hormone extraction and quantification, as thoroughly described in the subchapter 2.6 of Material and methods. Interestingly, quantification analysis revealed that cortisol concentration was significantly reduced (P value <0.0028) in *vhl*$^{-/-}$ larvae (92,7 fg/larva), compared to *vhl* siblings (321 fg/larva) (**figure 5.4A**). On the other hand, cortisol was significantly increased (P value <0.0001) in *arnt1* mutants (487.5 fg/larva), compared to *arnt1* siblings (325 fg/larva) (**figure 5.4B**).

Taken together, these data confirmed my hypothesis and showed for the first time that in zebrafish larvae the HIF signalling can act as negative regulator both of GR transcriptional activity and of steroidogenesis. Indeed, if only GR transcriptional activity was blocked by HIF, cortisol levels would be expected to be higher in *vhl* mutants. This is because by blocking GR (i.e. as occurs in *gr*$^{-/-}$ larvae), the GC-GR mediated negative feedback cannot occur anymore and this makes larvae hypercortisolaemic (Faught, Best and Vijayan, 2016; Facchinello *et al.*, 2017). Importantly, since *vhl*$^{-/-}$ larvae are characterized both by downregulated GR transcriptional activity and decreased cortisol levels, this strongly indicates that HIF

signalling can act both at the level of the pituitary gland (to inhibit *pomca* expression) and intracellularly to block GR transcriptional activity itself.

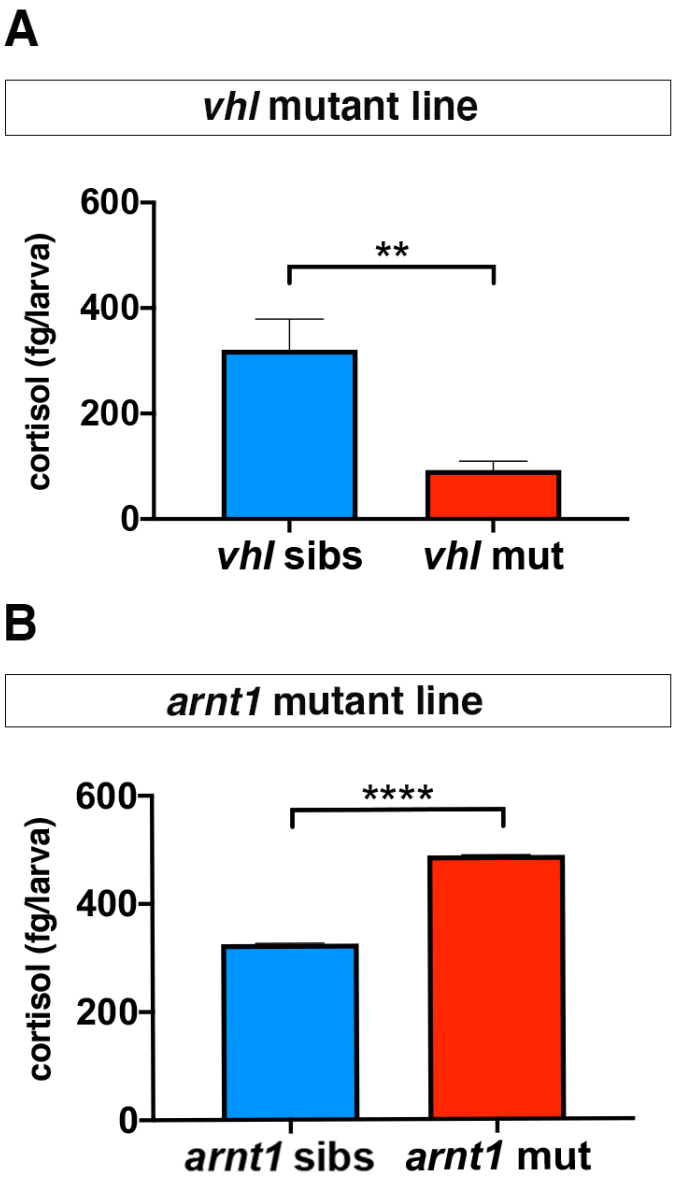

Figure 5.4 A. Steroid quantification results showed a significantly reduced cortisol concentration (P value <0;0028) in *vhl* mutants (92.7 fg/larva, in triplicate), compared to *vhl* siblings (321 fg/larva, in triplicate) at 5 dpf. **B.** Furthermore, a significantly increased cortisol concentration (P value <0;0001) was quantified in *arnt1* mutants (487.5 fg/larva, in triplicate), compared to *arnt1* wild-types larvae (325 fg/larva, in triplicate) at 5 dpf; unpaired t-test (**P < 0.01; ****P <0.001).

5.4. Discussion

Previous *in vitro* studies highlighted the potential for crosstalk between HIF and GC pathways. However, insights about how the interplay between these two major signalling pathways precisely occurs *in vivo* are still fragmentary and scarce. To this end, I was particularly keen to answer to the following question: is HIF pathway contributing to GC functions? If so, how is this occurring?

In this regard, I initially investigated how HIF signalling was able to affect the expression of selected GC target genes. To do so, I set up to perform RTqPCR analysis on two opposite mutant lines, characterised by an overexpressed (*vhl* $^{-/-}$) and a downregulated (*arnt1*$^{-/-}$) HIF pathway, respectively.

Collectively, my data show that the strong activation of the HIF signalling pathway, induced by *vhl* mutation, is able to blunt the GR transcriptional regulation, as judged by *fkbp5* expression. Vice versa, the inhibition of the HIF pathway, induced by *arnt1* loss of function, derepressed it. Furthermore, betamethasone treatment performed on the aforementioned mutant lines, followed by RTqPCR analysis, confirmed these data. Indeed, by triggering a further upregulation of the HIF signalling in *vhl*$^{-/-}$ larvae (as observed via hypoxia reporter expression), BME strengthens the HIF-mediated inhibition of the GC response, which in turn cannot be upregulated as strongly as occur in wild-types. In particular, this occur because the administration of synthetic GCs, by directly acting downstream of the HPI axis, is able to overcome the HIF-mediate negative regulation of the GC signalling.

By contrast, in the *arnt1* loss of function scenario, since HIF signalling cannot blunt GC responsiveness anymore, BME can further upregulate GC reporters. Furthermore, since these experiments were carried out under normal atmospheric

oxygen conditions, it is plausible to infer that even the low normoxic HIF activity nonetheless suffices to attenuate GR transcriptional regulation.

Then, in order to check whether this was due to any potential effect played by HIF signalling on steroidogenesis (Tan *et al.*, 2017) I quantified the expression of steroidogenesis-related genes (*pomca* and *cyp17a2*) both in *vhl*$^{-/-}$ and in *arnt1*$^{-/-}$ larvae, via whole-mount *in situ* hybridization analysis. Unexpectedly, both mutants showed downregulation of *pomca*. However, *arnt1*$^{-/-}$ larvae, which were characterized by an upregulated GC responsiveness, showed also an upregulated *cyp17a2* expression. Vice versa, *vhl*$^{-/-}$ larvae which have a downregulated GC response, displayed a downregulated *cyp17a2* expression.

As a consequence of the above considerations, taking into account the qPCR data on *fkbp5* expression in both mutant lines, I assume that in an *arnt1* knock-out scenario, the downregulation of *pomca* occurs as a consequence of the GC induced negative feedback loop, aimed to tune cortisol biosynthesis.

This assumption is also coherent with the upregulated basal cortisol levels quantified in these mutants. On the other hand, when HIF signalling is upregulated (in *vhl*$^{-/-}$), I infer that the downregulation both of *pomca* and *cyp17a2* may occur via HIF-mediated activity, which leads to the observed low cortisol levels and suppressed GR activity. Indeed, GCs control a plethora of physiological processes, act on almost every tissue and organ in the body to preserve homeostasis and have a strong anti-inflammatory and immunosuppressive activities. For this reason, the HPA/I axis must finely control their secretion (Oakley and Cidlowski, 2013).

Since previous studies in my laboratory demonstrated that GCs also act as HIF activators (Santhakumar *et al.*, 2012; Vettori *et al.*, 2017), I speculate that HIF pathway can in turn control cortisol levels by acting on *pomca*. This would allow HIF signalling

not only to monitor its own levels, but also to ensure homeostasis. Of note, the fact that HIF is particularly expressed in the brain, where it was found to directly act on *POMC* transcription to mediate glucose sensing in mice, (Sharp, Bergeron and Bernaudin, 2001; Baranova *et al.*, 2007; Fan *et al.*, 2009; Zhang *et al.*, 2011), would allow to strengthen my hypothesis about the negative regulatory function played by HIF on *pomca* expression. Moreover, since the GC circadian production in teleost is tuned at the level of the pituitary gland and several studies described the presence of links between HIF signalling and circadian rhythms (Egg *et al.*, 2013, 2014; Pelster and Egg, 2015; Peek *et al.*, 2017), this further enhances the strict relationship observed between GC and HIF signalling pathways.

Finally, as HIF signalling is a primary controller of cellular pro-inflammatory responses to hypoxia (Imtiyaz and Simon, 2010; Eltzschig and Carmeliet, 2011; Palazon *et al.*, 2014), which would counteract the anti-inflammatory activity played by GC, I infer that the concurrent expression of both upregulated HIF and GC pathways would be detrimental to homeostasis. In addition, since chronically elevated HIF level may have deleterious effects on an organism (i.e. on energy balance, immune system, blood circulation etc.), the need of HIF signalling to tune the stress response and avoid an uncontrolled systemic overexpression of the HIF pathway itself is warranted.

Importantly, my data would also be consistent with previous work which showed that exposure to hypoxia leads to downregulation of steroidogenic genes (*StAR, cyp11c1, cyp19a, cyp19b, hmgcr* and *hsd17b2*) in 72 hpf larvae, whilst zHIF-α loss of function triggered the upregulation especially of *StAR*, *cyp17a1* and *cyp11b2* (Tan *et al.*, 2017).

In this regard, to further test my hypothesis and confirm my assumptions, I set up to extract and quantify cortisol levels both in a HIF upregulated (*vhl*$^{-/-}$) and HIF

downregulated scenario (*arnt1*$^{-/-}$) in 5 dpf larvae. In particular, I predicted to observe reduced levels of endogenous GCs in *vhl*$^{-/-}$ and normal or even increased levels in *arnt1*$^{-/-}$ larvae. Importantly, the fact that cortisol levels were reduced in *vhl* mutant larvae and were upregulated in *arnt1* mutants, is coherent with my hypothesis.

Cumulatively, the HIF-mediated negative regulation of *pomca* seems to be a logic homeostatic interaction: cortisol increases HIF, which then reduces GR activity, that in the end should lead to less HIF signalling. For all these reasons, my data allow to fill the gaps and to provide a logic explanation on how this crosstalk may occur *in vivo* (**figure 5.5**).

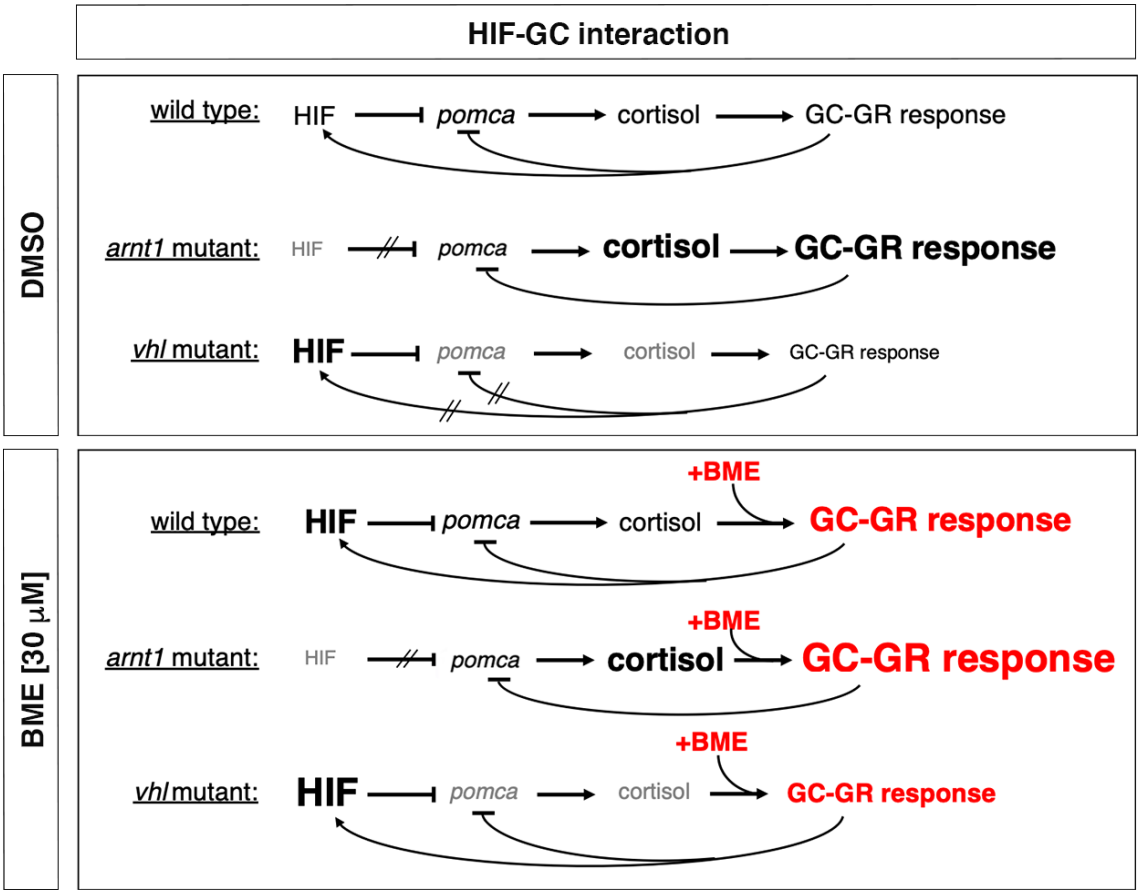

Figure 5.5 Speculative schemes of how the putative HIF-GC crosstalk occurs in wildtypes and how it is affected both in *arnt1*$^{-/-}$ and in *vhl*$^{-/-}$ larvae at 5 dpf, after BME [30 µM] treatment. In all the cases, *since* betamethasone acts downstream of the HPI axis, by directly binding to Gr, it is able to upregulate GC target genes expression. Consequently, since GCs are able to stimulate *the* HIF signalling, as expected, I observed an increase*d phd3:eGFP*-related brightness both in wildtypes and in *vhl*$^{-/-}$. However, the fact that I did not observed any HIF upregulation both in *arnt1*$^{-/-}$ and in *arnt1*$^{-/-}$*;vhl*$^{-/-}$ *larvae*, highlighted the fact that the BME induced HIF signalling activation is an Arnt1 dependent mechanism.

6. GENERAL DISCUSSION AND FUTURE WORK

Homeostasis is a state of optimal functioning in an organism, based on internal, physical and chemical conditions, which is maintained by several regulatory mechanisms aimed to assure both survival and correct functioning of all vertebrate species' body (Biddlestone, Bandarra and Rocha, 2015).

In particular, one of the main stressors that perturbs homeostasis is represented by hypoxia. It is a common stressful condition to which cells must rapidly respond, which is characterized by the lack of appropriate oxygen supply to meet metabolic requirements (Bertout, Patel and Simon, 2008; Semenza, 2013). In this regard, one of the primary cellular apparatus that organisms developed to cope with reduced oxygen availability is represented by the hypoxia-inducible factor transcription factors (HIF) family. It consists of key regulators of the cellular response to low oxygen levels, whose aim is to promptly coordinate a series of metabolic changes (i.e. from aerobic to anaerobic metabolism) that allow the body to prevent metabolic shutdown and consequent death (Elks *et al.*, 2015). Indeed, if this mechanism either fails or is maladaptive can lead to a wide range of pathological conditions including stroke, inflammation, tissue ischemia, and the growth of solid tumours. This is because, hypoxia shares an interrelated connection with inflammation, as inflammatory states during hypoxic conditions usually occur as a consequence of a broad range of human diseases (Bartels, Grenz and Eltzschig, 2013).

In this regard, synthetic GCs, which are analogous to naturally occurring steroid hormones, have been used for years as anti-inflammatory medications for treating pathological conditions that are linked to hypoxia (i.e., asthma, rheumatoid arthritis, chronic obstructive pulmonary disease, ischemic injury, etc.).

This is because GCs represent a well-known group of lipophilic steroid hormones synthetized and released by the interrenal tissue in teleosts, in response to stress. In particular, the latter is regulated by the hypothalamus-pituitary-interrenal (HPI) axis, which is the equivalent of the mammalian hypothalamus-pituitary-adrenal (HPA) axis. Moreover, cortisol is the main form of GC both in humans and teleosts and control a variety of physiological processes comprising inflammation, glucose homeostasis, stress response and intermediary metabolism.

In this respect, while several *in vitro* studies highlighted the presence of a crosstalk between hypoxia-inducible factors and GCs, (Kodama *et al.*, 2003; Leonard *et al.*, 2005; Wagner *et al.*, 2008; Zhang *et al.*, 2015, 2016) many questions remain unanswered and the argument is still debated. To this end, this study builds on previous knowledge regarding the interplay between these two major signalling pathways and provides further insights related to the role of HIF signalling on GC responsiveness and vice versa. Of note, it is particularly important to study and shed light on this discussed topic for the following reasons: a) by teasing out how this crosstalk occurs *in vivo* researchers might find new routes to downregulate HIF signalling for clinical purposes; b) by understanding how GCs act on HIF and vice versa, it will be also possible to reduce both the presence of adverse effects and the GC resistance, which nowadays limit their clinical use. Therefore, extending the research on how precisely this interplay occurs *in vivo*, may have a wide physiological significance in health and disease and may help researchers to develop more effective anti-inflammatory drugs in the future.

To this end, the zebrafish (*Danio rerio*) has been selected because it is an effective *in vivo* model organism to study how and to what degree hypoxic signalling affects the endogenous GC response and vice versa. Indeed, zebrafish share all the

components of the human HIF and GC signalling pathways and it has been demonstrated to be a very informative and genetically tractable organism for studying both hypoxia and the stress response both in physiological and pathophysiological conditions (van Rooijen *et al.*, 2011; Santhakumar *et al.*, 2012; Ziv *et al.*, 2012; Elks *et al.*, 2015; Faught and Vijayan, 2018b). In this regard, this thesis presents novel *in vivo* data, based on the use of zebrafish larvae, focused on the crosstalk between these two major signalling pathways.

As a base for starting the genetic analysis of this crosstalk, the generation both of *arnt1* and *gr* null mutant lines was warranted in order to downregulate both HIF and GR signalling respectively. To achieve this, a discriminative experiment was designed to insert each mutation in the well-established *vhl*$^{+/-}$(*phd3:eGFP*) mutant background (Rooijen *et al.*, 2009; Santhakumar *et al.*, 2012), where HIF signalling is strongly upregulated. The following step was to determine the importance both of *arnt1* and *arnt2* in the overall HIF response. To this end, phenotypic analysis carried out on 5 dpf double mutant larvae derived from the *arnt1*$^{+/-}$*;vhl*$^{+/-}$ mutant line allowed to show the presence of a mild upregulation of the HIF signalling coupled to a more rescued phenotype in them, compared to the one observed in *vhl*$^{-/-}$ larvae. However, *arnt1*$^{-/-}$*;vhl*$^{-/-}$ larvae beyond 5 dpf displayed only partial recovery from the *vhl* phenotype, as they developed well till 15 dpf, but then failed to grow and thrive compared to their wild-type siblings.

Another important aspect to consider is that unlike both *vhl* and *arnt2* mutants, which are embryonic lethal by 8–10 dpf (Hill *et al.*, 2009; Rooijen *et al.*, 2009), *arnt1*$^{-/-}$ larvae showed to be viable and fertile. Furthermore, my data confirmed that even if Arnt1 is not essential for survival, it is necessary in the liver and in organs outside the central nervous system for HIF−α function. By contrast, it was possible to verify that

Arnt2 isoform is especially required in the developing central nervous system, in accordance with previous study (Hill *et al.*, 2009). As a consequence of the above considerations, the similarities observed in terms of HIF reporter brightness both in *arnt1*$^{-/-}$;*vhl*$^{-/-}$ and *arnt2*$^{-/-}$;*vhl*$^{-/-}$ larvae (obtained via CRISPant technology) suggested that there is not a strong functional separation between the two isoforms. It is also possible to conclude that both Arnt1 and Arnt2 have partially overlapping functions *in vivo* and that both contribute to assure the HIF response. However, a more in-depth analysis of the expression pattern of these two isoforms coupled to molecular analysis will help to elucidate which is their involvement in the HIF signalling at early developmental stages in zebrafish larvae.

With respect to the effect of HIF signalling and GC responsiveness, it was particularly interesting to note that a strong activation of the HIF signalling (in *vhl*$^{-/-}$ larvae) can blunt GR transcriptional regulation as judged by RTqPCR analysis, whereas *arnt1* loss of function is able to derepress it. Moreover, as my experiments have been performed at normal atmospheric oxygen conditions, it was possible to deduce that normoxic HIF activity nevertheless suffices to mitigate GR transcriptional regulation. This is important because there were no clear indications so far about the control mechanism performed by HIF on GC responsiveness. Indeed, the majority of the data about it derived from i*n vitro* studies, where no functional HPI axis with its GC-GR mediated negative feedback loop are present (Kodama *et al.*, 2003; Leonard *et al.*, 2005; Wagner *et al.*, 2008; Gaber *et al.*, 2011; Zhang *et al.*, 2015). For this reason, showing and confirming the presence of this mechanism would be able to clarify how the crosstalk between HIF and GC pathway occurs *in vivo.* Moreover, this would underscore a novel model of interaction between these two major signalling pathways.

In this regard, an initial confirmation of this hypothesis was obtained by quantifying the steroidogenesis-related genes expression (*pomca* and *cyp17a2*) both in *vhl* and in *arnt1* mutant lines via whole-mount in situ hybridization. Indeed, both *vhl*$^{-/-}$ and in *arnt1*$^{-/-}$ larvae displayed a downregulated *pomca* expression at the level of the pituitary gland. However, *arnt1*$^{-/-}$ larvae displayed upregulated *cyp17a2* expression, which was instead downregulated *in vhl*$^{-/-}$ larvae. Furthermore, by considering the quantitative analysis on GR target genes in these mutants, it was possible to infer that in an *arnt1* knock-out scenario (where HIF is suppressed), *pomca* downregulation occurs as a result of the GC/GR-mediated negative feedback loop aimed to restrain cortisol biosynthesis. This was also confirmed by the presence of upregulated basal cortisol levels coupled to an increased GC responsiveness in this mutant line (**figure 5.6**). On the other hand, in *vhl*$^{-/-}$ (where HIF is upregulated) the fact that both cortisol levels and GC response were downregulated in the presence of *pomca* and *cyp17a2* inhibition, strengthened the hypothesis that this might occur due to a direct HIF-mediated activity on *pomca* expression.

Indeed, GCs control a plethora of physiological processes, act on almost all the tissues and organs in the body and have a strong anti-inflammatory and immunosuppressive actions. For these reasons, their production must be finely controlled by the HPA/I axis (R. Oakley, 2013). Moreover, even if it is rare and counterintuitive that a GC-resistant condition coincides with low cortisol levels (as observed in BME treated *vhl* mutants), I speculate that HIF signalling can act as a second controller of the GC-mediated stress response (in addition to cortisol levels themselves). Indeed, as previous work in my laboratory highlighted that GCs also act as HIF activators (Santhakumar *et al.*, 2012; Vettori *et al.*, 2017) I infer that HIF may in turn control cortisol levels by acting on *pomca* expression. This would allow HIF

signalling not only to manage its own levels, but also to assure both stress resolution and homeostasis. Of note, the reason for hypothesising that HIF signalling would counteract the anti-inflammatory GC activity, resides in the fact that the simultaneous expression of both upregulated HIF and GC pathway would be detrimental to homeostasis. Indeed, HIF is a master regulator of cellular pro-inflammatory responses to hypoxia, whereas GCs have a potent anti-inflammatory and immune suppressive activity.

Of note, my hypothesis would also be in accordance with a previous research showing that hypoxia exposure resulted in the downregulation of steroidogenic genes (*StAR*, *cyp19b, cyp19a, cyp11c1*, *hsd17b2* and *hmgcr*) in 72 hpf larvae, whilst zHIF-α loss of function stimulated the upregulation specifically of *StAR*, *cyp11b2* and *cyp17a1* (Tan *et al.*, 2017). Importantly, the fact that cortisol levels were reduced in *vhl*$^{-/-}$ and upregulated in *arnt1*$^{-/-}$ is consistent with my assumption. In addition, the fact that in teleost GCs biosynthesis is finely regulated by the hypothalamus-pituitary gland activity in a circadian way and multiple studies showed a direct connection between HIF signalling and circadian rhythms (Egg *et al.*, 2013, 2014; Pelster and Egg, 2015; Peek *et al.*, 2017), this further confirmed the tight interplay observed between GC and HIF signalling pathways. As a consequence of the above considerations, the HIF-mediated *pomca* negative regulation seems to be a logic homeostatic response.

Consequently, another important aspect to analyse in the future is related to the HIF signalling regulation of the GC responsiveness in the presence of *arnt1* and/or *gr* loss of function (*arnt1*$^{-/-}$; *vhl*$^{-/-}$ and *gr*$^{-/-}$; *vhl*$^{-/-}$ larvae), where HIF pathway is partially attenuated. This would be particularly interest to achieve via cortisol quantification coupled to molecular analysis, because it will allow to deepen the knowledge on the HIF-GC crosstalk also in these intermediate scenarios.

With respect to the role of GCs in the HIF signalling, it is important to notice that *gr* mutation is able to generate an efficient, but not complete rescue of the *vhl* phenotype. Moreover, the fact that *gr*$^{-/-}$;*vhl*$^{-/-}$ survived much longer than *vhl* mutants (>21 dpf), and that similarly to *arnt1*$^{-/-}$;*vhl*$^{-/-}$, failed to grow and thrive when compared to siblings, confirmed it. It is also interesting to note that previous work from my lab (Vettori *et al.*, 2017) established that activation of the GC signalling negatively regulates VHL in human liver cells. However, my current data derived from *in vivo* genetic analysis on these mutants reveal that in zebrafish larvae there must be a different interaction's point between these two pathways. This is because a further activation of the HIF reporter was observed following BME treatment in the absence both of Vhl and Vll. Cumulatively, my data allowed to show for the first time in an *in vivo* animal model that GR is fundamental to ensure high HIF signalling levels. This is interesting because by knowing the importance of GCs in ensuring HIF pathway, it would allow to use GR inhibitors to attenuate an overstated HIF response, and to elicit a more controlled reinstatement of the homeostasis. Nevertheless, since at present the precise molecular mechanism behind it is still unknown, more research towards this direction (i.e. ChIP seq, pull-down assay) is warranted.

Importantly, data related to the effect of betamethasone treatment in *arnt1*$^{-/-}$ larvae revealed that although betamethasone can upregulate *fkbp5* expression (Vettori *et al.*, 2017), unexpectedly it failed to stimulate the HIF signalling. This was also observed in the *arnt1*$^{-/-}$;*vhl*$^{-/-}$ larvae whose *phd3:eGFP* expression unvaried after BME treatment. Here, I speculate that this would be best explained by assuming that a BME-Gr complex would preferentially act on a HIFα/ARNT1 but not a HIFα/ARNT2 complex. However, more analysis is needed to test whether this occurs also in mammalian cells.

Finally, the importance of GCs in the HIF pathway was further analysed by studying the Mr contribution to the HIF signalling itself. Indeed, nowadays nothing is known about it. Moreover, a recent work by Faught and Vijayan, 2018 demonstrated that both Gr and Mr are involved in the regulation both of zebrafish stress axis activation and function. Surprisingly, the fact that *mr CRISPR* injection in a *vhl*$^{-/-}$ background triggered a significant reduction of HIF reporter brightness, compared to uninjected *vhl*$^{-/-}$ larvae highlighted for the first time *in vivo* the importance of mineralocorticoid receptor in assuring high HIF levels. In addition, the further reduction of the HIF reporter expression following the additional removal of *mr* in a *gr*$^{-/-}$*;vhl*$^{-/-}$ background allowed to strengthen these data.

Cumulatively, it was possible to show that both the glucocorticoid receptor and mineralocorticoid receptor play a key role in enforcing the HIF signalling in the zebrafish. Moreover, this hypothesis is consistent with Faught and Vijayan, 2018 work, showing that both Gr and Mr signalling are involved in the regulation of the GC negative feedback. For these reasons, since HIF signalling plays a pivotal role in tumour growth and is proven difficult to downregulate i*n vivo*, this outcome can have a wider significance in health and disease. In this regard, my research indicates that the modulation of Gr and Mr might be a potential avenue.

Another important clinical application could be related to the mitigation of GC resistance. Indeed, it is well known that the loss of GC negative feedback, followed by hypercortisolaemia is linked to increased physiological stress and seems to contribute to anxiety, depression and post-traumatic stress disorders (Griffiths *et al.*, 2012). However, recent studies have debated about cortisol's role as pathophysiological benchmark of major depressive disorder, by stating that the link between GCs and depression is correlative rather than causal (Qin *et al.*, 2019; Nandam *et al.*, 2020). In

this regard, the use of Mr inhibitors in combination with iron chelators (i.e EDTA, deferiprone)/PHD inhibitors (i.e dimethyloxalylglycine, DMOG) could help stabilize HIF in order to both counteract the exacerbated GC production and to simultaneously avoid any possible cortisol-MR mediated activity. This could also be useful to reduce long-term use GC related side effects. On the other hand, since synthetic GCs are commonly used for acute and chronic inflammatory disorders treatments, a combined use with HIF blocking chemicals and/or oxygen treatment could help reducing HIF overexpression and to potentiate GC-related effects. In accordance with this assumption, the fact that dexamethasone (GC agonist) has been recently shown to decrease mortality in hospitalised patients with COVID-19 that require mechanical ventilation, is promising and deserves further researching.

Of note, future work that could bring to any potential drug development would include additional preclinical testing both *in vitro* and *in vivo* to better elucidate how HIF-GC interaction occurs specifically at molecular level. In particular, I believe that a multidisciplinary study characterized by molecular biology, biophysics (*in vitro*) and inflammation model (*in vivo*) approach could be exploited to this purpose. Firstly, the use of ChIP sequencing, proximity ligation assay and Fluorescence Resonance Energy Transfer (FRET) assay, could help uncovering which genes, domains, HRE/GRE are involved and if GC-GR and HIF physically interact. Secondly, to understand whether HIF-GR interplay occurs at DNA level or, as predicted by Kodama et al., 2003, via LBD, a GR-LBD plasmidic construct could be injected into $gr^{+/-}$ (*phd3:eGFP*) incross-derived zebrafish embryos following treated with a HIF activator drug (i.e FG4592 compound). Indeed, since $gr^{-/-}$ showed low HIF levels, the chemical treatment should not be able to upregulate HIF pathway in the uninjected group. Vice versa, if this occur in the injected group, it will mean that the HIF-GC interaction requires the GR-LBD to take place.

Thirdly, a mouse model for inflammation would help corroborating how HIF affects GC signalling and may have a strong clinical relevance. Indeed, what is clinically often an issue is that people with severe inflammatory phenotype are usually resistant to GCs. In this regard, since I observed that upregulated HIF levels suppress GR activity, being able to efficiently block HIF in the inflamed tissue could increase GC treatment efficacy, especially in resistant patients.

In conclusion, my study stresses the importance of the GC pathway in driving HIF signalling. In addition, a negative regulatory role performed by HIF in regulating both GR responsiveness and steroidogenesis was uncovered as shown via RTqPCR, WISH and steroid hormone quantification. A novel mineralocorticoid receptor contribution to the HIF-GC crosstalk was also highlighted. Here, although Mr contribution to HIF response in other organisms remains unclear, my data suggests that research into its function is warranted. Finally, original zebrafish mutant lines (*gr*$^{+/-}$*;vhl*$^{+/-}$*, arnt1*$^{+/-}$*;vhl*$^{+/-}$ *and arnt1*$^{+/-}$*;gr*$^{+/-}$*;vhl*$^{+/-}$) which helped to better comprehend how the interplay between HIF and GCs occurs *in vivo* were created and deeply described. For these reasons, I believe that this work could pave the way for further *in vivo* analysis aimed to accurately identify the broad crosstalk behind these two major signalling pathways.

7. REFERENCES

1. Alsop, D. and Vijayan, M. (2009) 'The zebrafish stress axis: Molecular fallout from the teleost-specific genome duplication event', *General and Comparative Endocrinology*. Elsevier Inc., 161(1), pp. 62–66. doi: 10.1016/j.ygcen.2008.09.011.

2. Alsop, D. and Vijayan, M. M. (2008) 'Development of the corticosteroid stress axis and receptor expression in zebrafish.', *American journal of physiology. Regulatory, integrative and comparative physiology*, 294(3), pp. R711–R719. doi: 10.1152/ajpregu.00671.2007.

3. Andreasen, E. A. *et al.* (2002) 'Tissue-Specific Expression of AHR2, ARNT2, and CYP1A in Zebrafish Embryos and Larvae: Effects of Developmental Stage and 2,3,7,8-Tetrachlorodibenzo-p-dioxin Exposure', *Toxicological Sciences*, 68(2), pp. 403–419. doi: 10.1093/toxsci/68.2.403.

4. Ang, S. O. *et al.* (2002) 'Disruption of oxygen homeostasis underlies congenital Chuvash polycythemia', *Nature genetics*, 32(4), p. 614—621. doi: 10.1038/ng1019.

5. Appelhoff, R. J. *et al.* (2004) 'Differential function of the prolyl hydroxylases PHD1, PHD2, and PHD3 in the regulation of hypoxia-inducible factor.', *The Journal of biological chemistry*. United States, 279(37), pp. 38458–38465. doi: 10.1074/jbc.M406026200.

6. Aprelikova, O. *et al.* (2004) 'Regulation of HIF prolyl hydroxylases by hypoxia-inducible factors.', *Journal of cellular biochemistry*. United States, 92(3), pp. 491–501. doi: 10.1002/jcb.20067.

7. Aronoff, S. L. *et al.* (2004) 'Glucose Metabolism and Regulation: Beyond Insulin and Glucagon', *Diabetes Spectrum*. American Diabetes Association, 17(3), pp. 183–190. doi: 10.2337/diaspect.17.3.183.

8. Baker, M. E. and Katsu, Y. (2017) '30 YEARS OF THE MINERALOCORTICOID RECEPTOR: Evolution of the mineralocorticoid receptor: sequence, structure and function', *Journal of Endocrinology*. Bristol, UK: Bioscientifica Ltd, 234(1), pp. T1–T16. doi: 10.1530/JOE-16-0661.

9. Bamberger, C. M., Schulte, H. M. and Chrousos, G. P. (1996) 'Molecular Determinants of Glucocorticoid Receptor Function and Tissue Sensitivity to Glucocorticoids', *Endocrine Reviews*, 17(3), pp. 245–261. doi: 10.1210/edrv-17-3-245.

10. Baranova, O. *et al.* (2007) 'Neuron-Specific Inactivation of the Hypoxia Inducible Factor 1α Increases Brain Injury in a Mouse Model of Transient Focal Cerebral Ischemia', *The Journal of Neuroscience*, 27(23), pp. 6320 LP – 6332. doi: 10.1523/JNEUROSCI.0449-07.2007.

11. Barnes, P. J. (2011) 'Glucocorticosteroids: current and future directions', *British Journal of Pharmacology*. John Wiley & Sons, Ltd (10.1111), 163(1), pp. 29–43. doi: 10.1111/j.1476-5381.2010.01199.x.

12. Barnes, P. J. and Adcock, I. M. (2009) 'Glucocorticoid resistance in inflammatory diseases', *The Lancet*. Elsevier, 373(9678), pp. 1905–1917. doi: 10.1016/S0140-6736(09)60326-3.

13. Bartels, K., Grenz, A. and Eltzschig, H. K. (2013) 'Hypoxia and inflammation are two sides of the same coin', *Proceedings of the National Academy of Sciences of the United States of America*. 2013/11/01. National Academy of Sciences, 110(46), pp. 18351–18352. doi: 10.1073/pnas.1318345110.

14. Basu, M. *et al.* (2002) 'Glucocorticoids as prophylaxis against acute mountain sickness', *Clinical Endocrinology*. John Wiley & Sons, Ltd, 57(6), pp. 761–767. doi: 10.1046/j.1365-2265.2002.01664.x.

15. Behrooz, A. and Ismail-Beigi, F. (1997) 'Dual control of glut1 glucose transporter

gene expression by hypoxia and by inhibition of oxidative phosphorylation', *J Biol Chem*, 272(9), pp. 5555–5562. Available at: http://www.ncbi.nlm.nih.gov/entrez/query.fcgi?cmd=Retrieve&db=PubMed&dopt=Citation&list_uids=9038162.

16. van den Berghe, G. (1991) 'The role of the liver in metabolic homeostasis: Implications for inborn errors of metabolism', *Journal of Inherited Metabolic Disease*, 14(4), pp. 407–420. doi: 10.1007/BF01797914.

17. Berra, E. *et al.* (2001) 'Hypoxia-inducible factor-1α (HIF-1α) escapes O 2 -driven proteasomal degradation irrespective of its subcellular localization: nucleus or cytoplasm', *EMBO reports*, 2(7), pp. 615–620. doi: 10.1093/embo-reports/kve130.

18. Bertout, J. A., Patel, S. A. and Simon, M. C. (2008) 'The impact of O2 availability on human cancer', *Nature reviews. Cancer*. 2008/11/06, 8(12), pp. 967–975. doi: 10.1038/nrc2540.

19. Bianchi, L., Tacchini, L. and Cairo, G. (1999) 'HIF-1-mediated activation of transferrin receptor gene transcription by iron chelation', *Nucleic Acids Research*, 27(21), pp. 4223–4227. doi: 10.1093/nar/27.21.4223.

20. Biddlestone, J., Bandarra, D. and Rocha, S. (2015) 'The role of hypoxia in inflammatory disease (review)', *International journal of molecular medicine*. 2015/01/27. D.A. Spandidos, 35(4), pp. 859–869. doi: 10.3892/ijmm.2015.2079.

21. Binder, E. B. (2009) 'The role of FKBP5, a co-chaperone of the glucocorticoid receptor in the pathogenesis and therapy of affective and anxiety disorders', *Psychoneuroendocrinology*. Pergamon, 34, pp. S186–S195. doi: 10.1016/J.PSYNEUEN.2009.05.021.

22. van den Bos, R. *et al.* (2020) 'Early Life Glucocorticoid Exposure Modulates Immune Function in Zebrafish (Danio rerio) Larvae', *Frontiers in Immunology*.

Frontiers Media S.A., 11, p. 727. doi: 10.3389/fimmu.2020.00727.

23. Bremer, A. A. and Miller, W. L. (2014) 'Regulation of Steroidogenesis', in *Cellular Endocrinology in Health and Disease*. Elsevier Inc., pp. 207–227. doi: 10.1016/B978-0-12-408134-5.00013-5.

24. Burger, A. *et al.* (2016) 'Maximizing mutagenesis with solubilized CRISPR-Cas9 ribonucleoprotein complexes', *Development*, 143(11), pp. 2025 LP – 2037. doi: 10.1242/dev.134809.

25. Busillo, J. M. and Cidlowski, J. A. (2013) 'The five Rs of glucocorticoid action during inflammation: Ready, reinforce, repress, resolve, and restore', *Trends in Endocrinology and Metabolism*. doi: 10.1016/j.tem.2012.11.005.

26. Buss, J. L. *et al.* (2004) 'Iron chelators in cancer chemotherapy.', *Current topics in medicinal chemistry*. United Arab Emirates, 4(15), pp. 1623–1635. doi: 10.2174/1568026043387269.

27. Chandel, N. S. *et al.* (2000) 'Reactive oxygen species generated at mitochondrial Complex III stabilize hypoxia-inducible factor-1α during hypoxia: A mechanism of O2 sensing', *Journal of Biological Chemistry*. J Biol Chem, 275(33), pp. 25130–25138. doi: 10.1074/jbc.M001914200.

28. Charmandari, E., Tsigos, C. and Chrousos, G. (2005) 'ENDOCRINOLOGY OF THE STRESS RESPONSE [1]', *Annual Review of Physiology*, 67(1), pp. 259–284. doi: 10.1146/annurev.physiol.67.040403.120816.

29. Charron, C. E. *et al.* (2009) 'Hypoxia-inducible Factor 1α Induces Corticosteroid-insensitive Inflammation via Reduction of Histone Deacetylase-2 Transcription', *Journal of Biological Chemistry*. American Society for Biochemistry and Molecular Biology, 284(52), pp. 36047–36054. doi: 10.1074/JBC.M109.025387.

30. Chatzopoulou, A. *et al.* (2015) 'Transcriptional and Metabolic Effects of

Glucocorticoid Receptor α and β Signaling in Zebrafish', *Endocrinology*, 156(5), pp. 1757–1769. doi: 10.1210/en.2014-1941.

31. Chrousos, G. and Kino, T. (2009) 'Glucocorticoid Signaling in the Cell: Expanding Clinical Implications to Complex Human Behavioral and Somatic Disorders', 100(2), pp. 130–134. doi: 10.1016/j.pestbp.2011.02.012.Investigations.

32. Chrousos, G. P. and Kino, T. (2005) 'Intracellular glucocorticoid signaling: a formerly simple system turns stochastic.', *Science's STKE : signal transduction knowledge environment*, 2005(304), p. pe48. doi: 10.1126/stke.3042005pe48.

33. Cohen, H. T. and McGovern, F. J. (2005) 'Renal-cell carcinoma.', *The New England journal of medicine*. United States, 353(23), pp. 2477–2490. doi: 10.1056/NEJMra043172.

34. Coll, A. P. and Yeo, G. S. H. (2013) 'The hypothalamus and metabolism: Integrating signals to control energy and glucose homeostasis', *Current Opinion in Pharmacology*. Elsevier Ltd, pp. 970–976. doi: 10.1016/j.coph.2013.09.010.

35. Consoli, A. (1992) 'Role of Liver in Pathophysiology of NIDDM', *Diabetes Care*, 15(3), pp. 430–441. doi: 10.2337/diacare.15.3.430.

36. Covello, K. L. and Simon, M. C. (2004) 'HIFs, Hypoxia, and Vascular Development', in *Current Topics in Developmental Biology*, pp. 37–54. doi: 10.1016/S0070-2153(04)62002-3.

37. Cruz, S. A. *et al.* (2013) 'Glucocorticoid Receptor, but Not Mineralocorticoid Receptor, Mediates Cortisol Regulation of Epidermal Ionocyte Development and Ion Transport in Zebrafish (Danio Rerio)', *PLOS ONE*. Public Library of Science, 8(10), p. e77997. Available at: https://doi.org/10.1371/journal.pone.0077997.

38. Cummins, E. P. *et al.* (2006) 'Prolyl hydroxylase-1 negatively regulates IkappaB kinase-beta, giving insight into hypoxia-induced NFkappaB activity.', *Proceedings of*

the National Academy of Sciences of the United States of America, 103(48), pp. 18154–18159. doi: 10.1073/pnas.0602235103.

39. Cummins, E. P. *et al.* (2007) 'Hypoxic Regulation of NF-??B Signaling', *Methods in Enzymology*, 435(07), pp. 479–492. doi: 10.1016/S0076-6879(07)35025-8.

40. Cummins, E. P. and Taylor, C. T. (2005) 'Hypoxia-responsive transcription factors', *Pflugers Archiv European Journal of Physiology*, 450(6), pp. 363–371. doi: 10.1007/s00424-005-1413-7.

41. Dallman, M. F. *et al.* (1987) 'Regulation of ACTH secretion: variations on a theme of B.', *Recent progress in hormone research*. United States, 43, pp. 113–173. doi: 10.1016/b978-0-12-571143-2.50010-1.

42. Dardzinski, B. J. *et al.* (2000) 'Increased plasma beta-hydroxybutyrate, preserved cerebral energy metabolism, and amelioration of brain damage during neonatal hypoxia ischemia with dexamethasone pretreatment', *Pediatric research*, 48(2), pp. 248–255. doi: 10.1203/00006450-200008000-00021.

43. Davies, T. H., Ning, Y. M. and Sánchez, E. R. (2005) 'Differential control of glucocorticoid receptor hormone-binding function by tetratricopeptide repeat (TPR) proteins and the immunosuppressive ligand FK506', *Biochemistry*, 44(6), pp. 2030–2038. doi: 10.1021/bi048503v.

44. Dittrich, A. *et al.* (2012) 'Glucocorticoids increase interleukin-6–dependent gene induction by interfering with the expression of the suppressor of cytokine signaling 3 feedback inhibitor', *Hepatology*. John Wiley & Sons, Ltd, 55(1), pp. 256–266. doi: 10.1002/hep.24655.

45. Drutel, G. *et al.* (1996) 'Cloning and Selective Expression in Brain and Kidney of ARNT2 Homologous to the Ah Receptor Nuclear Translocator (ARNT)', *Biochemical and Biophysical Research Communications*. Academic Press, 225(2), pp. 333–339. doi:

10.1006/BBRC.1996.1176.

46. Duan, C. (2016) 'Hypoxia-inducible factor 3 biology: complexities and emerging themes.', *American journal of physiology. Cell physiology*, 310(4), pp. C260-9. doi: 10.1152/ajpcell.00315.2015.

47. Duque, E. de A. and Munhoz, C. D. (2016) 'The Pro-inflammatory Effects of Glucocorticoids in the Brain ', *Frontiers in Endocrinology* , p. 78. Available at: https://www.frontiersin.org/article/10.3389/fendo.2016.00078.

48. Eachus, H. *et al.* (2017) 'Genetic disruption of 21-hydroxylase in zebrafish causes interrenal hyperplasia', *Endocrinology*, 158(12), pp. 4165–4173. doi: 10.1210/en.2017-00549.

49. Ebersole, J. L. *et al.* (2018) 'Hypoxia-inducible transcription factors, HIF1A and HIF2A, increase in aging mucosal tissues', *Immunology*. 2018/02/14. John Wiley and Sons Inc., 154(3), pp. 452–464. doi: 10.1111/imm.12894.

50. Egg, M. *et al.* (2013) 'Linking Oxygen to Time: The Bidirectional Interaction Between the Hypoxic Signaling Pathway and the Circadian Clock', *Chronobiology International*. Taylor & Francis, 30(4), pp. 510–529. doi: 10.3109/07420528.2012.754447.

51. Egg, M. *et al.* (2014) 'Chronodisruption increases cardiovascular risk in zebrafish via reduced clearance of senescent erythrocytes', *Chronobiology international*, 31(5), p. 680—689. doi: 10.3109/07420528.2014.889703.

52. Eguchi, H. *et al.* (1997) 'A nuclear localization signal of human aryl hydrocarbon receptor nuclear translocator/hypoxia-inducible factor 1β is a novel bipartite type recognized by the two components of nuclear pore-targeting complex', *Journal of Biological Chemistry*. J Biol Chem, 272(28), pp. 17640–17647. doi: 10.1074/jbc.272.28.17640.

53. Elks, P. M. *et al.* (2011) 'Activation of hypoxia-inducible factor-1α (Hif-1α) delays inflammation resolution by reducing neutrophil apoptosis and reverse migration in a zebrafish inflammation model.', *Blood*. United States, 118(3), pp. 712–722. doi: 10.1182/blood-2010-12-324186.

54. Elks, P. M. *et al.* (2015) 'Exploring the HIFs, buts and maybes of hypoxia signalling in disease: lessons from zebrafish models', *Disease Models & Mechanisms*, 8(11), pp. 1349–1360. doi: 10.1242/dmm.021865.

55. Eltzschig, H. K. and Carmeliet, P. (2011) 'Hypoxia and inflammation', *The New England journal of medicine*, 364(7), pp. 656–665. doi: 10.1056/NEJMra0910283.

56. Elvert, G. *et al.* (2003) 'Cooperative interaction of hypoxia-inducible factor-2α (HIF-2α) and Ets-1 in the transcriptional activation of vascular endothelial growth factor receptor-2 (Flk-1)', *Journal of Biological Chemistry*. American Society for Biochemistry and Molecular Biology, 278(9), pp. 7520–7530. doi: 10.1074/jbc.M211298200.

57. Epstein, A. C. R. *et al.* (2001) 'C. elegans EGL-9 and Mammalian Homologs Define a Family of Dioxygenases that Regulate HIF by Prolyl Hydroxylation', *Cell*, 107(1), pp. 43–54. doi: https://doi.org/10.1016/S0092-8674(01)00507-4.

58. Escoter-Torres, L. *et al.* (2019) 'Fighting the fire: Mechanisms of inflammatory gene regulation by the glucocorticoid receptor', *Frontiers in Immunology*. Frontiers Media S.A., p. 1859. doi: 10.3389/fimmu.2019.01859.

59. Facchinello, N. *et al.* (2017) 'nr3c1 null mutant zebrafish are viable and reveal DNA-binding-independent activities of the glucocorticoid receptor', *Scientific Reports*. London: Nature Publishing Group UK, 7, p. 4371. doi: 10.1038/s41598-017-04535-6.

60. Fan, X. *et al.* (2009) 'The role and regulation of hypoxia-inducible factor-1α expression in brain development and neonatal hypoxic–ischemic brain injury', *Brain*

Research Reviews. Elsevier, 62(1), pp. 99–108. doi: 10.1016/J.BRAINRESREV.2009.09.006.

61. Faught, E., Best, C. and Vijayan, M. M. (2016) 'Maternal stress-associated cortisol stimulation may protect embryos from cortisol excess in zebrafish', *Royal Society Open Science*, 3(2). doi: 10.1098/rsos.160032.

62. Faught, E. and Vijayan, M. M. (2018a) 'Maternal stress and fish reproduction: The role of cortisol revisited', *Fish and Fisheries*, 19(6). doi: 10.1111/faf.12309.

63. Faught, E. and Vijayan, M. M. (2018b) 'The mineralocorticoid receptor is essential for stress axis regulation in zebrafish larvae', *Scientific Reports*. Springer US, 8(1), pp. 1–11. doi: 10.1038/s41598-018-36681-w.

64. Fromage, G. (2012) 'Steroids: what are they and what is their mechanism of action?', *Journal of Aesthetic Nursing*. Mark Allen Group, 1(4), pp. 198–201. doi: 10.12968/joan.2012.1.4.198.

65. Fukuda, R. *et al.* (2007) 'HIF-1 Regulates Cytochrome Oxidase Subunits to Optimize Efficiency of Respiration in Hypoxic Cells', *Cell*, 129(1), pp. 111–122. doi: 10.1016/j.cell.2007.01.047.

66. Gaber, T. *et al.* (2011) 'Macrophage Migration Inhibitory Factor Counterregulates Dexamethasone-Mediated Suppression of Hypoxia-Inducible Factor-1α Function and Differentially Influences Human CD4⁺ T Cell Proliferation under Hypoxia', *The Journal of Immunology*, 186(2), pp. 764 LP – 774. doi: 10.4049/jimmunol.0903421.

67. Geer, E. B., Islam, J. and Buettner, C. (2014) 'Mechanisms of glucocorticoid-induced insulin resistance: focus on adipose tissue function and lipid metabolism', *Endocrinology and metabolism clinics of North America*, 43(1), pp. 75–102. doi: 10.1016/j.ecl.2013.10.005.

68. Glanemann, M. *et al.* (2004) 'Ischemic preconditioning and methylprednisolone both equally reduce hepatic ischemia/reperfusion injury', *Surgery*, 135(2), pp. 203–214. doi: 10.1016/j.surg.2003.08.011.

69. Gnarra, J. R. *et al.* (1997) 'Defective placental vasculogenesis causes embryonic lethality in VHL-deficient mice.', *Proceedings of the National Academy of Sciences of the United States of America*, 94(17), pp. 9102–9107. doi: 10.1073/pnas.94.17.9102.

70. Gonzalez Nunez, V., Gonzalez-Sarmiento, R. and Rodrı́guez, R. E. (2003) 'Identification of two proopiomelanocortin genes in zebrafish (Danio rerio)', *Molecular Brain Research*, 120(1), pp. 1–8. doi: https://doi.org/10.1016/j.molbrainres.2003.09.012.

71. Gordan, J. D. *et al.* (2007) 'HIF-2alpha promotes hypoxic cell proliferation by enhancing c-myc transcriptional activity', *Cancer cell*, 11(4), pp. 335–347. doi: 10.1016/j.ccr.2007.02.006.

72. Gordeuk, V. R. *et al.* (2004) 'Congenital disorder of oxygen sensing: association of the homozygous Chuvash polycythemia VHL mutation with thrombosis and vascular abnormalities but not tumors.', *Blood*. United States, 103(10), pp. 3924–3932. doi: 10.1182/blood-2003-07-2535.

73. Greenald, D. *et al.* (2015) 'Genome-wide mapping of Hif-1α binding sites in zebrafish.', *BMC genomics*. BMC Genomics, 16, p. 923. doi: 10.1186/s12864-015-2169-x.

74. Griffiths, B. B. *et al.* (2012) 'A zebrafish model of glucocorticoid resistance shows serotonergic modulation of the stress response.', *Frontiers in behavioral neuroscience*, 6(October), p. 68. doi: 10.3389/fnbeh.2012.00068.

75. Groeneweg, F. L. *et al.* (2011) 'Rapid non-genomic effects of corticosteroids and their role in the central stress response.', *The Journal of endocrinology*. England,

209(2), pp. 153–167. doi: 10.1530/JOE-10-0472.

76. Groulx, I. and Lee, S. (2002) 'Oxygen-dependent ubiquitination and degradation of hypoxia-inducible factor requires nuclear-cytoplasmic trafficking of the von Hippel-Lindau tumor suppressor protein', *Molecular and cellular biology*. American Society for Microbiology, 22(15), pp. 5319–5336. doi: 10.1128/mcb.22.15.5319-5336.2002.

77. Guenther, M. G., Barak, O. and Lazar, M. A. (2001) 'The SMRT and N-CoR corepressors are activating cofactors for histone deacetylase 3', *Molecular and cellular biology*. American Society for Microbiology, 21(18), pp. 6091–6101. doi: 10.1128/mcb.21.18.6091-6101.2001.

78. de Guia, R. M. *et al.* (2014) 'Glucocorticoid hormones and energy homeostasis', *Hormone molecular biology and clinical investigation*, 19(2), p. 117—128. doi: 10.1515/hmbci-2014-0021.

79. Haase, V. H. (2010) 'Hypoxic regulation of erythropoiesis and iron metabolism.', *American journal of physiology. Renal physiology*, 299(1), pp. F1-13. doi: 10.1152/ajprenal.00174.2010.

80. Hansen, I. A. *et al.* (2003) 'The pro-opiomelanocortin gene of the zebrafish (Danio rerio)', *Biochemical and Biophysical Research Communications*, 303(4), pp. 1121–1128. doi: https://doi.org/10.1016/S0006-291X(03)00475-3.

81. Hatamoto, K. and Shingyoji, C. (2008) 'Cyclical training enhances the melanophore responses of zebrafish to background colours', *Pigment Cell & Melanoma Research*. John Wiley & Sons, Ltd (10.1111), 21(3), pp. 397–406. doi: 10.1111/j.1755-148X.2008.00445.x.

82. Hatcher, H. C. *et al.* (2009) 'Synthetic and natural iron chelators: therapeutic potential and clinical use', *Future medicinal chemistry*, 1(9), pp. 1643–1670. doi: 10.4155/fmc.09.121.

83. Heikkilä, M. *et al.* (2011) 'Roles of the human hypoxia-inducible factor (HIF)-3α variants in the hypoxia response', *Cellular and Molecular Life Sciences*, 68(23), pp. 3885–3901. doi: 10.1007/s00018-011-0679-5.

84. Henze, A.-T. and Acker, T. (2010) 'Feedback regulators of hypoxia-inducible factors and their role in cancer biology', *Cell Cycle*. Taylor & Francis, 9(14), pp. 2821–2835. doi: 10.4161/cc.9.14.12249.

85. Hickey, M. M. and Simon, M. C. (2006) 'Regulation of Angiogenesis by Hypoxia and Hypoxia-Inducible Factors', *Current Topics in Developmental Biology*, 76, pp. 217–257. doi: 10.1016/S0070-2153(06)76007-0.

86. Hill, A. J. *et al.* (2009) 'Potential Roles of Arnt2 in Zebrafish Larval Development', *Zebrafish*. 140 Huguenot Street, 3rd FloorNew Rochelle, NY 10801USA: Mary Ann Liebert, Inc., 6(1), pp. 79–91. doi: 10.1089/zeb.2008.0536.

87. Hirose, K. *et al.* (1996) 'cDNA cloning and tissue-specific expression of a novel basic helix-loop-helix/PAS factor (Arnt2) with close sequence similarity to the aryl hydrocarbon receptor nuclear translocator (Arnt)', *Molecular and cellular biology*, 16(4), pp. 1706–1713. doi: 10.1128/mcb.16.4.1706.

88. Holmquist-Mengelbier, L. *et al.* (2006) 'Recruitment of HIF-1α and HIF-2α to common target genes is differentially regulated in neuroblastoma: HIF-2α promotes an aggressive phenotype', *Cancer Cell*. Cell Press, 10(5), pp. 413–423. doi: 10.1016/j.ccr.2006.08.026.

89. Hruscha, A. *et al.* (2013) 'Efficient CRISPR/Cas9 genome editing with low off-target effects in zebrafish', *Development*, 140(May), pp. 4982–4987. doi: 10.1242/dev.099085.

90. Hu, C.-J. *et al.* (2007) 'The N-terminal transactivation domain confers target gene specificity of hypoxia-inducible factors HIF-1alpha and HIF-2alpha', *Molecular*

biology of the cell. 2007/09/05. The American Society for Cell Biology, 18(11), pp. 4528–4542. doi: 10.1091/mbc.e06-05-0419.

91. Hu, C. *et al.* (2003) 'Differential Roles of Hypoxia-Inducible Factor 1 alpha (HIF-1 alpha) and HIF-2 alpha in Hypoxic Gene Regulation.', *Molecular and Cellular Biology*, 23(24), pp. 9361–9374. doi: 10.1128/MCB.23.24.9361.

92. Huang, Y. *et al.* (2009) 'Hypoxia down-regulates glucocorticoid receptor alpha and attenuates the anti-inflammatory actions of dexamethasone in human alveolar epithelial A549 cells', *Life Sciences*, 85(3–4), pp. 107–112. doi: 10.1016/j.lfs.2009.04.026.

93. Imtiyaz, H. Z. and Simon, M. C. (2010) 'Hypoxia-inducible factors as essential regulators of inflammation', *Current topics in microbiology and immunology*, 345, pp. 105–120. doi: 10.1007/82_2010_74.

94. Ivan, M. and Kaelin Jr, W. G. (2017) 'The EGLN-HIF O(2)-Sensing System: Multiple Inputs and Feedbacks', *Molecular cell*, 66(6), pp. 772–779. doi: 10.1016/j.molcel.2017.06.002.

95. Iwai, K. *et al.* (1999) 'Identification of the von Hippel-Lindau tumor-suppressor protein as part of an active E3 ubiquitin ligase complex', *Proceedings of the National Academy of Sciences of the United States of America*, 96(22), pp. 12436–12441. doi: 10.1073/pnas.96.22.12436.

96. Jain, S. *et al.* (1998) 'Expression of ARNT, ARNT2, HIF1α, HIF2α and Ah receptor mRNAs in the developing mouse', *Mechanisms of Development*. Elsevier, 73(1), pp. 117–123. doi: 10.1016/S0925-4773(98)00038-0.

97. Jones, M. T., Hillhouse, E. W. and Burden, J. L. (1977) 'Dynamics and mechanics of corticosteroid feedback at the hypothalamus and anterior pituitary gland.', *The Journal of endocrinology*. England, 73(3), pp. 405–417. doi: 10.1677/joe.0.0730405.

98. Kaelin, W. G. J. and Ratcliffe, P. J. (2008) 'Oxygen sensing by metazoans: the central role of the HIF hydroxylase pathway.', *Molecular cell*. United States, 30(4), pp. 393–402. doi: 10.1016/j.molcel.2008.04.009.

99. Kallio, P. J. *et al.* (1999) 'Regulation of the hypoxia-inducible transcription factor 1alpha by the ubiquitin-proteasome pathway.', *The Journal of biological chemistry*. United States, 274(10), pp. 6519–6525. doi: 10.1074/jbc.274.10.6519.

100. Kapitsinou, P. P. and Haase, V. H. (2008) 'The VHL tumor suppressor and HIF: insights from genetic studies in mice.', *Cell death and differentiation*, 15(4), pp. 650–659. doi: 10.1038/sj.cdd.4402313.

101. Karlsson, J., von Hofsten, J. and Olsson, P.-E. (2001) 'Generating Transparent Zebrafish: A Refined Method to Improve Detection of Gene Expression During Embryonic Development', *Marine Biotechnology*, 3(6), pp. 522–527. doi: 10.1007/s1012601-0053-4.

102. Khacho, M. *et al.* (2008) 'Cancer-causing mutations in a novel transcription-dependent nuclear export motif of VHL abrogate oxygen-dependent degradation of hypoxia-inducible factor.', *Molecular and cellular biology*, 28(1), pp. 302–314. doi: 10.1128/MCB.01044-07.

103. Khurana, A. *et al.* (2006) 'Regulation of the ring finger E3 ligase Siah2 by p38 MAPK', *The Journal of biological chemistry*. 2006/09/25, 281(46), pp. 35316–35326. doi: 10.1074/jbc.M606568200.

104. Kim, H. R. *et al.* (2017) 'Chapter 18 - Zebrafish as a model for von Hippel Lindau and hypoxia-inducible factor signaling', in Detrich, H. W., Westerfield, M., and Zon, L. I. B. T.-M. in C. B. (eds) *The Zebrafish*. Academic Press, pp. 497–523. doi: https://doi.org/10.1016/bs.mcb.2016.07.001.

105. Kim, H. R. *et al.* (2020) 'Investigation of the role of VHL-HIF signaling in DNA

repair and apoptosis in zebrafish', *Oncotarget*. Impact Journals LLC, 11(13), pp. 1109–1130. doi: 10.18632/oncotarget.27521.

106. Kim, J. W. *et al.* (2006) 'HIF-1-mediated expression of pyruvate dehydrogenase kinase: A metabolic switch required for cellular adaptation to hypoxia', *Cell Metabolism*, 3(3), pp. 177–185. doi: 10.1016/j.cmet.2006.02.002.

107. Kim, W. Y. and Kaelin, W. G. (2004) 'Role of VHL gene mutation in human cancer', *Journal of Clinical Oncology*. American Society of Clinical Oncology, pp. 4991–5004. doi: 10.1200/JCO.2004.05.061.

108. Kimmel, C. B. *et al.* (1995) 'Stages of Embryonic Development of the Zebrafish', *Developmental Dynamics*, 203, pp. 253–310. doi: 10.1002/aja.1002030302.

109. Klimova, T. and Chandel, N. S. (2008) 'Mitochondrial complex III regulates hypoxic activation of HIF', *Cell Death and Differentiation*. Cell Death Differ, pp. 660–666. doi: 10.1038/sj.cdd.4402307.

110. de Kloet, E. R., Joëls, M. and Holsboer, F. (2005) 'Stress and the brain: from adaptation to disease', *Nature Reviews Neuroscience*, 6(6), pp. 463–475. doi: 10.1038/nrn1683.

111. Köblitz, L. *et al.* (2015) 'Developmental Expression and Hypoxic Induction of Hypoxia Inducible Transcription Factors in the Zebrafish.', *PloS one*, 10(6), p. e0128938. doi: 10.1371/journal.pone.0128938.

112. Kodama, T. *et al.* (2003) 'Role of the glucocorticoid receptor for regulation of hypoxia-dependent gene expression', *Journal of Biological Chemistry*, 278(35), pp. 33384–33391. doi: 10.1074/jbc.M302581200.

113. Koh, M. Y. *et al.* (2012) 'The Hypoxia-Associated Factor Switches Cells from HIF-1α– to HIF-2α–Dependent Signaling Promoting Stem Cell Characteristics, Aggressive Tumor Growth and Invasion', *Cancer Research*, 71(11), pp. 4015–4027. doi:

10.1158/0008-5472.CAN-10-4142.

114. Koh, M. Y. and Powis, G. (2012) 'Passing the baton: The HIF switch', *Trends in Biochemical Sciences*, 37(9), pp. 364–372. doi: 10.1016/j.tibs.2012.06.004.

115. Koivunen, P. *et al.* (2004) 'Catalytic Properties of the Asparaginyl Hydroxylase (FIH) in the Oxygen Sensing Pathway Are Distinct from Those of Its Prolyl 4-Hydroxylases', *Journal of Biological Chemistry* , 279(11), pp. 9899–9904. doi: 10.1074/jbc.M312254200.

116. Kowalewski, M. P., Gram, A. and Boos, A. (2015) 'The role of hypoxia and HIF1α in the regulation of STAR-mediated steroidogenesis in granulosa cells', *Molecular and Cellular Endocrinology*. Elsevier, 401, pp. 35–44. doi: 10.1016/J.MCE.2014.11.023.

117. Kramer, B. M. R. *et al.* (2001) 'Dynamics and plasticity of peptidergic control centres in the retino-brain-pituitary system of Xenopus laevis', *Microscopy Research and Technique*. John Wiley & Sons, Ltd, 54(3), pp. 188–199. doi: 10.1002/jemt.1132.

118. Krieg, M. *et al.* (2000) 'Up-regulation of hypoxia-inducible factors HIF-1alpha and HIF-2alpha under normoxic conditions in renal carcinoma cells by von Hippel-Lindau tumor suppressor gene loss of function.', *Oncogene*, 19, pp. 5435–5443. doi: 10.1038/sj.onc.1203938.

119. Krug Ii, R. G. *et al.* (2014) 'A transgenic zebrafish model for monitoring glucocorticoid receptor activity', *Genes, Brain and Behavior*, 13, pp. 478–487. doi: 10.1111/gbb.12135.

120. Kuo, T. *et al.* (2015) 'Regulation of Glucose Homeostasis by Glucocorticoids', in Wang, J.-C. and Harris, C. (eds) *Glucocorticoid Signaling: From Molecules to Mice to Man*. New York, NY: Springer New York, pp. 99–126. doi: 10.1007/978-1-4939-2895-8_5.

121. Kuo, T., Harris, C. and Wang, J.-C. (2013) 'Metabolic functions of glucocorticoid receptor in skeletal muscle', *Molecular and Cellular Endocrinology*, 380(1–2), pp. 79–

88. doi: 10.1016/j.mce.2013.03.003.

122. Kurrasch, D. M. *et al.* (2009) 'Neuroendocrine transcriptional programs adapt dynamically to the supply and demand for neuropeptides as revealed in NSF mutant zebrafish', *Neural development*. BioMed Central, 4, p. 22. doi: 10.1186/1749-8104-4-22.

123. Labun, K. *et al.* (2016) 'CHOPCHOP v2: a web tool for the next generation of CRISPR genome engineering', *Nucleic Acids Research*, 44(W1), pp. W272–W276. doi: 10.1093/nar/gkw398.

124. Lando, D. *et al.* (2002) 'FIH-1 is an asparaginyl hydroxylase enzyme that regulates the transcriptional activity of hypoxia-inducible factor', *Genes & development*. Cold Spring Harbor Laboratory Press, 16(12), pp. 1466–1471. doi: 10.1101/gad.991402.

125. Langlais, D. *et al.* (2008) 'Regulatory Network Analyses Reveal Genome-Wide Potentiation of LIF Signaling by Glucocorticoids and Define an Innate Cell Defense Response', *PLOS Genetics*. Public Library of Science, 4(10), p. e1000224. Available at: https://doi.org/10.1371/journal.pgen.1000224.

126. Langlais, D. *et al.* (2012) 'The Stat3/GR Interaction Code: Predictive Value of Direct/Indirect DNA Recruitment for Transcription Outcome', *Molecular Cell*. Cell Press, 47(1), pp. 38–49. doi: 10.1016/J.MOLCEL.2012.04.021.

127. Laryea, G. *et al.* (2015) 'Dissection of glucocorticoid receptor-mediated inhibition of the hypothalamic-pituitary-adrenal axis by gene targeting in mice', *Frontiers in neuroendocrinology*. 2014/09/27, 36, pp. 150–164. doi: 10.1016/j.yfrne.2014.09.002.

128. Le, P. P. *et al.* (2005) 'Glucocorticoid receptor-dependent gene regulatory networks', *PLoS Genetics*, 1(2), pp. 0159–0170. doi: 10.1371/journal.pgen.0010016.

129. Leonard, M. O. *et al.* (2005) 'Potentiation of Glucocorticoid Activity in Hypoxia through Induction of the Glucocorticoid Receptor', *The Journal of Immunology*, 174, pp. 2250–2257. doi: 10.4049/jimmunol.174.4.2250.

130. Li, G., Wang, S. and Gelehrter, T. D. (2003) 'Identification of Glucocorticoid Receptor Domains Involved in Transrepression of Transforming Growth Factor-β Action', *Journal of Biological Chemistry*, 278(43), pp. 41779–41788. doi: 10.1074/jbc.M305350200.

131. Li, H., Dong, L. and Whitlock, J. P. (1994) 'Transcriptional activation function of the mouse Ah receptor nuclear translocator.', *Journal of Biological Chemistry* , 269(45), pp. 28098–28105. Available at: http://www.jbc.org/content/269/45/28098.abstract.

132. Li, Q. F. *et al.* (2006) 'Hypoxia upregulates hypoxia inducible factor (HIF)-3α expression in lung epithelial cells: characterization and comparison with HIF-1α', *Cell Research*, 16(6), pp. 548–558. doi: 10.1038/sj.cr.7310072.

133. Limbourg, F. P. *et al.* (2002) 'Rapid nontranscriptional activation of endothelial nitric oxide synthase mediates increased cerebral blood flow and stroke protection by corticosteroids', *The Journal of Clinical Investigation*. American Society for Clinical Investigation, 110(11), pp. 1729–1738. doi: 10.1172/JCI15481.

134. Lin, D. *et al.* (1995) 'Role of steroidogenic acute regulatory protein in adrenal and gonadal steroidogenesis.', *Science (New York, N.Y.)*. United States, 267(5205), pp. 1828–1831. doi: 10.1126/science.7892608.

135. Lisy, K. and Peet, D. J. (2008) 'Turn me on: regulating HIF transcriptional activity', *Cell Death & Differentiation*, 15(4), pp. 642–649. doi: 10.1038/sj.cdd.4402315.

136. Livak, K. J. and Schmittgen, T. D. (2001) 'Analysis of Relative Gene Expression Data Using Real-Time Quantitative PCR and the 2−ΔΔCT Method', *Methods*. Academic Press, 25(4), pp. 402–408. doi: 10.1006/METH.2001.1262.

137. Loboda, A., Jozkowicz, A. and Dulak, J. (2010) 'HIF-1 and HIF-2 transcription factors--similar but not identical.', *Molecules and cells*, 29(5), pp. 435–442. doi: 10.1007/s10059-010-0067-2.

138. Löhr, H. and Hammerschmidt, M. (2011) 'Zebrafish in endocrine systems: recent advances and implications for human disease.', *Annual review of physiology*. United States, 73, pp. 183–211. doi: 10.1146/annurev-physiol-012110-142320.

139. Lonser, R. R. *et al.* (2003) 'von Hippel-Lindau disease.', *Lancet (London, England)*. England, 361(9374), pp. 2059–2067. doi: 10.1016/S0140-6736(03)13643-4.

140. Macfarlane, D. P., Forbes, S. and Walker, B. R. (2008) 'Glucocorticoids and fatty acid metabolism in humans: Fuelling fat redistribution in the metabolic syndrome', *Journal of Endocrinology*, 197(2), pp. 189–204. doi: 10.1677/JOE-08-0054.

141. Majmundar, A. J., Wong, W. J. and Simon, M. C. (2010) 'Hypoxia-Inducible Factors and the Response to Hypoxic Stress', *Molecular Cell*, 40(2), pp. 294–309. doi: 10.1016/j.molcel.2010.09.022.

142. Makino, Y. *et al.* (2007) 'Transcriptional up-regulation of inhibitory PAS domain protein gene expression by hypoxia-inducible factor 1 (HIF-1): a negative feedback regulatory circuit in HIF-1-mediated signaling in hypoxic cells.', *The Journal of biological chemistry*. American Society for Biochemistry and Molecular Biology, 282(19), pp. 14073–82. doi: 10.1074/jbc.M700732200.

143. Mangelsdorf, D. J. *et al.* (1995) 'The nuclear receptor superfamily: the second decade.', *Cell*, 83(6), pp. 835–839. doi: 10.1016/0092-8674(95)90199-x.

144. De Marco, R. J. *et al.* (2013) 'Optogenetic elevation of endogenous glucocorticoid level in larval zebrafish', *Front Neural Circuits*, 7(May), p. 82. doi: 10.3389/fncir.2013.00082.

145. Marzolla, V. *et al.* (2012) 'The role of the mineralocorticoid receptor in adipocyte biology and fat metabolism.', *Molecular and cellular endocrinology*. Ireland, 350(2), pp. 281–288. doi: 10.1016/j.mce.2011.09.011.

146. Merkulov, V. M. and Merkulova, T. I. (2012) 'Glucocorticoid receptor isoforms generated by alternative splicing and alternative translation initiation', *Russian Journal of Genetics: Applied Research*, 2(3), pp. 205–213. doi: 10.1134/S2079059712030070.

147. Michaud, J. L. *et al.* (2000) 'ARNT2 acts as the dimerization partner of SIM1 for the development of the hypothalamus', *Mechanisms of Development*, 90(2), pp. 253–261. doi: 10.1016/S0925-4773(99)00328-7.

148. Minchenko, A. *et al.* (2002) 'Hypoxia-inducible Factor-1-mediated Expression of the 6- Phosphofructo-2-kinase/fructose-2,6-bisphosphatase-3 (PFKFB3) Gene', *J Biol Chem*, 277(8), pp. 6183–6187. doi: 10.1074/jbc.M110978200.

149. Mitre-Aguilar, I. B., Cabrera-Quintero, A. J. and Zentella-Dehesa, A. (2015) 'Genomic and non-genomic effects of glucocorticoids: implications for breast cancer', *International journal of clinical and experimental pathology*. e-Century Publishing Corporation, 8(1), pp. 1–10. Available at: https://www.ncbi.nlm.nih.gov/pubmed/25755688.

150. Moghadam-Kia, S. and Werth, V. P. (2010) 'Prevention and treatment of systemic glucocorticoid side effects', *International Journal of Dermatology*. John Wiley & Sons, Ltd (10.1111), 49(3), pp. 239–248. doi: 10.1111/j.1365-4632.2009.04322.x.

151. Mole, D. R. *et al.* (2009) 'Genome-wide association of hypoxia-inducible factor (HIF)-1alpha and HIF-2alpha DNA binding with expression profiling of hypoxia-inducible transcripts.', *The Journal of biological chemistry*, 284(25), pp. 16767–16775. doi: 10.1074/jbc.M901790200.

152. Mommsen, T. P., Vijayan, M. M. and Moon, T. W. (1999) 'Cortisol in teleosts:

Dynamics, mechanisms of action, and metabolic regulation', *Reviews in Fish Biology and Fisheries*. Springer, pp. 211–268. doi: 10.1023/A:1008924418720.

153. Moniz, S., Biddlestone, J. and Rocha, S. (2014) 'Grow$_2$: the HIF system, energy homeostasis and the cell cycle.', *Histology and histopathology*. Spain, 29(5), pp. 589–600. doi: 10.14670/HH-29.10.589.

154. Montague, T. G. *et al.* (2014) 'CHOPCHOP: a CRISPR/Cas9 and TALEN web tool for genome editing', *Nucleic acids research*. 2014/05/26. Oxford University Press, 42(Web Server issue), pp. W401–W407. doi: 10.1093/nar/gku410.

155. Montgomery, M. T. *et al.* (1990) 'The use of glucocorticosteroids to lessen the inflammatory sequelae following third molar surgery', *Journal of Oral and Maxillofacial Surgery*. W.B. Saunders, 48(2), pp. 179–187. doi: 10.1016/S0278-2391(10)80207-1.

156. Moroz, E. *et al.* (2009) 'Real-Time Imaging of HIF-1α Stabilization and Degradation', *PLOS ONE*. Public Library of Science, 4(4), p. e5077. Available at: https://doi.org/10.1371/journal.pone.0005077.

157. Mountjoy, K. G. *et al.* (1994) 'Localization of the melanocortin-4 receptor (MC4-R) in neuroendocrine and autonomic control circuits in the brain.', *Molecular endocrinology (Baltimore, Md.)*. United States, 8(10), pp. 1298–1308. doi: 10.1210/mend.8.10.7854347.

158. Munck, A., Guyre, P. M. and Holbrook, N. J. (1984) 'Physiological functions of glucocorticoids in stress and their relation to pharmacological actions.', *Endocrine reviews*. United States, 5(1), pp. 25–44. doi: 10.1210/edrv-5-1-25.

159. Murani, E. *et al.* (2019) 'Transcriptome Responses to Dexamethasone Depending on Dose and Glucocorticoid Receptor Sensitivity in the Liver', *Frontiers in genetics*. Frontiers Media S.A., 10, p. 559. doi: 10.3389/fgene.2019.00559.

160. Murdoch, C., Muthana, M. and Lewis, C. E. (2005) 'Hypoxia Regulates

Macrophage Functions in Inflammation', *The Journal of Immunology*, 175(10), pp. 6257 LP – 6263. doi: 10.4049/jimmunol.175.10.6257.

161. Muto, A. *et al.* (2005) 'Forward Genetic Analysis of Visual Behavior in Zebrafish', *PLOS Genetics*. Public Library of Science, 1(5), p. e66. Available at: https://doi.org/10.1371/journal.pgen.0010066.

162. Muto, A. *et al.* (2013) 'Glucocorticoid receptor activity regulates light adaptation in the zebrafish retina.', *Frontiers in neural circuits*, 7(September), p. 145. doi: 10.3389/fncir.2013.00145.

163. Nakayama, K. *et al.* (2004) 'Siah2 regulates stability of prolyl-hydroxylases, controls HIF1alpha abundance, and modulates physiological responses to hypoxia.', *Cell*. United States, 117(7), pp. 941–952. doi: 10.1016/j.cell.2004.06.001.

164. Nandam, L. S. *et al.* (2020) 'Cortisol and Major Depressive Disorder-Translating Findings From Humans to Animal Models and Back', *Frontiers in psychiatry*. Frontiers Media S.A., 10, p. 974. doi: 10.3389/fpsyt.2019.00974.

165. Nath, B. and Szabo, G. (2012) 'Hypoxia and hypoxia inducible factors: Diverse roles in liver diseases', *Hepatology*, 55(2), pp. 622–633. doi: 10.1002/hep.25497.

166. Neeck, G., Renkawitz, R. and Eggert, M. (2002) 'Molecular aspects of glucocorticoid hormone action in rheumatoid arthritis', *Cytokines, Cellular & Molecular Therapy*, 7(2), pp. 61–69. doi: 10.1080/13684730412331302081.

167. Neff, M. M. *et al.* (1998) 'dCAPS, a simple technique for the genetic analysis of single nucleotide polymorphisms: experimental applications in Arabidopsis thaliana genetics', *The Plant Journal*. John Wiley & Sons, Ltd (10.1111), 14(3), pp. 387–392. doi: 10.1046/j.1365-313X.1998.00124.x.

168. Nesan, D. *et al.* (2012) 'Glucocorticoid Receptor Signaling Is Essential for Mesoderm Formation and Muscle Development in Zebrafish', *Endocrinology*, 153(3),

pp. 1288–1300. doi: 10.1210/en.2011-1559.

169. Nesan, D. and Vijayan, M. M. (2013) 'Role of glucocorticoid in developmental programming: Evidence from zebrafish', *General and Comparative Endocrinology*. doi: 10.1016/j.ygcen.2012.10.006.

170. Nesan, D. and Vijayan, M. M. (2016) 'Maternal Cortisol Mediates Hypothalamus-Pituitary-Interrenal Axis Development in Zebrafish.', *Scientific reports*. Nature Publishing Group, 6(November 2015), p. 22582. doi: 10.1038/srep22582.

171. Nicolaides, N. C. *et al.* (2010) 'The human glucocorticoid receptor: Molecular basis of biologic function', *Steroids*, 75(1), pp. 1–12. doi: 10.1016/j.steroids.2009.09.002.

172. Nicolaides, N. C. *et al.* (2015) 'Stress, the Stress System and the Role of Glucocorticoids', *Neuroimmunomodulation*, 22(1–2), pp. 6–19. doi: 10.1159/000362736.

173. Nikolaus, S., Fölscn, U. and Schreiber, S. (2000) *Immunopharmacology of 5-aminosalicylic acid and of glucocorticoids in the therapy of inflammatory bowel disease*, *Hepato-gastroenterology*.

174. Nyhan, M. J., O'Sullivan, G. C. and McKenna, S. L. (2008) 'Role of the VHL (von Hippel-Lindau) gene in renal cancer: a multifunctional tumour suppressor.', *Biochemical Society transactions*. England, 36(Pt 3), pp. 472–478. doi: 10.1042/BST0360472.

175. O'Reilly, M. W. *et al.* (2016) '11-Oxygenated C19 Steroids Are the Predominant Androgens in Polycystic Ovary Syndrome', *The Journal of clinical endocrinology and metabolism*. Endocrine Society, 102(3), pp. 840–848. doi: 10.1210/jc.2016-3285.

176. Oakley, R. H. and Cidlowski, J. A. (2011) 'Cellular processing of the glucocorticoid receptor gene and protein: New mechanisms for generating tissue-

specific actions of glucocorticoids', *Journal of Biological Chemistry*, 286(5), pp. 3177–3184. doi: 10.1074/jbc.R110.179325.

177. Oakley, R. H. and Cidlowski, J. A. (2013) 'The biology of the glucocorticoid receptor: New signaling mechanisms in health and disease', *Journal of Allergy and Clinical Immunology*, 132(5). doi: 10.1016/j.jaci.2013.09.007.

178. Pajusola, K. *et al.* (2005) 'Stabilized HIF-1alpha is superior to VEGF for angiogenesis in skeletal muscle via adeno-associated virus gene transfer.', *The FASEB journal : official publication of the Federation of American Societies for Experimental Biology*, 19(10), pp. 1365–1367. doi: 10.1096/fj.05-3720fje.

179. Palazon, A. *et al.* (2014) 'HIF transcription factors, inflammation, and immunity', *Immunity*, 41(4), pp. 518–528. doi: 10.1016/j.immuni.2014.09.008.

180. Pan, Y. *et al.* (2007) 'Multiple factors affecting cellular redox status and energy metabolism modulate hypoxia-inducible factor prolyl hydroxylase activity in vivo and in vitro.', *Molecular and cellular biology*, 27(3), pp. 912–925. doi: 10.1128/MCB.01223-06.

181. Panettieri, R. A. *et al.* (2019) 'Non-genomic Effects of Glucocorticoids: An Updated View', *Trends in Pharmacological Sciences*. doi: 10.1016/j.tips.2018.11.002.

182. Papandreou, I. *et al.* (2006) 'HIF-1 mediates adaptation to hypoxia by actively downregulating mitochondrial oxygen consumption', *Cell Metabolism*, 3(3), pp. 187–197. doi: 10.1016/j.cmet.2006.01.012.

183. Parichy, D. M. *et al.* (2009) 'Normal Table of Post-Embryonic Zebrafish Development: Staging by Externally Visible Anatomy of the Living Fish', *Developmental dynamics : an official publication of the American Association of Anatomists*, 238(12), pp. 2975–3015. doi: 10.1002/dvdy.22113.

184. Peek, C. B. *et al.* (2017) 'Circadian Clock Interaction with HIF1α Mediates

Oxygenic Metabolism and Anaerobic Glycolysis in Skeletal Muscle', *Cell metabolism*. 2016/10/20, 25(1), pp. 86–92. doi: 10.1016/j.cmet.2016.09.010.

185. Pelster, B. and Egg, M. (2015) 'Multiplicity of Hypoxia-Inducible Transcription Factors and Their Connection to the Circadian Clock in the Zebrafish*', *Physiological and Biochemical Zoology*, 88(2), pp. 146–157. doi: 10.1086/679751.

186. Pelster, B. and Egg, M. (2018) 'Hypoxia-inducible transcription factors in fish: expression, function and interconnection with the circadian clock', *The Journal of Experimental Biology*, 221(13), p. jeb163709. doi: 10.1242/jeb.163709.

187. Pescador, N. *et al.* (2005) 'Identification of a functional hypoxia-responsive element that regulates the expression of the egl nine homologue 3 (egln3/phd3) gene', *The Biochemical journal*. Portland Press Ltd., 390(Pt 1), pp. 189–197. doi: 10.1042/BJ20042121.

188. Place, T. L. *et al.* (2013) 'Prolyl-4-hydroxylase 3 (PHD3) expression is downregulated during epithelial-to-mesenchymal transition', *PloS one*. Public Library of Science, 8(12), pp. e83021–e83021. doi: 10.1371/journal.pone.0083021.

189. Pollenz, R. S., Sattler, C. A. and Poland, A. (1994) 'The aryl hydrocarbon receptor and aryl hydrocarbon receptor nuclear translocator protein show distinct subcellular localizations in Hepa 1c1c7 cells by immunofluorescence microscopy.', *Molecular pharmacology*. United States, 45(3), pp. 428–438.

190. Prager, E. M. and Johnson, L. R. (2009) 'Stress at the synapse: signal transduction mechanisms of adrenal steroids at neuronal membranes.', *Science signaling*. United States, 2(86), p. re5. doi: 10.1126/scisignal.286re5.

191. Prasch, A. L. *et al.* (2006) 'Identification of Zebrafish ARNT1 Homologs: 2,3,7,8-Tetrachlorodibenzo-p-dioxin Toxicity in the Developing Zebrafish Requires ARNT1', *Molecular Pharmacology*, 69(3), pp. 776 LP – 787. doi:

10.1124/mol.105.016873.

192. Presman, D. M. and Hager, G. L. (2017) 'More than meets the dimer: What is the quaternary structure of the glucocorticoid receptor?', *Transcription*. doi: 10.1080/21541264.2016.1249045.

193. Qin, D. *et al.* (2019) 'Chronic Glucocorticoid Exposure Induces Depression-Like Phenotype in Rhesus Macaque (Macaca Mulatta) ', *Frontiers in Neuroscience* , p. 188. Available at: https://www.frontiersin.org/article/10.3389/fnins.2019.00188.

194. R. Oakley, J. C. (2013) 'The Biology of the Glucocorticoid Receptor: New Signaling Mechanism in Health and Disease', *J allergy clin inmunol*, 132(5), pp. 1033–1044. doi: 10.1016/j.jaci.2013.09.007.The.

195. Rafacho, A. *et al.* (2014) 'Glucocorticoid treatment and endocrine pancreas function: Implications for glucose homeostasis, insulin resistance and diabetes', *Journal of Endocrinology*, 223(3), pp. R49–R62. doi: 10.1530/JOE-14-0373.

196. Rahtu-Korpela, L. *et al.* (2014) 'HIF prolyl 4-hydroxylase-2 inhibition improves glucose and lipid metabolism and protects against obesity and metabolic dysfunction', *Diabetes*, 63(10), pp. 3324–3333. doi: 10.2337/db14-0472.

197. Ramamoorthy, S. and Cidlowski, J. A. (2013) 'Exploring the molecular mechanisms of glucocorticoid receptor action from sensitivity to resistance', *Endocrine development*. 2013/02/01, 24, pp. 41–56. doi: 10.1159/000342502.

198. Ramamoorthy, S. and Cidlowski, J. A. (2016) 'Corticosteroids. Mechanisms of Action in Health and Disease', *Rheumatic Disease Clinics of North America*. doi: 10.1016/j.rdc.2015.08.002.

199. Rankin, E. B. *et al.* (2009) 'Hypoxia-inducible factor 2 regulates hepatic lipid metabolism', *Mol.Cell Biol.*, 29(16), pp. 4527–4538. doi: MCB.00200-09 [pii];10.1128/MCB.00200-09 [doi].

200. Raval, R. R. *et al.* (2005) 'Contrasting properties of hypoxia-inducible factor 1 (HIF-1) and HIF-2 in von Hippel-Lindau-associated renal cell carcinoma.', *Molecular and cellular biology*, 25(13), pp. 5675–86. doi: 10.1128/MCB.25.13.5675-5686.2005.

201. Reichardt, H. M. *et al.* (1998) 'DNA Binding of the Glucocorticoid Receptor Is Not Essential for Survival', *Cell*. Cell Press, 93(4), pp. 531–541. doi: 10.1016/S0092-8674(00)81183-6.

202. Revollo, J. R. and Cidlowski, J. A. (2009) 'Mechanisms generating diversity in glucocorticoid receptor signaling', *Annals of the New York Academy of Sciences*, 1179, pp. 167–178. doi: 10.1111/j.1749-6632.2009.04986.x.

203. Robertson, A. L. *et al.* (2014) 'A Zebrafish Compound Screen Reveals Modulation of Neutrophil Reverse Migration as an Anti-Inflammatory Mechanism Anne', 6(225). doi: 10.1126/scitranslmed.3007672.A.

204. Robertson, C. E. *et al.* (2014) 'Hypoxia-inducible factor-1 mediates adaptive developmental plasticity of hypoxia tolerance in zebrafish, Danio rerio.', *Proceedings. Biological sciences / The Royal Society*, 281(1786), pp. 20140637-. doi: 10.1098/rspb.2014.0637.

205. van Rooijen, E. *et al.* (2009) 'Zebrafish mutants in the von Hippel-Lindau tumor suppressor display a hypoxic response and recapitulate key aspects of Chuvash polycythemia', *Blood*, 113(25), pp. 6449 LP – 6460. doi: 10.1182/blood-2008-07-167890.

206. van Rooijen, E. *et al.* (2011) *A Zebrafish Model for VHL and Hypoxia Signaling*. Third Edit, *Methods in Cell Biology*. Third Edit. Elsevier Inc. doi: 10.1016/B978-0-12-381320-6.00007-2.

207. Ruas, J. L. and Poellinger, L. (2005) 'Hypoxia-dependent activation of HIF into a transcriptional regulator', *Seminars in Cell and Developmental Biology*. Elsevier Ltd, pp.

514–522. doi: 10.1016/j.semcdb.2005.04.001.

208. Safronova, O. and Morita, I. (2010) 'Transcriptome remodeling in hypoxic inflammation.', *Journal of dental research*. United States, 89(5), pp. 430–444. doi: 10.1177/0022034510366813.

209. Sanderson, B. A. *et al.* (2014) 'Modification of gel architecture and TBE/TAE buffer composition to minimize heating during agarose gel electrophoresis', *Analytical Biochemistry*. Academic Press, 454, pp. 44–52. doi: 10.1016/J.AB.2014.03.003.

210. Santhakumar, K. *et al.* (2012) 'A zebrafish model to study and therapeutically manipulate hypoxia signaling in tumorigenesis', *Cancer Research*, 72(16), pp. 4017–4027. doi: 10.1158/0008-5472.CAN-11-3148.

211. Schaaf, M.J.M., Chatzopoulou, A. and Spaink, H. P. (2009) 'The zebrafish as a model system for glucocorticoid receptor research', *Comparative Biochemistry and Physiology Part A: Molecular & Integrative Physiology*. Pergamon, 153(1), pp. 75–82. doi: 10.1016/J.CBPA.2008.12.014.

212. Schaaf, M. J. M. and Cidlowski, J. A. (2002) 'Molecular mechanisms of glucocorticoid action and resistance', *Journal of Steroid Biochemistry and Molecular Biology*, 83(1–5), pp. 37–48. doi: 10.1016/S0960-0760(02)00263-7.

213. Schild, Y. *et al.* (2020) 'Hif-1alpha stabilisation is protective against infection in zebrafish comorbid models', *The FEBS Journal*. John Wiley & Sons, Ltd, n/a(n/a). doi: 10.1111/febs.15433.

214. Schmidt, F. and Braunbeck, T. (2011) 'Alterations along the Hypothalamic-Pituitary-Thyroid Axis of the Zebrafish (*Danio rerio*) after Exposure to Propylthiouracil', *Journal of Thyroid Research*. Edited by J. R. Wall. SAGE-Hindawi Access to Research, 2011, p. 376243. doi: 10.4061/2011/376243.

215. Schödel, J. *et al.* (2011) 'High-resolution genome-wide mapping of HIF-binding

sites by ChIP-seq', *Blood*. Blood, 117(23). doi: 10.1182/blood-2010-10-314427.

216. Schofield, C. J. and Ratcliffe, P. J. (2004) 'Oxygen sensing by HIF hydroxylases', *Nature Reviews Molecular Cell Biology*, 5(5), pp. 343–354. doi: 10.1038/nrm1366.

217. Schoneveld, O. J. L. M., Gaemers, I. C. and Lamers, W. H. (2004) 'Mechanisms of glucocorticoid signalling', *Biochimica et Biophysica Acta - Gene Structure and Expression*, 1680(2), pp. 114–128. doi: 10.1016/j.bbaexp.2004.09.004.

218. Scortegagna, M. *et al.* (2005) 'HIF-2α regulates murine hematopoietic development in an erythropoietin-dependent manner', *Blood*. American Society of Hematology, 105(8), pp. 3133–3140. doi: 10.1182/blood-2004-05-1695.

219. Semenza, G. *et al.* (1996) 'Hypoxia Response Elements in the Aldolase A, Enolase 1,and Lactate Dehydrogenase A Gene Promoters Contain Essential Binding Sites for Hypoxia-inducible Factor 1', *Journal of Biological Chemistry*, 271(51), pp. 32529–32537. doi: 10.1074/jbc.271.51.32529.

220. Semenza, G. L. (2001) 'HIF-1 and mechanisms of hypoxia sensing', *Current Opinion in Cell Biology*, 13(2), pp. 167–171. doi: 10.1016/S0955-0674(00)00194-0.

221. Semenza, G. L. (2011a) 'Hypoxia. Cross talk between oxygen sensing and the cell cycle machinery', *American Journal of Physiology-Cell Physiology*. American Physiological Society, 301(3), pp. C550–C552. doi: 10.1152/ajpcell.00176.2011.

222. Semenza, G. L. (2011b) 'Oxygen Sensing, Homeostasis, and Disease', *New England Journal of Medicine*. Massachusetts Medical Society, 365(6), pp. 537–547. doi: 10.1056/NEJMra1011165.

223. Semenza, G. L. (2012) 'Hypoxia-inducible factors: mediators of cancer progression and targets for cancer therapy.', *Trends in pharmacological sciences*, 33(4), pp. 207–214. doi: 10.1016/j.tips.2012.01.005.

224. Semenza, G. L. (2013) 'HIF-1 mediates metabolic responses to intratumoral

hypoxia and oncogenic mutations', *Journal of Clinical Investigation*, 123(9), pp. 3664–3671. doi: 10.1172/JCI67230.

225. Sharp, F. R., Bergeron, M. and Bernaudin, M. (2001) 'Hypoxia-inducible factor in brain', in Roach, R. C., Wagner, P. D., and Hackett, P. H. (eds) *Hypoxia: From Genes to the Bedside*. Boston, MA: Springer US, pp. 273–291. doi: 10.1007/978-1-4757-3401-0_18.

226. Shay, J. E. S. and Simon, M. C. (2012) 'Hypoxia-inducible factors : Crosstalk between inflammation and metabolism', 23, pp. 389–394.

227. Shi, C. *et al.* (2020) 'Hyperandrogenism in POMCa-deficient zebrafish enhances somatic growth without increasing adiposity', *Journal of Molecular Cell Biology*, 12(4), pp. 291–304. doi: 10.1093/jmcb/mjz053.

228. Siddiq, A., Aminova, L. R. and Ratan, R. R. (2007) 'Hypoxia inducible factor prolyl 4-hydroxylase enzymes: center stage in the battle against hypoxia, metabolic compromise and oxidative stress.', *Neurochemical research*, 32(4–5), pp. 931–946. doi: 10.1007/s11064-006-9268-7.

229. Simon, M. C. and Keith, B. (2008) 'The role of oxygen availability in embryonic development and stem cell function', *Nature Reviews Molecular Cell Biology*, 9(4), pp. 285–296. doi: 10.1038/nrm2354.

230. Singleman, C. and Holtzman, N. G. (2014) 'Growth and maturation in the zebrafish, Danio rerio: a staging tool for teaching and research', *Zebrafish*. 2014/06/30. Mary Ann Liebert, Inc., 11(4), pp. 396–406. doi: 10.1089/zeb.2014.0976.

231. Smith, S. M. and Vale, W. W. (2006) 'The role of the hypothalamic-pituitary-adrenal axis in neuroendocrine responses to stress', *Dialogues in clinical neuroscience*. Les Laboratoires Servier, 8(4), pp. 383–395. Available at: https://pubmed.ncbi.nlm.nih.gov/17290797.

232. Smith, T. G. *et al.* (2006) 'Mutation of von Hippel-Lindau tumour suppressor and

human cardiopulmonary physiology.', *PLoS medicine*, 3(7), p. e290. doi: 10.1371/journal.pmed.0030290.

233. Solaini, G. *et al.* (2010) 'Hypoxia and mitochondrial oxidative metabolism.', *Biochimica et biophysica acta*. Netherlands, 1797(6–7), pp. 1171–1177. doi: 10.1016/j.bbabio.2010.02.011.

234. Spiga, F. *et al.* (2014) 'HPA axis-rhythms', *Comprehensive Physiology*, 4(3). doi: 10.1002/cphy.c140003.

235. Stahn, C. and Buttgereit, F. (2008) 'Genomic and nongenomic effects of glucocorticoids', *Nature Clinical Practice Rheumatology*. Nature Publishing Group, 4, p. 525. Available at: https://doi.org/10.1038/ncprheum0898.

236. Stellato, C. (2004) 'Post-transcriptional and nongenomic effects of glucocorticoids.', *Proceedings of the American Thoracic Society*, 1(11), pp. 255–263. doi: 10.1513/pats.200402-015MS.

237. Stocco, D. M. and Clark, B. J. (1996) 'Regulation of the acute production of steroids in steroidogenic cells.', *Endocrine reviews*. United States, 17(3), pp. 221–244. doi: 10.1210/edrv-17-3-221.

238. Stroka, D. and Candinas, D. (2010) 'Hypoxia-Inducible Factor-1 Signaling System', in Dufour, J. F. and Clavien, P. A. (eds) *Signaling Pathways in Liver Diseases*. doi: 10.1007/978-3-642-00150-5_27.

239. Sun, Y.-Y. *et al.* (2010) 'Glucocorticoid Protection of Oligodendrocytes against Excitotoxin Involving Hypoxia-Inducible Factor-1 in a Cell-Type-Specific Manner', *Journal of Neuroscience*, 30(28), pp. 9621–9630. doi: 10.1523/JNEUROSCI.2295-10.2010.

240. Surjit, M. *et al.* (2011) 'Widespread Negative Response Elements Mediate Direct Repression by Agonist- Liganded Glucocorticoid Receptor', *Cell*. Elsevier, 145(2), pp.

224–241. doi: 10.1016/j.cell.2011.03.027.

241. Suzuki, T. *et al.* (2014) 'Hypoxia and fatty liver', *World Journal of Gastroenterology*, 20(41), pp. 15087–15097. doi: 10.3748/wjg.v20.i41.15087.

242. Tan, T. *et al.* (2017) 'Overexpression and Knockdown of Hypoxia-Inducible Factor 1 Disrupt the Expression of Steroidogenic Enzyme Genes and Early Embryonic Development in Zebrafish', *Gene regulation and systems biology*. SAGE Publications, 11, pp. 1177625017713193–1177625017713193. doi: 10.1177/1177625017713193.

243. Tanguay, R. L. *et al.* (2000) 'Identification and expression of alternatively spliced aryl hydrocarbon nuclear translocator 2 (ARNT2) cDNAs from zebrafish with distinct functions', *Biochimica et Biophysica Acta (BBA) - Gene Structure and Expression*, 1494(1–2), pp. 117–128. doi: 10.1016/S0167-4781(00)00225-6.

244. Thisse, C. and Thisse, B. (2008) 'High-resolution in situ hybridization to whole-mount zebrafish embryos', *Nature Protocols*. Nature Publishing Group, 3, p. 59. Available at: https://doi.org/10.1038/nprot.2007.514.

245. Timmermans, S., Souffriau, J. and Libert, C. (2019) 'A General Introduction to Glucocorticoid Biology', *Frontiers in immunology*. Frontiers Media S.A., 10, p. 1545. doi: 10.3389/fimmu.2019.01545.

246. To, T. T. *et al.* (2007) 'Pituitary-Interrenal Interaction in Zebrafish Interrenal Organ Development', *Molecular Endocrinology*, 21(2), pp. 472–485. doi: 10.1210/me.2006-0216.

247. Tokarz, J. *et al.* (2013) 'Zebrafish and steroids: What do we know and what do we need to know?', *Journal of Steroid Biochemistry and Molecular Biology*. doi: 10.1016/j.jsbmb.2013.01.003.

248. Tokudome, S. *et al.* (2009) 'Glucocorticoid protects rodent hearts from ischemia / reperfusion injury by activating lipocalin-type prostaglandin D synthase – derived

PGD 2 biosynthesis', 119(6). doi: 10.1172/JCI37413.mentally.

249. Tsigos, C. and Chrousos, G. P. (2002) 'Hypothalamic-pituitary-adrenal axis, neuroendocrine factors and stress.', *Journal of psychosomatic research*. England, 53(4), pp. 865–871. doi: 10.1016/s0022-3999(02)00429-4.

250. Uchida, T. *et al.* (2004) 'Prolonged Hypoxia Differentially Regulates Hypoxia-inducible Factor (HIF)-1α and HIF-2α Expression in Lung Epithelial Cells: IMPLICATION OF NATURAL ANTISENSE HIF-1α ', *Journal of Biological Chemistry* , 279(15), pp. 14871–14878. doi: 10.1074/jbc.M400461200.

251. Uhlenhaut, N. H. *et al.* (2013) 'Insights into Negative Regulation by the Glucocorticoid Receptor from Genome-wide Profiling of Inflammatory Cistromes', *Molecular Cell*, 49(1). doi: 10.1016/j.molcel.2012.10.013.

252. Ulrich-Lai, Y. M. and Herman, J. P. (2009) 'Neural regulation of endocrine and autonomic stress responses.', *Nature reviews. Neuroscience*, 10(6), pp. 397–409. doi: 10.1038/nrn2647.

253. Vandevyver, S. *et al.* (2013) 'New insights into the anti-inflammatory mechanisms of glucocorticoids: An emerging role for glucocorticoid-receptor-mediated transactivation', *Endocrinology*. doi: 10.1210/en.2012-2045.

254. Varshney, G. K. *et al.* (2015) 'High-throughput gene targeting and phenotyping in zebrafish using CRISPR/Cas9', *Genome Research*, 5(1), pp. 1–10. doi: 10.1101/gr.186379.114.Freely.

255. Vegiopoulos, A. and Herzig, S. (2007) 'Glucocorticoids, metabolism and metabolic diseases', *Molecular and Cellular Endocrinology*, 275(1–2), pp. 43–61. doi: 10.1016/j.mce.2007.05.015.

256. Vettori, A. *et al.* (2017) 'Glucocorticoids promote Von Hippel Lindau degradation and Hif-1α stabilization', *Proceedings of the National Academy of Sciences*,

p. 201705338. doi: 10.1073/pnas.1705338114.

257. Wagle, M., Mathur, P. and Guo, S. (2011) 'Corticotropin-Releasing Factor Critical for Zebrafish Camouflage Behavior Is Regulated by Light and Sensitive to Ethanol', *The Journal of Neuroscience*, 31(1), pp. 214 LP – 224. doi: 10.1523/JNEUROSCI.3339-10.2011.

258. Wagner, A. E. *et al.* (2008) 'Dexamethasone impairs hypoxia-inducible factor-1 function', *Biochemical and Biophysical Research Communications*, 372(2), pp. 336–340. doi: 10.1016/j.bbrc.2008.05.061.

259. Walisser, J. A., Bunger, M. K., Glover, E. and Bradfield, C. A. (2004) 'Gestational exposure of Ahr and Arnt hypomorphs to dioxin rescues vascular development', *Proceedings of the National Academy of Sciences of the United States of America*. 2004/11/15. National Academy of Sciences, 101(47), pp. 16677–16682. doi: 10.1073/pnas.0404379101.

260. Walisser, J. A., Bunger, M. K., Glover, E., Harstad, E. B., *et al.* (2004) 'Patent Ductus Venosus and Dioxin Resistance in Mice Harboring a Hypomorphic Arnt Allele', *Journal of Biological Chemistry* , 279(16), pp. 16326–16331. doi: 10.1074/jbc.M400784200.

261. Walmsley, S. R. *et al.* (2011) 'Prolyl hydroxylase 3 (PHD3) is essential for hypoxic regulation of neutrophilic inflammation in humans and mice.', *The Journal of clinical investigation*, 121(3), pp. 1053–1063. doi: 10.1172/JCI43273.

262. Wang, C. *et al.* (2019) 'Extensive epigenomic integration of the glucocorticoid response in primary human monocytes and in vitro derived macrophages', *Scientific Reports*, 9(1), p. 2772. doi: 10.1038/s41598-019-39395-9.

263. Wang, W. D. *et al.* (2000) 'Overexpression of a Zebrafish ARNT2-like Factor Represses CYP1A Transcription in ZLE Cells', *Marine biotechnology (New York, N.Y.)*, 2(4), p. 376—386. Available at: http://europepmc.org/abstract/MED/10960127.

264. Warnecke, C. *et al.* (2004) 'Differentiating the functional role of hypoxia-inducible factor (HIF)-1α and HIF-2α (EPAS-1) by the use of RNA interference: erythropoietin is a HIF-2α target gene in Hep3B and Kelly cells', *The FASEB Journal*. Wiley, 18(12), pp. 1462–1464. doi: 10.1096/fj.04-1640fje.

265. Webb, J. D., Coleman, M. L. and Pugh, C. W. (2009) 'Hypoxia, hypoxia-inducible factors (HIF), HIF hydroxylases and oxygen sensing.', *Cellular and molecular life sciences : CMLS*. Switzerland, 66(22), pp. 3539–3554. doi: 10.1007/s00018-009-0147-7.

266. Weger, B. D. *et al.* (2016) 'Extensive Regulation of Diurnal Transcription and Metabolism by Glucocorticoids', *PLOS Genetics*. Public Library of Science, 12(12), p. e1006512. Available at: https://doi.org/10.1371/journal.pgen.1006512.

267. Weger, M. *et al.* (2018) 'Expression and activity profiling of the steroidogenic enzymes of glucocorticoid biosynthesis and the fdx1 co-factors in zebrafish', *Journal of Neuroendocrinology*, 30(4), pp. 1–15. doi: 10.1111/jne.12586.

268. Wenger, R. H., Stiehl, D. P. and Camenisch, G. (2005) 'Integration of oxygen signaling at the consensus HRE.', *Science's STKE : signal transduction knowledge environment*. American Association for the Advancement of Science, pp. re12–re12. doi: 10.1126/stke.3062005re12.

269. Whirledge, S. and Cidlowski, J. A. (2013) 'A role for glucocorticoids in stress-impaired reproduction: beyond the hypothalamus and pituitary', *Endocrinology*. 2013/09/24. Endocrine Society, 154(12), pp. 4450–4468. doi: 10.1210/en.2013-1652.

270. Wilson, K. S. *et al.* (2013) 'Physiological roles of glucocorticoids during early embryonic development of the zebrafish (Danio rerio)', *The Journal of Physiology*. John Wiley & Sons, Ltd, 591(24), pp. 6209–6220. doi: 10.1113/jphysiol.2013.256826.

271. Wright, A. D., Brearey, S. P. and Imray, C. H. E. (2008) 'High hopes at high

altitudes: pharmacotherapy for acute mountain sickness and high-altitude cerebral and pulmonary oedema', *Expert Opinion on Pharmacotherapy*, 9(1), pp. 119–127. doi: 10.1517/14656566.9.1.119.

272. Wu, R. S. *et al.* (2018) 'A Rapid Method for Directed Gene Knockout for Screening in G0 Zebrafish', *Developmental Cell*. Elsevier Inc., 46(1), pp. 112-125.e4. doi: 10.1016/j.devcel.2018.06.003.

273. Xie, Y. *et al.* (2019) 'Glucocorticoids inhibit macrophage differentiation towards a pro-inflammatory phenotype upon wounding without affecting their migration', *bioRxiv*, p. 473926. doi: 10.1101/473926.

274. Yamamoto, Y., Yin, M. J. and Gaynor, R. B. (2000) 'IkappaB kinase alpha (IKKalpha) regulation of IKKbeta kinase activity', *Molecular and cellular biology*. American Society for Microbiology, 20(10), pp. 3655–3666. doi: 10.1128/mcb.20.10.3655-3666.2000.

275. Yu, C.-Y. *et al.* (2010) 'Genome-Wide Analysis of Glucocorticoid Receptor Binding Regions in Adipocytes Reveal Gene Network Involved in Triglyceride Homeostasis', *PLOS ONE*. Public Library of Science, 5(12), p. e15188. Available at: https://doi.org/10.1371/journal.pone.0015188.

276. Yudt, M. R. and Cidlowski, J. A. (2001) 'Molecular Identification and Characterization of A and B Forms of the Glucocorticoid Receptor', *Molecular Endocrinology*, 15(7), pp. 1093–1103. doi: 10.1210/mend.15.7.0667.

277. Yudt, M. R. and Cidlowski, J. a (2002) 'The glucocorticoid receptor: coding a diversity of proteins and responses through a single gene.', *Molecular endocrinology (Baltimore, Md.)*, 16(8), pp. 1719–26. doi: 10.1210/me.2002-0106.

278. Zhang, C. *et al.* (2015) 'Effects of hypoxia inducible factor-1α on apoptotic inhibition and glucocorticoid receptor downregulation by dexamethasone in AtT-20

cells', *BMC Endocrine Disorders*. BMC Endocrine Disorders, 15(24), pp. 1–9. doi: 10.1186/s12902-015-0017-2.

279. Zhang, F. L. *et al.* (2012) 'Hypoxia-inducible factor 1-mediated human GATA1 induction promotes erythroid differentiation under hypoxic conditions', *Journal of Cellular and Molecular Medicine*, 16(8), pp. 1889–1899. doi: 10.1111/j.1582-4934.2011.01484.x.

280. Zhang, H. *et al.* (2007) 'HIF-1 Inhibits Mitochondrial Biogenesis and Cellular Respiration in VHL-Deficient Renal Cell Carcinoma by Repression of C-MYC Activity', *Cancer Cell*, 11(5), pp. 407–420. doi: 10.1016/j.ccr.2007.04.001.

281. Zhang, H. *et al.* (2008) 'Mitochondrial autophagy is an HIF-1-dependent adaptive metabolic response to hypoxia.', *The Journal of biological chemistry*, 283(16), pp. 10892–903. doi: 10.1074/jbc.M800102200.

282. Zhang, H. *et al.* (2011) 'Hypoxia-Inducible Factor Directs POMC Gene to Mediate Hypothalamic Glucose Sensing and Energy Balance Regulation', *PLOS Biology*. Public Library of Science, 9(7), p. e1001112. Available at: https://doi.org/10.1371/journal.pbio.1001112.

283. Zhang, P. *et al.* (2014) 'Hypoxia-Inducible Factor 3 Is an Oxygen-Dependent Transcription Activator and Regulates a Distinct Transcriptional Response to Hypoxia', *Cell Reports*, 6(6), pp. 1110–1121. doi: 10.1016/j.celrep.2014.02.011.

284. Zhang, P. *et al.* (2016) 'Down-regulation of GR?? expression and inhibition of its nuclear translocation by hypoxia', *Life Sciences*, 146, pp. 92–99. doi: 10.1016/j.lfs.2015.12.059.

285. Ziv, L. *et al.* (2012) 'An affective disorder in zebrafish with mutation of the glucocorticoid receptor', *Molecular Psychiatry*. Nature Publishing Group, 18(6), pp. 681–691. doi: 10.1038/mp.2012.64.

WEBSITES:

https://chopchop.cbu.uib.no/

www.graphpad.com

http://helix.wustl.edu/dcaps/

https://assets.thermofisher.com/TFS-Assets/LSG/manuals/cms_042380.pdf

BOOKS:

Kino T. Glucocorticoid Receptor. [Updated 2017 Aug 15]. In: Feingold KR, Anawalt B, Boyce A, et al., editors. Endotext [Internet]. South Dartmouth (MA): MDText.com, Inc.; 2000-. Available from: https://www.ncbi.nlm.nih.gov/books/NBK279171/